

Aus dem  
Institut für Pharmakologie und Klinische Pharmakologie  
der Heinrich-Heine-Universität Düsseldorf  
Direktor: Univ.-Prof. Dr. Jens W. Fischer

**Transkriptionelle und metabolische Regulation der Hyaluronsäurematrix  
im Rahmen der Tumorprogression**

Habilitationsschrift  
zur Erlangung der *Venia Legendi*  
für das Fach Klinische Pharmakologie

vorgelegt von  
Dr. med. Dr. rer. nat. Sören Twarock

2021

*Ein Mensch schaut in der Zeit zurück  
und sieht: Sein Unglück war sein Glück.*

Eugen Roth (1895 – 1976)

In Liebe und Dankbarkeit meiner Familie gewidmet.

# Inhaltsverzeichnis

<b><i>Inhaltsverzeichnis</i></b> .....	<b>3</b>
<b><i>Abkürzungsverzeichnis</i></b> .....	<b>4</b>
<b><i>Abbildungsverzeichnis</i></b> .....	<b>5</b>
<b>A. Einleitung</b> .....	<b>6</b>
1. Neoplasien.....	6
2. Die Tumormikroumgebung.....	7
3. Die extrazelluläre Matrix .....	8
4. Das Hyaluronsäure-System.....	9
<b>B. Zielsetzung</b> .....	<b>10</b>
<b>C. Zusammenfassung relevanter Publikationen</b> .....	<b>10</b>
<b>I. Hyaluronsäure-Effekte im Tumormikromilieu</b> .....	<b>13</b>
1. Einfluss der Hyaluronsäure auf Zell-Matrix-Kontakte und die Tumorzellproliferation <i>in vitro</i> .....	13
2. Regulation der HA-Synthese durch EGF, HA-Verteilung zwischen Tumor und Stroma und Auswirkung der HA-Inhibition auf die Tumorprogression <i>in vivo</i> .....	16
3. Synergistische Reduktion der Proliferation und Migration von ESCC-Zellen durch gleichzeitige Inhibition des EGF-Rezeptor-Signalwegs und der Hyaluronsäure-Synthese .....	19
<b>II. Transkriptionelle Regulation der Hyaluronsäure-Synthese in ESCC</b> .....	<b>20</b>
1. Prostaglandine und Hyaluronsäure-Synthese .....	20
2. ESCC-Zellen modulieren die Chemokin-Expression und die Hyaluronsäuresynthese in Fibroblasten ...	22
<b>III. Metabolische Regulation der Hyaluronsäure-Synthese in ESCC</b> .....	<b>23</b>
1. Einfluss einer diabetischen Stoffwechsellage auf Hyaluronsäuresynthese und Tumorprogression .....	23
2. Eine Inhibition der Hyaluronsäurematrix verbessert die Tumor-hemmende Wirkung von Dichloressigsäure <i>in vitro</i> und <i>in vivo</i> .....	27
<b>D. Zusammenfassung der Ergebnisse und perspektivischer Ausblick</b> .....	<b>32</b>
<b>E. Literatur</b> .....	<b>35</b>
<b>F. Danksagung</b> .....	<b>39</b>
<b>G. Originalarbeiten</b> .....	<b>40</b>

## Abkürzungsverzeichnis

4-MU	4-Methylumbelliferon
ANOVA	Varianzanalyse ( <i>analysis of variance</i> )
CEMIP	<i>Cell migration-inducing and hyaluronan-binding protein</i> (KIAA1199)
EGF	Epithelialer Wachstumsfaktor ( <i>epithelial growth factor</i> )
EGFR	EGF Rezeptor
ESCC	Ösophageale Plattenepithelkarzinomzellen ( <i>esophageal squamous cancer cells</i> )
EZM	Extrazelluläre Matrix
FAK	Fokale Adhäsiionskinase
G6P	Glukose-6-Phosphat
GLUT	Glukose-Transporter
HA	Hyaluronsäure (Hyaluronan)
HABP	Hyaluronsäure-bindendes Protein
HAS	Hyaluronsäure-Synthase
HYAL	Hyaluronidase
IGFR	Insulin-ähnlicher Wachstumsfaktor-Rezeptor
IRS-1	Insulin-Rezeptor-Substrat 1
MMP	Matrix-Metalloproteasen
qPCR	quantitative Echtzeit-PCR
RHAMM	<i>Receptor for Hyaluronan Mediated Motility</i> (HMMR, CD168)
$\alpha$ SMA	$\alpha$ -Glattmuskel-Aktin ( $\alpha$ -smooth muscle actin)
SEM	Standardfehler des Mittelwertes ( <i>standard error of mean</i> )
shRNA	Haarnadel-Interferenz-RNA ( <i>small hairpin RNA</i> )
siRNA	Interferenz-RNA ( <i>small interfering RNA</i> )
TKI	Tyrosinkinase-Inhibitoren
TLR	<i>Toll-like receptor</i>
TMU	Tumormikroumgebung
TNM	Tumor-Klassifikation (Tumor, Nodus, Metastasen)

## Abbildungsverzeichnis

Abb. 1: Charakteristika maligner Neoplasien .....	6
Abb. 2: Komponenten der Tumormikroumgebung .....	7
Abb. 3: Komponenten der extrazellulären Matrix .....	8
Abb. 4: Komponenten des Hyaluronsäuresystems .....	9
Abb. 5: Effekte der Hyaluronsäure-Matrix auf die Tumorprogression von ESCC .....	12
Abb. 6: Verringerung der Anzahl HA-assoziierter Filopodien, Auflösung von fokalen Adhäisonskomplexen und Degradation der fokalen Adhäisonskinase unter HA-Synthese-Inhibition durch 4-MU .....	13
Abb. 7: Nachbildung der Effekte von 4-MU auf Zellmorphologie, Filopodien und FAK-Spaltung durch einen lentiviral vermittelten Knockdown von <i>HAS3</i> und <i>HAS2</i> .....	14
Abb. 8: Abhängigkeit der Filopodien-Abnahme und FAK-Degradation von HA-Rezeptoren .....	15
Abb. 9: Korrelation der HAS3-Genexpression mit der Tumorgröße nach TNM-Klassifikation und der EGFR-Expression in Schnitten von gesunder Mukosa und humanen ESCC .....	16
Abb. 10: Hemmung des Tumorwachstums von xenotransplantierten OSC1-Zellen in Nacktmäusen durch Behandlung mit 4-MU .....	18
Abb. 11: Hemmung des Tumorwachstums von xenotransplantierten OSC1-Zellen durch lenti-viralen Knockdown von HAS3 .....	18
Abb. 12: Auswirkungen von 4-MU und tumorzellspezifischem HAS3-Knockdown auf die Proliferationsrate in OSC1-Xenografts .....	19
Abb. 13: Immunhistochemischer Nachweis von Hyaluronsäure (HA), Cyclooxygenase-2 (COX-2) und CD44 in menschlichem Ösophaguskarzinomgewebe .....	20
Abb. 14: HAS-Isoform-Expression in OSC1/2-Zellen unter Stimulation der Prostaglandin-Rezeptoren .....	21
Abb. 15: Intrazelluläre cAMP-Spiegel nach Stimulation des Prostaglandin-Signalwegs .....	21
Abb. 16: Abhängigkeit der HA-Synthese von extrazellulären Glukosekonzentrationen .....	24
Abb. 17: Metabolische Konkurrenz zwischen Glykolyse und HA-Synthese .....	25
Abb. 18: Verstärkung der HA-abhängigen Tumorprogression durch Hyperglykämie und Insulin-Depletion in einem Typ-1-Diabetes-Nacktmaus-Xenograft-Modell .....	26
Abb. 19: Gesteigerte Bildung der Hyaluronsäure-Matrix in Ösophaguskarzinomzellen unter DCA .....	27
Abb. 20: Umschaltung des Metabolismus von KYSE-410-Zellen von Glykolyse auf oxidative Phosphorylierung durch DCA .....	28
Abb. 21: Steigerung der Konzentration des frühen Glykolyse-Metaboliten Glucose-6-Phosphat und des HAS-Substrats UDP-N-Acetylglucosamin unter DCA .....	28
Abb. 22: Erhöhung des für Vorstufen der HA-Synthese benötigten Metaboliten Acetyl-CoA über die Aktivierung des mitochondrialen Krebs-Zyklus durch DCA .....	29
Abb. 23: Erhöhte Protein-O-GlcNAcylierung unter DCA .....	29
Abb. 24: Reduktion des Volumens von ESCC-Zell-Sphäroiden und eine damit einhergehende Apoptose-Induktion unter Kombination von DCA mit 4-MU .....	30
Abb. 25: Reduktion von Tumorwachstum und -proliferation und Induktion von HA-Synthese und Apoptose durch die Kombination von DCA und 4-MU in einem Tumorregressionsmodell <i>in vivo</i> .....	31
Abb. 26: Zusammenfassung der Ergebnisse der in diesem Manuscript zusammengefassten Veröffentlichungen. Vom Autor eigens für dieses Manuscript erstelltes Schema .....	32
Abb. 27: Hyaluronsäure-bindende Proteine, Proteoglykane und Interaktionen zwischen Kollagen, Elastin und Hyaluronsäure .....	33

## A. Einleitung

### 1. Neoplasien

Neoplastische Krankheitsbilder stellen zusammen mit kardiovaskulären Erkrankungen die häufigsten Todesursachen weltweit dar (Sung et al. 2021) und haben diese in Ländern mit hohem Einkommen mittlerweile sogar als führende Todesursache abgelöst (Mahase 2019). Während sich benigne Neoplasien in erster Linie durch eine stark erhöhte Zellteilungsrate auszeichnen, die sich klinisch durch Verdrängung anderer Gewebe und Strukturen oder die Produktion von systemisch wirksamen Hormonen bemerkbar machen, kommen im Falle der malignen Neoplasien eine Invasion anderer Gewebearten und eine hämatogene oder lymphogene Nah- und Fernmetastasierung hinzu, die zu paraneoplastischen Syndromen und einer stark verminderten Lebenserwartung führen können.

Die zellulären Charakteristika von malignen Neoplasien wurden von Weinberg und Hanahan in den beiden vielbeachteten Publikationen *Hallmarks of Cancer* (Hanahan and Weinberg 2000, Hanahan and Weinberg 2011) zusammengefasst. Zu den ursprünglich formulierten sechs Merkmalen erniedrigte Apoptoserate, dauerhaftes proliferatives Wachstum, Unempfindlichkeit gegenüber wachstums-hemmenden Signalen, Invasion und Metastasierung sowie Immortalisierung und Induktion von Neoangiogenese kamen später die vier weiteren Eigenschaften deregulierter Energiehaushalt, Immunevasion, Inflammation und Genominstabilität hinzu.

Die Therapie von Neoplasien basiert auf drei Säulen: chirurgische Maßnahmen, ionisierende Strahlung und pharmakologische Therapie. Die klassische pharmakologische zytostatische Therapie, wie sie in den 1940er Jahren erstmals eingesetzt wurde, wirkt über eine Inhibition des Wachstums schnellproliferierender Zellen. Neben neoplastischen Zellen sind dies unter anderem auch hämatopoetische Zellen, Keimzellen, Immunzellen und epitheliale Zellen. Daraus ergeben sich die starken Nebenwirkungen dieser Therapiestrategie wie Knochenmarktoxizität, Übelkeit und Erbrechen, Diarrhoe, Haarausfall und Keimzellschädigung. Einige Wirkstoffklassen wie die Alkyantien bergen zusätzlich das Risiko der Induktion von zeitversetzt auftretenden Sekundärneoplasien. Seit den späten 1990er Jahren wurden zunehmend zielgerichtete Tumortherapeutika („targeted therapy“) entwickelt und klinisch angewandt, die tumorentitätsspezifische Zielproteine blockieren und so zu geringeren unspezifischen Nebenwirkungen und einer stärkeren Wirksamkeit geführt haben. Prominente Beispiele sind die monoklonalen Antikörper („-mabs“) und die Tyrosinkinaseinhibitoren (TKI, „-nibe“). Eine aktuelle Entwicklung stellen die Immuncheckpoint-Inhibitoren dar, die die Antwort des Immunsystems auf das neoplastische Gewebe steigern und so zu einer immunvermittelten Lyse der transformierten Zellen führen können. Trotz dieser faszinierenden Entwicklungen der letzten Jahrzehnte bleibt die Wirksamkeit der neuen Therapieverfahren dennoch oft hinter den Erwartungen zurück: Die Fünf-Jahres-Überlebenszeiten konnten über die vergangenen Jahrzehnte zwar schrittweise verlängert werden, ein dauerhafter kurativer Ansatz ist meist aber nur in frühen Krankheitsphasen und bei bestimmten Tumorentitäten erreichbar. Oft wird die Wirksamkeit von Chemotherapie-Regimen auch durch das Auftreten lebensbedrohlicher Nebenwirkungen limitiert.

Charakteristika maligner Neoplasien

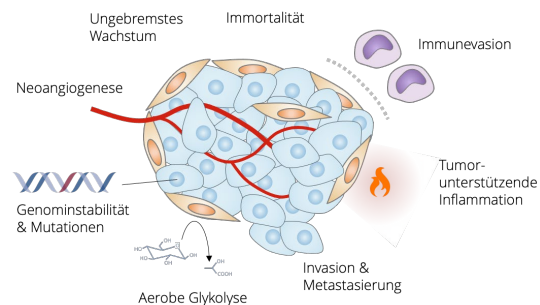


Abb. 1: Charakteristika maligner Neoplasien

Vom Autor eigens für dieses Manuskript erstelltes Schema.

## 2. Die Tumormikroumgebung

Die Tumormikroumgebung (TMU, auch: das Tumormikromilieu) besteht aus zellulären und extrazellulären Komponenten: Wichtige Zellarten sind mesenchymale Zellen wie Fibroblasten oder mesenchymale Stromazellen (MSC), Immunzellen wie Makrophagen, dendritische Zellen und Lymphozyten sowie endotheliale Zellen, deren Anteil im Rahmen der tumorassoziierten Neoangiogenese stark zunehmen kann (Arneth 2019, Farc and Cristea 2021). Tumor- und Stromazellen synthetisieren die Komponenten der extrazellulären Matrix (EZM); da diese Moleküle nicht nur aus Protein-, sondern auch aus Kohlenhydrat-Vorstufen synthetisiert werden, hängt ihre Produktion entscheidend vom zellulären Metabolismus der beteiligten Zellarten ab (Lau and Heiden 2020, Montenegro and Indraccolo 2020).

Die wechselseitigen Zell-Zell- und Zell-EZM-Interaktionen zwischen Tumor- und Stromazellen bilden ein dynamisches System, das den Tumorzellen ermöglicht, die Stromazellen derart zu beeinflussen, dass sie ihre bisherige Funktion verlieren und neue Phänotypen ausprägen, die die Entwicklung und Invasion von Tumorzellen begünstigen. Dieser Prozess, der mitunter auch als *Hijacking* bezeichnet wird (Baghban et al. 2020), erklärt die auf den ersten Blick unerwartete Beobachtung, dass eine starke Infiltration des Tumorgewebes mit Immunzellen nicht zu einer Eradikation der Tumorzellen führt, sondern vielmehr zu einer gesteigerten Tumorprogression (Duan et al. 2020).

Bisher wurden bereits einige charakteristische Veränderungen der TMU während der Tumorgenese und -progression nachgewiesen: Die Bildung von hypoxischen Nischen, eine Ansäuerung durch verstärkte Laktat-Exkretion, weitere metabolische Verschiebungen, veränderte physiko-chemische Eigenschaften sowie die Beeinflussung der Aktivität von Immun- und Nervenzellen (Jin and Jin 2020). In den letzten Jahren hat sich die TMU daher als zentrales Thema der Tumorforschung etabliert. In diesem Rahmen werden auch die Auswirkungen bereits zugelassener Arzneistoffe auf die TMU untersucht und ihr Einsatz als aktive Modulatoren der TMU geprüft; unter diesen Arzneistoffen finden sich interessanterweise unter anderem häufig verwendete Medikamente wie Cyclooxygenase-Hemmer, das Antidiabetikum Metformin, HMG-CoA-Reduktase-Hemmer („Statine“) und Beta-Blocker (Jin and Jin 2020).

Während sich viele neuartige Therapieansätze auf die Therapie spezifischer Untertypen verschiedener Neoplasien konzentrieren, könnte die TMU Zielstrukturen enthalten, die einen universelleren Ansatz zur Tumortherapie darstellen. Um systemische Nebenwirkungen dieser Therapieansätze auf weitere Gewebetypen zu vermeiden, ist es essentiell, die Veränderungen der EZM in der Tumorgenese genau zu charakterisieren und die ablaufenden Interaktionen zwischen Tumor- und Stromazellen während der Tumorprogression zu verstehen.

Die Komponenten der Tumormikroumgebung

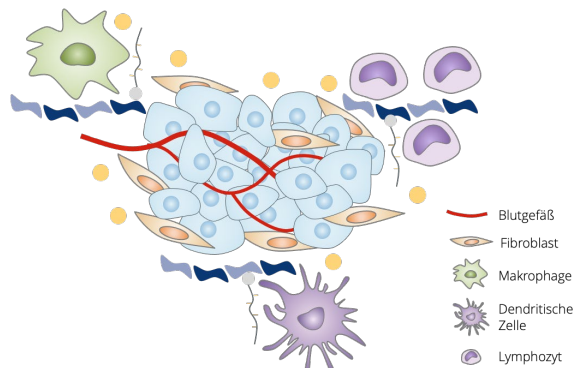


Abb. 2: Komponenten der Tumormikroumgebung.

Vom Autor eigens für dieses Manuskript erstelltes Schema.

### 3. Die extrazelluläre Matrix

Die EZM ist ein hochspezialisiertes, dynamisches und plastisches Gerüst, in das die Zellen der Gewebe eingebettet sind. Die EZM besteht einerseits aus fibrillären Komponenten wie Kollagenen, Fibronectin und Elastin und andererseits aus nicht-fibrillären Molekülen wie Proteoglykanen, Hyaluronsäure und Glykoproteinen. Diese makromolekularen Komponenten bilden komplexe Netzwerke, die durch Bindung an Oberflächenrezeptoren mit den Zellen kommunizieren und intrazelluläre Signaltransduktionskaskaden beeinflussen können. Weitere wichtige Komponenten sind die Matrixabbauenden Enzyme wie Kollagenasen, Hyaluronidasen und Matrix-Metalloproteasen (MMP), die die strukturgebenden Komponenten degradieren können und so hochaktive niedermolekulare Produkte entstehen lassen. Weitere in der Matrix gebundene Proteine wie Wachstumsfaktoren können auf diesem Wege freigesetzt werden und ihrerseits Zellfunktionen modulieren (Theocharis et al. 2019).

Durch diese Dynamik sorgt die EZM einerseits für eine strukturelle Integrität von Geweben und bedingt dadurch deren charakteristische mechanische Eigenschaften; andererseits reguliert sie aber auch die Gewebshomöostase und beeinflusst den Phänotyp, die Proliferation und das Überleben der eingebetteten Zellen sowie deren Antwort auf externe Noxen oder eine Inflammation. Da die EZM sich dynamisch an die aktuellen Zustände und Erfordernisse des Gewebes anpasst und diese mitbedingt, variiert die molekulare Zusammensetzung und Struktur der EZM sowohl stark zwischen den verschiedenen Gewebetypen als auch bei verschiedenen physiologischen und pathophysiologischen Zuständen wie der normalen Gewebereparatur oder der Progression verschiedener Krankheiten. Eine pathologisch veränderte Matrix kann auf diese Weise die Progression einer Erkrankung unterstützen und aufrechterhalten. Dies wurde im Rahmen von genetischen Mutationen von Matrixgenen gezeigt, betrifft aber auch eine Vielzahl wichtiger Systemerkrankungen wie kardiovaskulären und neoplastischen Krankheitsbildern, entzündlichen Erkrankungen wie Osteoarthritis und chronisch-entzündliche Darmerkrankungen, Fibrose und Hautalterung (Theocharis et al. 2019).

Eine Erforschung der zugrundeliegenden Veränderungen in der EZM könnte daher zum tieferen Verständnis vieler Krankheitsbilder beitragen und spezifische Veränderungen aufzeigen, die für Diagnostik und Therapie relevant werden können.

Die Komponenten der extrazellulären Matrix

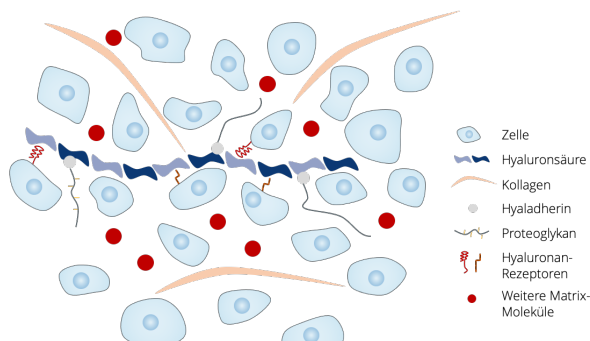


Abb. 3: Komponenten der extrazellulären Matrix

Vom Autor eigens für dieses Manuskript erstelltes Schema.

## 4. Das Hyaluronsäure-System

Die Hyaluronsäure (HA) ist ein langketiges Glykosaminoglykan und neben Kollagen eine Hauptkomponente der EZM. Sie erfüllt wichtige Funktionen bei der Organisation und Hydratisierung des Gewebes und reguliert über die Interaktion mit spezifischen Zelloberflächenrezeptoren wie CD44, RHAMM, LYVE1, HARE oder TLR2/4 sowie diversen Bindungsmolekülen unter anderem zelluläre Funktionen wie Proliferation und Migration (Turley et al. 2002). Die Umsatzrate, die

Konzentration und die molekulare Größe der HA werden durch intrazelluläre Stoffwechselwege reguliert, die sich auf die Aktivität und Expression der HA-Synthasen (HAS1-3) und den Abbau der HA durch Hyaluronidasen (HYAL1-2, PH-20, CEMIP) auswirken.

Von entscheidender Bedeutung für die oft auch gegensätzlichen biologischen Wirkungen der HA ist die Polysaccharid-Kettenlänge bzw. das Molekulargewicht: So vermittelt hochmolekulare HA ( $2 \times 10^3$ - $10^5$  Saccharid-Einheiten, Molekulargewicht  $4 \times 10^2$ - $2 \times 10^4$  kDa) die Hydratisierung von Geweben sowie die Unterdrückung von Angiogenese und Immunreaktionen. HA Fragmente hingegen fördern Neoangiogenese, Inflammation und Zellmigration und unterdrücken die Apoptose von Tumorzellen (Stern et al. 2006, Erickson and Stern 2012).

Trotz des relativ einfachen chemischen Aufbaus vermittelt HA so über verschiedene Molekülgrößen und Gewebekonzentrationen ein breites Spektrum an physiologischen und pathologischen Vorgängen, wie die Morphogenese, Wundheilung und Entzündung. Über analoge Wege fördert ein dysreguliertes HA-System aber auch die Tumorprogression, Neoangiogenese und Chemotherapieresistenz (Caon et al. 2020) oder kann den Umbau von Geweben in Rahmen kardiovaskulärer Erkrankungen negativ beeinflussen (Grandch et al. 2018).

Neuere metabolische Untersuchungen zeigen, dass die Synthese von HA einerseits durch den zellulären Metabolismus reguliert wird (Twarock et al. 2019), andererseits aber auch zelluläre Funktionen über die Reprogrammierung des zellulären Stoffwechsels regulieren kann (Chanmee et al. 2016). Ein aktueller Review gibt einen guten Überblick über die Charakteristika, die Regulation und die Funktionen der HA (Kobayashi et al. 2020).

Mittlerweile ist gut belegt, dass eine HA-reiche Matrix eine spezifische Tumormikroumgebung schafft, die die Angiogenese, Invasion, Metastasierung, Immunevasion und Chemotherapieresistenz von Tumoren begünstigt und damit eine vielversprechende Zielstruktur darstellt (Chanmee et al. 2016). Die Publikationen in dieser Arbeit haben zu diesen Erkenntnissen beigetragen und pharmakologische Therapieoptionen aufgezeigt.

### Das Hyaluronsäure-System

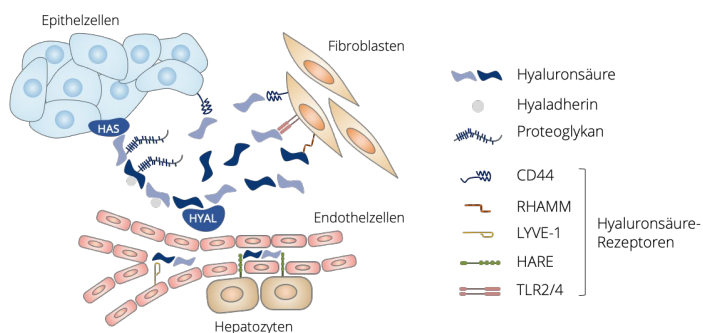


Abb. 4: Komponenten des Hyaluronsäuresystems

Vom Autor eigens für dieses Manuskript erstelltes Schema.

## B. Zielsetzung

Die im Folgenden beschriebenen Projekte hatten zum Ziel, die Beteiligung einer HA-reichen Tumormikroumgebung an der Tumorprogression zu untersuchen und pharmakologische Angriffspunkte in diesem System zu identifizieren. Dies erfolgte am Modell des ösophagealen Plattenepithelkarzinoms (ESCC).

Im Speziellen wurden in den hier vorgestellten Publikationen folgende Ziele verfolgt:

- I. **Charakterisierung der Auswirkungen** einer HA-reichen Matrix auf die Tumorprogression ösophagealer Plattenepithelkarzinomzellen
- II. **Identifizierung von Signalwegen**, die eine **transkriptionelle Regulation** der HA-Synthasen, Hyaluronidasen und HA-Rezeptoren bewirken und dadurch potentielle pharmakologische Angriffspunkte zur Modulation des HA-Systems darstellen könnten
- III. **Untersuchung von metabolischen Regulationsmechanismen** der HA-Synthese und deren Beeinflussung durch Pharmaka oder durch eine diabetische Stoffwechsellage

## C. Zusammenfassung relevanter Publikationen

Die Besprechung der folgenden Publikationen erfolgt nicht chronologisch nach Veröffentlichungsdatum, sondern entsprechend der im vorausgegangenen Abschnitt dargestellten Zielsetzungen. Die Publikationen im ersten Abschnitt fokussieren sich auf die Charakterisierung des HA-Systems in ösophagealen Plattenepithelkarzinomzellen, um dessen Stellenwert für die Tumorprogression zu definieren. In den folgenden beiden Abschnitten erfolgt dann die Analyse der Regulationsmöglichkeiten durch transkriptionelle und metabolische Faktoren. In diesem Zusammenhang werden fünf Publikationen in Erstautorschaft genauer erläutert. Zusätzlich wird kurz auf zwei thematisch passende Veröffentlichungen in Koautorenschaft eingegangen.

Eine Übersicht über die in diesen Projekten untersuchten Prozesse und die eingesetzten Pharmaka ist in **Abb. 5** dargestellt.

### I. Hyaluronsäure-Effekte im Tumormikromilieu

- a. In *Twarock et al. JBC 2010* wurde der **Einfluss von HA auf die Stabilisierung von Zell-Matrix-Kontakten** untersucht. Der experimentell induzierte Verlust von HA-Zell-Interaktionen destabilisierte fokale Adhäsionen über eine gesteigerte Degradation der fokalen Adhäsionskinase (FAK) und führte so zu einem Verlust von Filopodien. Dieser Effekt war über RHAMM vermittelt und ging *in vitro* mit einer verringerten Tumorzellproliferation einher.
- b. In *Twarock et al. Mol Cancer 2011* wurde ein **Zusammenhang der HAS-Expression mit der Expression des epithelialen Wachstumsfaktor-Rezeptors (EGFR)** in humanen Tumorschnitten und eine regulatorische Verbindung dieser beiden Proteine *in vitro* nachgewiesen. Im Mausmodell wurde der **Anteil der Tumor- und Stromaanteile an der HA-Synthese im Tumorgewebe** untersucht und die Auswirkung einer Inhibition der HA-Synthese mittels oral verabreichten **4-MU** oder tumorzellspezifischer HAS3-shRNA auf die Tumorprogression *in vivo* quantifiziert.
- c. In *Kretschmer et al. BJP 2015* wurde der **synergistische Effekt einer gleichzeitigen Hemmung des EGFR-Signalwegs** mittels **Erlotinib** und der **HA-Synthese** mittels **4-MU** oder shRNA gegen

CD44 und RHAMM auf die Proliferation und Migration von verschiedenen ESCC-Zelllinien und das Wachstum von multizellulären Tumor-Sphäroiden *in vitro* untersucht.

## **II. Transkriptionelle Regulation des Hyaluronsäuresystems**

- a. In Twarock et al. *BJP* 2009 wurde der Einfluss des **Prostaglandin-Rezeptor-Signalwegs** auf die **Expression der HA-Synthasen** in verschiedenen ESCC-Zelllinien untersucht. In den untersuchten Zelllinien konnte überraschenderweise im Gegensatz zu Untersuchungen anderer Zellarten eine Entkopplung dieser beiden Signalwege beobachtet werden.
- b. In Kretschmer et al. *JBC* 2016 wurden die **parakrinen Effekte von ESCC auf Fibroblasten** analysiert. Eine direkte Interaktion zwischen den beiden Zellarten stimulierte über eine durch Cadherin gesteuerte Signalkaskade die HAS2-Transkription. Zusätzlich zeigte sich unter der direkten Co-Kultur eine modulierte Chemokin- und  $\alpha$ -SMC-Expression in den Fibroblasten sowie eine HA-vermittelte erhöhte Adhäsion von CD4 $^{+}$ -Zellen an das Tumorgewebe.

## **III. Metabolische Regulation des Hyaluronsäuresystems**

- a. In Twarock et al. *Int J Cancer* 2017 wurden die **Auswirkungen einer diabetischen Stoffwechsellage** – Hyperglykämie und gestörte Insulin-Signaltransduktion – auf die HA-Synthese und die dadurch beeinflusste Tumorprogression untersucht. In einem Nacktmausmodell konnte *in vivo* beobachtet werden, dass eine Stoffwechsellage entsprechend einem Diabetes mellitus Typ I eine vermehrte Bildung von tumorassozierter HA-Matrix bewirkte, was wiederum die Tumorprogression und Neoangiogenese beschleunigte. Dieser Prozess wurde durch die orale Gabe von **4-MU** effektiv abgeschwächt. Die Aufklärung der zugrundeliegenden Mechanismen erfolgte in ESCC-Zellen *in vitro*. Hier wurde eine von der **Glucose-Konzentration abhängige Steigerung der HA-Synthese** festgestellt. Im Gegensatz dazu **verringerte** eine Zugabe von **Insulin die HA-Synthese**. Dieser Effekt konnte durch die gezielte Ausschaltung von Genen, die direkt oder indirekt die Glykolyse steigern, umgekehrt werden. Daraus konnte geschlossen werden, dass Insulin durch Steigerung der Glykolyse der HA-Synthese die Substrate entziehen kann. Die gesteigerte HA-Synthese unter diabetischen Bedingungen förderte *in vitro* Invasion, Verankerungsunabhängiges Wachstum und Adhäsion von ESCC an Endothelzellen.
- b. In Twarock et al. *BJP* 2019 wurden die **Wirkungen des Pyruvat-Dehydrogenase-Kinase-Inhibitors Dichloracetat (DCA)** auf die HA-Synthese untersucht und die gleichzeitige Hemmung der anti-apoptotischen HA-Matrix durch **4-MU als synergistisches Wirkprinzip getestet**. In Zellkulturversuchen mit ESCC-Zellen zeigte sich *in vitro* eine Zunahme der HA-Synthese unter **DCA**-Behandlung. Diese Beobachtung konnte in weiteren Versuchen unter anderem auf eine gesteigerte Acetyl-CoA-Konzentration unter **DCA** zurückgeführt werden, der ein Anstieg des Metaboliten UDP-N-Acetylglucosamin (UDP-GlcNAc) folgte. Dieser dient als Substrat für HAS-Enzyme und kann durch den Prozess der O-GlcNAcylierung die Aktivität von Proteinen wie der HASen steigern. Die synergistische tumorhemmende Wirkung der Kombination von **DCA** und **4-MU** wurde in 2D- und 3D-Zellkulturen und in einem Nacktmaus-Tumor-Xenograft-Regressionsmodell demonstriert.

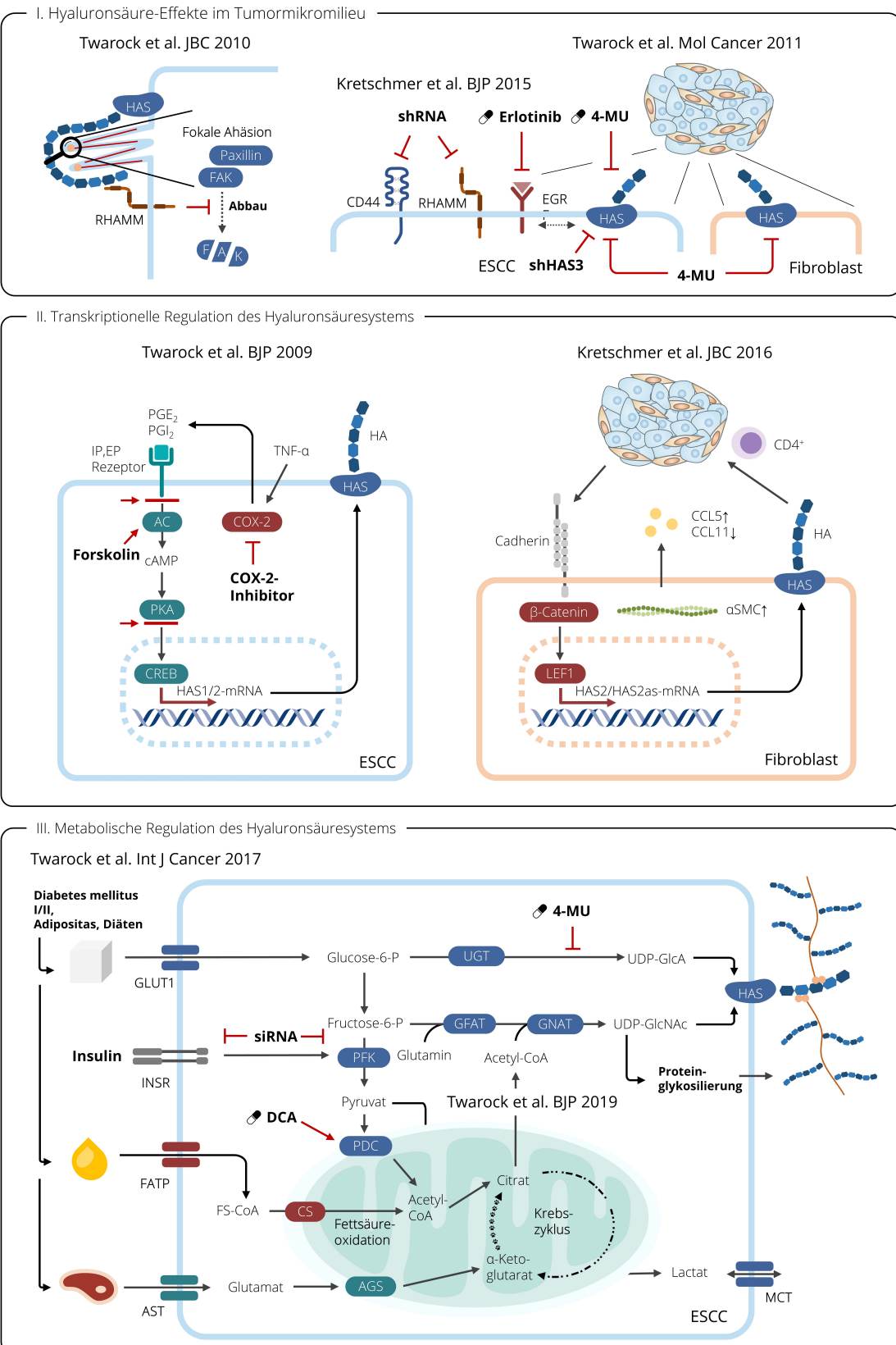


**Abb. 5: Effekte der Hyaluronsäure-Matrix auf die Tumorprogression von ESCC.**

Beschreibung siehe Text. AGS: Aspartat-Glutamat-Shuttle, AST: Aminosäure-Transporter, CS: Carnitin-Shuttle, FATP: Fettsäure-Transporter, GFAT; GNAT: GLUT1: Glucose-Transporter 1, HA: Hyaluronsäure, INSR: Insulin-Rezeptor, MCT: Monocarboxylat-Transporter 1, PDC: Pyruvat-Dehydrogenase-Komplex, UDP-GlcA: Uridindiphosphat-Glucuronsäure, UDP-GlcNAc: Uridindiphosphat-N-Acetylglucosamin. Vom Autor eigens für dieses Manuskript erstelltes Schema.

## I. Hyaluronsäure-Effekte im Tumormikromilieu

### 1. Einfluss der Hyaluronsäure auf Zell-Matrix-Kontakte und die Tumorzellproliferation *in vitro*

**Originalarbeit:** Twarock, S., Tammi, M. I., Savani, R. C. and Fischer, J. W. (2010). Hyaluronan stabilizes focal adhesions, filopodia, and the proliferative phenotype in esophageal squamous carcinoma cells. *J Biol Chem* 285(30): 23276-23284 (Twarock et al. 2010).

**Copyright:** Diese Veröffentlichung wurde unter den Bedingungen einer Creative Commons CC-BY-4.0-Lizenz (open access) beim Verlag Elsevier veröffentlicht. Diese erlaubt die freie Verwendung aller Inhalte unter Angabe der Originalquelle.

In dieser Veröffentlichung wurde die Rolle der HA in der Stabilisierung der perizellulären Matrix und zellulärer Protrusionen mit Kontakt zur Matrix untersucht. Dabei wurden verschiedene Methoden zur Reduktion der HA-Interaktion mit den Tumorzellen eingesetzt:

- Pharmakologische Inhibition der HA-Synthese durch den niedermolekularen HA-Synthese-Inhibitor **4-Methylumbelliferon (4-MU)**
- Interferenz-RNA gegen **HA-Synthase-Isoformen** (HAS2 und HAS3)
- Verdrängung der perizellulären HA durch das Peptid **Pep-1**
- Abbau der HA über exogen zugegebene **Hyaluronidase** und
- siRNA-vermittelter Knockdown der **HA-Rezeptoren CD44 und RHAMM**.

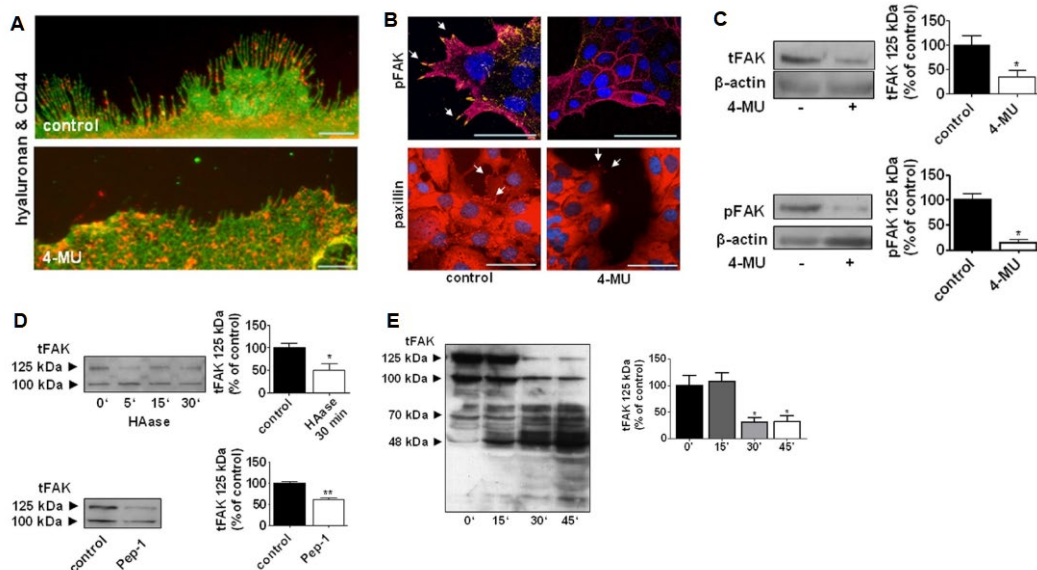


**Abb. 6: Verringern der Anzahl HA-assozierter Filopodien, Auflösung von fokalen Adhäsionskomplexen und Degradation der fokalen Adhäsionskinase unter HA-Synthese-Inhibition durch 4-MU.**

A Die Assoziation von HA mit Filopodien wurde in fixierten OSC1-Zellen durch Immunfärbung von CD44 (grün) und affinitätshistochimischer Färbung von HA (rot) verifiziert. Repräsentative Bilder, Skalenbalken 5 μm. Die Inhibition der HA-Synthese durch 4-MU (0,3 mM, 24 h) reduzierte die HA-Menge und Filopodien-Anzahl. B Die Immunfärbungen von pFAK (orange, Pfeile) und CD44 (magenta) sowie von Paxillin (rot, Pfeile) zeigten eine Abnahme fokaler Adhäsionen als Reaktion auf die Behandlung mit 4-MU. Repräsentative Bilder, Skalenbalken 50 μm. C Immunoblots zeigten eine Abnahme von Gesamt-FAK (tFAK) und phosphorylierter FAK (pFAK) unter 4-MU (0,3 mM, 24 h). D Sowohl der Verdau von perizellulärer HA mit *Streptomyces* Hyaluronidase (HAase, 5 U/ml, 5-30 min, oberes Panel) im Vergleich zur unbehandelten Kontrolle als auch die Behandlung mit dem HA-verdrängenden Peptid Pep-1 (500 g/ml, 24 h, unteres Panel) im Vergleich zum scrambled Peptid (Kontrolle) führten zu einer ausgeprägten tFAK-Spaltung. E Die Degradation der FAK begann zwischen 15 und 30 min nach der Applikation von 4-MU und erreichte nach 45 min ein Maximum. Verwendet wurde ein Antikörper gegen den C-Terminus von FAK. C-E Dargestellt sind repräsentative Immunoblots und deren quantitative Analyse nach densitometrischem Scannen. Mittelwert ± SEM, n=3, \*p<0,05, \*\*p<0,01 gegenüber der jeweiligen Kontrolle. Veröffentlicht unter einer CC-BY-4.0-Lizenz beim Verlag Elsevier, die eine freie Verwendung unter Angabe der Quelle erlaubt.

Als Ergebnis zeigte sich, dass HA eine stabilisierende Wirkung auf Zell-Matrix-Interaktionen über fokale Adhäsionen aufweist. Entsprechend kam es unter einer HA-Depletion mittels **4-MU** zu einer Rückbildung zellulärer Filopodien (**Abb. 6A**), die auf eine Abnahme von Komponenten der fokalen Adhäsionen — die phosphorylierte fokale Adhäsionskinase (pFAK) und Paxillin — zurückgeführt werden konnte (**Abb. 6B**). Immunoblots zeigten zudem, dass nicht nur die phosphorylierte Form der fokalen Adhäsionskinase abnahm, sondern auch die unphosphorylierte Proteinmenge sank (**Abb. 6C**). Dieser Effekt trat auch unter dem Einsatz von Hyaluronidase und Pep-1 auf (**Abb. 6D**) und konnte schließlich auf die Degradation der FAK unter diesen Bedingungen zurückgeführt werden (**Abb. 6E**). Dieser Mechanismus wurde in weiteren ösophagealen Plattenepithelkarzinom-Zelllinien bestätigt. In der Folge verringerte sich auch die Migrations- und Proliferations-Aktivität der Zellen (hier nicht gezeigt).

Eine detaillierte Untersuchung der beteiligten Proteine des HA-Systems zeigte, dass ein transkriptioneller Knockdown beider relevanter HA-Synthase-Isoformen (HAS2 und HAS3) diesen Degradation-Prozesses einleiten konnte, HAS3 als Hauptisoform aber einen größeren Anteil an diesem Prozess hatte (**Abb. 7A**). Analog folgte im ähnlichen Verhältnis eine Degradation der FAK (**Abb. 7B**). Sowohl unter 4-MU als auch unter HAS2/3-Silencing kam es zu einer Abnahme der ERK- und AKT-Phosphorylierung sowie zu einer Erniedrigung der Proliferation und Migration (Daten hier nicht gezeigt).

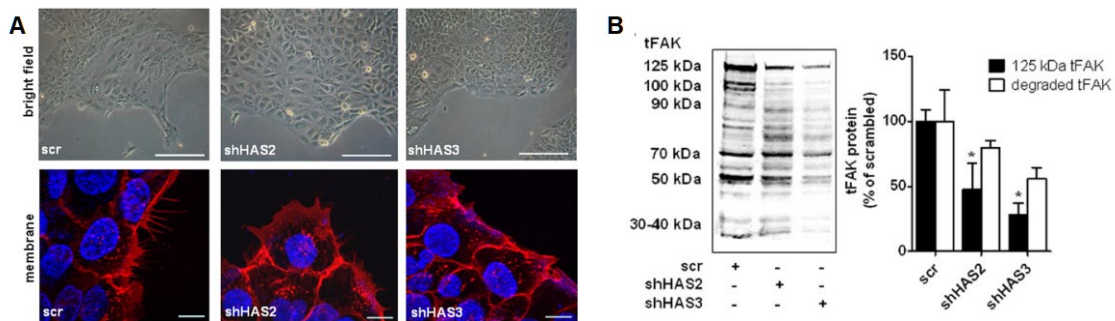


**Abb. 7:** Nachbildung der Effekte von 4-MU auf Zellmorphologie, Filopodien und FAK-Spaltung durch einen lentiviralen Knockdown von HAS3 und HAS2.

**A Oberes Panel** Die Lichtmikroskopie lebender Zellen zeigte eine Veränderung der Zellform nach lentiviraler Infektion mit shHAS3 und in geringerem Ausmaß mit shHAS2. Diese Formveränderung wies eine starke Ähnlichkeit zu denjenigen auf, die nach der Behandlung mit 4-MU beobachtet wurde. **Unteres Panel** Die Färbung der fixierten Zellen mit dem Membran-Marker WGA Alexa Fluor 555 Konjugat zeigte eine Abnahme der Anzahl und Größe der Filopodien. Auch diese Effekte waren nach Knockdown von HAS3 am stärksten ausgeprägt, traten aber auch beim Knockdown von HAS2 auf. Die Effekte des HAS-Knockdowns wurden 5 Tage nach der Infektion ausgewertet und eine nicht gegen humane Gene gerichtete shRNA (scr, *scrambled*) wurde als Kontrolle verwendet. Abgebildet sind repräsentative Bilder von n=3 Experimenten, Skalenbalken 500 µm. **B** Analog zu diesen Beobachtungen steigerte shHAS3 die Spaltung von FAK stärker als shHAS2. Nachweis durch Immunoblot, quantitative Analyse von 125-kDa FAK (tFAK) und von degradierten FAK-Fragmenten nach Normalisierung auf Tubulin und auf *scrambled* Kontrollen (scr). n=3, Mittelwert ± SEM, \*p<0,05 versus *scrambled* shRNA. Veröffentlicht unter einer CC-BY-4.0-Lizenz beim Verlag Elsevier, die eine freie Verwendung unter Angabe der Quelle erlaubt.

In einem letzten Schritt wurde untersucht, ob die bisher beobachteten Effekte mechanistisch über die beiden HA-Rezeptoren CD44 und RHAMM vermittelt werden. Die Immunfärbung zeigte, dass CD44 in den OSC1-Kulturen stark und gleichmäßig exprimiert wurde. Die Behandlung mit 4-MU führte zu einer randständigen Betonung der Färbung (**Abb. 8A**). RHAMM wurde ebenfalls exprimiert, aber seine Expression schien durch die Behandlung mit 4-MU nicht beeinflusst zu werden (**Abb. 8B**). Zur Aufklärung der Beteiligung der HA-Rezeptoren an der Filopodienintegrität und Zellform wurden ein lentiviralem vermittelten Knockdown von CD44 und RHAMM mit shRNA und eine Färbung der Membran mit WGA Alexa Fluor 555 Konjugat verwendet. Im Vergleich zur *scrambled control* shRNA zeigte sich, dass shCD44 keinen Effekt auf die Filopodienstabilität hatte (**Abb. 8C**), während shRHAMM den Verlust von Filopodien induzierte (**Abb. 8D**). Analog zu diesen Beobachtungen steigerte nur shRHAMM die Spaltung von FAK (**Abb. 8E**). Die zelluläre Proliferation und Migration wurden hingegen von beiden untersuchten Rezeptoren beeinflusst (Daten hier nicht gezeigt).

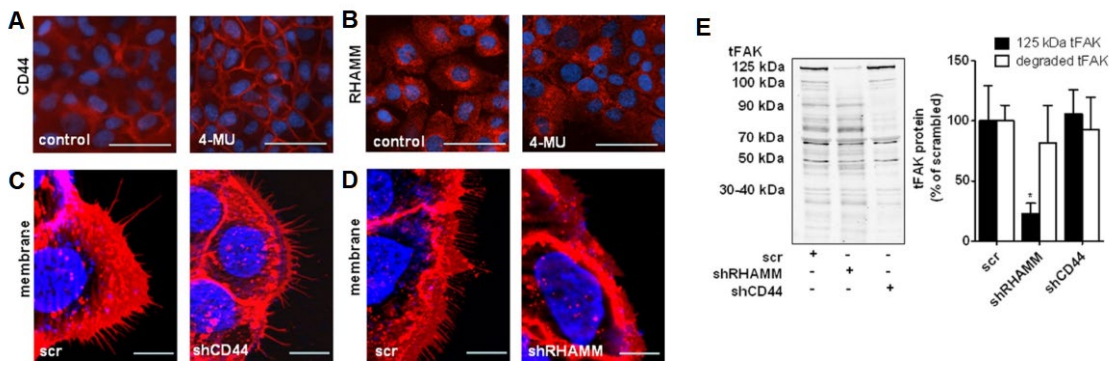


**Abb. 8: Abhängigkeit der Filopodien-Abnahme und FAK-Degradation von HA-Rezeptoren.**

**A** Die immunzytologische Färbung auf CD44 (rot) und Kerne (blau) in OSC1-Kulturen ± 300 µM 4-MU zeigte eine Zunahme der randständigen CD44-Expression unter 4-MU. **B** Die immunzytologische Färbung auf RHAMM (rot) und Kerne (blau) in OSC1-Kulturen ± 300 µM 4-MU zeigte keine Unterschiede zwischen den beiden Konditionen. **A-B** Repräsentative Bilder, Maßstabsbalken 50 µm. Die Überprüfung der Filopodienstabilität erfolgte durch einen lentiviralen vermittelten Knockdown von **C** CD44 und **D** RHAMM mit shRNA. Die Färbung der Membran mit WGA Alexa Fluor 555 Konjugat (rot) und Kerne (blau) im Vergleich zu *scrambled* control shRNA (scr) zeigte, dass nur RHAMM einen Effekt auf die Filopodienstabilität hatte. Die Effekte des RHAMM- und CD44-Knockdowns wurden 5 Tage nach der Infektion gemessen. Dargestellt sind repräsentative Bilder von n=3 Experimenten, Skalenbalken 20 µm. **E** Nachweis der Spaltung von FAK durch Immunoblot, quantitative Analyse von 125-kDa FAK (tFAK) und degradierten FAK-Fragmenten nach Normalisierung auf Tubulin und auf *scrambled* (scr) Kontrollen. n=3, Mittelwert ± SEM, \*p<0,05 versus *scrambled* shRNA. Veröffentlicht unter einer CC-BY-4.0-Lizenz beim Verlag Elsevier, die eine freie Verwendung unter Angabe der Quelle erlaubt.

Zusammenfassend wurde in dieser Arbeit ein neuer Mechanismus identifiziert, über den HA Zell-Matrix-Kontakte in Form von fokalen Adhäsionen stabilisierte und die Proliferation und Migration von Tumorzellen unterstützte. Die Abhängigkeit der unter 4-MU beobachteten Wirkungen von dessen hemmenden Effekt auf das HA-System wurde durch shRNA-Experimente und die Nutzung weiterer HA-System-inhibierender Prinzipien bestätigt. Mechanistisch wurde eine Beteiligung beider HA-Synthase-Isoformen (HAS2 und 3) sowie des HA-Rezeptors RHAMM identifiziert. RHAMM könnte daher eine interessante zukünftige Zielstruktur zur Therapie des Ösophaguskarzinoms darstellen.

## 2. Regulation der HA-Synthese durch EGF, HA-Verteilung zwischen Tumor und Stroma und Auswirkung der HA-Inhibition auf die Tumorprogression *in vivo*

**Originalarbeit:** Twarock, S., Freudenberger, T., Poscher, E., Dai, G., Jannasch, K., Dullin, C., Alves, F., Prenzel, K., Knoefel, W. T., Stoeklein, N. H., Savani, R. C., Homey, B. and Fischer, J. W. (2011). Inhibition of oesophageal squamous cell carcinoma progression by *in vivo* targeting of hyaluronan synthesis. Mol Cancer 10: 30 (Twarock et al. 2011).

**Copyright:** Diese Veröffentlichung wurde unter den Bedingungen einer Creative Commons CC-BY-2.0-Lizenz (open access) beim Verlag BMC-Springer veröffentlicht. Diese erlaubt die freie Verwendung aller Inhalte unter Angabe der Originalquelle.

Die Ziele dieser Arbeit waren, die Expression und Regulation der HAS-Isoformen in humanen ESCC *in vitro* und *in vivo* genauer zu charakterisieren mit speziellem Fokus auf den Anteil von Tumor- und Stromagewebe.

Im ersten Teil dieser Arbeit wurde ein Zusammenhang zwischen dem epithelialen Wachstumsfaktor-Rezeptor (EGFR) und HAS3 in humanen ESCC Biopsien und in der Zellkultur detektiert und durch den Einsatz von zwei pharmakologischen Wirkstoffen bestätigt.

Mittels qPCR wurde dafür die Genexpression der HAS3 in humanen Biopsien aus gesunder Mukosa und Plattenepithelkarzinomen des Ösophagus verglichen. Dieser Vergleich ergab eine signifikant höhere Expression der enzymatisch aktiven Variante 1 der HAS3 (HAS3v1) in SCC (**Abb. 9A**). Eine Stratifizierung nach TNM-Klassifikation zeigte darüber hinaus eine Abnahme der Varianz bei größerer Tumorausdehnung, klassifiziert als T2-T4 (**Abb. 9B**).

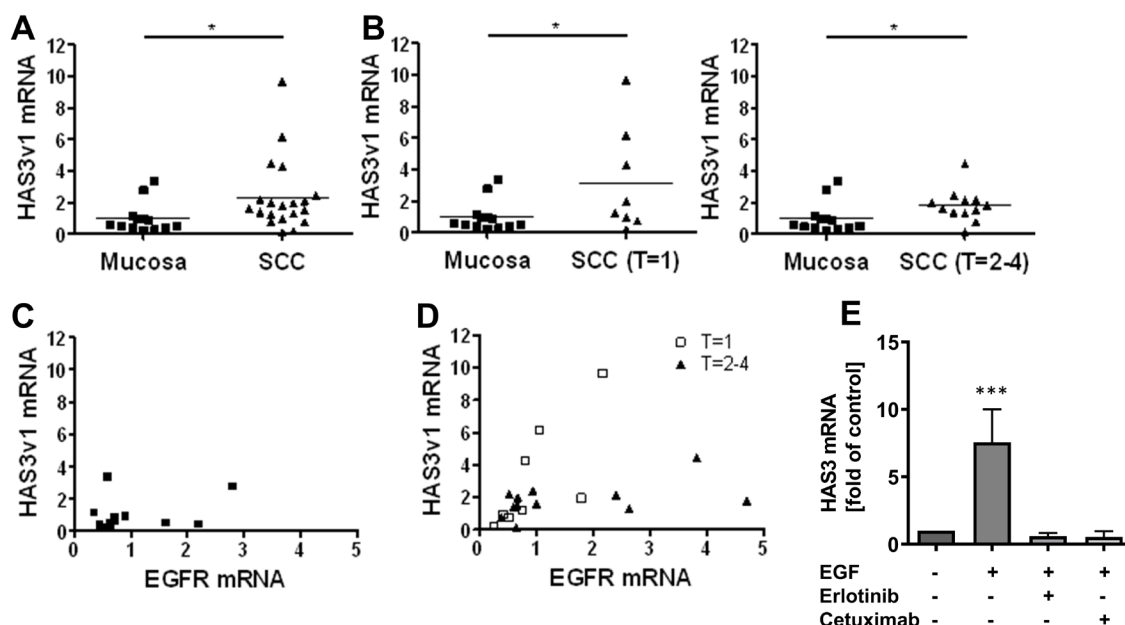


**Abb. 9:** Korrelation der HAS3-Genexpression mit der Tumogröße nach TNM-Klassifikation und der EGFR-Expression in Schnitten von gesunder Mukosa und humanen ESCC.

qPCR auf HAS3-mRNA aus Biopsieproben von **A** normaler Mukosa (n=13) und **B** humanem ESCC differenziert nach TNM-Staging (Tumogröße T, Lymphknotenbefall N und Vorhandensein von Metastasen M) (n = 20), Mittelwert  $\pm$  SEM, \*p < 0,05. Die EGFR-Expression wurde in den gleichen Biopsieproben wie in **A** bestimmt und mit der HAS3-Expression in **C** normaler Mukosa und in **D** ESCC korreliert. **E** Stimulation der HAS3-mRNA-Expression durch EGF in der humanen ESCC-Zelllinie OSC1. Dieser Effekt wurde durch den Einsatz des EGFR-Tyrosinkinase Inhibitors Erlotinib und des Anti-EGFR-Antikörpers Cetuximab aufgehoben. Mittelwerte  $\pm$  SEM; n = 3-5; \*\*\*p < 0,001. Veröffentlicht unter einer CC-BY-2.0-Lizenz beim Verlag BMC-Springer, die eine freie Verwendung unter Angabe der Quelle erlaubt.

Weitere Untersuchungen ergaben, dass die mRNA-Expression von HAS3 positiv mit der mRNA-Expression des EGF-Rezeptors (HER1, ErbB1) in Tumorzellen korrelierte, während in normaler Mukosa keine Korrelation existierte (**Abb. 9CD**). Interessanterweise zeigten die Tumorproben des Grades T1 eine steilere Korrelation als die des Grades T2-4. Dies könnte auf eine stärkere Abhängigkeit der frühen Tumorgrade vom EGF-Signalweg zur Aufrechterhaltung der HAS3-Aktivität hinweisen. In der Zellkultur wurde der Stellenwert dieser beobachteten Korrelation mechanistisch weiter analysiert. In Übereinstimmung mit den vorherigen Befunden führte die Aktivierung des EGF-Rezeptors im Zellkulturmodell zur Induktion der HAS3-mRNA-Expression in ESCC-Zellen. Durch den Einsatz pharmakologischer, für den Einsatz am Menschen zugelassener, Inhibitoren des EGFR-Signalweges konnte im Anschluss dieser Befund weiter gestützt werden: sowohl der EGF-Rezeptor-Tyrosinkinase-Inhibitor **Erlotinib** als auch der monoklonalen Anti-EGFR-Antikörper **Cetuximab** senkten die EGFR-induzierte Steigerung der HAS3-Expression wieder auf das Ausgangsniveau ab (**Abb. 9E**).

Im zweiten Teil dieser Arbeit wurden die Erkenntnisse aus den *in vitro*-Untersuchungen im Kapitel I.1 zur Beteiligung der HA an einem aktivierten Phänotyp der ESCC-Tumorzellen in einem Nacktmausmodell-Tumor-Xenograft-Modell *in vivo* untersucht. Ziel war es, die Auswirkungen einer systemischen pharmakologischen HA-Synthese-Inhibition mittels **4-MU** auf die Tumor- und Stroma-Matrix zu untersuchen und einen Vergleich zu einem lentiviralen Knockdown von HAS3 in den Tumorzellen mittels einer small-hairpin-Interferenz RNA (shHAS3) zu ziehen. Auf diese Weise sollte der Anteil von Tumor- und Stromazellen an der HA-Produktion im Tumorgewebe bestimmt werden.

Als Ergebnis zeigte sich, dass die Inhibition der Tumorzell-ständigen HA-Produktion ausreichte, um die Effekte der systemischen Inhibition der HA-Synthese nachzubilden. Sowohl Tumorwachstum als auch morphologische Veränderungen ähnelten stark zwischen der 4-MU-behandelten Gruppe (**Abb. 10**) und der shHAS3-Gruppe (**Abb. 11**). Zudem konnte in beiden Gruppen unter der Behandlung eine Abnahme proliferierender Zellkerne detektiert werden; die proliferierenden Zellen beschränkten sich jeweils auf die Grenzfläche zwischen Tumorzellen und Stromazellen (**Abb. 12**).

Die in dieser Arbeit identifizierte Regulation der HA-Synthese durch EGF legte die Basis für weitere Experimente zum Synergismus einer EGFR- und HA-Synthese-Inhibition (siehe Kapitel I.3). Zudem zeigte diese Arbeit die Wirksamkeit einer pharmakologischen HA-Inhibition durch **4-MU** auf die Tumorprogression *in vivo* und charakterisierte die HA-Verteilung zwischen Tumor und Stroma während einer solchen Behandlung.

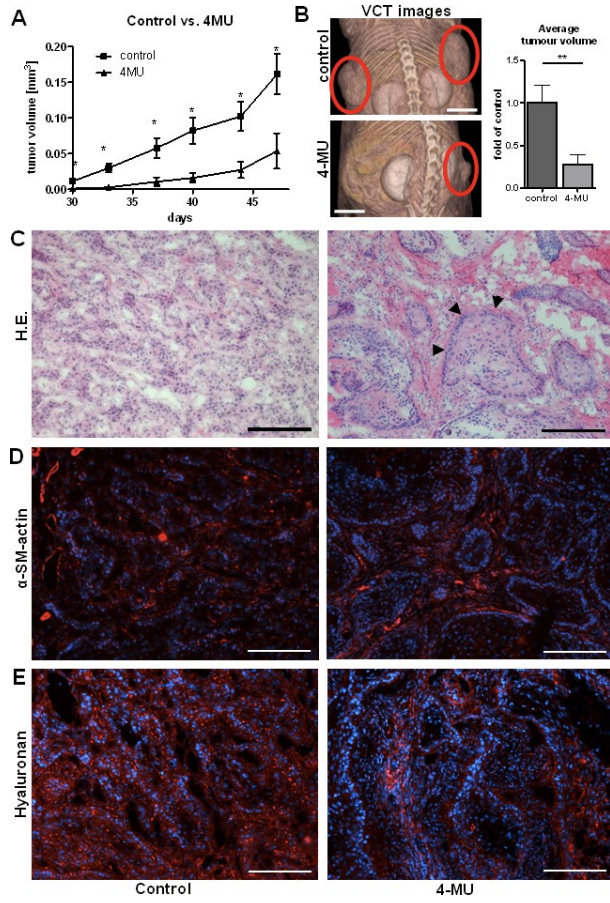


**Abb. 10:** Hemmung des Tumorwachstums von xenotransplantierten OSC1-Zellen in Nacktmäusen durch Behandlung mit 4-MU.

Nacktmäusen wurden  $10^6$  OSC1-Zellen subkutan injiziert und das Tumorwachstum wurde über 47 Tage beobachtet. **A** Tumorvolumen, bestimmt durch Schieblehren-Messungen; Mittelwert  $\pm$  SEM, n=21 (Kontrolle), n=17 (4-MU); \*p < 0,05. **B** Repräsentative fpVCT-Bilder von Kontrollmäusen und 4-MU-behandelten Mäusen nach 47 Tagen. Skalenbalken 1 cm. Die durchschnittlichen Tumorvolumina nach Tötung der Mäuse am Ende des Experiments, gemessen mittels fpVCT, zeigten eine signifikante Reduktion des Tumorvolumens in der 4-MU-Gruppe. **C** Mit H&E gefärbte Kryo-Schnitte zeigten einen charakteristischen Tumor-Phänotyp in den mit 4-MU behandelten Mäusen. Dieser Phänotyp war gekennzeichnet durch größere Tumorzellcluster mit einer zellreichen Randregion (Pfeile) und ausgeprägtem Tumorstroma. **D** Stromale Fibroblasten wurden auf *alpha-smooth muscle actin* gefärbt (rot). **E** Die HA-Färbung (rot) war sowohl mit Tumorzellen als auch mit Stromagewebe assoziiert und wurde durch die Behandlung mit 4-MU deutlich reduziert. **C-E** Repräsentative Bilder von n = 6 (Kontrolle) und n = 7 (shHAS3) Experimenten, Skalenbalken 200  $\mu\text{m}$ . Veröffentlicht unter einer CC-BY-2.0-Lizenz beim Verlag BMC-Springer, die eine freie Verwendung unter Angabe der Quelle erlaubt.

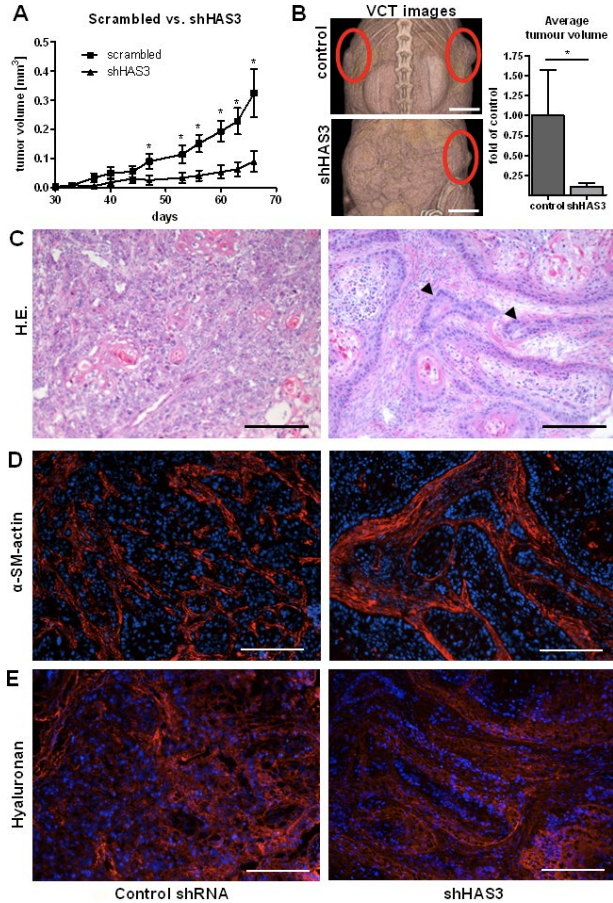


**Abb. 11:** Hemmung des Tumorwachstums von xenotransplantierten OSC1-Zellen durch lenti-viralen Knockdown von HAS3.

Nacktmäuse erhielten subkutane Injektionen von  $10^6$  OSC1-Zellen, die *in vitro* mit einem Lentivirus transduziert worden waren, das entweder scrambled shRNA (Kontrolle) oder shHAS3 enthielt. **A** Das Tumorwachstum wurde durch Schieblehren-Messungen über 65 Tage ermittelt. Mittelwert  $\pm$  SEM, n = 6 (Kontrolle), n=7 (shHAS3); \*p < 0,05. **B** Repräsentative fpVCT-Bilder von Mäusen nach 65 Tagen, Skalenbalken 1 cm. Die durchschnittlichen Tumorvolumina nach der Tötung der Mäuse am Ende des Experiments, gemessen mittels fpVCT, zeigten ebenfalls eine signifikante Reduktion des Tumorvolumens in der shHAS3-Gruppe. **C** Die H&E-Färbung zeigte Veränderungen in der Tumormorphologie, die denen nach 4-MU sehr ähnlich waren (vgl. Abb. links). **D** Das Tumorstroma wurde durch Färbung von *alpha-smooth muscle actin* (rot) sichtbar gemacht. **E** Die Xenotransplantation von shHAS3-Tumorzellen verursachte eine Umverteilung der HA-Färbung, die spezifisch in der äußeren Schicht der Tumorzellcluster lokalisiert war. **C-E** Dargestellt sind repräsentative Bilder von n = 6 (Kontrolle) und n = 7 (shHAS3) Experimenten, Skalenbalken, 200  $\mu\text{m}$ . Veröffentlicht unter einer CC-BY-2.0-Lizenz beim Verlag BMC-Springer, die eine freie Verwendung unter Angabe der Quelle erlaubt.

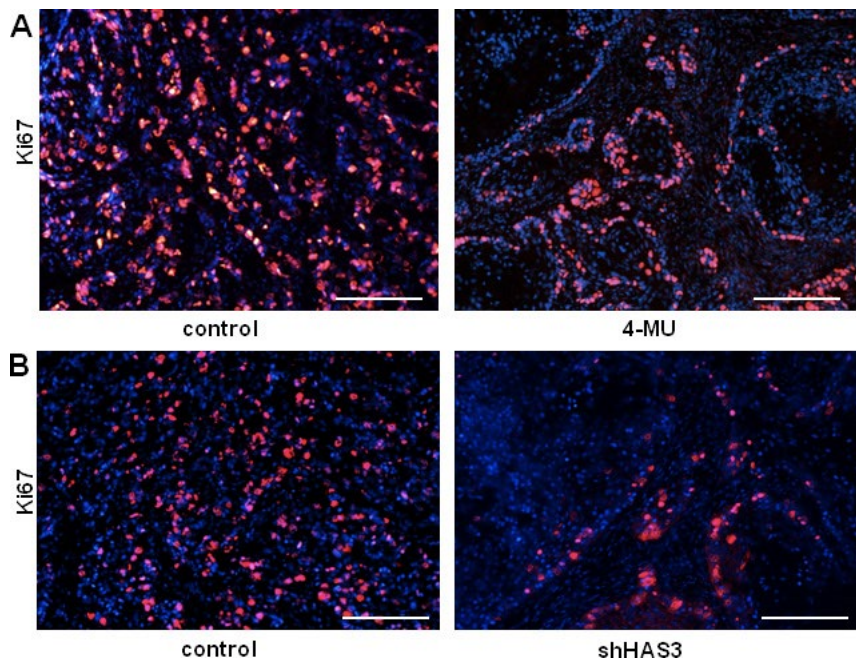


**Abb. 12: Auswirkungen von 4-MU und tumorzellspezifischem HAS3-Knockdown auf die Proliferationsrate in OSC1-Xenografts.**

Die Rate proliferierender Zellen in Tumorschnitten aus dem Nacktmaus-Xenograft-Modell wurde durch die immunzytologische Färbung von humanem Ki67 (rot) und Kernen (blau) bestimmt. **A** Die Behandlung mit 4-MU reduzierte den Anteil proliferierender Zellen; die Verteilung beschränkte sich auf die Grenzfläche zwischen Tumorzellen und Stromazellen. **B** Die Ki67-Färbung war in den mit shHAS3 transduzierten Tumorzellen deutlich reduziert. Auch hier beschränkten sich die proliferierenden Zellen auf die Randbereiche der Tumorzellinseln. Skalenbalken 200 µm. Gezeigt sind repräsentative Bilder von n = 6 (Kontrolle) und n = 7 (shHAS3) Experimenten. Veröffentlicht unter einer CC-BY-2.0-Lizenz beim Verlag BMC-Springer, die eine freie Verwendung unter Angabe der Quelle erlaubt.

### 3. Synergistische Reduktion der Proliferation und Migration von ESCC-Zellen durch gleichzeitige Inhibition des EGF-Rezeptor-Signalwegs und der Hyaluronsäure-Synthese

Originalarbeit: Kretschmer, I., Freudenberger, T., Twarock, S. and Fischer, J. W. (2015). Synergistic effect of targeting the epidermal growth factor receptor and hyaluronan synthesis in oesophageal squamous cell carcinoma cells. Br J Pharmacol (Kretschmer et al. 2015).

In dieser Arbeit wurde eine pharmakologische Kombinationstherapie aus dem EGFR-Tyrosinkinase-Inhibitor (TKI) Erlotinib und dem niedermolekularen HA-Synthese-Inhibitor 4-MU untersucht. Die Spezifität der Wirkung von 4-MU auf das HA-System wurde über eine genetische Ausschaltung der HA-Rezeptoren CD44 und RHAMM bestätigt.

Die Kombinationstherapie hemmte synergistisch die Proliferation und Migration von verschiedenen ESCC-Zelllinien und das Wachstum von multizellulären Tumor-Sphäroiden. In weiteren Experimenten wurde eine verringerte ERK-Phosphorylierung als möglicher Mechanismus dieser Effekte identifiziert.

Zusammenfassend zeigte die Kombination von 4-MU und Erlotinib eine vielversprechende Anti-Tumor-Wirksamkeit in verschiedenen ESCC-Zelllinien. Diese Beobachtung könnte eine Grundlage für den klinischen Einsatz dieser Substanzkombination darstellen.

## II. Transkriptionelle Regulation der Hyaluronsäure-Synthese in ESCC

### 1. Prostaglandine und Hyaluronsäure-Synthese

Originalarbeit: Twarock, S., Rock, K., Sarbia, M., Weber, A. A., Janicke, R. U. and Fischer, J. W. (2009). Synthesis of hyaluronan in oesophageal cancer cells is uncoupled from the prostaglandin-cAMP pathway. Br J Pharmacol 157(2): 234-243 (Twarock et al. 2009).

**Copyright:** Die Verwendung des Bildmaterials aus dieser Veröffentlichung erfolgt mit freundlicher Genehmigung des Verlags John Wiley and Sons. Lizenzierungsdatum 09.07.2021, Lizenznummer: 5104680153238.

Der Hintergrund dieser Arbeit war die in der Literatur gut belegte Überexpression der Cyclooxygenase-2 (COX-2) in gastrointestinalen Tumoren (Hashemi Goradel et al. 2019) und die Beobachtung, dass die von der COX-2 synthetisierten Prostaglandine in humanen vaskulären glatten Muskelzellen (hSMC) eine transkriptionelle Steigerung der HA-Synthase 1 und 2 (HAS1 und HAS2) bewirken (Sussmann et al. 2004). Sowohl für die von der COX-2 gebildeten Prostaglandine als auch für eine übermäßige HA-Produktion sind tumorfördernde Effekte bekannt. In der hier beschriebenen Arbeit sollte daher untersucht werden, ob die für glatte Gefäßmuskelzellen beschriebene Verbindung dieser beiden Systeme analog in Tumorzellen zu finden ist.

Sowohl COX-2 als auch HA und CD44 konnten immunhistochemisch in über 90% der untersuchten Gewebeschnitte von Ösophaguskarzinomen detektiert werden (**Abb. 13**).

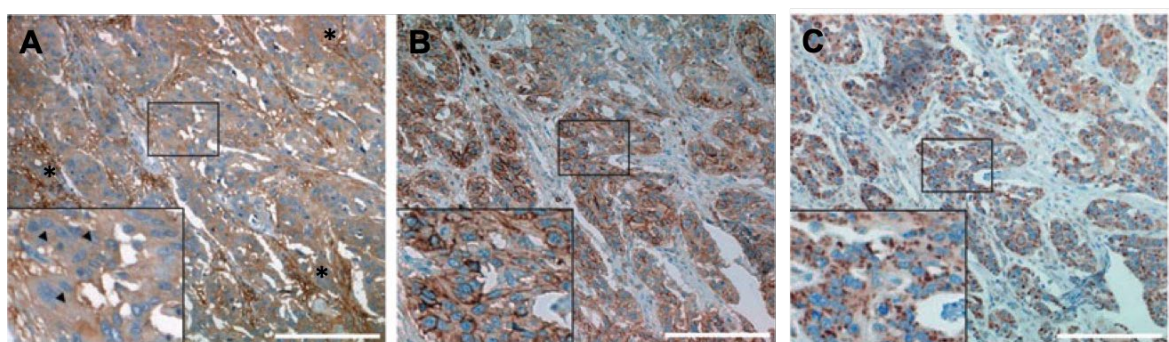


**Abb. 13:** Immunhistochemischer Nachweis von Hyaluronsäure (HA), Cyclooxygenase-2 (COX-2) und CD44 in menschlichem Ösophaguskarzinomgewebe.

Abgebildet sind repräsentative Schnitte von menschlichen Speiseröhrentumoren, n= 69. Um die räumlichen Beziehungen von HA, COX-2 und CD44 zu beurteilen, wurden konsekutive Schnitte angefärbt. **A** HA wurde sowohl im Tumorzellparenchym als auch in Stromazellen nachgewiesen; Sternchen zeigen die Akkumulation von HA im Tumorstroma; Inset, Vergrößerung des angezeigten Bereichs eines Tumorzellclusters, der auch HA innerhalb der Tumorzellen zeigt (Pfeilspitzen). **B** COX-2 und **C** CD44 wurden hauptsächlich in Tumorzellinseln nachgewiesen. Insgesamt wies die Mehrheit (>90%) der Proben eine starke Expression aller drei Proteine auf. Maßstabsbalken 200  $\mu$ m. Verwendung erfolgt mit freundlicher Genehmigung des Verlags John Wiley and Sons.

Die von der COX-2 synthetisierten Prostaglandine wirken als Liganden an verschiedenen Prostaglandin-Rezeptoren. Die in dieser Arbeit untersuchten EP2-, EP4- und IP-Rezeptoren weisen die Gemeinsamkeit auf, dass sie über ein G-Protein vom Gs-Typ die cAMP-Spiegel der Zelle steigern können, was in der Folge über eine Aktivierung eines *cAMP response element-binding protein* (CREB) die Transkription von Zielgenen steigern kann. In den folgenden Versuchen wurden die an diesem Signaltransduktionsweg beteiligten Komponenten daher näher untersucht. Die verwendeten Tumorzelllinien wiesen folgende Besonderheiten auf: OSC1-Zellen exprimieren hauptsächlich COX-1, OSC2-Zellen COX-2 und die HeLa-Zelllinien D98 und H21 zeigen eine TNF $\alpha$ -abhängige Induzierbarkeit der COX-2.

RT-PCR-Analysen zeigten, dass OSC1- und OSC2-Zellen unter basalen Bedingungen HAS2, HAS3, COX-2 und die Gs-gekoppelten EP2- und EP4-Prostaglandin-Rezeptoren exprimierten aber nur eine schwache IP-Rezeptor-Expression aufwiesen. Allerdings induzierte weder die Stimulation mit dem PGI<sub>2</sub>-

Analogon Iloprost noch die Zugabe von exogenem PGE<sub>2</sub> oder Forskolin die mRNA-Expression von HAS1, HAS2 oder HAS3 in OSC1- und OSC2-Zellen (**Abb. 14**).

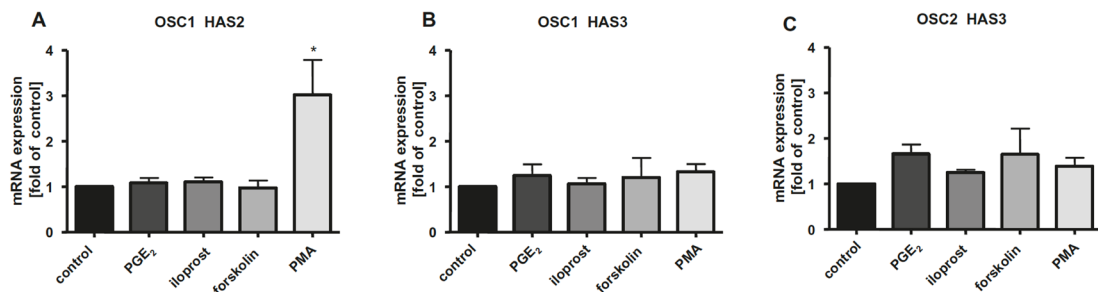


**Abb. 14: HAS-Isoform-Expression in OSC1/2-Zellen unter Stimulation der Prostaglandin-Rezeptoren.**

Die Zellen wurden für 6 h mit dem Prostazyklin (PGI<sub>2</sub>)-Analogon Iloprost (100 nmol/L), PGE<sub>2</sub> (100 nmol/L), Forskolin (10 mmol/L) oder mit PMA (100 nmol/L) als Positivkontrolle stimuliert. Dargestellt sind die Ergebnisse einer RT-PCR aus drei bis fünf unabhängigen Experimenten (Mittelwert  $\pm$  SEM, \*p < 0,05). Die HAS2/3-mRNA-Expression wurde auf GAPDH normalisiert. **A** Nur der PKC-Aktivator Phorbolmyristacetat (PMA) führte zu einem Anstieg der HAS2 mRNA-Transkription in OSC1-Zellen. **B, C** HAS3 mRNA-Spiegel wurden durch keinen Stimulus verändert. HAS1 mRNA war nicht nachweisbar (nicht gezeigt). Verwendung erfolgt mit freundlicher Genehmigung des Verlags John Wiley and Sons.

Weitere Untersuchungen ergaben, dass eine exogene Prostanoid-Stimulation in OSC2-Zellen keinen intrazellulären cAMP-Anstieg auslöste, während PGE<sub>2</sub> in OSC1-Zelle und Iloprost in Fibroblasten zu einer deutlichen cAMP-Zunahme führten (**Abb. 15**). Auch in den beiden HeLa-Zelllinien konnte keine Regulation der HAS-Expression oder HA-Sekretion unter COX-2-Induktion mit TNF $\alpha$  oder Inhibition mit Etoricoxib beobachtet werden (Daten hier nicht gezeigt).

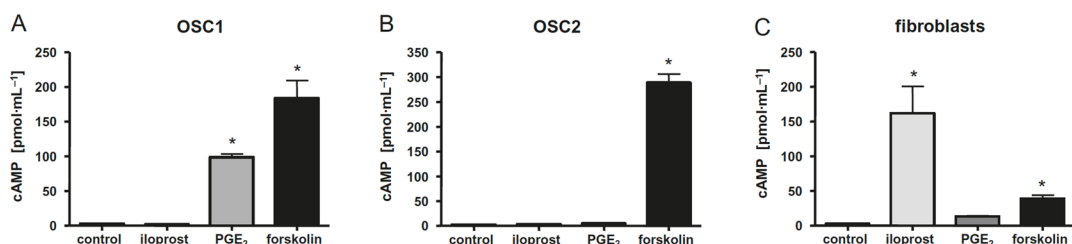


**Abb. 15: Intrazelluläre cAMP-Spiegel nach Stimulation des Prostaglandin-Signalwegs.**

Die intrazellulären cAMP-Spiegel wurden mittels Radioimmunoassay bestimmt. Zur Untersuchung der cAMP-Antwort wurden OSC1- und OSC2-Zellen sowie Fibroblasten mit Wirkstoffen stimuliert, von denen bekannt ist, dass sie den cAMP-Spiegel induzieren. Der Aktivator der Adenylylatzyklase Forskolin wurde als Positivkontrolle verwendet. **A** In OSC1-Zellen kam es unter PGE2-Stimulation und Forskolin zu einem cAMP-Anstieg. **B** In OSC2-Zellen führte keine exogene Prostanoid-Stimulation zu einem cAMP-Anstieg. **C** Fibroblasten reagierten auf das stabile Prostacyclin-Analogon Iloprost mit einem ausgeprägten cAMP-Anstieg, der höher als die Forskolin-Kontrolle ausfiel. Repräsentative Ergebnisse aus vier unabhängigen Experimenten. Mittelwert  $\pm$  SEM, \*p < 0,05. Verwendung erfolgt mit freundlicher Genehmigung des Verlags John Wiley and Sons.

Aus diesen Ergebnissen kann geschlossen werden, dass in Ösophagus- und HeLa-Krebszellen die Expression der HAS-Isoformen nicht über den Prostaglandin-cAMP-Signalweg reguliert wird. Anhand der verschiedenen Prostaglandin-Rezeptor-Muster zwischen OSC1/2-Zellen und Fibroblasten lässt sich vermuten, dass die Stimulation der HAS1 und 2 in Fibroblasten und glatten Gefäßmuskelzellen über Prostacyclin und den IP-Rezeptor-Signalweg reguliert wird, dieser Weg in den Tumorzellen aber keine relevante Rolle spielt. Dennoch könnte dieser Mechanismus in der Beeinflussung des Tumorstromas von Bedeutung sein, da dieses zu einem großen Teil aus *cancer-associated-fibroblasts* (CAFs) besteht und in diesem System vom Tumor sezernierte Prostaglandine die HAS2-Expression im Stroma erhöhen könnten. Dieser Mechanismus könnte für die in **Abb. 13** gezeigten hohen HA-Mengen in den humanen Tumorschnitten mitverantwortlich sein. Interessanterweise konnte in einer neueren Arbeit in der

Brustkrebszelllinie MDA-MB-231 ein Zusammenhang zwischen COX2-Expression und HAS2-Expression gefunden werden (Stasinopoulos et al. 2008). Dies lässt vermuten, dass sich die entsprechenden Prostaglandin-Signalwege in verschiedenen Tumorentitäten stark unterscheiden können.

## 2. ESCC-Zellen modulieren die Chemokin-Expression und die Hyaluronsäure-synthese in Fibroblasten

Originalarbeit: Kretschmer, I., Freudenberger, T., Twarock, S., Yamaguchi, Y., Grandoch, M. and Fischer, J. W. (2016). Esophageal Squamous Cell Carcinoma Cells Modulate Chemokine Expression and Hyaluronan Synthesis in Fibroblasts. *J Biol Chem* 291(8): 4091-4106 (Kretschmer et al. 2016).

Das Ziel dieser Arbeit war es, die Interaktion von Tumor- und Stromazellen in Bezug auf HA und die Chemokinexpression zu charakterisieren. Hierzu wurden als Tumorzellen die ESCC-Zelllinie Kyse 410 und stellvertretend für Stromazellen Hautfibroblasten und Tumor-assoziierte Fibroblasten (*cancer-associated fibroblasts*, CAF) verwendet, die aus einem Nacktmaus-Tumor-Xenograft-Modell stammten.

Eine erste interessante Beobachtung in dieser Arbeit war, dass KYSE-410-Zellen die mRNA-Expression der HA-Synthase 2 (Has2) in Fibroblasten nur in direkten Co-Kulturen induzierten; zwei verschiedene indirekte Co-Kultur-Ansätze führten nicht zu einer Stimulation. In weiteren Versuchen wurde mit dem  $\beta$ -Catenin/LEF1-Signalweg entsprechend ein Mechanismus für diese Stimulation identifiziert, der durch Zell-Zell-Kontakte aktiviert wird. Analog zur Stimulation der Has2-mRNA wurde in diesen Experimenten auch die Has2-Antisense-RNA (Has2as) reguliert.

Im Folgenden wurde die Auswirkung eines Knockdowns von Has2 in den Hautfibroblasten auf die KYSE410-Zellen und Hautfibroblasten untersucht. Dieser hatte keine Auswirkungen auf epithelial-mesenchymale Übergangsmarker, Proliferation und Migration der KYSE410-Zellen in der Co-Kultur; es konnte aber in den Hautfibroblasten eine Abnahme der Gen-Expression des Myofibroblastenmarkers  $\alpha$ -Glattmuskel-Aktin ( $\alpha$ SMA) detektiert werden.

In weiteren Experimenten wurde unter Co-Kultur-Bedingungen eine Hochregulation des Chemokins CCL5 und eine Herunterregulation von CCL11 sowohl in Hautfibroblasten als auch in CAFs detektiert. Außerdem wurde festgestellt, dass HA die Adhäsion von CD4 $^{+}$ -, aber nicht von CD8 $^{+}$ -Zellen an Xenograft-Tumorgewebe fördert.

Zusammenfassend zeigt diese Arbeit, dass die direkte Co-Kultur von Ösophaguskarzinomzellen und Fibroblasten die stromale HA-Synthese über den  $\beta$ -Catenin/LEF1-Weg induziert und das Chemokinprofil der stromalen Fibroblasten verändert, was wiederum die Immunantwort des Tumors beeinflussen könnte.

### III. Metabolische Regulation der Hyaluronsäure-Synthese in ESCC

HA besteht als Glykosaminoglykan überwiegend aus Metaboliten des Glukose-Stoffwechsels. In den folgenden Projekten wurde daher untersucht, inwiefern und auf welche Weise metabolische Verschiebungen innerhalb dieses Stoffwechselwegs die Menge der synthetisierten HA mitbeeinflussen können und welche Auswirkungen dies auf das Tumorwachstum hat.

#### 1. Einfluss einer diabetischen Stoffwechsellage auf Hyaluronsäuresynthese und Tumorprogression

Originalarbeit: Twarock, S., Reichert, C., Peters, U., Gorski, D. J., Rock, K. and Fischer, J. W. (2017). Hyperglycaemia and aberrated insulin signalling stimulate tumour progression via induction of the extracellular matrix component hyaluronan. *Int J Cancer* 141(4): 791-804 (Twarock et al. 2017).

**Copyright:** Die Verwendung des Bildmaterials aus dieser Veröffentlichung erfolgt mit freundlicher Genehmigung des Verlags John Wiley and Sons. Lizenzierungsdatum 09.07.2021, Lizenznummer: 5104681412256.

In epidemiologische Studien wurde eine höhere Inzidenz verschiedener Tumorentitäten unter Patienten mit Diabetes mellitus Typ 1 und Typ 2 festgestellt (Giovannucci et al. 2010). Zu diesen zählt auch das Ösophaguskarzinom (Huang et al. 2012), für das außerdem eine Assoziation zwischen gesteigertem Nüchternblutzucker und erhöhter Mortalität beschrieben wurde (Jee et al. 2005, Stocks et al. 2009). Die zugrundeliegenden Pathomechanismen sind Gegenstand der aktuellen Forschung; derzeit werden der direkte Einfluss der **Hyperglykämie** auf das Tumorzellwachstum, die **anabolen Wirkungen** von erhöhten **Insulin**-Konzentrationen sowie die verstärkte Produktion **inflammatorischer Zytokine** durch das Fettgewebe bei Adipositas als Ursachen angenommen und untersucht (Vigneri et al. 2009). Hinweise für die genannten Mechanismen ergeben sich auch aus der Erkenntnis, dass die Pharmakotherapie mit insulinotropen Antidiabetika die Tumorzidenz steigert (Currie et al. 2009), während eine Behandlung mit Metformin das Risiko einer Krebsentstehung (Evans et al. 2005) und die Mortalitätsrate (Landman et al. 2010) senken kann.

Für den direkten Einfluss einer **Hyperglykämie** gibt es einige Hinweise: Durch die metabolische Umstellung von mitochondrialer oxidativer Phosphorylierung auf die aerobe Glykolyse („Warburg Effekt“) kommt es zu einer weitgehenden Abhängigkeit der Tumorzellen von der Glukoseversorgung (Warburg 1956, Vander Heiden et al. 2009). Zusätzlich werden durch die chronische Hyperglykämie eine Vielzahl von Signalwegen aktiviert, die die Proliferation und Invasion erhöhen und die Einleitung einer Apoptose inhibieren können (Duan et al. 2014, Ryu et al. 2014).

Neben seiner anabolen Wirkung, die zu einer Stimulation der zellulären Proliferation führt, ist die wichtigste Funktion von **Insulin** die Steuerung des Glukose-Metabolismus. Hierbei sind vor allem zwei Mechanismen von Bedeutung: die **Erhöhung der Glukose-Aufnahme** in die Zelle und die **Förderung der Glukose-Metabolisierung** in der Glykolyse und im Pentosephosphatweg. Da in den meisten Tumorzellen die Glukose-Aufnahme allerdings – im Rahmen des „Warburg-Effektes“ – über Insulin-unabhängige Glucose-Transporter-Isoformen wie GLUT1 und GLUT3 stattfindet (Medina and Owen 2002), überwiegen hier die Mechanismen zur Steuerung der Metabolisierung von Glukose.

HA wird in der Zelle hauptsächlich aus Vorstufen synthetisiert, die in den ersten Schritten der Glykolyse aus Glukose entstehen. Auf Grundlage der vorher geschilderten Erkenntnisse wurde daher in diesem Projekt untersucht, inwiefern die HA-Synthese in ösophagealen Plattenepithelkarzinomzellen einerseits von der Glukose-Verfügbarkeit und andererseits von der Aktivität anderer Glukose-verbrauchender biochemischer Metabolisierungswege, wie der Glykolyse und dem Pentosephosphatweg, abhängt. Die Arbeitshypothese lautete, dass eine hyperglykämische Stoffwechselslage in Zusammenspiel mit einer vorhandenen Insulinresistenz zu einer gesteigerten HA-Synthese führen könnte. Da HA tumorfördernde Eigenschaften besitzt, könnte dieser Mechanismus zur Aggressivität und Chemotherapie-Resistenz von Tumorzellen beitragen.

Zellkultur-Versuche, in denen den Tumorzellen verschiedene Glukose-Konzentrationen angeboten wurden, zeigten eine konzentrationsabhängige Steigerung der extrazellulären HA-Menge im Zellüberstand (**Abb. 16A**) als auch der perizellulären HA-Matrix (**Abb. 16B**) sowohl unter An- als auch Abwesenheit von Serum.

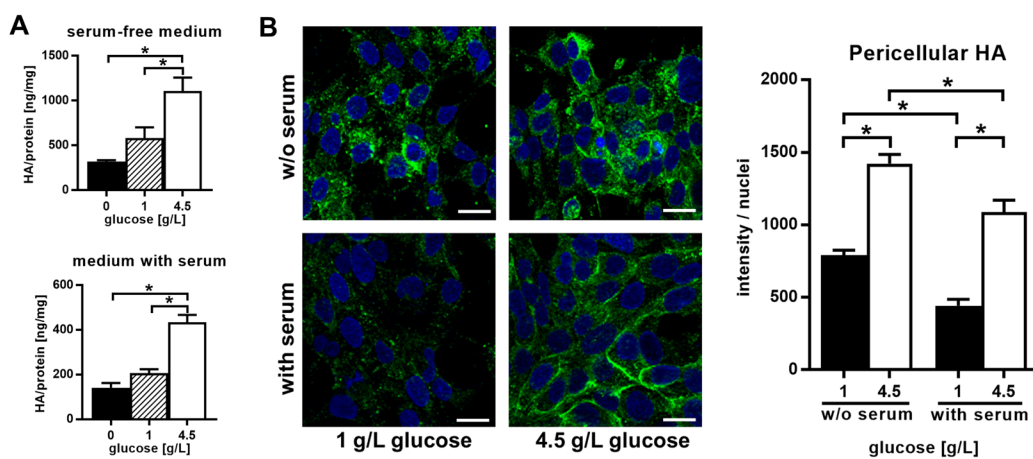


**Abb. 16: Abhängigkeit der HA-Synthese von extrazellulären Glukosekonzentrationen.**

A HA-Konzentrationen im Medium von OSC1-Zellen normalisiert auf zelluläres Protein unter verschiedenen Glukosekonzentration mit und ohne Serum (10% FCS) nach 24 h gemessen mittels HA-Bindungsprotein (HABP)-Assay. B Perizellulärer HA-Mantel der OSC1-Zellen unter niedriger und hoher Glukosekonzentration mit und ohne Serum visualisiert durch HA-Affinitätszytochemie nach 24 h. HABP, grün, Zellkerne blau (Hoechst). Maßstabsbalken 10 µm. Mittelwerte ± SEM, n=3, \*p < 0,05. Verwendung erfolgt mit freundlicher Genehmigung des Verlags John Wiley and Sons.

In den folgenden Versuchen wurde der Effekt von Insulin-gesteuerten Signalkaskaden auf die HA-Synthese untersucht. Dies folgte der oben beschriebenen Annahme, dass HA mit anderen metabolischen Wegen in Konkurrenz steht, die ebenfalls Glukose verbrauchen.

Eine Inhibition der Glykolyse durch Ausschaltung ihres Schlüsselenzyms Phosphofructokinase M führte demnach wie erwartet zu einem deutlichen Anstieg der HA-Produktion, während die Konzentration des Endmetaboliten der aeroben Glykolyse Laktat stark abnahm (**Abb. 17A**). Eine Steigerung der Glykolyse durch Stimulation mit Insulin hatte dementsprechend einen gegenläufigen Effekt (**Abb. 17B**). Dieser konnte wiederum durch das Ausschalten des Insulinrezeptors umgekehrt werden (**Abb. 17C**). In weiteren hier nicht gezeigten Zellkultur-Experimenten wurde in dieser Arbeit die funktionelle Bedeutung dieser Prozesse für die Proliferation, die Invasion, das verankerungsunabhängige Wachstum und die Adhäsion von ESCC an Endothelzellen *in vitro* nachgewiesen.

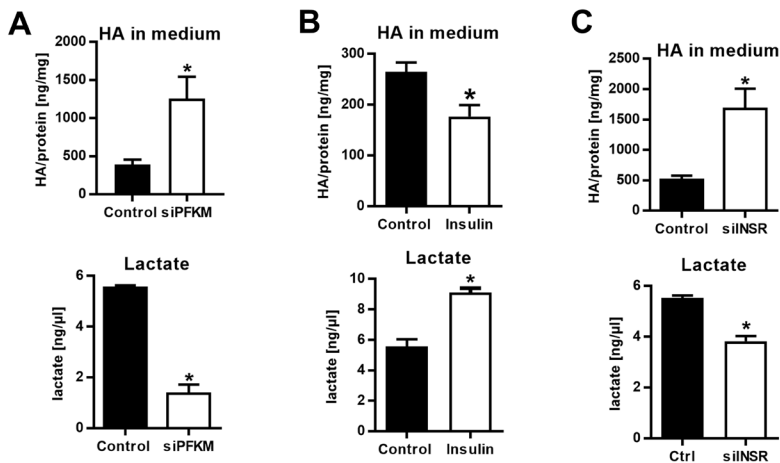


**Abb. 17: Metabolische Konkurrenz zwischen Glykolyse und HA-Synthese.**

A Die genetische Ausschaltung der Phosphofructokinase M (PFKM) – ein Schlüsselenzym der Glykolyse – hemmt die Glykolyse zu Lactat und lenkt die Glukoseverwertung in Richtung HA-Synthese um. B Die Stimulation mit Insulin (50 nM, 24 h) steigerte die Glykolyse zu Lactat und senkte dadurch die HA-Synthese. C Die genetische Ausschaltung des Insulinrezeptors (INSR) kehrte die Effekte von Insulin auf die Lactat- und HA-Spiegel um. HA im Überstand wurde mittels HABP-Assay, Lactat mittels kolorimetrischem Assay gemessen, beides in Anwesenheit von Serum nach 24 h. Mittelwerte  $\pm$  SEM, n=3-4, \*p < 0,05. Verwendung erfolgt mit freundlicher Genehmigung des Verlags John Wiley and Sons.

Die *in vivo* Relevanz der beschriebenen Zellkultur-basierten Ergebnisse wurde schließlich in einem Streptozotocin-induzierten diabetischen Nacktmaus-Tumor-Xenograft-Modell überprüft. Dieses ist geprägt von einer systemischen Hyperglykämie und einem Mangel an Insulin. Wie in **Abb. 18A** dargestellt, wiesen die diabetischen Mäuse ein wesentlich stärkeres Tumorgewicht auf als die nicht-diabetischen Tiere; das Tumorgewicht in beiden Gruppen wurde durch die Fütterung mit dem HA-Synthese-Inhibitor **4-MU** deutlich gesenkt. Die Überlebenszeit der diabetischen Tiere wurde in einer Kaplan-Meier-Kurve aufgetragen (**Abb. 18B**); aus dieser konnte eine signifikant lebensverlängernde Wirkung von **4-MU** in dieser Gruppe abgelesen werden. Die histologische Aufarbeitung der entsprechenden Tumorschnitte zeigte, dass die Tumoren in der diabetischen Gruppe einen höheren HA-Anteil aufwiesen als die der nicht-diabetischen Gruppe und dass **4-MU** die HA-Menge in beiden Gruppen reduzierte (**Abb. 18C**). Die Vaskularisierung, quantifiziert über eine Färbung auf CD31 (**Abb. 18D**), sowie die Proliferationsrate, gemessen über die Anfärbung Ki67-positiver Zellkerne (**Abb. 18E**) wurde durch **4-MU** nur in der diabetischen Gruppe gesenkt. Die Auswertung apoptotischer Zellen mittels TUNEL-Färbung ergab, dass **4-MU** wiederum nur in der diabetischen Gruppe zu einer ausgeprägten Zunahme der Apoptose führte (**Abb. 18F**).

Zusammengefasst zeigt diese Arbeit, dass eine hyperglykämische Stoffwechselzustand und ein gestörter Insulin-Signalweg die Tumorprogression über eine Induktion der HA-Synthese fördern können und dass dieser Prozess durch die Behandlung mit **4-MU**, einem pharmakologischen Inhibitor der HA-Synthese, effektiv abgeschwächt werden kann. Somit könnte die unter diesen Bedingungen stattfindende Verschiebung der Glukoseverwertung von Glukose-Katabolismus hin zum HA-Anabolismus eine wichtige Verbindung zwischen Diabetes und Tumorprogression darstellen und die therapeutische Hemmung der HA-Synthese durch **4-MU** einen vielversprechenden Ansatz für die Tumorbehandlung bei diabetischen Patienten bieten.

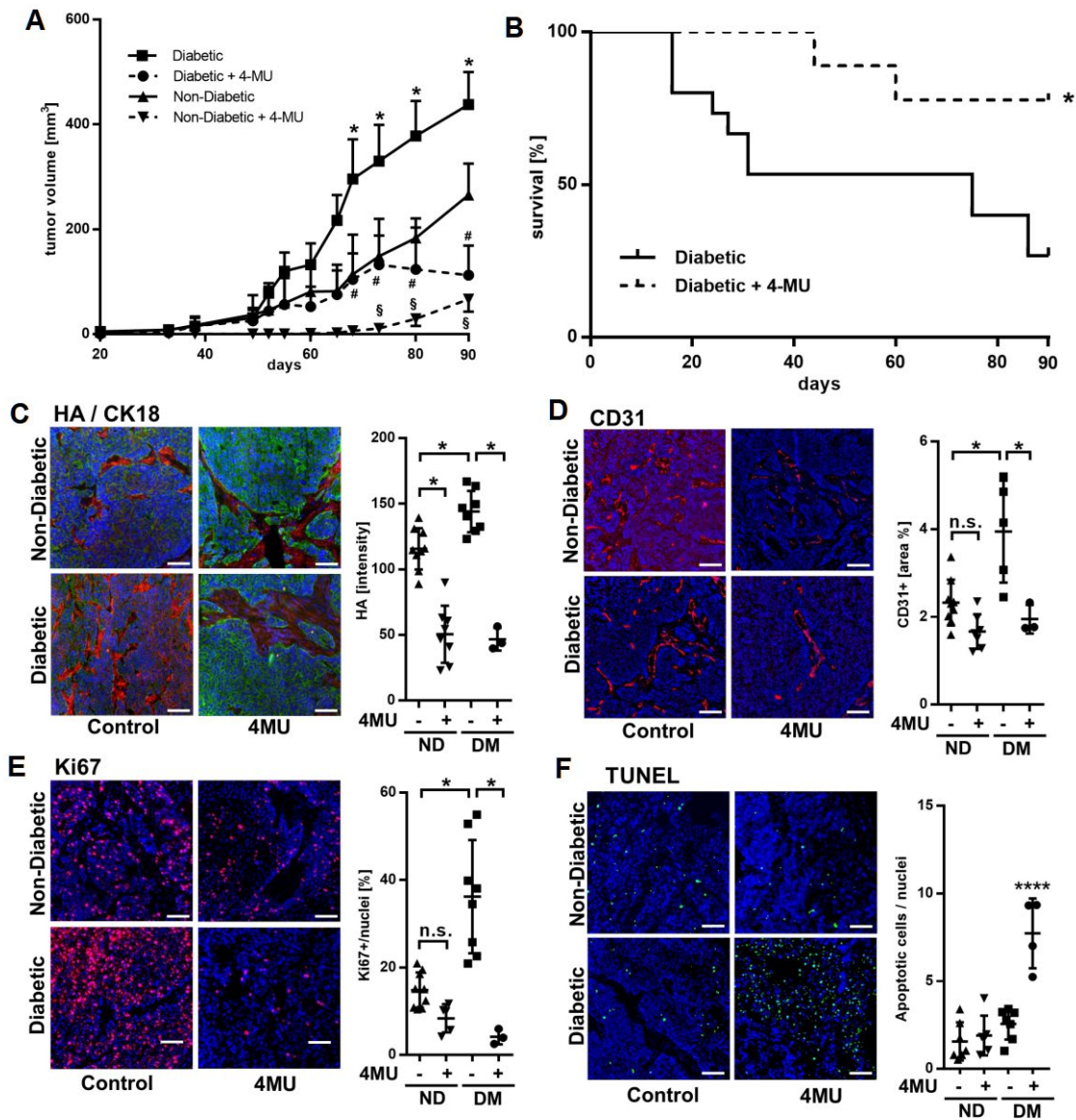


**Abb. 18:** Verstärkung der HA-abhängigen Tumorprogression durch Hyperglykämie und Insulin-Depletion in einem Typ-1-Diabetes-Nacktmaus-Xenograft-Modell.

A OSC1-Xenotransplant-Tumorwachstum über 90 Tage in diabetischen und nicht-diabetischen Mäusen mit (gestrichelte Linien) oder ohne (durchgezogene Linien) orale Applikation des HA-Synthese-Inhibitors 4-MU. Zwei-Wege-ANOVA mit Tukey's Post-Test: \*p < 0,05 diabetisch vs. nicht-diabetisch; #p < 0,05 diabetisch vs. diabetisch mit 4-MU; \$p < 0,05 nicht-diabetisch vs. nicht-diabetisch mit 4-MU. B Kaplan-Meier-Überlebenskurve von diabetischen Nacktmäusen mit Tumoren ± 4-MU-Behandlung innerhalb von 90 Tagen nach Xenotransplantation. Beobachtet wurden 15 diabetische Mäuse ohne 4-MU-Behandlung vs. 9 diabetische Mäuse mit 4-MU-Behandlung. Am Ende des Experiments waren 4 diabetische Mäuse ohne 4-MU-Behandlung und 7 4-MU behandelte diabetische Mäuse noch am Leben. Log-rank (Mantel-Cox) Test: \*p < 0,05. C HA-Färbung (HABP, rot) im Tumor (Cytokeratin 18, CK18, grün) und im Stroma, Zellkerne (blau, Hoechst). Quantifizierung von 9 nicht-diabetischen (ND), 8 diabetischen (DM), 8 ND + 4-MU und 3 DM + 4-MU Tumoren. D Endothelzellsfärzung (CD31-Färbung, rot) und Zellkerne (blau, Hoechst). Quantifizierung von 9 nicht-diabetischen (ND), 5 diabetischen (DM), 7 ND + 4-MU und 3 DM + 4-MU Tumoren. E Proliferationsrate im Tumorgewebe (Ki67-Färbung, rot), Zellkerne (blau, Hoechst). Quantifizierung von 9 nicht-diabetischen (ND), 8 diabetischen (DM), 5 ND + 4-MU und 3 DM + 4-MU Tumoren. F Apoptotische Zellen (TUNEL-Färbung, grün) und Zellkerne (blau, Hoechst). Quantifizierung von 7 nicht-diabetischen (ND), 6 diabetischen (DM), 7 ND + 4-MU und 4 DM + 4-MU Tumoren. C-F Repräsentative Bilder, Maßstabsbalken 100 µm, Darstellung als Streudiagramme mit Mittelwert ± SEM. Statistische Signifikanz wurde mit Ein-Weg-ANOVA bestimmt: \*p < 0,05, \*\*\*\*p < 0,0001. Verwendung erfolgt mit freundlicher Genehmigung des Verlags John Wiley and Sons.

## 2. Eine Inhibition der Hyaluronsäurematrix verbessert die Tumor-hemmende Wirkung von Dichloressigsäure *in vitro* und *in vivo*

Originalarbeit: Twarock, S., Reichert, C., Bach, K., Reiners, O., Kretschmer, I., Gorski, D. J., Gorges, K., Grandoch, M. and Fischer, J. W. (2019). Inhibition of the hyaluronan matrix enhances metabolic anticancer therapy by dichloroacetate *in vitro* and *in vivo*. Br J Pharmacol 176(23): 4474-4490 (Twarock et al. 2019).

**Copyright:** Diese Veröffentlichung wurde unter den Bedingungen einer Creative Commons CC-BY-NC-ND 4.0-Lizenz (open access) beim Verlag Wiley veröffentlicht. Diese erlaubt die freie Verwendung aller Inhalte unter Angabe der Originalquelle. Vorsorglich wurde eine Lizenz angefordert: 5104690425109 vom 09.07.2021.

Die aerobe Glykolyse ist ein einzigartiges Merkmal von Tumorzellen, das mehrere Vorteile für die Krebsprogression mit sich bringt wie z. B. eine Apoptose-Resistenz. Das niedermolekulare Pharmakon Dichloracetat (DCA) ist ein Pyruvat-Dehydrogenase-Kinase-Inhibitor, der die oxidative Phosphorylierung wiederherstellt und bei einer Vielzahl von Krebsentitäten eine Apoptose induziert. Seine therapeutische Wirksamkeit wird jedoch durch Resistenzmechanismen und dosislimitierende Nebenwirkungen begrenzt. Ziel dieser Studie war es daher, die Rolle der anti-apoptotischen HA-Matrix in diesem Kontext zu untersuchen und die Inhibition der HA-Synthese durch 4-MU als eine mögliche zusätzliche Behandlungsoption zu testen, um die Wirksamkeit von DCA zu steigern.

In einem ersten Schritt wurde ein potentieller metabolischer Zusammenhang zwischen DCA-Behandlung und HA-Matrix-Synthese *in vitro* untersucht. Im Ergebnis zeigte sich eine dosisabhängige Zunahme der HA-Menge im Zellüberstand (**Abb. 19A**) und perizellulär (**Abb. 19B**).

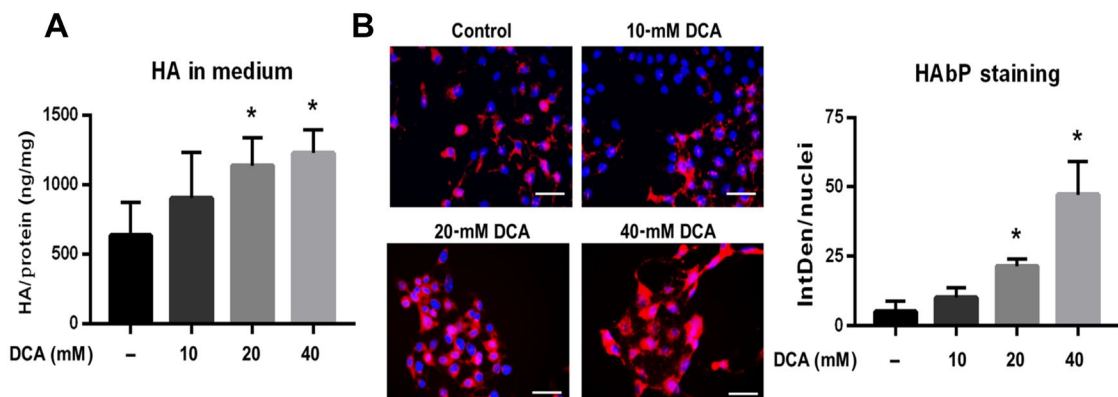


**Abb. 19: Gesteigerte Bildung der Hyaluronsäure-Matrix in Ösophaguskarzinomzellen unter DCA.**

KYSE-410-Zellen wurden 72 Stunden lang mit 10, 20 oder 40 mM Dichloracetat (DCA) inkubiert und auf ihren HA-Gehalt analysiert. **A** Die HA-Konzentration im Medium wurde mit einem ELISA-ähnlichen Immunaffinitätsassay gemessen und auf den Proteingehalt normalisiert ( $n = 6$ ). **B** Die perizelluläre HA-Matrix (rot) wurde mit einem HA-Bindungsprotein (HAbP) angefärbt und die integrierte Dichte (IntDen) auf die Anzahl der Zellkerne (Hoechst, blau) normalisiert ( $n = 7$ , jedes  $n$  steht für eine gepoolte Analyse von fünf Replikaten). Repräsentative Bilder, Maßstabsbalken 100  $\mu\text{m}$ . Verwendung erfolgt mit freundlicher Genehmigung des Verlags John Wiley and Sons.

Im nächsten Schritt sollten über die Quantifizierung verschiedener Metaboliten unter der Behandlung mit DCA Wirkmechanismen identifiziert werden, die an der Steigerung der HA-Synthese unter DCA beteiligt sein könnten. Zuerst wurde die metabolische Wirkung von DCA auf die Verschiebung der Energiegewinnung von Glykolyse zu oxydativer Phosphorylierung in den KYSE-410-Zellen überprüft und bestätigt: Die Glykolyse nahm dosisabhängig ab (**Abb. 20A**), während die mitochondriale ATP-Produktion bereits bei der kleinsten getesteten Dosis den Höhepunkt der Steigerung erreichte (**Abb. 20B**).

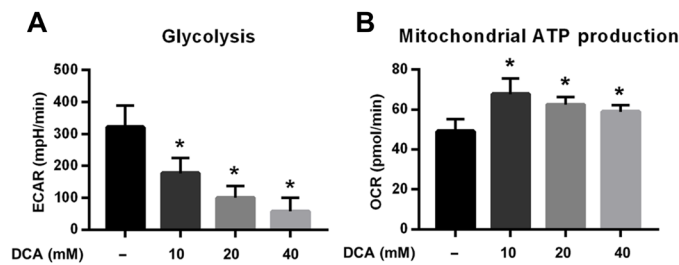


**Abb. 20:** Umschaltung des Metabolismus von KYSE-410-Zellen von Glykolyse auf oxidative Phosphorylierung durch DCA.

Eine Echtzeit-Stoffwechselanalyse mittels Seahorse XFe96 wurde genutzt, um die Auswirkungen von DCA auf Glykolyse und oxidative Phosphorylierung in KYSE-410-Zellen zu untersuchen.  $12 \times 10^3$  Zellen pro Well wurden 15 Minuten mit DCA präinkubiert. **A** Die Glykolyse-Aktivität wurde mit dem *Glycolysis Rate Assay Kit* als extrazelluläre Ansäuerungsrate (ECAR) bestimmt. **B** Die mitochondriale oxidative Phosphorylierung wurde mit dem *Mitochondrial Stress Test Kit* als Sauerstoffverbrauchsrate (OCR) gemessen. n=6, jedes n repräsentiert eine gepoolte Analyse von vier technischen Replikaten, Mittelwerte  $\pm$  SD, Einweg-ANOVA, \*p < 0,05. Verwendung erfolgt mit freundlicher Genehmigung des Verlags John Wiley and Sons.

Im Folgenden wurden drei Mechanismen identifiziert, über die DCA zu einer erhöhten HA-Synthese beitragen kann:

- Erhöhtes Substratangebot** durch Steigerung von Glucose-Metaboliten wie Glucose-6-Phosphat aufgrund eines Rückstaus in der Glykolyse
- Erhöhtes Intermediär-Metaboliten-Angebot** durch gesteigerte Produktion von Acetyl-CoA im Krebs-Zyklus
- Erhöhte O-GlcNAcylierung** von Proteinen wie den HAS-Enzymen, die mit einer Aktivierung einhergehen kann

Ad A. DCA verursachte einen dosisabhängigen Anstieg von Glucose-6-Phosphat (**Abb. 21A**), einem frühen Glykolyse-Metaboliten, der als Vorstufe von UDP-Glucuronsäure und UDP-N-Acetylglucosamin ein zentrales Substrat der HA-Synthese darstellt. Entsprechend stiegen auch die Spiegel von UDP-N-Acetylglucosamin an (**Abb. 21B**).

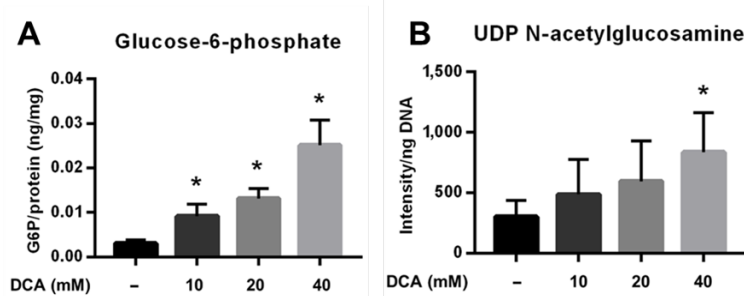


**Abb. 21:** Steigerung der Konzentration des frühen Glykolyse-Metaboliten Glucose-6-Phosphat und des HAS-Substrats UDP-N-Acetylglucosamin unter DCA.

A Die Glucose-6-Phosphat (G6P)-Konzentration wurde nach 3-tägiger DCA-Inkubation mittels kolorimetrischer Analyse gemessen. B Der HA-Vorläufer UDP-N-Acetylglucosamin wurde mittels ENVI-Carb-Säulen isoliert, durch Fluorophor-unterstützte Kohlenhydrat-Elektrophorese (FACE) quantifiziert und auf den Gesamt-DNA-Gehalt normiert. n=6, Mittelwerte  $\pm$  SD, Einweg-ANOVA, \*p < 0,05. Verwendung erfolgt mit freundlicher Genehmigung des Verlags John Wiley and Sons.

Ad B. DCA führt über die Reaktivierung des Krebs-Zyklus zu einem Anstieg von Acetyl-CoA im Zytosol (**Abb. 22A**). Um den mitochondrialen Metabolismus als Quelle dieses Anstiegs zu verifizieren, wurde die Aktivität der ATP-Citrat-Lyase, die am *Shuttling* von Acetyl-CoA aus dem Mitochondrium ins Zytosol beteiligt ist, durch SB204990 inhibiert. Durch diese Maßnahme konnte der zytosolische Anstieg von Acetyl-CoA unter DCA-Behandlung aufgehoben werden (**Abb. 22B**).

Weitere Messungen bestätigten schließlich den Zusammenhang dieses beobachteten Mechanismus mit der HA-Sekretion (**Abb. 22C**).

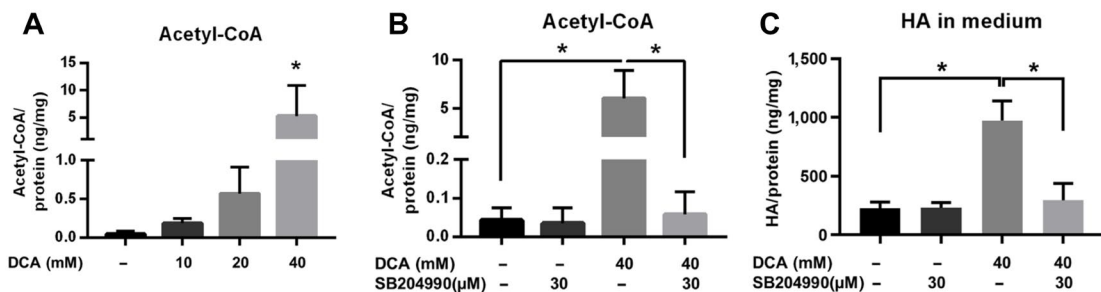


**Abb. 22:** Erhöhung des für Vorstufen der HA-Synthese benötigten Metaboliten Acetyl-CoA über die Aktivierung des mitochondrialen Krebs-Zyklus durch DCA.

A Dosisabhängige Steigerung der intrazellulären Acetyl-CoA-Konzentration durch DCA; gemessen über ein kolorimetrisches Verfahren. B Der ATP-Citrat-Lyase-Inhibitor SB204990 hemmt den Export von Acetyl-CoA aus den Mitochondrien in das Cytosol und wurde verwendet, um die Effekte von Dichloracetat auf die zelluläre Acetyl-CoA-Konzentration aufzuheben. C Messung der HA-Konzentration im Medium nach Hemmung des Acetyl-CoA-Shuttlings mit SB204990 durch einen ELISA-ähnlichen Immunaffinitätsassay. n=6, Mittelwerte  $\pm$  SD, Einweg-ANOVA, \*p < 0,05. Verwendung erfolgt mit freundlicher Genehmigung des Verlags John Wiley and Sons.

**Ad C.** Der unter A. beschriebene Anstieg von UDP-N-Acetylglucosamin führte zu einer erhöhten O-GlcNAcylierung von Proteinen, die durch die Behandlung mit dem O-GlcNAc-Transferase (OGT)-Inhibitor Alloxan aufgehoben werden konnte. Dieser Effekt wurde mit Immunoblot (**Abb. 23A**) und Immunfärbungen nachgewiesen (**Abb. 23B**).

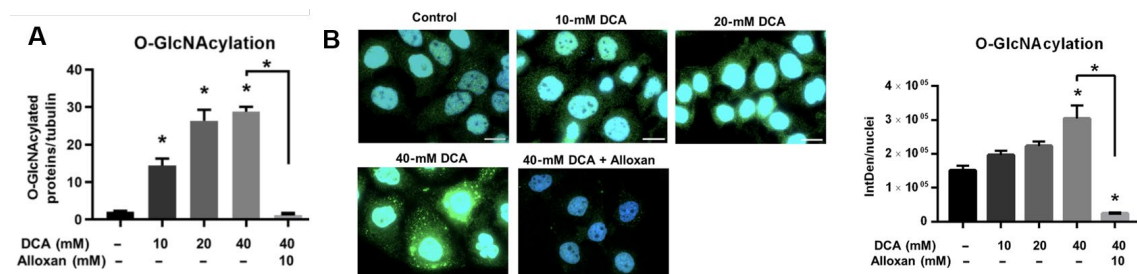


**Abb. 23:** Erhöhte Protein-O-GlcNAcylierung unter DCA.

Die dosisabhängig gesteigerte O-GlcNAcylierung der zellulären Proteine unter DCA wurde durch A Immunoblot-Analyse (n = 6) und B Immunfärbung (O-GlcNAcylierung, grün; Nuklei, blau) quantifiziert (n = 8, jedes n repräsentiert eine gepoolte Analyse von fünf technischen Replikaten). Durch Behandlung mit dem O-GlcNAc-Transferase (OGT)-Inhibitor Alloxan konnte dieser Effekt aufgehoben werden. Repräsentative Bilder, Maßstabsbalken 20 μm. Signifikanz durch Zwei-Wege-ANOVA ermittelt, \*p < 0,05 vs. Kontrolle (0 mM DCA) oder wie durch die Klammer angegeben. Verwendung erfolgt mit freundlicher Genehmigung des Verlags John Wiley and Sons.

Im Anschluss wurden die Auswirkungen und der Synergismus einer Kombination von DCA mit 4-MU in 2D- und 3D-Zellkulturen und in einem Nacktmaus-Tumor-Xenograft-Regressionsmodell untersucht. Im 3D-Tumorspheroidmodell hatte die Kombination der beiden Substanzen eine synergistische Wirkung auf die Reduktion der Spheroidgröße: Während die Monotherapien lediglich zu einem verlangsamten Wachstum führten, konnte die Kombinationstherapie sogar eine Verkleinerung des Spheroidvolumens bewirken (**Abb. 24A**).

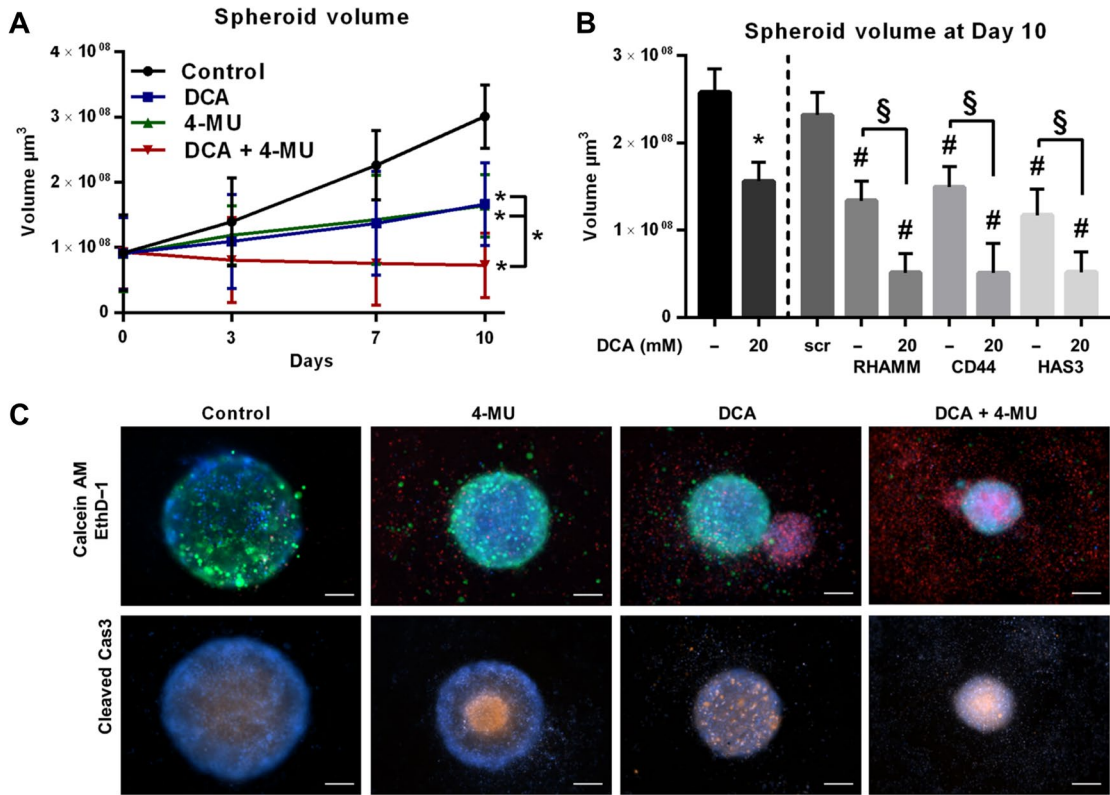


**Abb. 24:** Reduktion des Volumens von ESCC-Zell-Sphäroiden und eine damit einhergehende Apoptose-Induktion unter Kombination von DCA mit 4-MU.

A Sphäroid-Volumina von 24 Replikaten pro Bedingung wurden gemessen. 3D-Kulturen wurden 4 Tage nach Aussaat mit DCA (20 mM), 4-MU (300  $\mu\text{M}$ ) oder der Kombination aus beiden inkubiert und das Volumen über einen Zeitraum von 10 Tagen gemessen und lichtmikroskopisch beobachtet. Das Sphärenvolumen wurde auf Basis des Durchmessers mit der Formel  $V = 1/6 \times \pi \times d^3$  berechnet ( $n = 6$ ). B Einfluss eines siRNA-Knockdowns von RHAMM, CD44 und HAS3 in KYSE410-Zellen auf die Sphäroidbildung. Eine zusätzliche Stimulation mit 20 mM DCA wurde ab Tag 4 durchgeführt und die Zellen für 10 Tage inkubiert. Es wurde *scrambled* siRNA verwendet, um nachteilige Effekte der siRNA selbst auszuschließen ( $n = 6$ ; ein  $n$  umfasste 24 Sphäroide pro Bedingung). C An Tag 10 wurden die Sphäroide auf lebende (Calcein AM, grün) und tote (Ethidium Homodimer 1 [EthD-1], rot) Zellen (obere Reihe) oder auf gespaltene Caspase 3 (Cas3, orange, untere Reihe) gefärbt. Die Zellkerne wurden mit Hoechst (blau) gegenfärbt. Repräsentative Bilder, Maßstabsbalken 200  $\mu\text{m}$ . Mittelwerte  $\pm$  SD. Einweg-ANOVA, \* $p < 0,05$ , # $p < 0,05$  vs. *scrambled* Kontrolle, § $p < 0,05$  vs. alleinige siRNA-Behandlung. Verwendung erfolgt mit freundlicher Genehmigung des Verlags John Wiley and Sons.

Ähnliche synergistische Effekte ergaben sich auch bei einer Kombination von DCA mit siRNAs gegen die beiden HA-Rezeptoren RHAMM und CD44 sowie die HA-Synthase HAS3 (Abb. 24B). Die Färbung der Tumorspheroide auf tote, lebende und apoptotische Zellen zeigte eine deutliche Zunahme der toten und apoptotischen Zellen unter der Kombinationstherapie (Abb. 24C).

In einem Xenograft-Nacktmaus-Tumor-Regressionsmodell wurden schließlich die bisher erhobenen Daten verifiziert. Die Kombination von DCA und 4-MU erreichte als einzige Bedingung in diesem Versuch eine Regression der Tumogröße, während die einzelnen Substanzen lediglich zu einer Abschwächung des Tumorwachstums führten (Abb. 25A).

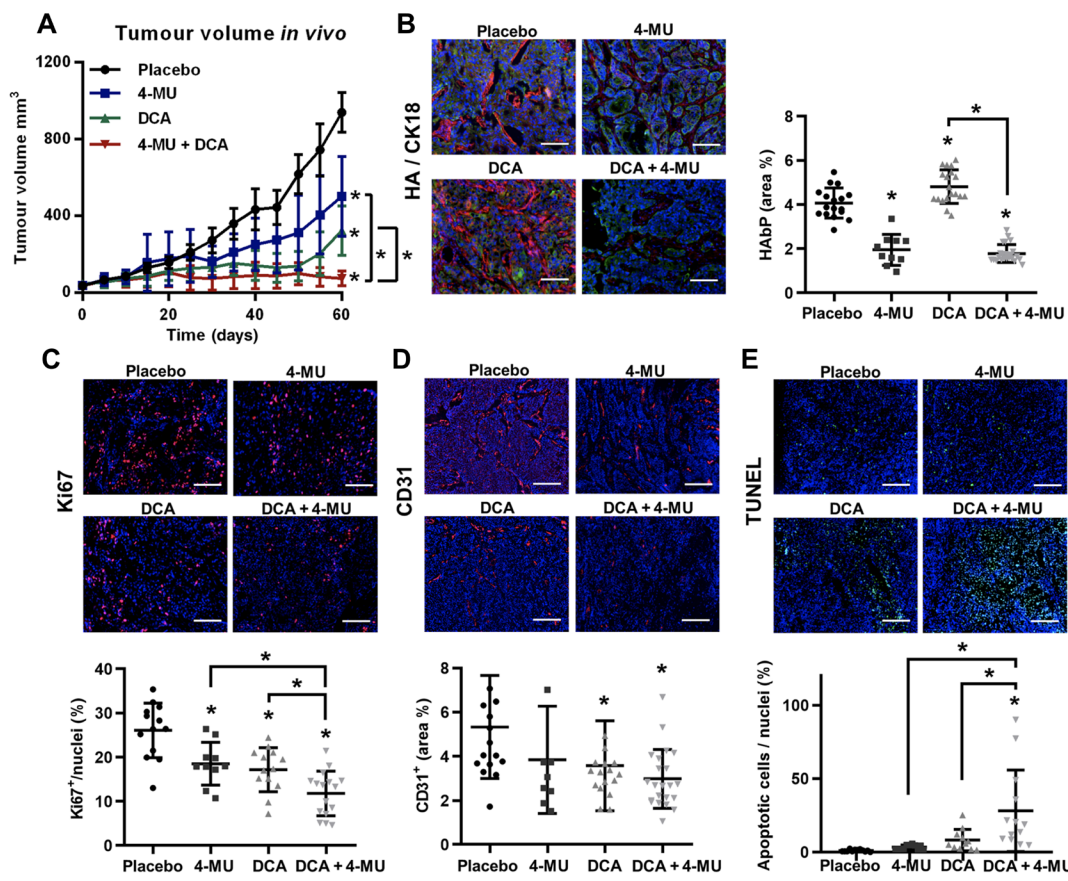


**Abb. 25: Reduktion von Tumorwachstum und -proliferation und Induktion von HA-Synthese und Apoptose durch die Kombination von DCA und 4-MU in einem Tumorregressionsmodell in vivo.**

A Die Behandlung mit den Testsubstanzen wurde begonnen, nachdem ein Tumorvolumen von  $> 30 \text{ mm}^3$  festgestellt wurde. Das Tumorwachstum wurde mit Messschiebern gemessen und über 60 Tage beobachtet. Placebo n = 15, 4-MU n = 9, Dichloroacetat n = 10, Dichloroacetat + 4-MU n = 13. Resttumoren wurden entnommen und Kryoschnitte angefertigt. Die Schnitte wurden gefärbt auf B HA (HABP, rot) im Tumor (CK18, grün) und Stroma, C proliferative Aktivität der Tumorzellen (Ki67, rot) und D Gefäße (CD31, rot). E Eine TUNEL-Färbung (grün) wurde verwendet, um die Apoptose-Rate zu messen. Repräsentative Bilder, Skalenbalken 100  $\mu\text{m}$ . Mittelwerte  $\pm$  SD. Ein-Weg-ANOVA, \*p < 0,05, signifikant verschieden von Placebo oder wie angegeben. Verwendung erfolgt mit freundlicher Genehmigung des Verlags John Wiley and Sons.

Die histologische Aufarbeitung der entsprechenden Tumorschnitte zeigte, dass die Tumoren in der **DCA** Gruppe in Übereinstimmung mit den *in-vitro*-Ergebnissen einen höheren HA-Anteil aufwiesen als die der Kontroll-Gruppe und dass **4-MU** die HA-Menge in beiden Gruppen reduzierte (**Abb. 25B**). Die Proliferationsrate, gemessen über die Anfärbung Ki67-positiver Zellkerne, verringerte sich am deutlichsten unter der Kombinationstherapie, die im Vergleich mit den Monotherapien eine nochmals signifikant erniedrigte Proliferationsrate aufwies (**Abb. 25C**). Die Vaskularisierung, quantifiziert über eine Färbung auf CD31, wurde signifikant nur in den beiden **DCA**-enthaltenden Gruppen gesenkt (**Abb. 25D**). Die Auswertung apoptotischer Zellen mittels TUNEL-Färbung ergab nur unter der Kombinationstherapie eine signifikante, stark ausgeprägte Zunahme der Apoptose (**Abb. 25E**).

Zusammenfassend wurden in dieser Arbeit verschiedene Mechanismen identifiziert, über die **DCA** die HA-Synthese verstärken kann. Die resultierende HA-reiche Mikroumgebung des Tumors stellt einen Faktor dar, der zur Chemotherapieresistenz beiträgt. Die Hemmung der HA-Synthese mittels 4-MU zeigte in Kombination mit **DCA** ausgeprägte synergistische Wirkungen auf die Proliferation und das Überleben von ESCC *in vitro* und *in vivo*. Die Kombination dieser beiden Medikamente, die bereits beim Menschen eingesetzten wurden, könnte eine interessante neue Tumortherapie darstellen.

## D. Zusammenfassung der Ergebnisse und perspektivischer Ausblick

Die Ergebnisse der in diesem Manuscript zusammengefassten Veröffentlichungen haben dazu beigetragen, die Beteiligung des HA-Systems an der Tumorprogression genauer zu verstehen, mechanistische Schnittpunkte zu weiteren zellulären Systemen, Signaltransduktionskaskaden und Stoffwechselwegen zu charakterisieren und die Funktionen der Hyaluronsäure für zelluläre Prozesse tiefer zu verstehen (Abb. 26). Durch die ausgeprägten tumorfördernden Aspekte und differentiellen Regulationen über Molekülgröße und verschiedene Rezeptoren bietet die Modulation des HA-Systems weitreichende Möglichkeiten, in die TMU einzugreifen. Entsprechend wurde daher der Einfluss verschiedener Pharmaka auf das HA-System untersucht und synergistische Substanz-Kombinationen identifiziert, die potentielle Kandidaten für eine klinische Tumor-Therapie darstellen könnten. Die Tatsache, dass viele der untersuchten Pharmaka bereits für andere Krankheitsbilder am Menschen angewandt wurden und eine gute Verträglichkeit aufweisen, erleichtert weitere Untersuchungen in klinischen Studien. Darüber hinaus zeigen die Arbeiten, dass eine Inhibition der Hyaluronsäure-Synthese ein vielversprechender Ansatz zur Verbesserung des Ansprechens auf herkömmliche zytostatische Therapieprinzipien darstellt und auch in anderen Konstellationen getestet werden sollte. Die Untersuchung der TMU erfolgt zunehmend unter der Anwendung von dreidimensionalen Kultursystemen, wie sie auch in einigen hier vorgestellten Publikationen (Kretschmer et al. 2015, Twarock et al. 2019) verwendet wurden. Eine weitere interessante Entwicklung zur Untersuchung der TMU sind Organoide und *Lab-on-Chip*-Ansätze (Baghban et al. 2020).

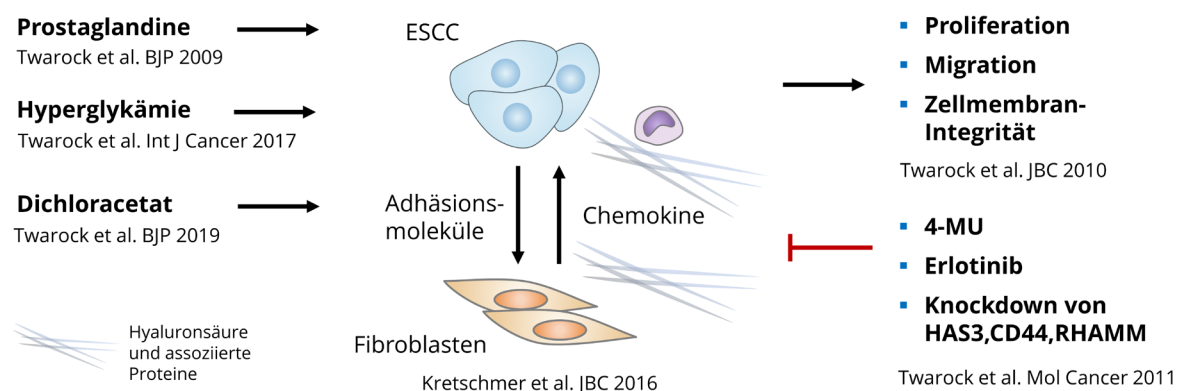


**Abb. 26: Zusammenfassung der Ergebnisse der in diesem Manuscript zusammengefassten Veröffentlichungen.** Vom Autor eigens für dieses Manuscript erstelltes Schema.

Da Fehlregulationen des HA-Systems wie eingangs beschrieben auch an der Pathogenese vieler weiterer Erkrankungen beteiligt sind, könnten die hier beschriebenen Mechanismen bezüglich der Regulation und pharmakologischen Beeinflussung des HA-Systems auch über die Tumorthерапie hinaus für andere Forschungsgebiete wie zum Beispiel kardiovaskuläre und immunologische Fragestellungen von Relevanz sein (Jiang et al. 2011, Grandoch et al. 2018, Ding et al. 2019).

Die hier vorgestellten Veröffentlichungen haben unter anderem Schnittstellen zu Systemen untersucht, die die Hyaluronsäure-Matrix beeinflussen können wie Prostaglandin-, EGFR- und Cadherin-Signalwege und metabolische Einflüsse. Ein interessanter zukünftiger Ansatz ist die Untersuchung des HA-Systems im Kontext einer Charakterisierung der übrigen Matrix-Komponenten in der Tumormikroumgebung. Bisher sind bereits einige Verbindungen zwischen HA und anderen Matrix-Komponenten bekannt. Diese im weitesten Sinne als Hyaladherine bezeichneten Proteine sind unter anderem die HA-Rezeptoren, Linker-Proteine wie TSG-6 und weitere Proteine mit HA-Bindungsstellen wie bestimmte Proteoglykane, die als Hyalektane bezeichnet werden und Aggrecan, Brevican,

Neurocan und Versican umfassen. Diese können an HA und an weitere Matrix-Bestandteile binden und so die Matrix stabilisieren. Niedermolekulare HA-Ketten und HA-Oligomere können wiederum über die Bindung an spezifische Rezeptoren eine Vielzahl an Transduktionswegen stimulieren. Weitere Hauptkomponenten der EZM sind Zucker-basierte Moleküle wie die Glykosaminoglykane, zu denen auch die HA gehört. Sie zeigen während der Krebsentwicklung deutliche Veränderungen in Molekulargewicht, Verteilung, Zusammensetzung und Modifikationen wie der Sulfatierung. Neben ihren Einsatz als diagnostische Marker werden sie als Zielstrukturen aber auch als Medikamenten-Delivery-Systeme diskutiert (Bertiaki et al. 2021). Eine Übersicht über Hyaluronsäure-bindende Proteine, Proteoglykane und beispielhafter Interaktionen zwischen Kollagen, Elastin und Hyaluronsäure bietet Abb. 27.

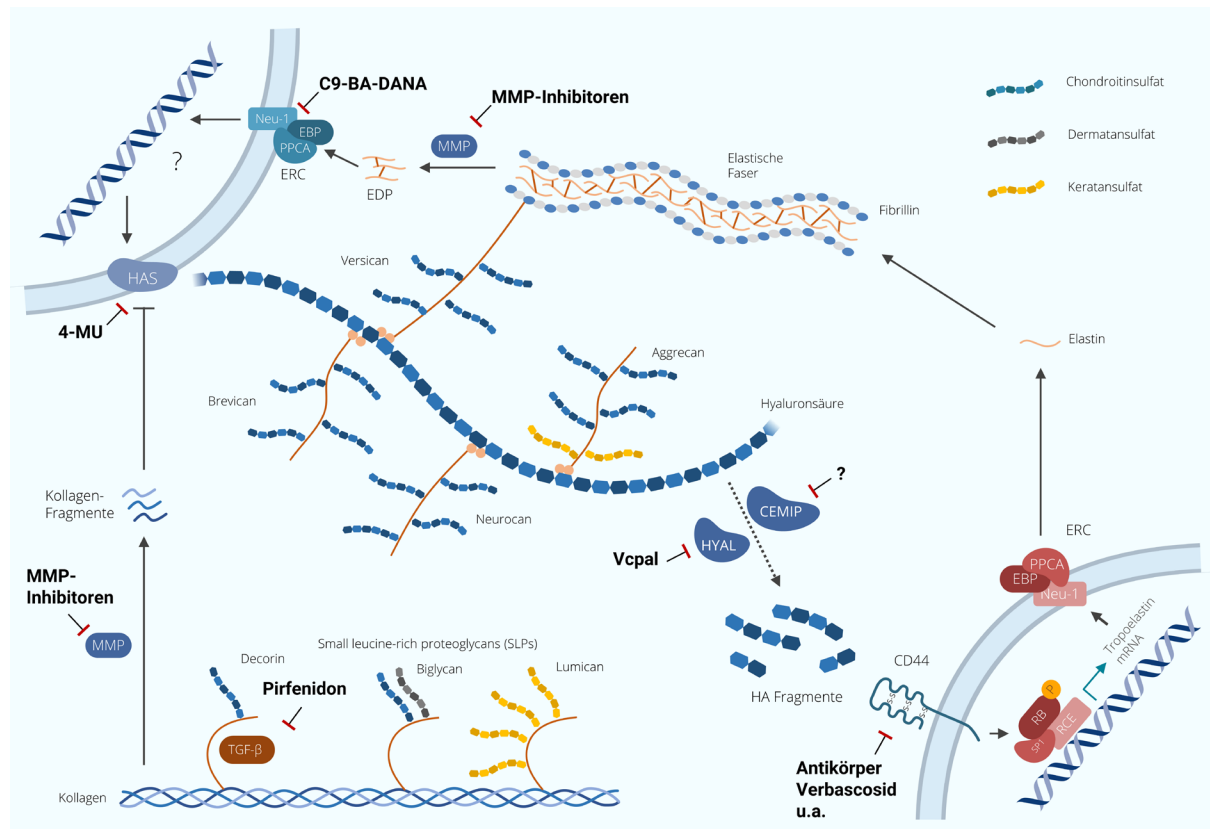


**Abb. 27:** Hyaluronsäure-bindende Proteine, Proteoglykane und Interaktionen zwischen Kollagen, Elastin und Hyaluronsäure.

ERC: Elastin-Rezeptor-Komplex, 4-MU: 4-Methylumbelliferon, PPCA: protective protein/cathepsin A, Neu-1: Neuraminidase-1, C9-BA-DANA: C9-butyl-amide-2,3-dehydro-N-acetylneurameric acid, Vcpal: Ascorbylpalmitat. Vom Autor eigens für dieses Manuskript erstelltes Schema.

Eine systematische Bestimmung dieser Zucker-basierten Moleküle erfolgt im Rahmen von Glykomik-Analysen. Es ist mittlerweile gut belegt, dass das Glykom nicht nur in Form unterschiedlicher Glykosylierungsmuster von Proteinen, sondern auch als Bestandteil von Proteoglykanen oder als eigenständige Polysaccharide für die hohe Diversität der EZM-Interaktionen verantwortlich und an vielen physiologischen und pathophysiologischen Prozessen beteiligt ist (Raghunathan et al. 2019). Die Untersuchung der kohlenhydratbasierten Strukturen der EZM ist im Gegensatz zu der Quantifizierung des intra- und extrazellulären Proteoms durch ihre Komplexität, Fragilität und Unzugänglichkeit für eine direkte analytische Messung eine Herausforderung. Der hohen Komplexität des Glykom-Netzwerks wird neuerdings zunehmend mit bioinformatischen Analysen begegnet (Kellman and Lewis 2021) und es wurden Hochdurchsatz-Analyseverfahren entwickelt, die eine Detektion der Glykan-Komponenten ermöglichen (Ricard-Blum 2020). Analog zu anderen „Omics“-Untersuchungsmethoden wird versucht,

mit dem Glykomics-Ansatz Netzwerke und Interaktionen zu identifizieren, die der Regulation spezifischer Prozesse dienen. Im Zuge der Forschungsbemühungen auf dem Gebiet der *GlycoScience* sind bereits Datenbank wie Glycosciences.DB (Bohm et al. 2019) und MatrixDB (Clerc et al. 2019) entstanden, die einen ersten Eindruck von den Möglichkeiten dieses Bereichs geben.

Aus pharmakologischer Perspektive wurden wie in der Einleitung beschrieben bereits eine Vielzahl zugelassener Arzneistoffe identifiziert, die neben ihrem Hauptwirkmechanismus als Modulatoren der extrazellulären Matrix fungieren können (Jin and Jin 2020) oder Strukturen der EZM als Hauptzielort aufweisen. Zu diesen gehören Pharmaka mit Wirkung auf Integrine, die unter anderem im kardiovaskulären Bereich (Twarock et al. 2016) oder in der Therapie der multiplen Sklerose (Polman et al. 2006) eingesetzt werden. Einen weiteren großen Forschungsbereich bilden die Inhibitoren von Matrix-abbauenden Enzymen wie die Matrix-Metallo-Protease (MMP)-Inhibitoren. Für das in diesem Manuskript beschriebene HA-System existieren bisher ebenfalls einige pharmakologische Ansätze mit niedermolekularen Substanzen. Beispiele sind der in den vorliegenden Arbeiten genutzte HA-Synthase-Inhibitor 4-MU (Kakizaki et al. 2004) und der Hyaluronidase-Inhibitor Ascorbylpalmitat (Botzki et al. 2004). Auch Für die Inhibition der CD44-Signaltransduktion wurden neben blockierenden Antikörpern (Maisel et al. 2016) mittlerweile niedermolekulare Substanzen (Liu and Finzel 2014, Wang et al. 2020) gefunden. Über die therapeutischen Möglichkeiten hinaus können die vom Tumor und der umgebenden Matrix sezernierten Moleküle auch als Marker zur Diagnose und Verlaufskontrolle der Tumorerkrankung verwendet werden (Baghban et al. 2020).

Die weitere Untersuchung der Komponenten der EZM birgt insgesamt die Möglichkeit einer Vielzahl von diagnostischen und therapeutischen Möglichkeiten nicht nur im Rahmen von neoplastischen, sondern auch kardiovaskulärer, fibrotischer und weiterer Erkrankungen. Daher bieten sich hier zukünftig unter Zuhilfenahme von Hochdurchsatzzanalysen in Kombination mit bioinformatischen Auswertungen, neuen dreidimensionalen EZM-Modellen und modernen molekularbiologischen Techniken viele interessante Ansätze zur weiteren Erforschung dieser Prozesse, die das Potential haben, die klinische Diagnostik und Therapie dieser Erkrankungen bereichern zu können.

## E. Literatur

- Arneth, B. (2019). *Tumor Microenvironment*. Medicina (Kaunas) 56(1).
- Baghban, R., Roshangar, L., Jahanban-Esfahlan, R., Seidi, K., Ebrahimi-Kalan, A., Jaymand, M., Kolahian, S., Javaheri, T. and Zare, P. (2020). *Tumor microenvironment complexity and therapeutic implications at a glance*. Cell Commun Signal 18(1): 59.
- Berdiaki, A., Neagu, M., Giataganas, E. M., Kuskov, A., Tsatsakis, A. M., Tzanakakis, G. N. and Nikitovic, D. (2021). *Glycosaminoglycans: Carriers and Targets for Tailored Anti-Cancer Therapy*. Biomolecules 11(3).
- Bohm, M., Bohne-Lang, A., Frank, M., Loss, A., Rojas-Macias, M. A. and Lutteke, T. (2019). *Glycosciences.DB: an annotated data collection linking glycomics and proteomics data (2018 update)*. Nucleic Acids Res 47(D1): D1195-D1201.
- Botzki, A., Rigden, D. J., Braun, S., Nukui, M., Salmen, S., Hoechstetter, J., Bernhardt, G., Dove, S., Jedrzejas, M. J. and Buschauer, A. (2004). *L-Ascorbic acid 6-hexadecanoate, a potent hyaluronidase inhibitor. X-ray structure and molecular modeling of enzyme-inhibitor complexes*. J Biol Chem 279(44): 45990-45997.
- Caon, I., Bartolini, B., Parnigoni, A., Carava, E., Moretto, P., Viola, M., Karousou, E., Vigetti, D. and Passi, A. (2020). *Revisiting the hallmarks of cancer: The role of hyaluronan*. Semin Cancer Biol 62: 9-19.
- Chanmee, T., Ontong, P. and Itano, N. (2016). *Hyaluronan: A modulator of the tumor microenvironment*. Cancer Lett 375(1): 20-30.
- Chanmee, T., Ontong, P., Izumikawa, T., Higashide, M., Mochizuki, N., Chokchaitaweesuk, C., Khansai, M., Nakajima, K., Kakizaki, I., Kongtawelert, P., Taniguchi, N. and Itano, N. (2016). *Hyaluronan Production Regulates Metabolic and Cancer Stem-like Properties of Breast Cancer Cells via Hexosamine Biosynthetic Pathway-coupled HIF-1 Signaling*. J Biol Chem 291(46): 24105-24120.
- Clerc, O., Deniaud, M., Vallet, S. D., Naba, A., Rivet, A., Perez, S., Thierry-Mieg, N. and Ricard-Blum, S. (2019). *MatrixDB: integration of new data with a focus on glycosaminoglycan interactions*. Nucleic Acids Res 47(D1): D376-D381.
- Currie, C. J., Poole, C. D. and Gale, E. A. (2009). *The influence of glucose-lowering therapies on cancer risk in type 2 diabetes*. Diabetologia 52(9): 1766-1777.
- Ding, H. Y., Xie, Y. N., Dong, Q., Kimata, K., Nishida, Y., Ishiguro, N. and Zhuo, L. S. (2019). *Roles of hyaluronan in cardiovascular and nervous system disorders*. J Zhejiang Univ Sci B 20(5): 428-436.
- Duan, Q., Zhang, H., Zheng, J. and Zhang, L. (2020). *Turning Cold into Hot: Firing up the Tumor Microenvironment*. Trends Cancer 6(7): 605-618.
- Duan, W., Shen, X., Lei, J., Xu, Q., Yu, Y., Li, R., Wu, E. and Ma, Q. (2014). *Hyperglycemia, a neglected factor during cancer progression*. Biomed Res Int 2014: 461917.
- Erickson, M. and Stern, R. (2012). *Chain gangs: new aspects of hyaluronan metabolism*. Biochem Res Int 2012: 893947.

- Evans, J. M., Donnelly, L. A., Emslie-Smith, A. M., Alessi, D. R. and Morris, A. D. (2005). *Metformin and reduced risk of cancer in diabetic patients*. BMJ 330(7503): 1304-1305.
- Farc, O. and Cristea, V. (2021). *An overview of the tumor microenvironment, from cells to complex networks (Review)*. Exp Ther Med 21(1): 96.
- Giovannucci, E., Harlan, D. M., Archer, M. C., Bergenstal, R. M., Gapstur, S. M., Habel, L. A., Pollak, M., Regensteiner, J. G. and Yee, D. (2010). *Diabetes and cancer: a consensus report*. Diabetes Care 33(7): 1674-1685.
- Grandoch, M., Bollyky, P. L. and Fischer, J. W. (2018). *Hyaluronan: A Master Switch Between Vascular Homeostasis and Inflammation*. Circ Res 122(10): 1341-1343.
- Hanahan, D. and Weinberg, R. A. (2000). *The hallmarks of cancer*. Cell 100(1): 57-70.
- Hanahan, D. and Weinberg, R. A. (2011). *Hallmarks of cancer: the next generation*. Cell 144(5): 646-674.
- Hashemi Goradel, N., Najafi, M., Salehi, E., Farhood, B. and Mortezaee, K. (2019). *Cyclooxygenase-2 in cancer: A review*. J Cell Physiol 234(5): 5683-5699.
- Huang, W., Ren, H., Ben, Q., Cai, Q., Zhu, W. and Li, Z. (2012). *Risk of esophageal cancer in diabetes mellitus: a meta-analysis of observational studies*. Cancer Causes Control 23(2): 263-272.
- Jee, S. H., Ohrr, H., Sull, J. W., Yun, J. E., Ji, M. and Samet, J. M. (2005). *Fasting serum glucose level and cancer risk in Korean men and women*. JAMA 293(2): 194-202.
- Jiang, D., Liang, J. and Noble, P. W. (2011). *Hyaluronan as an immune regulator in human diseases*. Physiol Rev 91(1): 221-264.
- Jin, M. Z. and Jin, W. L. (2020). *The updated landscape of tumor microenvironment and drug repurposing*. Signal Transduct Target Ther 5(1): 166.
- Kakizaki, I., Kojima, K., Takagaki, K., Endo, M., Kannagi, R., Ito, M., Maruo, Y., Sato, H., Yasuda, T., Mita, S., Kimata, K. and Itano, N. (2004). *A novel mechanism for the inhibition of hyaluronan biosynthesis by 4-methylumbellif erone*. J Biol Chem 279(32): 33281-33289.
- Kellman, B. P. and Lewis, N. E. (2021). *Big-Data Glycomics: Tools to Connect Glycan Biosynthesis to Extracellular Communication*. Trends Biochem Sci 46(4): 284-300.
- Kobayashi, T., Chanmee, T. and Itano, N. (2020). *Hyaluronan: Metabolism and Function*. Biomolecules 10(11).
- Kretschmer, I., Freudenberg, T., Twarock, S. and Fischer, J. W. (2015). *Synergistic effect of targeting the epidermal growth factor receptor and hyaluronan synthesis in oesophageal squamous cell carcinoma cells*. Br J Pharmacol.
- Kretschmer, I., Freudenberg, T., Twarock, S., Yamaguchi, Y., Grandoch, M. and Fischer, J. W. (2016). *Esophageal Squamous Cell Carcinoma Cells Modulate Chemokine Expression and Hyaluronan Synthesis in Fibroblasts*. J Biol Chem 291(8): 4091-4106.
- Landman, G. W., Kleefstra, N., van Hateren, K. J., Groenier, K. H., Gans, R. O. and Bilo, H. J. (2010). *Metformin associated with lower cancer mortality in type 2 diabetes: ZODIAC-16*. Diabetes Care 33(2): 322-326.

Lau, A. N. and Heiden, M. G. V. (2020). *Metabolism in the Tumor Microenvironment*. Annual Review of Cancer Biology 4(1): 17-40.

Liu, L. K. and Finzel, B. C. (2014). *Fragment-based identification of an inducible binding site on cell surface receptor CD44 for the design of protein-carbohydrate interaction inhibitors*. J Med Chem 57(6): 2714-2725.

Mahase, E. (2019). *Cancer overtakes CVD to become leading cause of death in high income countries*. BMJ 366: l5368.

Maisel, D., Birzele, F., Voss, E., Nopora, A., Bader, S., Friess, T., Goller, B., Laifenfeld, D., Weigand, S. and Runza, V. (2016). *Targeting Tumor Cells with Anti-CD44 Antibody Triggers Macrophage-Mediated Immune Modulatory Effects in a Cancer Xenograft Model*. PLoS One 11(7): e0159716.

Medina, R. A. and Owen, G. I. (2002). *Glucose transporters: expression, regulation and cancer*. Biol Res 35(1): 9-26.

Montenegro, F. and Indraccolo, S. (2020). *Metabolism in the Tumor Microenvironment*. Adv Exp Med Biol 1263: 1-11.

Polman, C. H., O'Connor, P. W., Havrdova, E., Hutchinson, M., Kappos, L., Miller, D. H., Phillips, J. T., Lublin, F. D., Giovannoni, G., Wajgt, A., Toal, M., Lynn, F., Panzara, M. A., Sandrock, A. W. and Investigators, A. (2006). *A randomized, placebo-controlled trial of natalizumab for relapsing multiple sclerosis*. N Engl J Med 354(9): 899-910.

Raghunathan, R., Sethi, M. K., Klein, J. A. and Zaia, J. (2019). *Proteomics, Glycomics, and Glycoproteomics of Matrisome Molecules*. Mol Cell Proteomics 18(11): 2138-2148.

Ricard-Blum, S. (2020). *Extracellular Matrix Omics*, Springer International Publishing.

Ryu, T. Y., Park, J. and Scherer, P. E. (2014). *Hyperglycemia as a risk factor for cancer progression*. Diabetes Metab J 38(5): 330-336.

Stasinopoulos, I., Mori, N. and Bhujwalla, Z. M. (2008). *The malignant phenotype of breast cancer cells is reduced by COX-2 silencing*. Neoplasia 10(11): 1163-1169.

Stern, R., Asari, A. A. and Sugahara, K. N. (2006). *Hyaluronan fragments: an information-rich system*. Eur J Cell Biol 85(8): 699-715.

Stocks, T., Rapp, K., Bjorge, T., Manjer, J., Ulmer, H., Selmer, R., Lukanova, A., Johansen, D., Concin, H., Tretli, S., Hallmans, G., Jonsson, H. and Stattin, P. (2009). *Blood glucose and risk of incident and fatal cancer in the metabolic syndrome and cancer project (me-can): analysis of six prospective cohorts*. PLoS Med 6(12): e1000201.

Sung, H., Ferlay, J., Siegel, R. L., Laversanne, M., Soerjomataram, I., Jemal, A. and Bray, F. (2021). *Global Cancer Statistics 2020: GLOBOCAN Estimates of Incidence and Mortality Worldwide for 36 Cancers in 185 Countries*. CA Cancer J Clin 71(3): 209-249.

Sussmann, M., Sarbia, M., Meyer-Kirchrath, J., Nusing, R. M., Schror, K. and Fischer, J. W. (2004). *Induction of hyaluronic acid synthase 2 (HAS2) in human vascular smooth muscle cells by vasodilatory prostaglandins*. Circ Res 94(5): 592-600.

Theocharis, A. D., Manou, D. and Karamanos, N. K. (2019). *The extracellular matrix as a multitasking player in disease*. FEBS J 286(15): 2830-2869.

Turley, E. A., Noble, P. W. and Bourguignon, L. Y. (2002). *Signaling properties of hyaluronan receptors*. J Biol Chem 277(7): 4589-4592.

Twarock, S., Bagheri, S., Bagheri, S. and Hohlfeld, T. (2016). *Platelet-vessel wall interactions and drug effects*. Pharmacol Ther 167: 74-84.

Twarock, S., Freudenberger, T., Poscher, E., Dai, G., Jannasch, K., Dullin, C., Alves, F., Prenzel, K., Knoefel, W. T., Stoecklein, N. H., Savani, R. C., Homey, B. and Fischer, J. W. (2011). *Inhibition of oesophageal squamous cell carcinoma progression by in vivo targeting of hyaluronan synthesis*. Mol Cancer 10: 30.

Twarock, S., Reichert, C., Bach, K., Reiners, O., Kretschmer, I., Gorski, D. J., Gorges, K., Grandoch, M. and Fischer, J. W. (2019). *Inhibition of the hyaluronan matrix enhances metabolic anticancer therapy by dichloroacetate in vitro and in vivo*. Br J Pharmacol 176(23): 4474-4490.

Twarock, S., Reichert, C., Peters, U., Gorski, D. J., Rock, K. and Fischer, J. W. (2017). *Hyperglycaemia and aberrated insulin signalling stimulate tumour progression via induction of the extracellular matrix component hyaluronan*. Int J Cancer 141(4): 791-804.

Twarock, S., Rock, K., Sarbia, M., Weber, A. A., Janicke, R. U. and Fischer, J. W. (2009). *Synthesis of hyaluronan in oesophageal cancer cells is uncoupled from the prostaglandin-cAMP pathway*. Br J Pharmacol 157(2): 234-243.

Twarock, S., Tammi, M. I., Savani, R. C. and Fischer, J. W. (2010). *Hyaluronan stabilizes focal adhesions, filopodia, and the proliferative phenotype in esophageal squamous carcinoma cells*. J Biol Chem 285(30): 23276-23284.

Vander Heiden, M. G., Cantley, L. C. and Thompson, C. B. (2009). *Understanding the Warburg effect: the metabolic requirements of cell proliferation*. Science 324(5930): 1029-1033.

Vigneri, P., Frasca, F., Sciacca, L., Pandini, G. and Vigneri, R. (2009). *Diabetes and cancer*. Endocr Relat Cancer 16(4): 1103-1123.

Wang, C., Wang, Z., Chen, C., Fu, X., Wang, J., Fei, X., Yan, X. and Xu, R. (2020). *A low MW inhibitor of CD44 dimerization for the treatment of glioblastoma*. Br J Pharmacol 177(13): 3009-3023.

Warburg, O. (1956). *On the origin of cancer cells*. Science 123(3191): 309-314.

## F. Danksagung

Ich danke meiner Familie und allen Kollegen, die mich stets im Erreichen meiner Ziele unterstützt haben. Herrn Prof. Jens Fischer danke ich für die Ermöglichung dieser Arbeit, meinen Kollegen Frau Prof. Maria Grandoch, Herrn Prof. Thomas Hohlfeld und Herrn Prof. Joachim Schmitt danke ich für das inspirierende und positive Arbeitsumfeld. Petra Pieres und Ramona Quednau danke ich für die Hilfe beim Gelingen dieser Arbeit.

Düsseldorf, März 2022 Sören Twarock

. . .  
-- -- --  
- - - - -  
-- -- --

## **G. Originalarbeiten**

Der Abdruck der folgenden dieser Habilitationsschrift zugrundeliegenden Originalarbeiten in Erstautorenschaft erfolgt chronologisch und wie oben angegeben entweder unter Berücksichtigung der Bedingungen einer Creative Common-Lizenz, die eine freie Verwendung aller Inhalte unter Angabe der Originalquelle erlaubt oder unter der freundlichen Genehmigung des Verlages John Wiley and Sons.

## RESEARCH PAPER

# Synthesis of hyaluronan in oesophageal cancer cells is uncoupled from the prostaglandin–cAMP pathway

S Twarock<sup>1</sup>, K Röck<sup>1</sup>, M Sarbia<sup>2</sup>, AA Weber<sup>1</sup>, RU Jänicke<sup>3</sup> and JW Fischer<sup>1</sup>

<sup>1</sup>Institut für Pharmakologie, Universitätsklinikum Essen, Universität Duisburg-Essen, Essen, Germany, <sup>2</sup>Pathologie der Technischen Universität München, München, Germany, and <sup>3</sup>Laboratory of Molecular Radiooncology, Clinic and Polyclinic for Radiation Therapy and Radio-oncology, Universitätsklinikum Düsseldorf, Düsseldorf, Germany

**Background and purpose:** Cyclooxygenase-2 (COX2) and hyaluronic acid (HA) are common in tumours and both independently promote tumour progression. Furthermore, COX2-dependent synthesis of prostaglandins (PGs) stimulates HA synthase-1 (HAS1) and HAS2 mRNA expression, together with HA synthesis via the cAMP/protein kinase A pathway in vascular smooth muscle cells. Therefore, the aim of the present study was to elucidate whether COX2-mediated PGs induce transcription of HAS isoforms in cancer cells as well.

**Experimental approach:** Human oesophageal squamous cell (OSC) carcinoma specimens were characterized with respect to HA, COX2 and CD44 expression by immunohistochemistry. OSC cell lines (OSC1, OSC2) and HeLa cell lines (D98, H21) were exposed to exogenous PG analogues (100 nmol·L<sup>-1</sup>), etoricoxib (10 µmol·L<sup>-1</sup>) and forskolin (10 µmol·L<sup>-1</sup>). Subsequently, cAMP levels, HA secretion and HAS isoform expression were determined by ELISA and real-time RT-PCR (reverse transcriptase polymerase chain reaction) respectively.

**Key results:** COX2, HA and CD44 were detected immunohistochemically in >90% of human oesophageal tumour samples. Under basal conditions, OSC1 and OSC2 cells express HAS2 and HAS3, COX2 and Gα<sub>s</sub>-coupled EP<sub>2</sub> and EP<sub>4</sub> PG receptors. Neither stimulation with the PGI<sub>2</sub> analogue, iloprost, addition of exogenous PGE<sub>2</sub> nor forskolin induced HAS1 or HAS2 mRNA expression in OSC1 and OSC2 cells. Furthermore, in HeLa cells after induction of COX2 by tumour necrosis factor α and subsequent PGE<sub>2</sub> release, inhibition of COX2 by etoricoxib did not affect HAS expression or HA secretion.

**Conclusions and implications:** We conclude that in oesophageal and HeLa cancer cells, HAS1/2 expression was not responsive to the PG/cAMP pathway.

*British Journal of Pharmacology* (2009) **157**, 234–243; doi:10.1111/j.1476-5381.2009.00138.x; published online 26 March 2009

**Keywords:** oesophageal cancer; COX2; etoricoxib; prostaglandins; hyaluronic acid

**Abbreviations:** COX2, cyclooxygenase-2; HA, hyaluronic acid, hyaluronan; HAS, hyaluronic acid synthase; hSMC, human vascular smooth muscle cell; OSC, oesophageal squamous cell; PG, prostaglandin; PMA, phorbol myristate acetate; TNF-α, tumour necrosis factor α

## Introduction

Oesophageal cancer is a rare but severe form of gastrointestinal cancer that is differentiated into adenocarcinomas and squamous cell carcinomas of the oesophagus. Squamous cell carcinomas are found in the upper two-thirds of the oesophagus and are mainly induced by alcohol and cigarette smoke. Adenocarcinomas are usually found in the lower third of the oesophagus and are preceded by metaplasia, referred to as Barrett's oesophagus (Enzinger and Mayer, 2003).

Cyclooxygenase (COX) is the key enzyme during synthesis of prostanoids [prostaglandins (PGs), prostacyclin, thromboxane A<sub>2</sub>]. These important mediators account for a variety of physiological and pathophysiological processes such as inflammation, constriction and dilatation of blood vessels, regulation of platelet aggregation and control of calcium regulation. COX catalyses the production of PGH<sub>2</sub> from its precursor arachidonic acid. Downstream enzymes like PGE<sub>2</sub> synthase and prostacyclin synthase account for the transformation of PGH<sub>2</sub> into the final products of the prostanoid family. The COX enzyme exists in two isoforms, COX1 that is responsible for the production of baseline levels of prostanoids and COX2 that is induced under pathological conditions and sustains inflammation. Prostanoids bind to a set of nine prostanoid receptors (Hata and Breyer, 2004; nomenclature follows Alexander *et al.*, 2008).

Correspondence: Professor Dr Jens W Fischer, Institut für Pharmakologie, Universitätsklinikum Essen, Universität Duisburg-Essen, Hufelandstrasse 55, D-45122 Essen, Germany. E-mail: j.fischer@uk-essen.de  
Received 18 July 2008; revised 20 October 2008; accepted 4 December 2008

Over-expression of COX isoforms, especially COX2, represents a well-known correlate of malignancy in a variety of cancers including those derived from colon (Kargman *et al.*, 1995), stomach (Uefuji *et al.*, 1998), lung (Wolff *et al.*, 1998), oesophagus (Zimmermann *et al.*, 1999), pancreas (Tucker *et al.*, 1999), liver (Shiota *et al.*, 1999), as well as head and neck tumours (Chan *et al.*, 1999). Treatment with COX2 inhibitors leads to decreased proliferation of a variety of tumours such as colorectal (Coffey *et al.*, 1997), oesophageal (Zimmermann *et al.*, 1999), prostate (Liu *et al.*, 1998) and breast cancer (Hong *et al.*, 1999). These effects can be reversed by addition of exogenous PGE<sub>2</sub> or PGF<sub>2α</sub>.

Hyaluronan (hyaluronic acid; HA), an unbranched polysaccharide, is composed of 2000–25 000 disaccharides of glucuronic acid and N-acetylglucosamine. Besides hydration and expansion of extracellular spaces, HA exhibits a plethora of physiological and pathophysiological functions that play a role in diverse processes including angiogenesis and inflammation involving signalling through HA receptors, CD44 and the receptor of HA-mediated motility (RHAMM). HA is produced by three isoforms of transmembrane HA synthase enzymes (HAS1–3) that link the two precursor molecules in an alternating manner and extrude the growing HA strand to the outside of the cell. While HAS1 and HAS2 produce HA up to 10<sup>7</sup> Da, HAS3 generates HA with an apparent molecular weight of approximately 10<sup>5</sup> Da. In this context, it is important to differentiate between HA of different molecular weights, because depending on its length, HA serves different functions (Stern *et al.*, 2006). An overproduction of HA in tumour cells such as breast cancer (Auvinen *et al.*, 1997), lung cancer (Horai *et al.*, 1981), colon cancer (Ropponen *et al.*, 1998), mesothelioma (Azumi *et al.*, 1992) or pancreatic cancer (Ringel *et al.*, 1999) results in elevated proliferation, migration, invasion, angiogenesis and resistance to apoptosis and cytostatic treatment. Urinary HA excretion is also an emerging prognostic marker for bladder cancer (Golshani *et al.*, 2007). Interestingly, COX2 and HA are often found in the same cancer cells.

Thus, both COX2 and HA are involved in promoting a variety of malignancies. Recently, it was discovered that PGE<sub>2</sub> and prostacyclin induce HAS1 and HAS2 mRNA expression in human vascular smooth muscle cells (hSMCs). This was proposed to be the outcome of an EP<sub>2</sub> or IP receptor-mediated activation of protein kinase A (PKA) and an increase in cAMP, that in turn binds to the cAMP-responsive element, a transcription site in the HAS2 promoter region (Monslow *et al.*, 2004; Sussmann *et al.*, 2004; van den Boom *et al.*, 2006). Based on these findings, we proposed, as a working hypothesis, that COX2-dependent PGs induce expression of HAS isoforms that subsequently give rise to HA-rich pericellular matrices, thereby promoting the malignant phenotype of cancer cells. The aim of the present study was to test this working hypothesis in oesophageal cancer cells.

## Methods

### Cell culture

The oesophageal cancer cell lines OSC1 and OSC2 (oesophageal squamous cell) and the HeLa cell lines H21 and D98 were

described previously (Defilippi *et al.*, 1987; Sarbia *et al.*, 1997). The cells were routinely maintained as monolayer cultures in RPMI-1640 supplemented with 10% foetal bovine serum, L-glutamine, penicillin and streptomycin at 37°C and 5% CO<sub>2</sub>. For experiments, cells were subjected to serum withdrawal for 24 h and subsequently treated with the test compounds.

### Immunohistochemical analysis of human tumour samples

The tumour samples were collected for diagnostic purposes and were examined by a senior pathologist (MS). Informed consent was obtained from patients or relatives. The present study was performed according to the Declaration of Helsinki. Immunohistochemical investigations were based on 69 patients (55 male; age range: 35–81 years) with squamous cell carcinoma of the oesophagus that underwent oesophageal resection without prior radio- or chemotherapy between 1978 and 1991 at the Department of Surgery, University of Düsseldorf. Subsequently, the resection specimens were fixed in buffered 4% formaldehyde. Pathological tumour stage was determined at the Department of Pathology, University of Düsseldorf according to standard procedures. For the purpose of this study, all cases were restaged according to the current TNM classification (Wittekind *et al.*, 2002). Accordingly, 26 cases were in pathological stage IIa (37.7%), 8 in stage IIb (11.6%) and 35 in stage III (50.7%).

For each of the tumours, one paraffin block including representative, non-necrotic tumour areas was selected. Three tissue cylinders with a diameter of 0.6 mm per tumour were punched from these areas and brought into a recipient paraffin block by using a tissue arraying instrument (Beecher Instruments, Silver Spring, MD, USA). Sections (4 µm) from the tissue microarrays were mounted on Superfrost-plus slides (Langenbrinck, Teningen, Germany, Order-No 030060) for the subsequent immunohistochemical study.

Sections were immunohistochemically stained by using antibodies against COX2 (Cayman Chemical, Ann Arbor, MI, USA, 1:150) and CD44v (Sigma-Aldrich, Munich, Germany, HPA005785, 1:500). HA was detected by using biotinylated HABP (Seikagaku Corp., Tokyo, Japan; 2 µg·mL<sup>-1</sup>) as described (Ripellino *et al.*, 1985). This staining procedure on paraffin-embedded sections detects expression of both, intracellular and extracellular HA. The sections were de-paraffinized and rehydrated in graded alcohol. Subsequently, for COX2 and CD44 detection, the sections were subjected to citrate buffer (pH 6.0) in a steamer at 100°C for 20 min. Primary antibody was applied overnight at 4°C. After application of the secondary antibody, antigen detection was performed by using diaminobenzidine as chromogen. Finally, the sections were counterstained with haematoxylin. Negative controls were treated identically to the tumour samples including antigen retrieval procedure with the exception that the primary antibody was replaced by non-immune serum. In negative controls no signals were detectable.

Using light microscopy, expression of HA, COX2 and CD44 was determined by a senior pathologist (MS). Cases were considered positive for expression when cancer cells in at least one out of three tissue cylinders per tumour case showed a distinctive extracellular/cytoplasmic (HA), cytoplasmic (COX2) or membranous expression pattern (CD44). Cases

were considered negative if cancer cells in all analysable tissue cylinders per case showed no immunoreactivity.

#### RNA isolation

Total RNA from treated cells was isolated by using Tri-Reagent (Sigma-Aldrich) according to the manufacturer's protocol. The RNA was quantitated by spectroscopic analysis at 260 nm with an Eppendorf photometer.

#### Quantification of gene expression

The expression levels of HAS1, HAS2 and HAS3 were analysed by real-time RT-PCR (reverse transcriptase polymerase chain reaction). For real-time RT-PCR quantification, total RNA (1 µg) was used for cDNA synthesis, and specific primers for human HAS isoforms were generated according to the known sequences HAS1 (NM\_001523.1), HAS2 (NM\_005328.1), HAS3 (NM\_005329.2) as follows: HAS-1: fwd 5'-TACAACCAG AAGTTCTGGG-3', rev 5'-CTGGAGGTGTACTTGGTAGC-3'; HAS-2: fwd 5'-GTGGATTATGTACAGGTTGTGA-3', rev 5'-TCCAACCATGGGATCTTCTT-3'; HAS-3: fwd 5'-GAGATGTC CAGATCCTCAACAA-3', rev 5'-CCCACTAATACTGCACAC-3'; GAPDH: fwd 5'-GTGAAGTCGGAGTCACG-3', rev 5'-TGAGGTCAATGAAGGGTC-3'. The relative mRNA expression levels were determined by using GAPDH as house

keeping gene and the  $2^{[-\Delta\Delta C(T)]}$  method. Values were then expressed as fold of respective controls.

Prostaglandin receptors were detected by RT-PCR using the following sequences: EP1: fwd 5'-GCGCTGCCATCTTCTCC-3', rev 5'-GGTACTGCAGCTCATAGC-3'; EP2: fwd 5'-GCTGGA CTATGGGCAGTACG-3', rev 5'-AACAGGAGGCCTAAGGA TGG-3'; EP3: fwd 5'-TCGGGCTCTCCTCGTTGTC-3', rev 5'-AGTGAAGCCAGGCGAACAGC-3'; EP4: fwd 5'-ACTACG TGGACAAGCGATTG-3', rev 5'-TCACAGAAGCAATTGGA TG-3'; IP: fwd 5'-GCGTCCTCTCTGCGCGCTGCCCTGCT GG-3', rev 5'-GGTCCCCATCTCACTGCTGTCAGG-3'.

#### Determination of the HA concentration

Cells were plated at a density of  $10^5$  cells per well in a 6 well plate and allowed to adhere for 24 h. The cells were cultured with or without stimulus for 6–24 h. HA released into the culture medium was quantified by using a commercially available assay based on HA-binding protein according to the manufacturer's instructions (Corgenix, Broomfield, CO, USA). Secreted HA was normalized to total cellular protein.

#### Quantification of PGI<sub>2</sub> and PGE<sub>2</sub> levels

Cell culture supernatants were collected at the indicated times and the concentration of 6-oxo-PGF<sub>1α</sub>, the stable hydrolysis

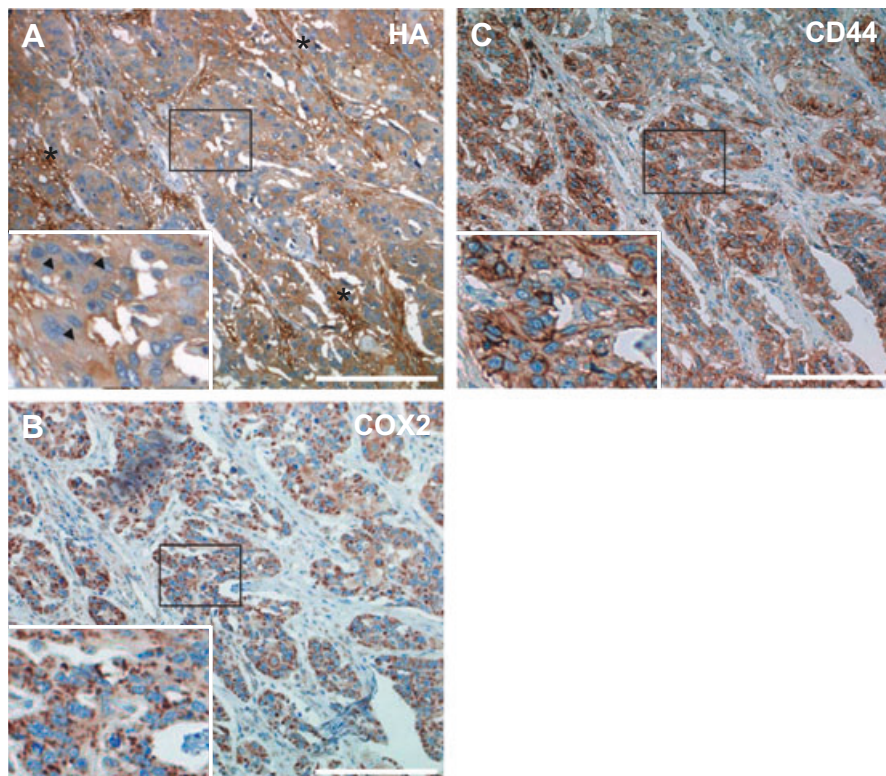


**Figure 1** Immunohistochemical detection of hyaluronic acid (HA), cyclooxygenase-2 (COX2) and CD44 in human oesophageal cancer tissue. Shown are sections of human oesophageal tumours, representative for 69 cases. To assess the spatial relationships of HA, COX2 and CD44, consecutive sections were stained. HA (A) was detected in both tumour cell parenchyma and stromal cells; asterisks indicate accumulation of HA in tumour stroma; inset, magnification of the indicated area of a tumour cell cluster demonstrating HA within the cancer cells as well (arrowheads). COX2 (B) and the HA receptor CD44 (C) were detected mainly in tumour cell islands. Taken together, the majority (>90%) of the specimens displayed a strong expression of all three proteins. The micrographs show representative sections (scale bar marks 200 µm).

product of PGI<sub>2</sub>, was determined by radioimmunoassay (RIA) as described previously (Sussmann *et al.*, 2004). PGE<sub>2</sub> was quantified by use of a commercially available ELISA assay (Prostaglandin E<sub>2</sub> EIA Kit – Monoclonal, Cayman Chemical, Ann Arbor, MI, USA).

#### *Measurement of intracellular cAMP concentrations*

Cells were seeded in 6 well plates in serum-free medium for 72 h. Then, the cells were washed twice with 2 mL of a balanced salt solution containing 130 mmol·L<sup>-1</sup> NaCl, 5.4 mmol·L<sup>-1</sup> KCl, 1.8 mmol·L<sup>-1</sup> CaCl<sub>2</sub>, 0.8 mmol·L<sup>-1</sup> MgCl<sub>2</sub>, 5.5 mmol·L<sup>-1</sup> glucose and 20 mmol·L<sup>-1</sup> HEPES, pH 7.3. Stimuli were added for 10 min. The reaction was stopped by removing the buffer and by addition of ice-cold ethanol (96%). Following evaporation of the ethanol, intracellular cAMP levels were determined by an RIA as described previously (Schröder and Schröer, 1993). All experiments were carried out in triplicate.

#### *Data analysis*

Data are presented as means  $\pm$  SEM of the indicated number of independent experiments. Statistical comparisons between groups were performed by using one-way ANOVA followed by the Bonferroni post test. A *P*-value  $<0.05$  was considered significant.

#### *Materials*

Reagents for RT-PCR and real-time RT-PCR were obtained from Qiagen (Hilden, Germany) and Invitrogen (Karlsruhe,

Germany). All cell culture reagents were obtained from Invitrogen or Sigma-Aldrich (Munich, Germany). Iloprost was kindly provided by Schering AG (Berlin, Germany). Forskolin, PGE<sub>2</sub> and human recombinant tumour necrosis factor  $\alpha$  (TNF- $\alpha$ ) were purchased from Sigma-Aldrich. Etoricoxib was bought from WITEGA Laboratorien Berlin-Adlershof GmbH (Berlin, Germany).

## Results

#### *Expression of HA, COX2 and CD44 in human oesophageal cancer sections*

Due to technical reasons, that is, detachment of tissue sections during immunohistochemical staining, only a subset of the 69 cases could be evaluated for expression of HA (61/69), COX2 (61/69) and CD44 (58/69). Expression of COX2 and CD44 was found in 100% of informative tumour samples, whereas accumulation of HA was found in 57 out of 61 samples (Figure 1A–C). HA was detected in tumour parenchyma (Figure 1A, inset, arrowheads) and even more pronounced in stromal cells (Figure 1A, asterisks). Because there is evidence that cancer cells tend to express large CD44 variants (Ponta *et al.*, 1994; 2003), an antibody detecting long CD44 variants was used. In consecutive sections CD44 and COX2 staining was observed in the cancer cells, whereas the stroma was predominantly negative (Figure 1B,C). Taken together, in the majority of cases co-localization of HA, COX2 and CD44 was observed in the cancer cells. Therefore, we

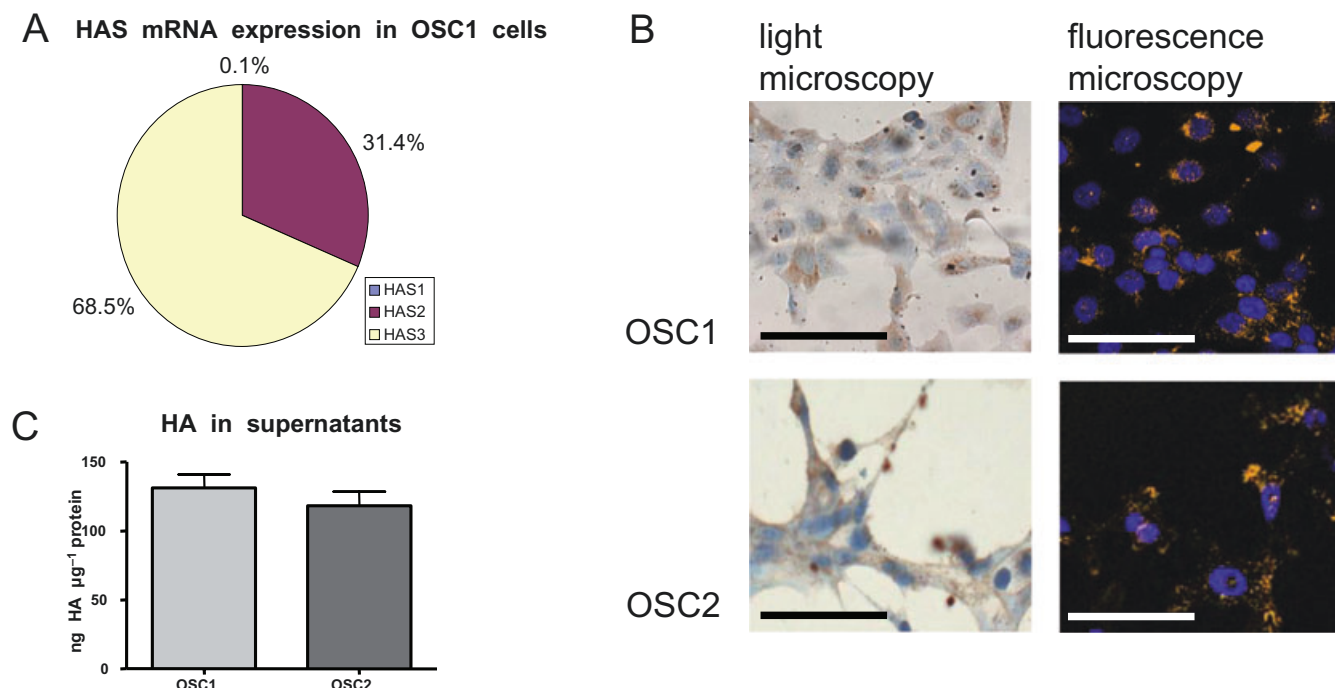


**Figure 2** Characterization of the hyaluronan system of oesophageal cancer cell lines (OSC1 and OSC2). (A) Expression of HAS2 and HAS3 in OSC1 and OSC2 cells was determined by quantitative real-time RT-PCR. In both cell lines, HAS1 mRNA expression was only barely detectable, whereas HAS2 and HAS3 could be detected in OSC1 cells at a ratio of about 1:2. In OSC2 cells, only HAS3 mRNA was detected (data not shown). (B) Affinity cytochemical staining showed membrane-bound patches of HA. Detection was performed by light microscopy (left column) and fluorescence staining (right column). The micrographs show representative reactions (scale bar marks 50 µm). (C) The quantification of HA in the supernatants of OSC1 and OSC2 cells revealed approximately equal amounts of secreted HA normalized to protein in both cell lines. Representative data from experiments are shown. HA, hyaluronic acid, hyaluronan; HAS, hyaluronic acid synthase; OSC, oesophageal squamous cell; RT-PCR, reverse transcriptase polymerase chain reaction.

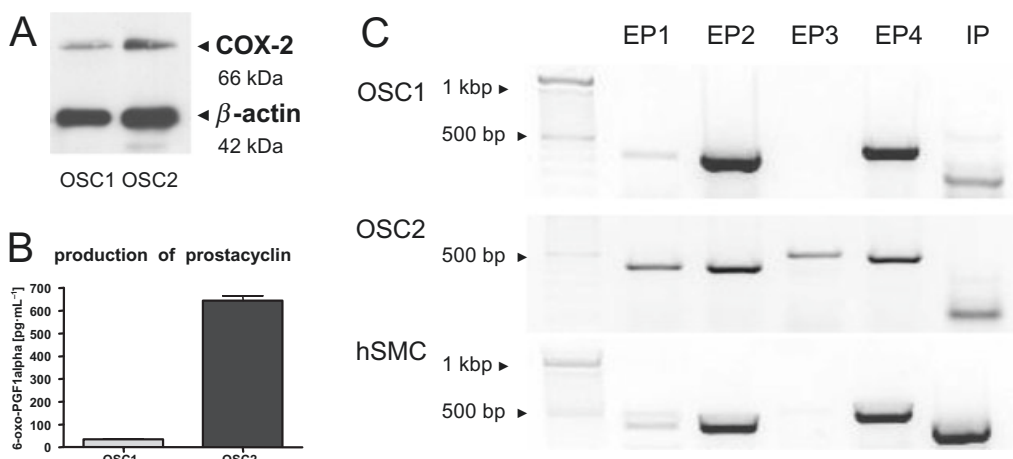


**Figure 3** Characterization of the COX2/PG system in OSC1 and OSC2 cells. (A) As shown by immunoblotting, COX2 was more abundantly expressed in OSC2 cells than in OSC1 cells. One representative immunoblot out of three is shown. (B) To determine the amount of PGs secreted by OSC1 and OSC2 cells, the prostacyclin metabolite, 6-oxo-PGF<sub>1</sub> <sub>$\alpha$</sub> , indicative of PG synthesis was determined in the supernatant. OSC2 cells produced approximately 12-fold more prostacyclin than OSC1 cells ( $n = 3$ , mean  $\pm$  SEM). (C) Expression of PG receptors by OSC1 and OSC2 cells was assessed by RT-PCR. Human smooth muscle cells were examined as control. All cells expressed EP<sub>1</sub>, EP<sub>2</sub>, EP<sub>4</sub> and IP receptors. Only OSC2 cells additionally expressed marked amounts of EP<sub>3</sub> receptor. Receptor bands were found at the expected sizes, EP<sub>1/2</sub> (450 bp), EP<sub>3/4</sub> (580 bp), IP (380/520 bp). Shown are the results of one representative experiment out of three. COX2, cyclooxygenase-2; hSMC, human vascular smooth muscle cell; OSC, oesophageal squamous cell; PG, prostaglandin; RT-PCR, reverse transcriptase polymerase chain reaction.

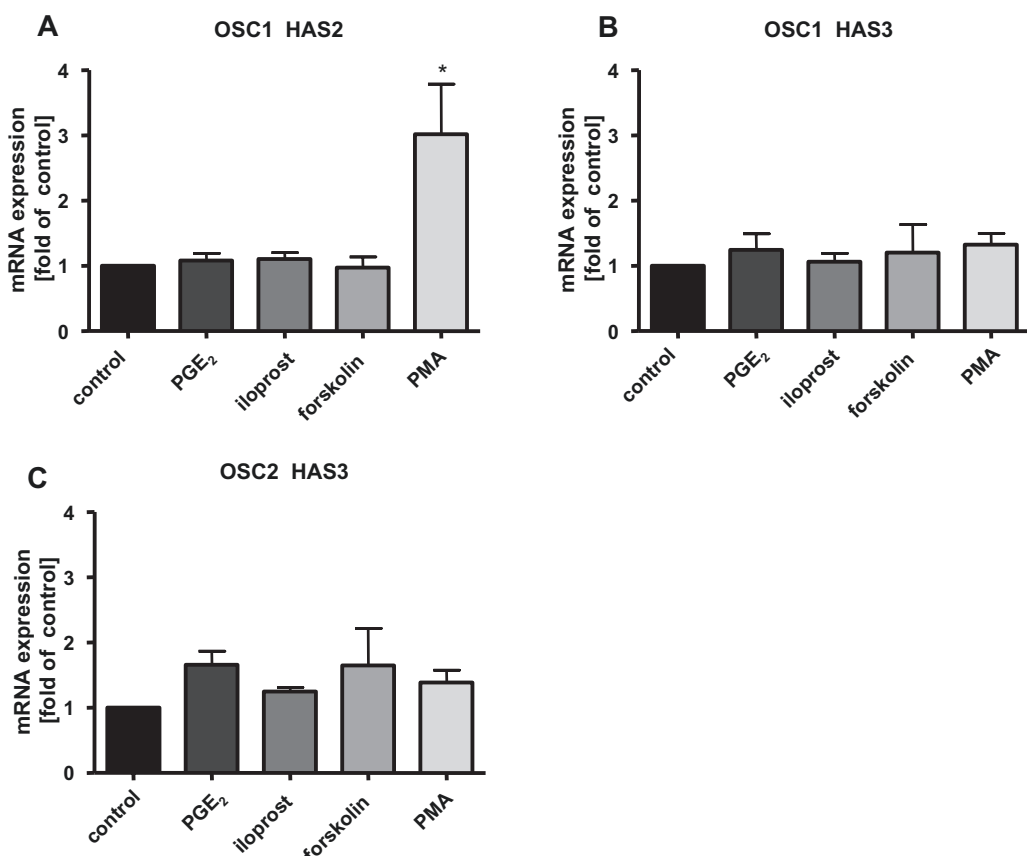


**Figure 4** HAS isoform expression in OSC1 and OSC2 cells. Cells were stimulated for 6 h with the prostacyclin (PGI<sub>2</sub>) analogue, iloprost (100 nmol·L<sup>-1</sup>), PGE<sub>2</sub> (100 nmol·L<sup>-1</sup>), forskolin (10  $\mu$ mol·L<sup>-1</sup>) or with PMA (100 nmol·L<sup>-1</sup>) as a positive control. Shown are the results of one real-time RT-PCR out of three to five independent experiments (mean  $\pm$  SEM, \* $P < 0.05$ ). The HAS2/3 mRNA expression was normalized to GAPDH. Surprisingly, neither PGE<sub>2</sub> nor iloprost or forskolin induced HAS2 mRNA in either cell line [OSC1, (A); OSC2, not shown]. Only PMA led to a strong increase of HAS2 mRNA transcription in OSC1 cells (A). HAS3 mRNA levels were not altered by any stimulus (B,C), HAS1 mRNA was not detectable (not shown). HAS, hyaluronic acid synthase; OSC, oesophageal squamous cell; PG, prostaglandin; PMA, phorbol myristate acetate; RT-PCR, reverse transcriptase polymerase chain reaction.

analysed *in vitro* whether COX2-dependent PGs would induce HA production in human oesophageal cancer cells.

#### Characterization of the HA system in the oesophageal cancer cell lines OSC1 and OSC2

Two oesophageal cancer cell lines exhibiting a different expression pattern of HAS isoforms were used in the subsequent experiments. In OSC1 cells, HAS2 and HAS3 mRNA were highly expressed at a ratio of about 1:2, while HAS1 mRNA was undetectable (Figure 2A). OSC2 cells, in contrast, only expressed HAS3 (not shown). HA was regularly found in both cell lines as pericellular HA as well as secreted HA in their supernatants. As shown by affinity cytochemistry, pericellular HA was distributed in both cell types as membrane-bound patches (Figure 2B), and both cell lines produced also approximately the same amount of HA (Figure 2C).

#### COX2 expression, PG production and PG receptor expression in OSC cells

Cyclooxygenase expression and activity in OSC1 and OSC2 cells were measured on protein and product level respectively. As shown by immunoblotting, COX was found to be constitutively expressed in both cell lines with OSC2 cells displaying a stronger protein expression, which is in accordance with a previous study (Zimmermann *et al.*, 1999) (Figure 3A). As an indicator for COX2 activity, the secretion of PGI<sub>2</sub> was quan-

tified. Consistent with the COX2 protein expression levels, PGI<sub>2</sub> levels were approximately 12 times higher in OSC2 cells compared with OSC1 cells (Figure 3B). Also the mRNAs of the corresponding prostacyclin (IP) and PGE receptors (EP<sub>1</sub>, EP<sub>2</sub>, EP<sub>4</sub>) were differentially expressed in both cell lines. Whereas OSC1 cells were found to abundantly express only the Gα<sub>i</sub>-coupled EP<sub>2</sub>, EP<sub>4</sub> and IP receptors, OSC2 cells expressed mRNA of all EP receptors and the IP receptor (Figure 3C).

#### Stimulation of OSC1 and OSC2 cells with PGs did not alter HAS isoform expression

Next we stimulated the cells with the prostacyclin (PGI<sub>2</sub>) analogue iloprost or with PGE<sub>2</sub> to assess their influence on HAS mRNA expression. Surprisingly, neither PGE<sub>2</sub> nor iloprost induced HAS1 mRNA or HAS2 mRNA in either OSC1 or OSC2 cells despite the fact that both cell lines abundantly express the IP, EP<sub>2</sub> and EP<sub>4</sub> receptors (see Figure 3C). To preclude the possibility that this deficiency is caused by a lack of cAMP induction due to inactive PG receptors, forskolin, an adenylylate cyclase activator was used to raise cAMP levels independently of PG receptor activity. However, forskolin had also no effect on the expression of the HAS2 mRNA (Figure 4A). Only phorbol myristate acetate (PMA), an activator of PKC that was used as a positive control, resulted in a strong increase in HAS2 mRNA transcription (Figure 4A). As, with the exception for PMA, none of the stimuli used was able to induce HAS2 mRNA expression, we hypothesized that HAS transcription

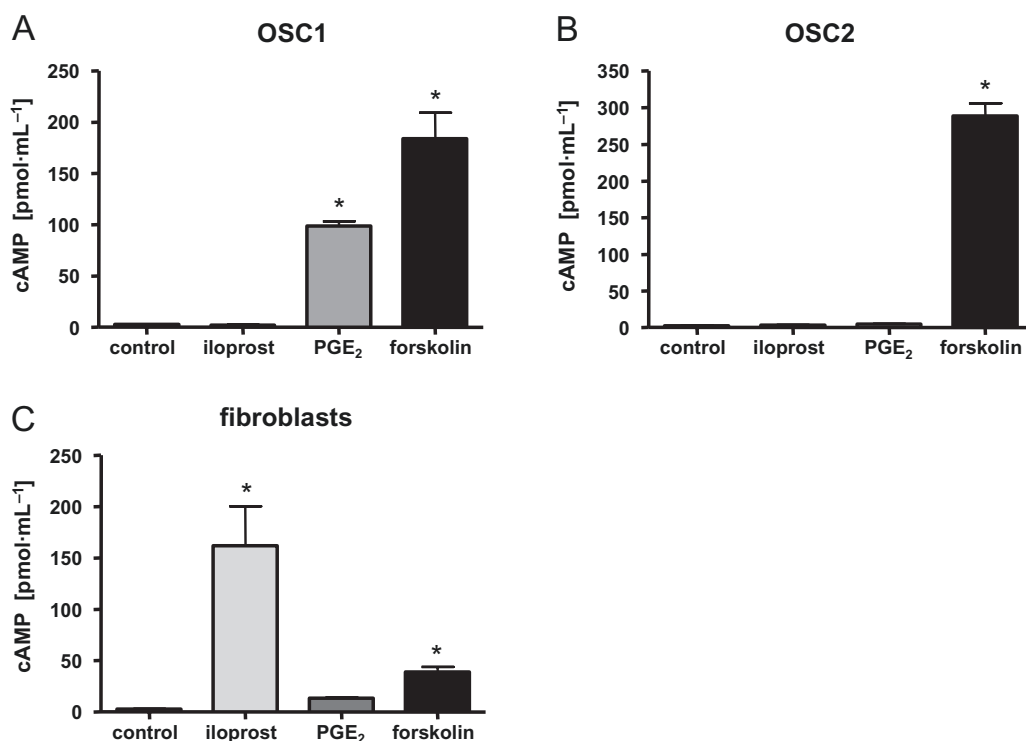


**Figure 5** Intracellular cAMP levels after stimulation of OSC1 and OSC2 cells and fibroblasts by iloprost, PGE<sub>2</sub> and forskolin. Intracellular cAMP levels were determined by radioimmunoassay. To examine the cAMP response, OSC1 (A) and OSC2 (B) cells were stimulated with agents known to induce cAMP levels. Human skin fibroblasts (C) were used as a positive control. Iloprost failed to induce cAMP increase in OSC1 and OSC2 cells, whereas it was able to raise cAMP levels in fibroblasts (C). PGE<sub>2</sub> stimulated cAMP production only in OSC1 cells (A), whereas forskolin led to an increase in cAMP levels in all tested cell types. Representative results from four independent experiments are shown and displayed as mean ± SEM; asterisk indicates a  $P$ -value  $< 0.05$ . OSC, oesophageal squamous cell; PG, prostaglandin.

might be uncoupled from the cAMP system in oesophageal cancer cells. In addition, HAS3 mRNA levels were not altered by any stimulus in either cell line (Figure 4B,C).

#### Induction of cAMP levels in response to prostaglandins

To verify that PG receptors were active and coupled to the  $G\alpha_s$  subunits in OSC cells, we performed cAMP assays to measure the activation of adenylyl cyclase in response to PGs. In contrast to the positive control in hSMCs (data not shown) and fibroblasts (Figure 5C), activation of the IP receptor by iloprost did not lead to an increase of cAMP in either OSC1 or OSC2 cells, suggesting that IP receptors are inactive (Figure 5A,B). On the other hand, PGE<sub>2</sub> stimulation resulted in a strong cAMP response, however, only in OSC1 cells (Figure 5A). The lack of a cAMP response in OSC2 cells might be due to receptor down-regulation because of the high endogenous PG levels in these cells (Figure 3B). Forskolin significantly increased cAMP levels in all examined cell lines proving the presence of functional adenylyl cyclase (Figure 5A–C). Thus, in OSC2 cells, both the IP and the EP receptors (EP<sub>2</sub> and EP<sub>4</sub>) did not induce cAMP formation, which may explain why HAS2 expression was not affected by PGs in these cells. However, in OSC1 cells, PGE<sub>2</sub> strongly induced cAMP production, suggesting that cAMP-dependent activation of HAS2 gene transcription was blocked downstream of cAMP in these cells.

#### Expression of the HAS isoforms in HeLa cells

To verify these results also in another cellular model, cancer cells known to produce large amounts of PGE<sub>2</sub> upon cytokine-induced COX2 expression were investigated. Therefore, two HeLa cell lines (D98, H21) exhibiting a TNF- $\alpha$ -inducible, COX2-dependent PG synthesis (Figure 6A,B) (Jänicke *et al.*, 1994; Totzke *et al.*, 2003) were used to assess the effects of endogenous PGE<sub>2</sub> on HAS mRNA expression. TNF- $\alpha$  had no effect on mRNA levels of HAS2 and HAS3 isoforms in both cell lines (Figure 6C,D) despite the dramatic induction of PGE<sub>2</sub> release (Figure 6A,B). Compatible with the conclusion that autocrine release of PGE<sub>2</sub> in response to TNF- $\alpha$  did not induce HAS2 or HAS3, no effect of the COX2 inhibitor etoricoxib on HAS expression was detected (Figure 6C,D). Interestingly, etoricoxib itself caused a slight induction of HAS2 in HeLa D98 cells that was, however, not significant. Taken together, these data further substantiate our conclusion that HAS mRNA expression is not regulated by PGs in cancer cells.

#### Discussion and conclusions

Previously it has been shown in hSMC that HAS1 and HAS2 are strongly induced by stimulation of the  $G\alpha_s$ -coupled IP and EP<sub>2</sub> receptors (Sussmann *et al.*, 2004; van den Boom *et al.*, 2006). Subsequently, it was reported that closure of the ductus arteriosus is also dependent on COX2-mediated PGE<sub>2</sub> synthe-

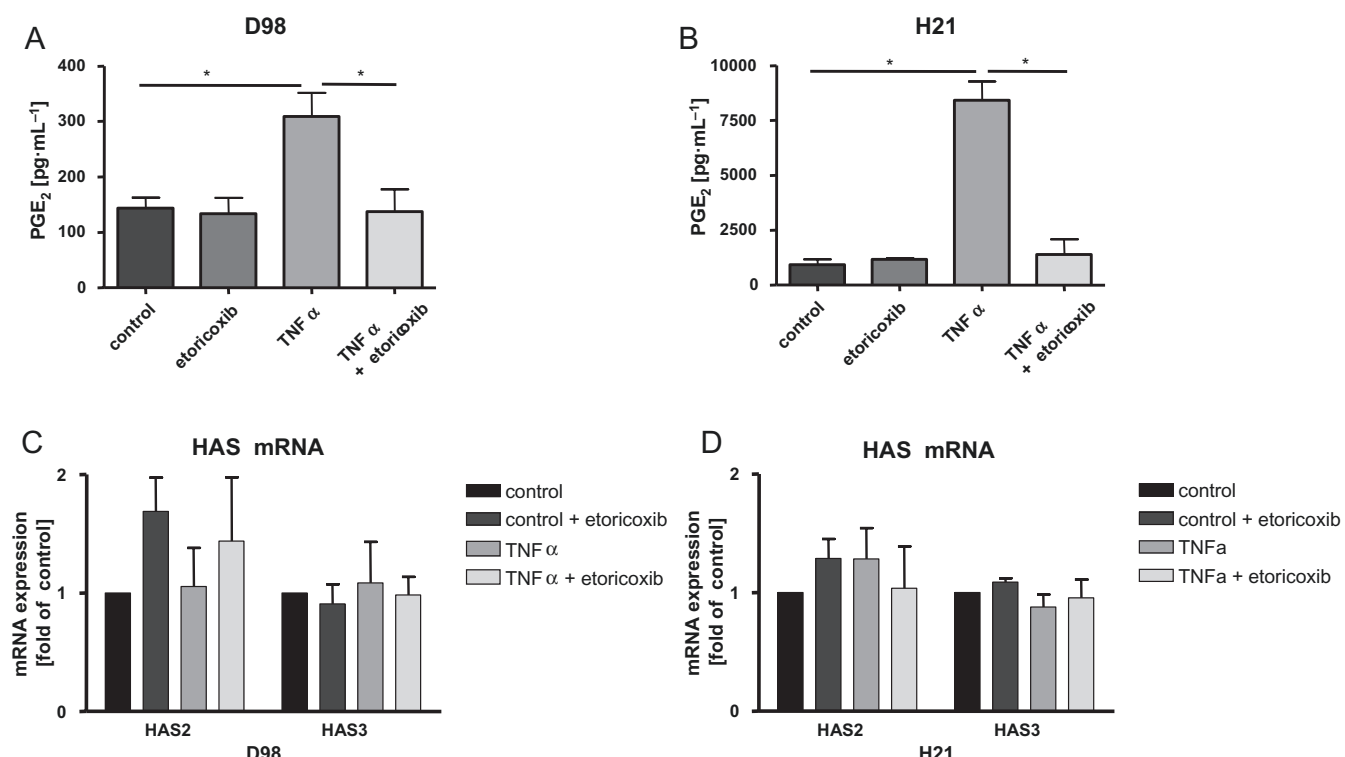


**Figure 6** HAS isoenzyme expression in HeLa cells. The HeLa cell lines D98 and H21 were stimulated with TNF- $\alpha$  (30 ng·mL<sup>-1</sup>) for 6 h in the absence or presence of the COX2 inhibitor etoricoxib (10  $\mu$ mol·L<sup>-1</sup>). The determination of PGE<sub>2</sub> levels revealed high endogenous PGE<sub>2</sub> synthesis in response to TNF- $\alpha$  that was responsive to etoricoxib (A,B). Real-time RT-PCR revealed that HAS2 and HAS3 mRNA levels were not regulated in response to COX2 and PG induction (C,D). HAS1 was not detectable (data not shown). The diagrams show representative results from three experiments (mean  $\pm$  SEM, \*P < 0.05). COX2, cyclooxygenase-2; HAS, hyaluronic acid synthase; PG, prostaglandin; RT-PCR, reverse transcriptase polymerase chain reaction; TNF- $\alpha$ , tumour necrosis factor  $\alpha$ .

sis and subsequent stimulation of HAS2-mediated HA synthesis via stimulation of the EP<sub>4</sub> receptor (Yokoyama *et al.*, 2006). Furthermore, it has been known for a long time that forskolin stimulates HA synthesis in oocytes thereby stimulating the rapid expansion of the pericellular matrix of oocytes (Fischer and Schröer, 2007). These findings suggest that the PG-mediated activation of HAS expression is a regulatory pathway of general importance. The fact that the majority of human oesophageal tumour samples were characterized by the presence of HA, COX2 and CD44 was compatible with the working hypothesis that COX2-mediated PG synthesis stimulates HA production in human tumours. However, *in vitro* in OSC1 and OSC2 cells, prostacyclin and PGE<sub>2</sub> did not induce HAS1 or HAS2 mRNA expression. In contrast, PMA, known to induce HAS2 transcription via activation of PKC (Feusi *et al.*, 1999; Pienimaki *et al.*, 2001; Anggiansah *et al.*, 2003) did up-regulate HAS transcription in both cell lines.

To investigate the reason for the absence of PG-mediated activation of HAS1/2 transcription, we analysed the prostanoid signalling pathway in more detail. RT-PCR analyses revealed that all the necessary receptors including the EP<sub>1-4</sub> and IP receptors are expressed in both OSC cell lines. Next, we pursued the question, if a loss of PG receptor-dependent induction of cAMP levels could be the reason for the lack of HAS2 induction in response to exogenous PGs. Forskolin, a direct cAMP inductor was used as positive control. Interestingly, in contrast to hSMC and fibroblasts, iloprost failed to stimulate cAMP production in either cell line. This might indicate that the IP receptor is either not expressed at the

protein level or desensitized. PGE<sub>2</sub> was able to raise cAMP levels in OSC1, but not in OSC2 cells, which are characterized by an abundant native overproduction of PGI<sub>2</sub> and PGE<sub>2</sub> (Zimmermann *et al.*, 1999) (Figure 3B), that in turn could cause a down-regulation of active EP receptors. Forskolin led to a strong increase of cAMP levels in both cell lines showing the presence of activatable adenylyl cyclase. However, forskolin failed to induce HAS2 mRNA as revealed by quantitative real-time RT-PCR (Figure 4). In conclusion, in OSC1 and OSC2 cells, the cAMP-mediated HAS2 mRNA induction might be inhibited downstream of cAMP generation. A possibility that might be considered in future studies is that epigenetic changes such as methylation of HAS2 promoter may occur. Another possibility for aberrant HAS2 mRNA expression was pointed out by Chao and Spicer who described a naturally occurring HAS2 antisense RNA (HASNT) that leads to inactivation of HAS2 gene expression (Chao and Spicer, 2005).

To further investigate the possibility that a highly elevated endogenous PG production could induce HAS2 mRNA in an autocrine manner and in turn permanently activate the HAS system, we used the two HeLa cell lines D98 and H21 that display strong COX2 induction in response to TNF- $\alpha$  (Jänicke *et al.*, 1994; Totzke *et al.*, 2003) and abundant production of PGE<sub>2</sub>. However, also in these cells no correlation between HAS mRNA expression and PGE<sub>2</sub> production was observed as indicated by the use of the COX2 inhibitor etoricoxib. These experiments show that the observed lack of response towards PG-mediated HAS expression is not restricted to oesophageal

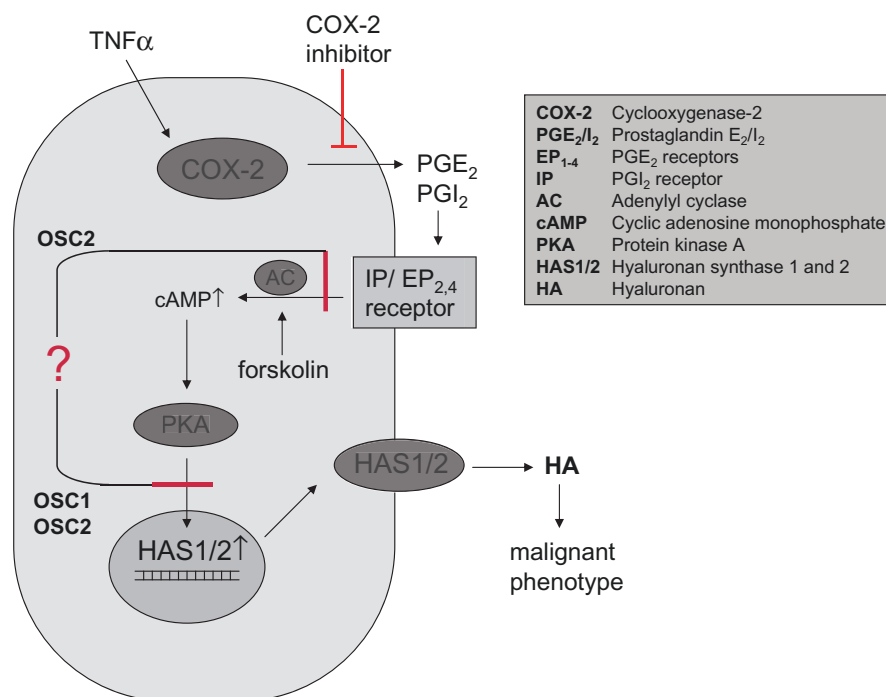


**Figure 7** Schematic illustration of the proposed stimulation of HAS isoform regulation by prostaglandins in cancer cells. According to our working hypothesis COX2-dependent prostaglandins (PGI<sub>2</sub> and PGE<sub>2</sub>) activate the G $\alpha_s$ -coupled IP and EP<sub>2/4</sub> receptors, raise intracellular cAMP levels and in turn activate HAS1 and HAS2 expression via PKA-mediated signals. The increased HA secretion stimulates a malignant tumour cell phenotype through signalling via HA receptors CD44 or receptor of HA-mediated motility (RHAMM). The present findings indicate that in oesophageal squamous cancer cells, OSC1 and OSC2, stimulation of HAS1 and HAS2 expression by prostaglandins is inhibited either at the level of prostaglandin receptor-stimulated cAMP induction (OSC2) and/or downstream of cAMP (OSC1, OSC2).

cancer cells and might therefore be relevant for cancer cells of varying origins.

Tofuku *et al.* showed that metastasis-associated properties of cancer cells such as invasion and proliferation are enhanced by lower molecular weight forms of HA that are characteristic of HAS3 activity (Itano and Kimata, 2002). In contrast, HAS2 is believed to deliver higher molecular weight HA that supports pericellular coat formation and thus inhibits a malignant tumour cell phenotype (Tofuku *et al.*, 2006) unless it is further processed by for example hyaluronidases (Stern, 2008). This hypothesis was corroborated by Bullard *et al.* (2003) who compared the primary colon carcinoma cell line SW480 and the corresponding lymph node metastasis cell line SW620. The expression levels of HAS3 mRNA were much higher in the metastasizing cells (Bullard *et al.*, 2003). Therefore, it is tempting to speculate that the observed absence of PG- and cAMP-dependent HAS2 mRNA induction is leading to a higher relative contribution of HAS3 to HA synthesis, which might support the malignant phenotype of OSC1 and OSC2 cells.

Taken together, the present data did not support our working hypothesis that COX2-dependent PGs induce HA synthesis in oesophageal cancer (Figure 7). In OSC2 cells, this is likely to have been caused by desensitized PG receptors, which did not lead to raised cAMP levels after stimulation. In OSC1 cells, the EP receptors induce cAMP levels in response to PGE<sub>2</sub>; however, HAS1 and HAS2 were not induced. Instead, we showed that in OSC1 and OSC2 cells, PG- and cAMP-dependent induction of HAS1/2 mRNA expression was not active. In future studies it should therefore be investigated whether epigenetic changes or natural occurring antisense RNA against HAS2 suppress the expression of HAS1 and HAS2 in these cancer cells.

## Acknowledgements

This research was supported by the Deutsche Forschungsgemeinschaft, SFB 612 (TP B9) and SFB728 (TP C6 and B1) and a fellowship of the Gründerstiftung zur Förderung von Forschung und wissenschaftlichen Nachwuchs an der Heinrich Heine Universität Düsseldorf.

## Conflict of interest

The authors state no conflict of interest.

## References

- Angiansah CL, Scott D, Poli A, Coleman PJ, Badrick E, Mason RM *et al.* (2003). Regulation of hyaluronan secretion into rabbit synovial joints in vivo by protein kinase C. *J Physiol* **550**: 631–640.
- Alexander SPH, Mathie A, Peters JA (2008). Guide to Receptors and Channels (GRAC), 3rd edn. *Br J Pharmacol* **153** (Suppl. 2): S1–S209.
- Auvinen PK, Parkkinen JJ, Johansson RT, Agren UM, Tammi RH, Eskelinen MJ *et al.* (1997). Expression of hyaluronan in benign and malignant breast lesions. *Int J Cancer* **74**: 477–481.
- Azumi N, Underhill CB, Kagan E, Sheibani K (1992). A novel biotinylated probe specific for hyaluronate. Its diagnostic value in diffuse malignant mesothelioma. *Am J Surg Pathol* **16**: 116–121.
- van den Boom M, Sarbia M, von Wnuck Lipski K, Mann P, Meyer-Kirchrath J, Rauch BH *et al.* (2006). Differential regulation of hyaluronic acid synthase isoforms in human saphenous vein smooth muscle cells: possible implications for vein graft stenosis. *Circ Res* **98**: 36–44.
- Bullard KM, Kim HR, Wheeler MA, Wilson CM, Neudauer CL, Simpson MA *et al.* (2003). Hyaluronan synthase-3 is upregulated in metastatic colon carcinoma cells and manipulation of expression alters matrix retention and cellular growth. *Int J Cancer* **107**: 739–746.
- Chan G, Boyle JO, Yang EK, Zhang F, Sacks PG, Shah JP *et al.* (1999). Cyclooxygenase-2 expression is up-regulated in squamous cell carcinoma of the head and neck. *Cancer Res* **59**: 991–994.
- Chao H, Spicer AP (2005). Natural antisense mRNAs to hyaluronan synthase 2 inhibit hyaluronan biosynthesis and cell proliferation. *J Biol Chem* **280**: 27513–27522.
- Coffey RJ, Hawkey CJ, Damstrup L, Graves-Deal R, Daniel VC, Dempsey PJ *et al.* (1997). Epidermal growth factor receptor activation induces nuclear targeting of cyclooxygenase-2, basolateral release of prostaglandins, and mitogenesis in polarizing colon cancer cells. *Proc Natl Acad Sci USA* **94**: 657–662.
- Defilippi P, Poupart P, Tavernier J, Fiers W, Content J (1987). Induction and regulation of mRNA encoding 26-kDa protein in human cell lines treated with recombinant human tumor necrosis factor. *Proc Natl Acad Sci USA* **84**: 4557–4561.
- Enzinger PC, Mayer RJ (2003). Esophageal cancer. *N Engl J Med* **349**: 2241–2252.
- Feusi E, Sun L, Sibalic A, Beck-Schimmer B, Oertli B, Wuthrich RP (1999). Enhanced hyaluronan synthesis in the MRL-Fas(lpr) kidney: role of cytokines. *Nephron* **83**: 66–73.
- Fischer JW, Schröer K (2007). Regulation of hyaluronan synthesis by vasodilatory prostaglandins. Implications for atherosclerosis. *Thromb Haemost* **98**: 287–295.
- Golshani R, Hautmann SH, Estrella V, Cohen BL, Kyle CC, Manoharan M *et al.* (2007). HAS1 expression in bladder cancer and its relation to urinary HA test. *Int J Cancer* **120**: 1712–1720.
- Hata AN, Breyer RM (2004). Pharmacology and signaling of prostaglandin receptors: multiple roles in inflammation and immune modulation. *Pharmacol Ther* **103**: 147–166.
- Hong SH, Avis I, Vos MD, Martinez A, Treton AM, Mulshine JL (1999). Relationship of arachidonic acid metabolizing enzyme expression in epithelial cancer cell lines to the growth effect of selective biochemical inhibitors. *Cancer Res* **59**: 2223–2228.
- Horai T, Nakamura N, Tateishi R, Hattori S (1981). Glycosaminoglycans in human lung cancer. *Cancer* **48**: 2016–21.
- Itano N, Kimata K (2002). Mammalian hyaluronan synthases. *IUBMB Life* **54**: 195–199.
- Jänicke RU, Lee FH, Porter AG (1994). Nuclear c-Myc plays an important role in the cytotoxicity of tumor necrosis factor alpha in tumor cells. *Mol Cell Biol* **14**: 5661–5670.
- Kargman SL, O'Neill GP, Vickers PJ, Evans JF, Mancini JA, Jothy S (1995). Expression of prostaglandin G/H synthase-1 and -2 protein in human colon cancer. *Cancer Res* **55**: 2556–2559.
- Liu XH, Yao S, Kirschenbaum A, Levine AC (1998). NS398, a selective cyclooxygenase-2 inhibitor, induces apoptosis and down-regulates bcl-2 expression in LNCaP cells. *Cancer Res* **58**: 4245–4249.
- Monslow J, Williams JD, Guy CA, Price IK, Craig KJ, Williams HJ *et al.* (2004). Identification and analysis of the promoter region of the human hyaluronan synthase 2 gene. *J Biol Chem* **279**: 20576–20581.
- Pienimaki JP, Rilla K, Fulop C, Sironen RK, Karvinen S, Pasonen S *et al.* (2001). Epidermal growth factor activates hyaluronan synthase 2 in epidermal keratinocytes and increases pericellular and intracellular hyaluronan. *J Biol Chem* **276**: 20428–20435.
- Ponta H, Sleeman J, Dall P, Moll J, Sherman L, Herrlich P (1994). CD44 isoforms in metastatic cancer. *Invasion Metastasis* **14**: 82–86.

- Ponta H, Sherman L, Herrlich PA (2003). CD44: from adhesion molecules to signalling regulators. *Nat Rev Mol Cell Biol* **4**: 33–45.
- Ringel J, Rychly J, Nebe B, Schmidt C, Muller P, Emmrich J et al. (1999). CD44, bFGF and hyaluronan in human pancreatic cancer cell lines. *Ann N Y Acad Sci* **880**: 238–242.
- Ripellino JA, Klinger MM, Margolis RU, Margolis RK (1985). The hyaluronic acid binding region as a specific probe for the localization of hyaluronic acid in tissue sections. Application to chick embryo and rat brain. *J Histochem Cytochem* **33**: 1060–1066.
- Ropponen K, Tammi M, Parkkinen J, Eskelinen M, Tammi R, Lippinen P et al. (1998). Tumor cell-associated hyaluronan as an unfavorable prognostic factor in colorectal cancer. *Cancer Res* **58**: 342–347.
- Sarbia M, Bosing N, Hildebrandt B, Koldovsky P, Gerharz CD, Gabbert HE (1997). Characterization of two newly established cell lines derived from squamous cell carcinomas of the oesophagus. *Anticancer Res* **17**: 2185–2192.
- Schröder H, Schröer K (1993). Prostacyclin-dependent cyclic AMP formation in endothelial cells. *Naunyn Schmiedebergs Arch Pharmacol* **347**: 101–104.
- Shiota G, Okubo M, Noumi T, Noguchi N, Oyama K, Takano Y et al. (1999). Cyclooxygenase-2 expression in hepatocellular carcinoma. *Hepatogastroenterology* **46**: 407–412.
- Stern R (2008). Hyaluronidases in cancer biology. *Semin Cancer Biol* **18**: 275–280.
- Stern R, Asari AA, Sugahara KN (2006). Hyaluronan fragments: an information-rich system. *Eur J Cell Biol* **85**: 699–715.
- Sussmann M, Sarbia M, Meyer-Kirchrath J, Nusing RM, Schror K, Fischer JW (2004). Induction of hyaluronic acid synthase 2 (HAS2) in human vascular smooth muscle cells by vasodilatory prostaglandins. *Circ Res* **94**: 592–600.
- Tofuku K, Yokouchi M, Murayama T, Minami S, Komiyama S (2006). HAS3-related hyaluronan enhances biological activities necessary for metastasis of osteosarcoma cells. *Int J Oncol* **29**: 175–183.
- Totzke G, Schulze-Osthoff K, Janicke RU (2003). Cyclooxygenase-2 (COX-2) inhibitors sensitize tumor cells specifically to death receptor-induced apoptosis independently of COX-2 inhibition. *Oncogene* **22**: 8021–8030.
- Tucker ON, Dannenberg AJ, Yang EK, Zhang F, Teng L, Daly JM et al. (1999). Cyclooxygenase-2 expression is up-regulated in human pancreatic cancer. *Cancer Res* **59**: 987–990.
- Uefuji K, Ichikura T, Mochizuki H, Shinomiya N (1998). Expression of cyclooxygenase-2 protein in gastric adenocarcinoma. *J Surg Oncol* **69**: 168–172.
- Wittekind C, Compton CC, Greene FL, Sabin LH (2002). TNM residual tumor classification revisited. *Cancer* **94**: 2511–2516.
- Wolff H, Saukkonen K, Anttila S, Karjalainen A, Vainio H, Ristimaki A (1998). Expression of cyclooxygenase-2 in human lung carcinoma. *Cancer Res* **58**: 4997–5001.
- Yokoyama U, Minamisawa S, Quan H, Ghatak S, Akaike T, Segi-Nishida E et al. (2006). Chronic activation of the prostaglandin receptor EP4 promotes hyaluronan-mediated neointimal formation in the ductus arteriosus. *J Clin Invest* **116**: 3026–3034.
- Zimmermann KC, Sarbia M, Weber AA, Borchard F, Gabbert HE, Schror K (1999). Cyclooxygenase-2 expression in human esophageal carcinoma. *Cancer Res* **59**: 198–204.

# Hyaluronan Stabilizes Focal Adhesions, Filopodia, and the Proliferative Phenotype in Esophageal Squamous Carcinoma Cells<sup>\*§</sup>

Received for publication, December 9, 2009, and in revised form, May 2, 2010 Published, JBC Papers in Press, May 12, 2010, DOI 10.1074/jbc.M109.093146

Sören Twarock<sup>†</sup>, Markku I. Tammi<sup>§</sup>, Rashmin C. Savani<sup>¶</sup>, and Jens W. Fischer<sup>†‡</sup>

From the <sup>†</sup>Institut für Pharmakologie, Universitätsklinikum Essen, Universität Duisburg-Essen, 45147 Essen, Germany, the <sup>§</sup>Institute of Biomedicine, Anatomy, University of Eastern Finland, FIN-70211, Kuopio, Finland, and the <sup>¶</sup>Divisions of Pulmonary and Vascular Biology and Neonatal-Perinatal Medicine, Department of Pediatrics, The University of Texas Southwestern Medical Center at Dallas, Dallas, Texas 75390

Hyaluronan (HA) is a polysaccharide component in the parenchyma and stroma of human esophageal squamous cell carcinoma (ESCC). Clinically, esophageal cancer represents a highly aggressive tumor type with poor prognosis resulting in a 5-year survival rate of 5%. The aim of the present study was the detailed analysis of the role of HA synthesis for ESCC phenotype *in vitro* using the ESCC cell line OSC1. In OSC1 cells, pericellular HA-matrix surrounding extended actin-dependent filopodia was detected. The small molecule inhibitor of HA synthesis, 4-methylumbelliflone (4-MU, 0.3 mM) caused loss of these filopodia and focal adhesions and inhibited proliferation and migration. In search of the underlying mechanism cleavage of focal adhesion kinase (FAK) was detected by immunoblotting. In addition, displacing HA by an HA-binding peptide (Pep-1, 500 µg/ml) and digestion of pericellular HA by hyaluronidase resulted in cleavage of focal adhesions. Furthermore, real-time reverse transcription PCR revealed that HA synthase 3 (HAS3) > HAS2 are the predominant HA-synthases in OSC1. Lentiviral transduction with shHAS3, and to a lesser extent with shHAS2, reduced intact FAK protein and filopodia as well as proliferation and migration. Furthermore, down-regulation by lentiviral shRNA of RHAMM (receptor of HA-mediated motility) but not CD44 induced loss of filopodia and caused FAK cleavage. In contrast, knockdown of both HA receptors inhibited proliferation and migration of OSC1. In conclusion, HA synthesis and, in turn, RHAMM and CD44 signaling promoted an activated phenotype of OSC1. Because RHAMM appears to support both filopodia, FAK, and the proliferative and migratory phenotype, it may be promising to explore RHAMM as a potential therapeutic target in esophageal cancer.

Hyaluronan (HA)<sup>2</sup> is produced by three isoforms of the hyaluronan synthase family (HAS1–3), which are located at the plasma membrane and extrude the growing HA polymer into the extracellular space. HAS isoenzymes produce HA of different chain lengths, and HA is subsequently degraded by hyaluronidases. HA is an unbranched high molecular weight polysaccharide that is composed of D-glucuronic acid  $\beta$ (1–3)-D-N-acetyl-glucosamine- $\beta$ (1–4) without further modifications. A variety of different types of cancer is characterized by high amounts of tumor cell-associated HA (*e.g.* colon and gastric cancer), and in some of these malignancies, such as colon cancer, tumor-associated HA is an independent prognostic factor for poor outcome (1–2). The activity of all three isoforms of the hyaluronan synthase family (HAS1–3) can be inhibited by 4-methylumbelliflone, which interferes with HAS activity by depleting the activated uridine diphosphate-glucuronic acid precursor pool (3). Consequently, 4-MU inhibits tumor progression in animal models (4–5). The biological effects of HA have largely been attributed to activation of the HA receptors RHAMM (receptor of HA-mediated motility, CD168) and CD44 (6). CD44 is an adhesion receptor and an HA receptor that serves, together with the expression of CD24 or CD133, as a surface marker for the tumorigenic potential of breast cancer and colon cancer cells (7–9) and is implicated in the HA-mediated chemoresistance of cancer cells (10). RHAMM is particularly interesting because it is a cytoplasmic protein that not only is exported into the extracellular compartment but also exerts oncogenic effects through both extracellular and intracellular functions (11–12). Importantly, RHAMM is believed to be transforming under control of RAS signaling in tumor cells (13) and to be required in part for the signaling of CD44 (11, 14). Furthermore, both CD44 and RHAMM can associate with the cytoskeleton (15–16) and control tumor cell invasiveness (17–18). In synthesis, the HA-rich matrix is important for a variety of aspects of tumor pathobiology, including anchorage-independent growth, migration, angiogenesis, suppression of apoptosis (2, 19), and metastasis (20–21).

\* This work was supported by a fellowship from the Gründerstiftung zur Förderung von Forschung und wissenschaftlichen Nachwuchs an der Heinrich Heine Universität Düsseldorf (to S. T.); National Institutes of Health Grants HL073896, HL079090, and HL075930 and the William Buchanan Chair in Pediatrics of the University of Texas Southwestern Medical Center, Dallas, TX (to R. C. S.); and the Academy of Finland, the Sigrid Juselius Foundation, and EVO Fund of Kuopio University Hospital (to M. I. T.).

§ The on-line version of this article (available at <http://www.jbc.org>) contains supplemental Fig. 1.

† To whom correspondence should be addressed: Institut für Pharmakologie, Universitätsklinikum Essen, Universität Duisburg-Essen, Hufelandstrasse 55, 45147 Essen, Germany. Tel.: 49-201-723-3460; Fax: 49-201-723-5968; E-mail: j.fischer@uk-essen.de.

<sup>2</sup> The abbreviations used are: HA, hyaluronan; ESCC, esophageal squamous cell carcinoma; 4-MU, 4-methylumbelliflone; FAK, focal adhesion kinase; HAS3, HA synthase 3; shRNA, short hairpin RNA; HABP, hyaluronan-binding protein; ERK, extracellular signal-regulated kinase; tFAK, total FAK; pFAK, phosphorylated FAK; FCS, fetal calf serum.



**TABLE 1**

shRNA sequences for lentiviral knockdown

Gene	shRNA
Human <i>HAS2</i>	5'-CCGGCGTCTCCTCTATGAAGAACACTCGAGTAGTTCTTCATAGAGGAGACGTTTG-3'
Human <i>HAS3</i>	5'-CCGGCGTCTACAACCTCTGTGTTCTCGAGAACACCAGAGAGTTGTAGAGCTTTG-3'
Human <i>RHAMM</i>	5'-CCGGCGTCTCCTATGAAGAACACTCGAGTAGTTCTTCATAGAGGAGACGTTTG-3'
Human <i>CD44</i>	5'-CCGGGCCATTAGTGAATTCAAACCTCGAGTTGAAATCAATAAGGGCTTTG-3'

With respect to esophageal cancer, it is known that HA accumulates in the parenchyma and stroma (22). However, the role of HA synthesis and the potential mechanistic links between HA synthesis, individual HAS enzymes and ESCC cell phenotype have not yet been explored.

The understanding of the role of the HA matrix in the pathophysiology of esophageal cancer may contribute to the definition of targets for novel HA-based therapeutic approaches. Therefore, the aim of the present study was to analyze the role of HA synthesis and individual HA receptors in human ESCC cells *in vitro*.

## EXPERIMENTAL PROCEDURES

**Materials**—Reagents were obtained from the indicated sources: 4-MU and latrunculin A from Sigma-Aldrich (Munich, Germany), AG82 from Calbiochem, Merck (Darmstadt, Germany); *Streptomyces* hyaluronidase from MP Biomedicals Germany (Eschwege, Germany); and a lentiviral gene silencing system MISSION™ from Sigma-Aldrich. Sequences are indicated in Table 1. Blocking anti-CD44 monoclonal antibody Hermes-1 was from Thermo Fisher Scientific (Bonn, Germany), and blocking anti-RHAMM IgG (R36) has been described previously (23). Pep-1 (GAHWQFNALTVR) and scrambled control peptide (SATPASAPYPLA) (24) were synthesized by Biosyntan (Berlin, Germany).

**Cell Culture**—OSC1 cells were a gift from M. Sarbia (25) and were used for experiments addressing molecular mechanisms throughout the present study. Key experiments were also performed in other ESCC lines (Kyse 30, -270, -410, -520)(26) obtained from DSMZ (German Collection of Microorganisms and Cell Cultures, Braunschweig, Germany). OSC1 and Kyse cells were maintained as monolayer cultures in RPMI 1640 (Sigma-Aldrich) supplemented with 10% fetal bovine serum, L-glutamine, penicillin, and streptomycin at 37 °C, 5% CO<sub>2</sub> and 95% humidified air. DNA synthesis was determined by [<sup>3</sup>H]thymidine incorporation, and migration was assessed using a microchemotaxis assay as described previously (27).

**Immunostaining**—Cultured cells were fixed for 20 min either with 3.7% paraformaldehyde in phosphate-buffered saline or with acetone:methanol (1:1) at -20 °C. HA was detected using biotinylated hyaluronan-binding protein (HABP, Seikagaku; 6 µg/ml) and fluorescein isothiocyanate- or Cy3-labeled streptavidin (Dako, Hamburg, Germany; 1:200) or Alexa 594-coupled HABP (28). Actin stress fibers were stained by fluorescein isothiocyanate-phalloidin and membranes by the membrane marker WGA Alexa Fluor® 555 conjugate (Invitrogen). Other primary antibodies used were rabbit anti-phospho-FAK (Tyr<sup>397</sup>, Santa Cruz Biotechnology; 1:500), monoclonal mouse anti-CD44H (R&D Systems, Wiesbaden, Germany; 1:500), mouse anti-paxillin (BD Transduction Laboratories; 1:500),

monoclonal mouse anti-β-tubulin I (Sigma-Aldrich; 1:20,000) and polyclonal anti-RHAMM (R36) (23). For detection, the appropriate secondary antibodies labeled either with fluorescein isothiocyanate or Cy3 (Sigma-Aldrich) were applied. Nuclei were counterstained by Hoechst 33342 solution (Invitrogen; 1:20,000).

**Blocking of RHAMM and CD44**—For blocking experiments, polyclonal anti-RHAMM (R36, 100 µg/ml) was applied for 1 h, and normal rabbit IgG (100 µg/ml) (AB-105-C, R&D Systems) was used as control. Blocking CD44 was performed by adding blocking anti-CD44 monoclonal antibody Hermes-1 (Thermo Fisher Scientific) (40 µg/ml) for 1 h, whereas control rat IgG<sub>2α</sub> (40 µg/ml) was used as control.

**Immunoblotting**—For Western blot analysis, whole cell lysates were separated on 10% SDS-PAGE and transferred to nitrocellulose, and the following primary antibodies were used: pAkt, Akt/PKB, pERK1/2, Erk1/2, pFAK (Cell Signaling Technology), FAK, cleaved FAK (C20) (Santa Cruz Biotechnology), β-actin (Abcam, Cambridge, UK), and tubulin (Sigma Aldrich) and were either detected by the appropriate horseradish peroxidase-coupled secondary antibodies or infrared fluorescent-coupled secondary antibodies, allowing fluorescent detection on a LI-COR Odyssey Infrared Imaging System.

**Determination of the HA and Proteoglycan Concentration in OSC1 Cell Culture Supernatants**—Cells were plated at a density of 10<sup>5</sup> cells per well in 6-well plates and allowed to adhere for 24 h. HA released into the culture medium was measured with an HABP-based commercial kit according to the manufacturer's instructions (Coragenix, Broomfield, CO). The quantity of HA was expressed per mg of total cellular protein. For proteoglycan secretion, cells were seeded at 2 × 10<sup>5</sup> cells per well in 6-well plates and kept for 24 h in growth medium in the presence of <sup>35</sup>SO<sub>4</sub><sup>2-</sup> (10 µCi/well, Hartmann Analytic). <sup>35</sup>S-labeled sulfated glycosaminoglycans were quantified using cetylpyridinium chloride (Sigma-Aldrich) precipitation as described by Wasteson *et al.* (29).

**Real-time Reverse Transcription-PCR**—Total RNA from OSC1 cells was isolated by using TriReagent® (Sigma-Aldrich), and cDNA was synthesized by using the Superscript III first-strand synthesis system (Invitrogen). The PCR reactions were performed by using the 7300 real-time PCR system (Applied Biosystems, Darmstadt, Germany) with SYBR Green PCR Master Mix (Applied Biosystems). Relative expression levels were compared by using real-time PCR with the 2<sup>-ΔΔC(T)</sup> method. The primer sequences of the genes of interest are given in Table 2.

**Lentiviral Knockdown**—HAS3, HAS2, CD44, and RHAMM knockdown were achieved by using the MISSION™ Lentiviral shRNA knockdown system (Sigma-Aldrich). The used shRNA

## Hyaluronan and Esophageal SCC Phenotype

sequences are stated in Table 2. A scrambled shRNA was used as a control. The transfer into the packaging line HEK 293T (ATCC) was performed with the lipofection reagent FuGENE 6 (Roche Applied Science, Mannheim, Germany). After 16 h, the

medium was changed to Iscove's modified Dulbecco's medium for better stability of the produced lentiviral particles. The next day, the lentiviruses were harvested, and target cells were transfected at a multiplicity of infection of 10 and kept for 5 days in normal growth medium before fixation.

**Statistical Analysis**—All data sets were analyzed either by analysis of variance and the Bonferroni post hoc test or by Student's *t* test as appropriate. Data are presented as means  $\pm$  S.E. Statistical significance was assigned at the level of  $p < 0.05$ .

## RESULTS

**4-MU Decreases Filopodia and Focal Adhesion Complexes**—Incubating OSC1 cells with 0.3 mM 4-MU decreased the total amount of HA secreted into the medium to  $50.7\% \pm 10.7\%$  ( $n = 3$ ,  $p < 0.05$ ) of that secreted by untreated OSC1 cells.

As a control, the effect of 4-MU on proteoglycan synthesis by incorporation of  $^{35}\text{SO}_4^{2-}$  into sulfated glycosaminoglycans chains was determined. Because 0.3 mM of 4-MU specifically inhibited HA synthesis without affecting sulfated proteoglycans ( $94.3\% \pm 1.5\%$ ,  $n = 3$  of control,  $p > 0.05$ ), this concentration was used throughout the study.

Interestingly, the shape of OSC1 cells changed remarkably in response to the inhibition of HA synthesis by 4-MU. These phenotypical changes comprised cell clustering, a uniform flat appearance, and smoother cell borders than those of untreated control cells (Fig. 1A, arrows). Moreover, a dramatic decrease in actin cytoskeleton staining (Fig. 1B) occurred in the presence of 4-MU. This finding suggests that 4-MU interferes with either actin fiber formation or actin fiber anchoring, e.g. disassembly of focal adhesion complexes. In contrast, the tubulin network remained intact in response to 4-MU (Fig. 1C, green). In addition, OSC1 regularly exhibited numerous filopodia, which were detectable by the WGA Alexa Fluor® 555 conjugate as membrane marker (Fig. 1C, red). Similar filopodia have been associated previously with tumor cell transformation (30). Notably, 4-MU caused rapid resolution of these protrusions within 1 h after application (Fig. 1C, right).

Confocal imaging of live cells that had been stained with Alexa

**TABLE 2**  
Primer sequences used for quantification of gene expression

Gene	Primer sequence
Human HAS1	5'-TACAAACCAGAACGTTCTGGG-3' 5'-CTGGAGGTGTACTTGGTAGC-3'
Human HAS2	5'-GTGGATTATGTACAGGTTGTGA-3' 5'-TCCAACCATGGGATCTTCTT-3'
Human HAS3	5'-GAGATGTCCAGATCTCAACAA-3' 5'-CCCACTAATACTGCACAC-3'
Human RHAMM	5'-GACCGTTACCATAACTATTGTC-3' 5'-CATCGATGCTCTTGGTG-3'
Human CD44	5'-GCTATTGAAAGCTTGAGAG-3' 5'-CGCAGATCGATTGAAATATAACC-3'
Human GAPDH	5'-GTGAGGTGGAGTCACAGC-3' 5'-TGAGGTCATGAAGGGGTC-3'

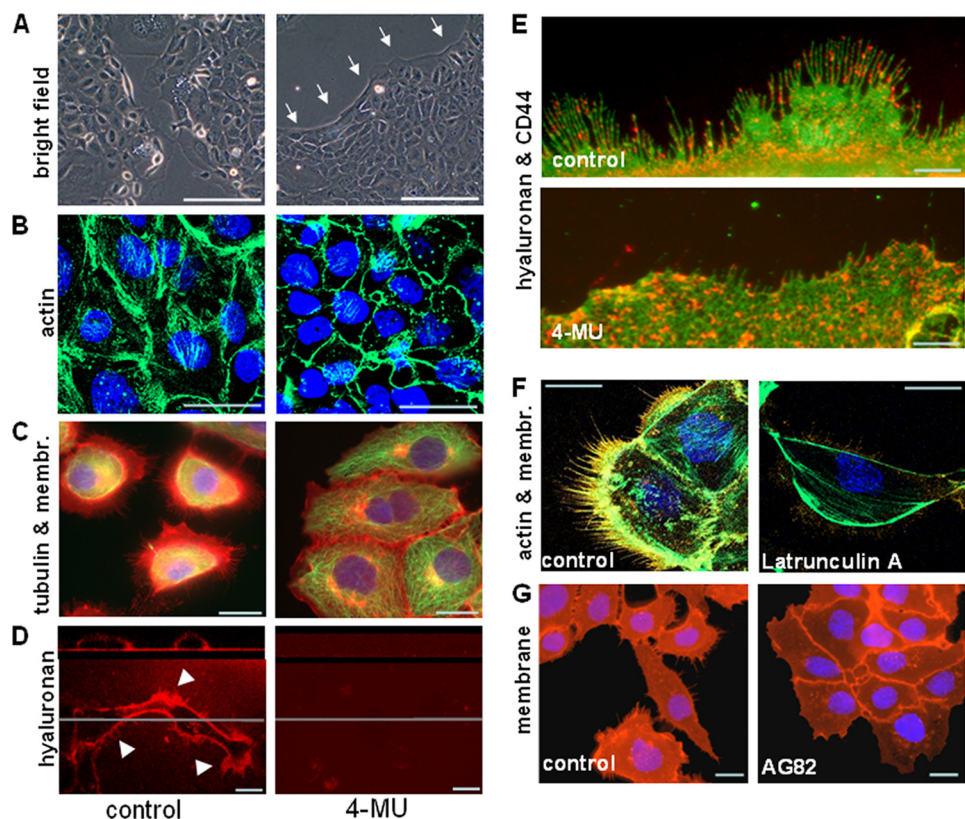


**FIGURE 1.** 4-MU causes changes in morphology, disruption of the actin cytoskeleton, and inhibition of HA-associated filopodia. *A*, treatment with 0.3 mM 4-MU for 24 h resulted in a dramatic change in the shape of OSC1 cells, including a uniform flat appearance, cluster formation, and smoother cell borders (arrows). Scale bars, 500  $\mu\text{m}$ . *B*, phalloidin staining revealed a reduction of actin cytoskeleton 24 h after the addition of 4-MU to OSC1 cells. Scale bars, 50  $\mu\text{m}$ . *C*, in controls, extensive filopodial protrusions were detected by staining of plasma membranes (membr.) with the WGA Alexa Fluor® 555 conjugate (red). The filopodia did not contain tubulin (green). Filopodia were no longer detectable 24 h after the addition of 4-MU (right panel). Scale bars, 20  $\mu\text{m}$ . *D*, the use of Alexa Fluor® 594-coupled HABP (red) during confocal microscopy of live cells showed a continuous pericellular HA coat covering also the filopodia (arrows). Hyaluronidase (20 units per ml) completely removed the pericellular HA signal (not shown). Importantly, after treatment with 4-MU for 24 h, the HA coat was no longer detectable. This finding suggests rapid turnover of the pericellular HA coat. Top, the xz-view; bottom, the xy-view. The orientation of the xz-analysis is indicated. Scale bars, 20  $\mu\text{m}$ . *E*, the association of the HA coat with the filopodia was verified in fixed OSC1 cells by immunostaining of CD44 (green) and affinity histochemistry of HA (red). Fluorescence microscopy showed that HA aggregates are still associated with the filopodia even after fixation. Scale bars, 5  $\mu\text{m}$ . *F*, staining actin (phalloidin, green) and the membrane (red) showed that the filopodia contained actin and that the filopodia were sensitive to the inhibitor of actin polymerization latrunculin A (2  $\mu\text{M}$ , 5 min). Scale bars, 20  $\mu\text{m}$ . *G*, filopodia showed a rapid response to inhibition of FAK by AG82 (10  $\mu\text{M}$ , 1 h), as shown by WGA Alexa Fluor® 555 conjugate (red). In this figure, the images compare untreated OSC1 cells in 10% FCS (control) with OSC1 treated with the indicated agents. Representative images from more than three experiments are shown. Scale bars, 20  $\mu\text{m}$ .

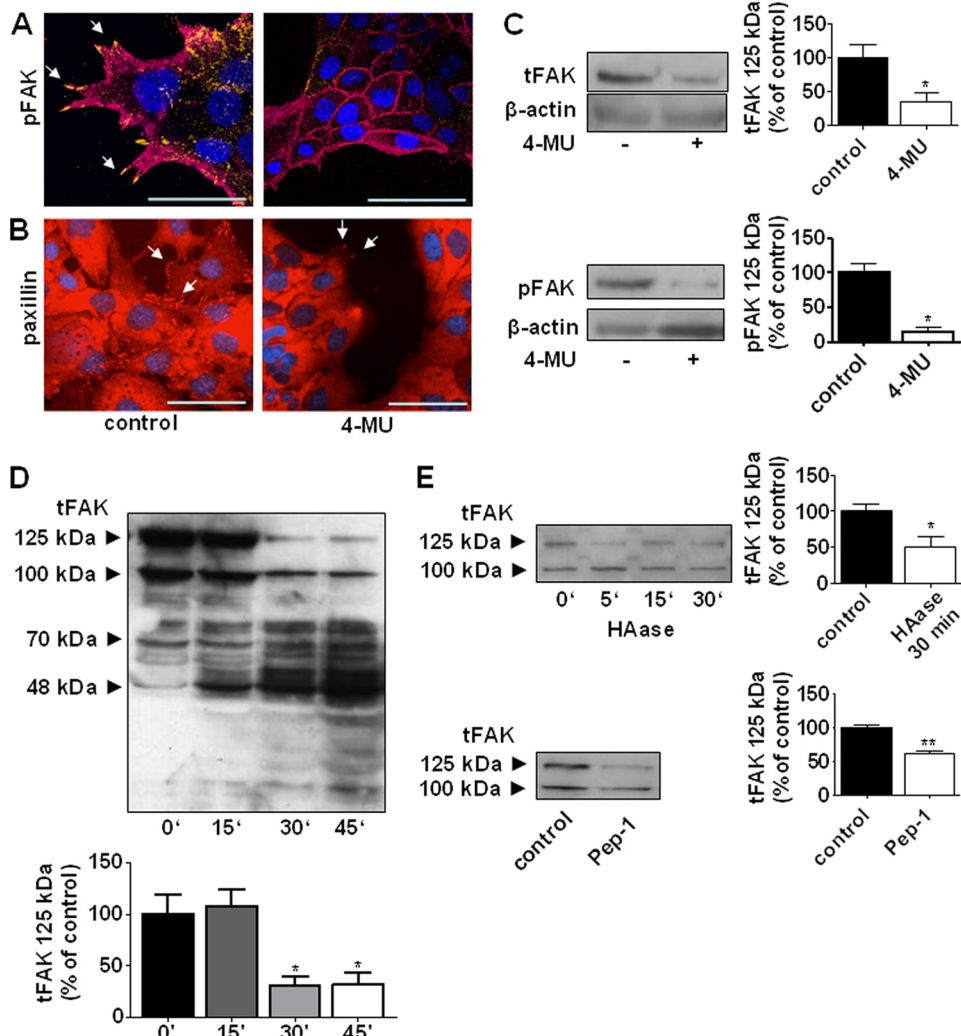


**FIGURE 2. Inhibition of HA synthesis results in FAK degradation and resolution of focal adhesion complexes.** *A*, OSC1 cells were treated for 24 h with 0.3 mM 4-MU. Double staining of CD44 (magenta) and pFAK (orange) revealed a decrease of pFAK in focal adhesions in response to treatment with 4-MU. Scale bars, 50  $\mu$ m. *B*, as an additional indication of focal adhesions, paxillin (red, arrows) was detected by immunostaining; the amount of paxillin in focal adhesions was strongly reduced by treatment with 4-MU. Scale bars, 50  $\mu$ m. *C*, immunoblots revealed strongly decreased levels of both tFAK and pFAK under the influence of 4-MU (0.3 mM, 24 h). Quantitative analysis of 125-kDa tFAK normalized to  $\beta$ -actin and to untreated control is shown. *D*, tFAK degradation in response to 4-MU began between 15 and 30 min after the application of 0.3 mM 4-MU, as detected by the use of an antibody targeting the C terminus of FAK. Quantitative data of 125-kDa tFAK are depicted below. *E*, both the digestion of pericellular HA with *Streptomyces* hyaluronidase (HAase, 5 units/ml, 5–30 min, upper panel) compared with untreated control and treatment with the HA-displacing peptide Pep-1 (500  $\mu$ g/ml, 24 h, lower panel) compared with scrambled peptide (control) led to pronounced tFAK cleavage. Quantitative data of 125-kDa tFAK are depicted. In this figure, representative immunoblots and the quantitative analysis (mean  $\pm$  S.E.,  $n = 3$ ) after densitometric scanning are presented. \*,  $p < 0.05$ ; \*\*,  $p < 0.01$  versus the respective control.

594-coupled HABP revealed a continuous pericellular HA matrix that covered the entire OSC1 cell, including the filopodial protrusions (Fig. 1*D*). Also, in fixed OSC1 cells stained for CD44 and HA, the association between HA and CD44-positive protrusions was obvious (Fig. 1*E*). Filopodia contained actin fibers as shown in Fig. 1*F*. Therefore, the inhibitor of actin polymerization latrunculin A (2  $\mu$ M, 5 min), was used to investigate the dependence of filopodia on the actin cytoskeleton. The incidence of filopodia was reduced in parallel to actin depolymerization, which began as early as 3 min after latrunculin A application (data not shown), whereas the cortical parts of the cytoskeleton were

still intact at this time. After 5 min, the inhibition of filopodia was almost complete (Fig. 1*F, right*).

Subsequently, the contribution of focal adhesion (FA) function to the maintenance of filopodia was analyzed by treatment with the FAK inhibitor AG82 (10  $\mu$ M, 1 h). AG82 completely inhibited the cell protrusions (Fig. 1*G*). Taken together, these results indicate that OSC1 cells extend actin-based filopodia that are dependent on HA synthesis and FAK activity.

**Inhibition of HA Synthesis Causes Cleavage of FAK**—To address the mechanism by which the inhibition of HA synthesis interferes with FAK and FAs, we used immunostaining of phosphorylated FAK (Fig. 2*A*, yellow) and paxillin (Fig. 2*B*, red) to analyze the distribution and activity of focal adhesion complexes after treatment with 4-MU. The levels of both pFAK and paxillin were dramatically lower in focal adhesions in response to 4-MU (24 h). In addition, we performed immunoblot analysis to measure the amount of total and phosphorylated FAK (Fig. 2*C*). In line with the results of immunofluorescence staining, these results showed a strong decrease in the levels of both total FAK (tFAK) and pFAK.

Using an antibody that detects C-terminal FAK cleavage products, we identified rapid cleavage of FAK starting between 15 and 30 min after the application of 4-MU as the reason for the reduction in tFAK (Fig. 2*D*). The most prominent bands run at 125, 100, 70, and 48 kDa; these findings are in agreement with those reported previously (31). To ensure that the

observed phenomena were specific responses to the inhibition of HA synthesis by 4-MU, we investigated the effects of other agents known to either degrade or displace HA. Indeed, we found that FAK degradation was also induced 5 min after the application of *Streptomyces* hyaluronidase (Fig. 2*E*, upper panel) and 24 h after the application of Pep-1 (500  $\mu$ g/ml), a hyaluronan binding and displacing peptide (24) (Fig. 2*E*, lower panel). To determine whether the formation of HA-dependent filopodia was specific to OSC1 or a more general phenomenon, we treated additional human ESCC cell lines with 4-MU. As shown in Fig. 3*A*, filopodia sensitive to 4-MU were detected also in other ESCC cell lines such as

## Hyaluronan and Esophageal SCC Phenotype

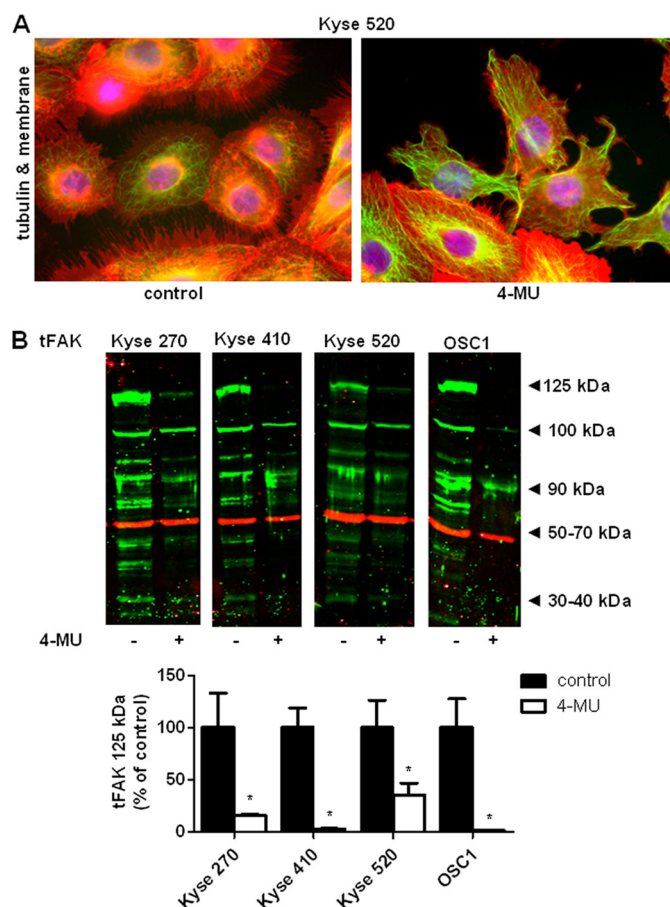


**FIGURE 3.** 4-MU inhibits filopodial protrusions and induces FAK degradation in ESCC Kyse cell lines. *A*, the ESCC cell line Kyse 520 exhibited filopodial protrusions that were sensitive to 4-MU (0.3 mM, 24 h). Cells were stained with a plasma membrane marker (WGA Alexa Fluor® 555 conjugate). *B*, FAK degradation in response to 4-MU was observed in four of five ESCC cell lines (Kyse 270, Kyse 410, Kyse 520, and OSC1) as detected by the use of an antibody targeting the C terminus of tFAK after the application of 0.3 mM 4-MU. Shown are representative immunoblots and quantitative analysis of the 125-kDa tFAK band after normalization to tubulin and as percentage of untreated controls ( $n = 3$ ; mean  $\pm$  S.E.). \*,  $p < 0.05$  versus untreated control cells.

Kyse 520. Furthermore, FAK degradation in response to 4-MU occurred in four out of five tested cell lines such as Kyse 520, 410, 270 (Fig. 3*B*). These results indicate that the pericellular HA matrix is required for filopodial plasma membrane extensions and suggest that the absence of HA results in rapid degradation of FAK and the breakdown of filopodia.

**Treatment with 4-MU Impairs Proliferation and Migration of OSC1 Cells**—In addition, the phosphorylation status of ERK1/2, an important downstream target of FAK, was analyzed between 5 min and 20 min after the addition of 4-MU. It was found that reduction of phosphorylation of ERK1/2 concurred with FAK cleavage at 20 min (Fig. 4, *A* and *B*).

In turn, incubation with 4-MU significantly inhibited proliferation, which was measured by [<sup>3</sup>H]thymidine incorporation in response to 10% fetal calf serum (FCS) and migration as determined by a modified Boyden chamber assay in response to 10% FCS: [<sup>3</sup>H]thymidine incorporation was  $61.7\% \pm 7.2\%$  that of untreated controls, and migration was

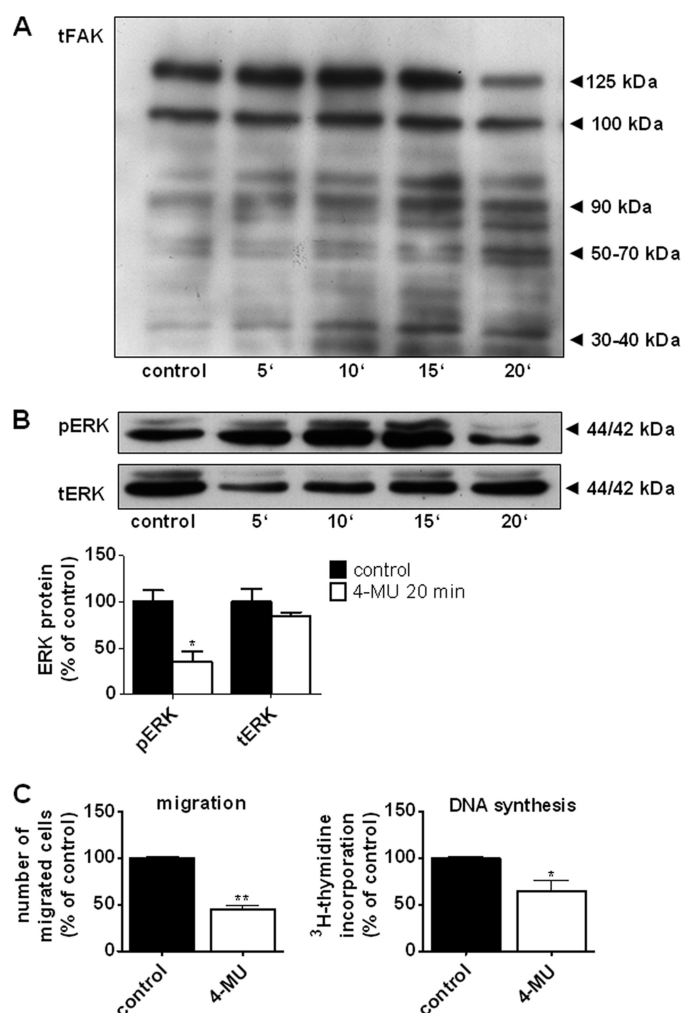


**FIGURE 4.** 4-MU-induced FAK cleavage coincides with decreased phosphorylation of ERK1/2 and reduced proliferation and migration. *A*, OSC1 cells were incubated with 4-MU (0.3 mM), and FAK degradation was detected with an antibody targeting the C terminus of tFAK starting at 20 min in OSC1 cells. *B*, time course of pERK1/2 and total ERK after the addition of 4-MU to OSC1 cells. The phosphorylation of ERK1/2 was strongly decreased starting at 20 min. Shown are representative immunoblots and quantitative analysis at 20 min of digitized blots. *C*, effect of 4-MU (0.3 mM) on migration toward FCS as determined in a 24-well microchemotaxis assay and DNA synthesis as determined by [<sup>3</sup>H]thymidine incorporation in response to FCS expressed as cpm per total cellular protein (mean  $\pm$  S.E.,  $n = 3$ ). \*,  $p < 0.05$ , \*\*,  $p < 0.01$  versus untreated control cells.

$45.4\% \pm 3.8\%$  that of untreated controls ( $n = 3–5$ , mean  $\pm$  S.E.,  $p < 0.05$ , Fig. 4*C*).

**Knockdown of HAS3 and HAS2 Causes FAK Degradation and Inhibition of Filopodia**—Because HAS3 and HAS2 are the main HAS isoforms in OSC1 cells, we investigated whether the molecular and cellular events mediating the inhibitory effects of 4-MU could be recapitulated by the knockdown of HAS3 or HAS2 in OSC1 cells *in vitro*. Knockdown of HAS3 and to a lesser extent of HAS2 reduced HA secretion into the medium (Fig. 5*A*) as expected from the relative expression levels of HAS2 and HAS3. In response to knockdown of HAS3, the phenotypical changes and the resolution of filopodia (Fig. 5*B*) closely resembled the changes produced by 4-MU. In addition, shHAS2 partially reduced filopodia as well and induced a smoother outline of cell clusters. Western blot analysis using the C-terminal FAK anti-

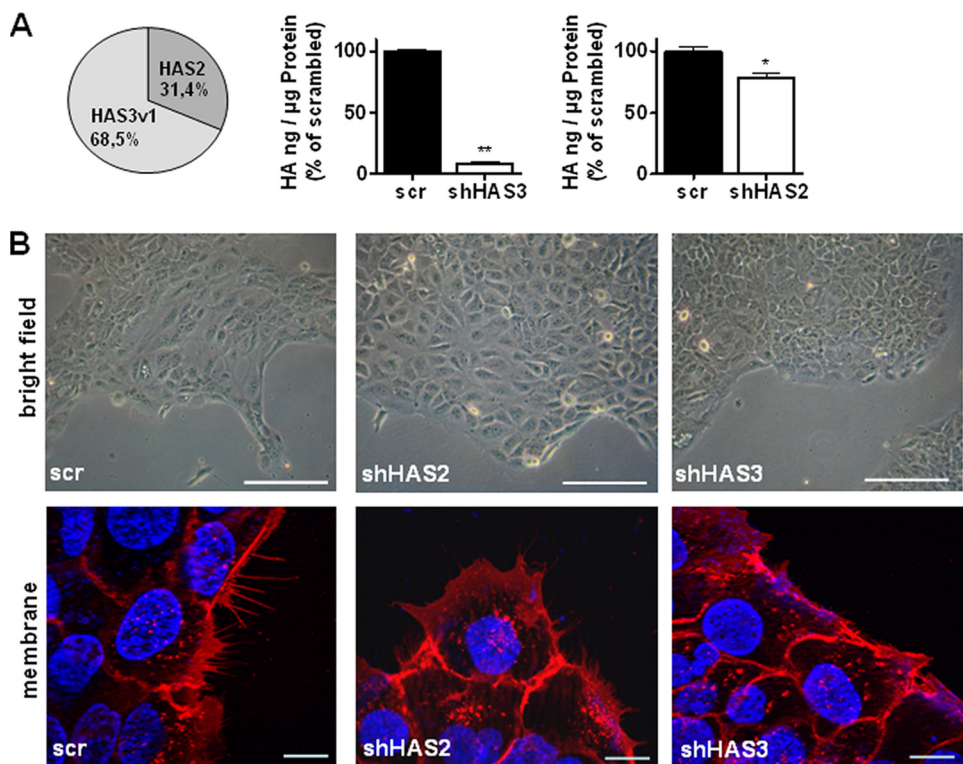


**FIGURE 5.** Lentiviral knockdown of HAS3 and HAS2 mimic the effects of 4-MU on cell morphology and filopodia. *A*, relative expression levels of HAS3 and HAS2 mRNA as determined by real-time reverse transcription-PCR. HA secretion was dramatically reduced after lentiviral knockdown of HAS3 and to a lesser extent by HAS2 shRNA. *B*, upper panel, light microscopy of live cells revealed a change in cell shape after infection with lentiviral shHAS3 and to a smaller degree with lentiviral shHAS2. This change in shape was similar to that observed after treatment with 4-MU (compare with Fig. 1). Lower panel, staining of fixed cells with membrane marker revealed a decrease in the number and the size of filopodia. These effects were most pronounced after knockdown of HAS3 but also were also present in the case of shHAS2. Scale bars, 500  $\mu$ m. The effects of the HAS knockdown were observed 5 days after infection and a nontargeting (scrambled) lentivirus was used as control. Shown are representative images of  $n = 3$  experiments (mean  $\pm$  S.E., \*,  $p < 0.05$ , \*\*,  $p < 0.01$ ). scr, scrambled.

body showed pronounced FAK cleavage after HAS3 and HAS2 knockdown (Fig. 6*A*). Concomitantly Akt/PKB and ERK phosphorylation were reduced by shHAS3 and shHAS2 (Fig. 6*B*). In turn, shHAS3 and shHAS2 reduced the proliferative and migratory response to FCS (Fig. 6*C*). Altogether, the cellular responses to HAS3 and HAS2 knockdown support the conclusion that HA synthesis plays a key role in the maintenance of filopodia and FAK protein levels as well as ERK and Akt/PKB signaling in OSC1 cells.

**Blockade of RHAMM but Not CD44 Induces FAK Degradation and Inhibits Filopodia**—OSC1 cells express both CD44 and RHAMM as identified by immunohistochemistry (Fig. 7, *A* and *B*). In response to 4-MU, CD44 was more pronounced in the circumference of the OSC1 cells, which might be due to a redistribution or due to the change in cell shape. In contrast, the expression pattern of RHAMM was not affected by 4-MU. To identify the HA receptors involved in the regulation of tFAK protein levels, and the maintenance of filopodia CD44 and RHAMM were down-regulated by lentiviral shRNA. Interestingly, shCD44 did not affect filopodial integrity (Fig. 7*C*) or tFAK levels (Fig. 8*A*). In contrast, shRHAMM led to a complete inhibition of filopodia (Fig. 7*D*) and a strong decrease in intact tFAK levels (Fig. 8*A*). However, both shRHAMM and shCD44 decreased Akt/PKB

and ERK1/2 phosphorylation (Fig. 8*B*) in OSC1 cells. Furthermore, both shCD44 and shRHAMM reduced proliferation and migration in response to FCS (Fig. 8*C*).

In addition to shRNA, blocking antibodies against CD44 (Hermes-1) and RHAMM (R36) were used. In line with the results obtained with shRNA, only blocking RHAMM caused loss of filopodia and FAK cleavage (*supplemental figure*). Blocking antibodies against CD44 inhibited Akt/PKB and ERK phosphorylation and blocking RHAMM by R36 resulted only in reduced Akt/PKB phosphorylation (*supplemental figure*). Thus, inhibiting RHAMM closely mimics all effects of 4-MU, shHAS3, and shHAS2, whereas inhibition of CD44 lacks the effects on filopodia and FAK. Therefore, it may be concluded that RHAMM plays a crucial role in transducing the effects of pericellular HA on the maintenance of FA and filopodial integrity in OSC1 cells, whereas both HA receptors are involved in ERK and Akt/PKB signaling.

## DISCUSSION

HA synthesis is not sufficient for malignant transformation (32), but HA, HA-binding proteins, and HA receptors provide a matrix environment that supports the malignant phenotype of cancer cells, stromal cell recruitment, and, thus, the progression of cancer (33). In human ESCC, HA accumulates in the parenchyma and stroma, and HA is produced by both tumor cells and stroma (22, 34). Here, an analysis of the molecular and cellular effects of HA synthesis on ESCC phenotype is provided.

In addition to the inhibition of proliferation and migration, 4-MU also repressed the formation of cell protrusions. These cell protrusions were reminiscent of the filopodia that have in previous studies been associated with the malignant phenotype of cancer cells (30). Furthermore, it was demonstrated recently that overexpression of HAS3 in several cell lines causes pronounced microvilli that were sensitive to 4-MU and hyaluronidase (28). Therefore, microvilli are thought to provide a scaffold to support the pericellular HA-matrix (28). The present results suggest that filopodia also can be dependent on HA-synthesis and pericellular HA. Furthermore, our findings suggest that the loss of filopodia and the change in cell shape are a consequence of FAK cleavage in response to the inhibition of HA synthesis. A likely candidate protease responsible for FAK degradation is calpain, which is involved in the physiological turnover of FAK and is

## Hyaluronan and Esophageal SCC Phenotype

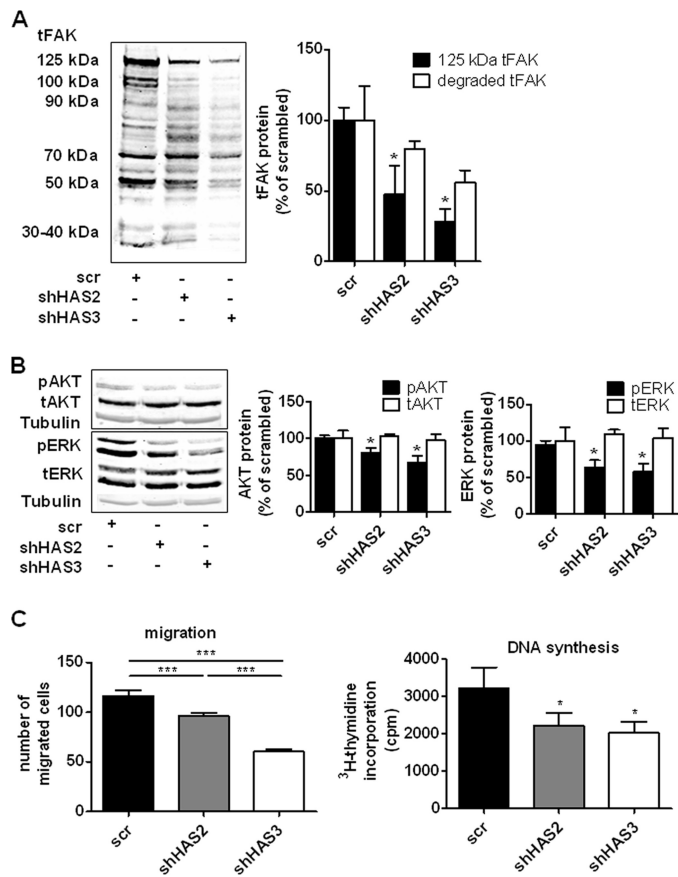


**FIGURE 6. Lentiviral knockdown of HAS3 and HAS2 cause FAK cleavage and inhibit proliferation and migration.** *A*, lentiviral knockdown of HAS3 and HAS2 was performed as described in Fig. 5. Increased cleavage of tFAK resulting in the loss of total intact 125-kDa FAK occurred after shHAS3 expression. This effect was present but less pronounced after knockdown of shHAS2. Quantitative analysis of 125-kDa tFAK and degraded tFAK (<125 kDa) after normalization to tubulin and to scrambled (scr) controls ( $n = 3$ , mean  $\pm$  S.E.). \*,  $p < 0.05$  versus scrambled shRNA. *B*, representative immunoblots of tAkt, pAkt, tERK, and pERK and quantitative data after densitometric scanning and normalization to tubulin and to scrambled controls ( $n = 3$ , mean  $\pm$  S.E.). \*,  $p < 0.05$  versus scrambled shRNA. The effects of HAS knockdown were observed 5 days after infection and compared with a nontargeting lentivirus as control. *C*, effect of shHAS3 and shHAS2 on migration toward FCS as determined in a 24-well microchemotaxis assay and on DNA synthesis as determined by [ $^3$ H]thymidine incorporation in response to FCS expressed as cpm per total cellular protein ( $n = 3$ , mean  $\pm$  S.E.). \*,  $p < 0.05$ , \*\*\*,  $p < 0.001$  versus scrambled shRNA. scr, scrambled.

also spatially associated with the focal adhesion complex (35).

It has been shown that cross-talk exists between the HA matrix and focal adhesions. Using H-ras-transformed C3 fibroblasts, Hall *et al.* (1994) demonstrated that HA leads to FAK tyrosine phosphorylation and augmented the formation of focal adhesions (36). Furthermore, in osteosarcoma cells, HA stimulates the phosphorylation of FAK and ERK1/2 (20). Despite the previously observed link between CD44 and FAK activation (37–38), CD44 blocking antibodies had no influence on FAK degradation in ESCC. In contrast, the present results from down-regulation of RHAMM by shRNA and blocking RHAMM by antibodies strongly suggest that the loss of RHAMM signaling induces subsequent FAK degradation. In addition, interference with RHAMM signaling by shRNA and R36 led to decreased phosphorylation of Akt/

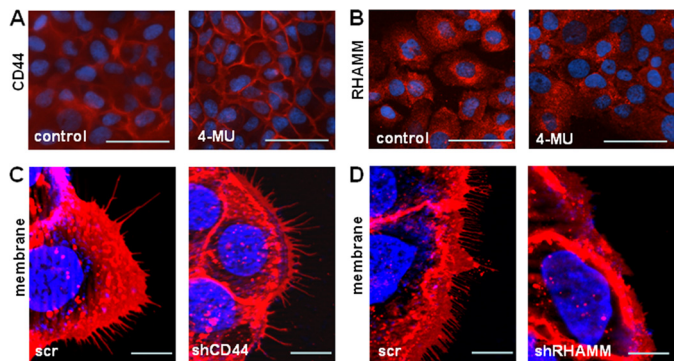


**FIGURE 7. Filopodia are dependent on RHAMM but not on CD44.** *A*, CD44 is strongly expressed and evenly distributed within the OSC1 cultures, as shown by immunostaining, and expression appeared more pronounced at the circumference of cells in response to treatment with 4-MU compared with untreated controls. *B*, RHAMM was expressed as well, but its expression appeared not to be affected by treatment with 4-MU compared with untreated control OSC1. Scale bar, 50  $\mu$ m. To elucidate the involvement of HA receptors in filopodial integrity and cell shape lentiviral shRNA vectors targeting CD44 (*C*) and RHAMM (*D*) were used and compared with scrambled control shRNA vectors. Membrane staining (WGA Alexa Fluor® 555 conjugate) showed that shCD44 had no effect on filopodia, whereas shRHAMM induced loss of filopodia. Scale bars, 20  $\mu$ m. The effects of the RHAMM and CD44 knockdown were observed 5 days after infection. Shown are representative images of  $n = 3$  experiments. scr, scrambled.

PKB, whereas ERK phosphorylation was responsive only to shRHAMM. This difference between the use of the blocking antibody R36 and shRNA might point toward a role of intracellular RHAMM for ERK phosphorylation in OSC1. Inhibition of CD44 by both shRNA and Hermes1 antibody led to decreased phosphorylation of Akt/PKB and ERK1/2. These findings suggest that both HA receptors are involved in the observed inhibition of the signaling response after interference with HA synthesis. The inhibition of Akt/PKB and ERK 1/2 signaling likely also explains the inhibition of growth and migration in response to 4-MU, shHAS3, shHAS2, shCD44, and shRHAMM because the activation of the Ras-MAPK and PI3-kinase pathways by HA have been shown to mediate promigratory and proproliferative phenotypes (32, 39–41) in cultured cancer cells. Interestingly, RHAMM is also a novel susceptibility gene for breast cancer, and its overexpression is positively correlated with the phosphorylation of ERK, metastasis, and poor survival for patients with breast cancer (42–43). RHAMM peptide vaccination is currently being successfully explored in phase 1 clinical trials of acute myeloid leukemia and multiple myeloma (44). The relevance of RHAMM for esophageal cancer is further emphasized by a microarray analysis showing that RHAMM is highly induced in human ESCC cell lines and correlating RHAMM expression with the TNM Classification of Malignant Tumors (TNM) stage of human esophageal carcinoma (45).

All considered, in OSC1 cells interference with HA production, digestion of HA, displacement of HA, and inhibition of RHAMM signaling all cause FAK cleavage, suggesting a strong cross-talk between FA and hyaluronan/RHAMM. This might be important for these tumor cells to regulate adhesion, migration, and proliferation. In contrast, CD44 participates in hyaluronan-mediated signaling through Akt/ERK and through these pathways may contribute to

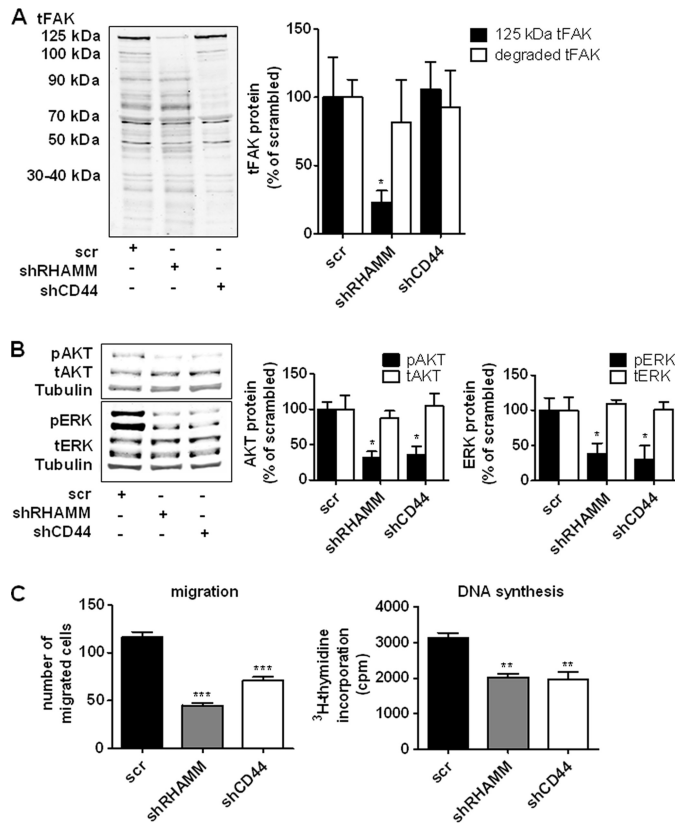


**FIGURE 8.** FAK cleavage is induced specifically by down-regulation of RHAMM. *A*, lentiviral shRNA targeting CD44 and RHAMM were used as in Fig. 7. Immunoblotting of tFAK and quantitative analysis of 125-kDa tFAK and degraded tFAK (<125 kDa) revealed that shCD44 had no effect on FAK, whereas shRHAMM induced pronounced FAK cleavage compared with the scrambled lentiviral vector. Data are normalized to tubulin and to scrambled control ( $n = 3$ , mean  $\pm$  S.E.). \*,  $p < 0.05$  versus scrambled control vector. *B*, phosphorylation of AKT and ERK1/2 were reduced by shRNA targeting both CD44 and RHAMM. Data were normalized to tubulin as loading control and to scrambled controls. *C*, both shCD44 and shRHAMM inhibited migration toward FCS as determined in a 24-well microchemotaxis assay and reduced DNA synthesis as determined by [<sup>3</sup>H]thymidine incorporation in response to FCS expressed as cpm per total cellular protein ( $n = 3$ ). \*\*,  $p < 0.01$ ; \*\*\*,  $p < 0.001$  versus scrambled control vector. scr, scrambled.

the control of migration and proliferation but has no effect on FAK and cell shape. FAK mediates many crucial events in cancer cell biology and signaling, including spreading, proliferation, migration, invasion, and metastasis (46–47); moreover, the promise of targeting FAK activity by antitumor therapy is supported by numerous studies. The novel interrelationship between HA/RHAMM and FAK turnover described here could therefore be important for a better understanding of these processes and for the development of new anticancer strategies.

## REFERENCES

- Ropponen, K., Tammi, M., Parkkinen, J., Eskelinen, M., Tammi, R., Lipponen, P., Agren, U., Alhava, E., and Kosma, V. M. (1998) *Cancer Res.* **58**, 342–347
- Toole, B. P. (2004) *Nat. Rev. Cancer* **4**, 528–539
- Kakizaki, I., Kojima, K., Takagaki, K., Endo, M., Kannagi, R., Ito, M., Maruo, Y., Sato, H., Yasuda, T., Mita, S., Kimata, K., and Itano, N. (2004) *J. Biol. Chem.* **279**, 33281–33289
- Nakazawa, H., Yoshihara, S., Kudo, D., Morohashi, H., Kakizaki, I., Kon, A., Takagaki, K., and Sasaki, M. (2006) *Cancer Chemother Pharmacol* **57**, 165–170
- Yoshihara, S., Kon, A., Kudo, D., Nakazawa, H., Kakizaki, I., Sasaki, M., Endo, M., and Takagaki, K. (2005) *FEBS Lett.* **579**, 2722–2726
- Turley, E. A., Noble, P. W., and Bourguignon, L. Y. W. (2002) *J. Biol. Chem.* **277**, 4589–4592
- Haraguchi, N., Ohkuma, M., Sakashita, H., Matsuzaki, S., Tanaka, F., Mimori, K., Kamohara, Y., Inoue, H., and Mori, M. (2008) *Ann Surg Oncol.* **15**, 2927–2933
- Mylonas, E., Giannopoulou, I., Fasomylakis, E., Nomikos, A., Magkou, C., Bakarakos, P., and Nakopoulou, L. (2008) *Hum. Pathol.* **39**, 1096–1102
- Shmelkov, S. V., Butler, J. M., Hooper, A. T., Hormigo, A., Kushner, J., Milde, T., St Clair, R., Baljevic, M., White, I., Jin, D. K., Chadburn, A., Murphy, A. J., Valenzuela, D. M., Gale, N. W., Thurston, G., Yancopoulos, G. D., D'Angelica, M., Kemeny, N., Lyden, D., and Rafii, S. (2008) *J. Clin. Invest.* **118**, 2111–2120
- Toole, B. P., and Slomiany, M. G. (2008) *Drug Resist. Updat.* **11**, 110–121
- Tolg, C., Hamilton, S. R., Nakrie, K. A., Kooshesh, F., Walton, P., McCarthy, J. B., Bissell, M. J., and Turley, E. A. (2006) *J. Cell Biol.* **175**, 1017–1028
- Maxwell, C. A., McCarthy, J., and Turley, E. (2008) *J. Cell Sci.* **121**, 925–932
- Hall, C. L., Yang, B., Yang, X., Zhang, S., Turley, M., Samuel, S., Lange, L. A., Wang, C., Curpen, G. D., Savani, R. C., Greenberg, A. H., and Turley, E. A. (1995) *Cell* **82**, 19–26
- Hamilton, S. R., Fard, S. F., Paiwand, F. F., Tolg, C., Veiseh, M., Wang, C., McCarthy, J. B., Bissell, M. J., Koropatnick, J., and Turley, E. A. (2007) *J. Biol. Chem.* **282**, 16667–16680
- Amieva, M. R., Litman, P., Huang, L., Ichimaru, E., and Furthmayr, H. (1999) *J. Cell Sci.* **112**, 111–125
- Underhill, C. B., and Toole, B. P. (1979) *J. Cell Biol.* **82**, 475–484
- Toole, B. P. (2002) *Glycobiology* **12**, 42
- Lesley, J., and Hyman, R. (1998) *Front Biosci.* **3**, d616–630
- Liu, N., Gao, F., Han, Z., Xu, X., Underhill, C. B., and Zhang, L. (2001) *Cancer Res.* **61**, 5207–5214
- Tofuku, K., Yokouchi, M., Murayama, T., Minami, S., and Komiya, S. (2006) *Int. J. Oncol.* **29**, 175–183
- Kim, S., Takahashi, H., Lin, W. W., Descargues, P., Grivennikov, S., Kim, Y., Luo, J. L., and Karin, M. (2009) *Nature* **457**, 102–106
- Wang, C., Tammi, M., Guo, H., and Tammi, R. (1996) *Am. J. Pathol.* **148**, 1861–1869
- Savani, R. C., Wang, C., Yang, B., Zhang, S., Kinsella, M. G., Wight, T. N., Stern, R., Nance, D. M., and Turley, E. A. (1995) *J. Clin. Invest.* **95**, 1158–1168
- Mummert, M. E., Mohamadzadeh, M., Mummert, D. I., Mizumoto, N., and Takashima, A. (2000) *J. Exp. Med.* **192**, 769–779
- Sarbia, M., Bösing, N., Hildebrandt, B., Koldovsky, P., Gerharz, C. D., and Gabbert, H. E. (1997) *Anticancer Res.* **17**, 2185–2192
- Shimada, Y., Imamura, M., Wagata, T., Yamaguchi, N., and Tobe, T. (1992) *Cancer* **69**, 277–284
- Dai, G., Freudenberg, T., Zipper, P., Melchior, A., Grether-Beck, S., Rabausch, B., de Groot, J., Twarock, S., Hanenberg, H., Homey, B., Krutmann, J., Reifenberger, J., and Fischer, J. W. (2007) *Am. J. Pathol.* **171**, 1451–1461
- Rilla, K., Tiihonen, R., Kultti, A., Tammi, M., and Tammi, R. (2008) *J. Histochem. Cytochem.* **56**, 901–910
- Wasteson, A., Uthne, K., and Westermark, B. (1973) *Biochem. J.* **136**, 1069–1074
- Kovbasnjuk, O., Mountazina, R., Baibakov, B., Wang, T., Elowsky, C., Choti, M. A., Kane, A., and Donowitz, M. (2005) *Proc. Natl. Acad. Sci. U.S.A.* **102**, 19087–19092
- Levkau, B., Herren, B., Koyama, H., Ross, R., and Raines, E. W. (1998) *J. Exp. Med.* **187**, 579–586
- Itano, N., Atsumi, F., Sawai, T., Yamada, Y., Miyaishi, O., Senga, T., Hamaguchi, M., and Kimata, K. (2002) *Proc. Natl. Acad. Sci. U.S.A.* **99**, 3609–3614
- Tammi, R. H., Kultti, A., Kosma, V. M., Pirinen, R., Auvinen, P., and Tammi, M. I. (2008) *Semin. Cancer Biol.* **18**, 288–295
- Twarock, S., Röck, K., Sarbia, M., Weber, A. A., Jänicke, R. U., and Fischer,

## Hyaluronan and Esophageal SCC Phenotype

- J. W. (2009) *Br. J. Pharmacol.* **157**, 234–243
35. Carragher, N. O., Fincham, V. J., Riley, D., and Frame, M. C. (2001) *J. Biol. Chem.* **276**, 4270–4275
36. Hall, C. L., Wang, C., Lange, L. A., and Turley, E. A. (1994) *J. Cell Biol.* **126**, 575–588
37. Bourguignon, L. Y., Zhu, H., Shao, L., and Chen, Y. W. (2000) *J. Biol. Chem.* **275**, 1829–1838
38. Fujita, Y., Kitagawa, M., Nakamura, S., Azuma, K., Ishii, G., Higashi, M., Kishi, H., Hiwasa, T., Koda, K., Nakajima, N., and Harigaya, K. (2002) *FEBS Lett.* **528**, 101–108
39. Camenisch, T. D., Spicer, A. P., Brehm-Gibson, T., Biesterfeldt, J., Augustine, M. L., Calabro, A., Jr., Kubalak, S., Klewer, S. E., and McDonald, J. A. (2000) *J. Clin. Invest.* **106**, 349–360
40. Sohara, Y., Ishiguro, N., Machida, K., Kurata, H., Thant, A. A., Senga, T., Matsuda, S., Kimata, K., Iwata, H., and Hamaguchi, M. (2001) *Mol. Biol. Cell* **12**, 1859–1868
41. Zoltan-Jones, A., Huang, L., Ghatak, S., and Toole, B. P. (2003) *J. Biol. Chem.* **278**, 45801–45810
42. Pujana, M. A., Han, J. D., Starita, L. M., Stevens, K. N., Tewari, M., Ahn, J. S., Rennert, G., Moreno, V., Kirchhoff, T., Gold, B., Assmann, V., Elshamy, W. M., Rual, J. F., Levine, D., Rozek, L. S., Gelman, R. S., Gunsalus, K. C., Greenberg, R. A., Sobhian, B., Bertin, N., Venkatesan, K., Ayivi-Guedehoussou, N., Solé, X., Hernández, P., Lázaro, C., Nathanson, K. L., Weber, B. L., Cusick, M. E., Hill, D. E., Offit, K., Livingston, D. M., Gruber, S. B., Parvin, J. D., and Vidal, M. (2007) *Nat. Genet.* **39**, 1338–1349
43. Wang, C., Thor, A. D., Moore, D. H., 2nd, Zhao, Y., Kerschmann, R., Stern, R., Watson, P. H., and Turley, E. A. (1998) *Clin. Cancer Res.* **4**, 567–576
44. Schmitt, M., Schmitt, A., Rojewski, M. T., Chen, J., Giannopoulos, K., Fei, F., Yu, Y., Götz, M., Heyduk, M., Ritter, G., Speiser, D. E., Gnijatic, S., Guillaume, P., Ringhoffer, M., Schlenk, R. F., Liebisch, P., Bunjes, D., Shiku, H., Dohner, H., and Greiner, J. (2008) *Blood* **111**, 1357–1365
45. Yamano, Y., Uzawa, K., Shinozuka, K., Fushimi, K., Ishigami, T., Nomura, H., Ogawara, K., Shiiba, M., Yokoe, H., and Tanzawa, H. (2008) *Int. J. Oncol.* **32**, 1001–1009
46. Owens, L. V., Xu, L., Craven, R. J., Dent, G. A., Weiner, T. M., Kornberg, L., Liu, E. T., and Cance, W. G. (1995) *Cancer Res.* **55**, 2752–2755
47. van Nimwegen, M. J., and van de Water, B. (2007) *Biochem. Pharmacol.* **73**, 597–609

RESEARCH

Open Access

# Inhibition of Oesophageal Squamous Cell Carcinoma Progression by *in vivo* Targeting of Hyaluronan Synthesis

Sören Twarock<sup>1</sup>, Till Freudenberger<sup>1</sup>, Eva Poscher<sup>1</sup>, Guang Dai<sup>1</sup>, Katharina Jannasch<sup>2</sup>, Christian Dullin<sup>2</sup>, Frauke Alves<sup>2</sup>, Klaus Prenzel<sup>3</sup>, Wolfram T Knoefel<sup>4</sup>, Nikolas H Stoecklein<sup>4</sup>, Rashmin C Savani<sup>5</sup>, Bernhard Homey<sup>6</sup> and Jens W Fischer<sup>1\*</sup>

## Abstract

**Background:** Oesophageal cancer is a highly aggressive tumour entity with at present poor prognosis. Therefore, novel treatment options are urgently needed. Hyaluronan (HA) is a polysaccharide present in the matrix of human oesophageal squamous cell carcinoma (ESCC). Importantly, *in vitro* ESCC cells critically depend on HA synthesis to maintain the proliferative phenotype. The aim of the present study is (1) to study HA-synthase (HAS) expression and regulation in human ESCC, and (2) to translate the *in vitro* results into a mouse xenograft model of human ESCC to study the effects of systemic versus tumour targeted HAS inhibition on proliferation and distribution of tumour-bound and stromal hyaluronan.

**Methods:** mRNA expression was investigated in human ESCC biopsies by semiquantitative real-time RT PCR. Furthermore, human ESCC were xenografted into NMRI nu/nu mice. The effects on tumour progression and morphology of 4-methylumbelliflone (4-MU), an inhibitor of HA-synthesis, and of lentiviral knock down of HA-synthase 3 (HAS3), the main HAS isoform in the human ESCC tissues and the human ESCC cell line used in this study, were determined. Tumour progression was monitored by calliper measurements and by flat-panel detector volume computed tomography (fpVCT). HA content, cellular composition and proliferation (Ki67) were determined histologically.

**Results:** mRNA of HAS isoform 3 (HAS3) was upregulated in human ESCC biopsies and HAS3 mRNA was positively correlated to expression of the epidermal growth factor (EGF) receptor. EGF was also proven to be a strong inducer of HAS3 mRNA expression *in vitro*. During the course of seven weeks, 4-MU inhibited progression of xenograft tumours. Interestingly, remodelling of the tumour into a more differentiated phenotype and inhibition of cell proliferation were observed. Lentiviral knockdown of HAS3 in human ESCC cells prior to xenografting mimicked all effects of 4-MU treatment suggesting that hyaluronan produced by ESCC is accountable for major changes in tumour environment *in vivo*.

**Conclusions:** Systemic inhibition of HA-synthesis and knockdown of tumour cell HAS3 cause decreased ESCC progression accompanied by tumour stroma remodelling and may therefore be used in novel approaches to ESCC therapy.

\* Correspondence: jens.fischer@uni-duesseldorf.de

<sup>1</sup>Institut für Pharmakologie und Klinische Pharmakologie, Universitätsklinikum Düsseldorf, Heinrich-Heine Universität Düsseldorf, 40225 Düsseldorf, Germany  
Full list of author information is available at the end of the article

## Background

Oesophageal cancer is the sixth leading cause of cancer deaths worldwide [1]. The mortality rate associated with oesophageal cancer is similar to its incidence rate because of its generally advanced stage at the time of diagnosis, its aggressive characteristics, and because of the paucity of effective treatment strategies. In spite of its poor prognosis, oesophageal cancer has not been well studied [2]. Two types of oesophageal cancer exist: adenocarcinoma, and oesophageal squamous cell carcinoma (ESCC), which corresponds to approximately 50% of all oesophageal cancers. Standard treatment for oesophageal cancer comprises surgery, chemoradiotherapy, and palliative chemotherapy with cisplatin, fluorouracil, and taxanes. However, the response to chemotherapy typically lasts only a few months, and the median survival time is less than one year [3]. Recent technical advances in surgery, the use of neoadjuvant chemoradiotherapy, and new cytotoxic drugs have increased the response rates but have had no meaningful effect on survival.

Hyaluronan (HA) is an unbranched high molecular weight polysaccharide that is composed of D-glucuronic acid beta(1-3)-D-N-acetyl-glucosamine beta(1-4). HA is produced by three isoforms of the hyaluronan synthase family (HAS1-3), which are located at the plasma membrane and extrude the growing HA polymer into the extracellular space [4]. Overexpression of either HAS2 or HAS3 in several tumour types such as prostate cancer [5], breast cancer [6,7], osteosarcoma [8] and colon carcinoma [9] is known to be associated with higher malignancy or metastasis. The activity of all three HAS isoenzymes can be inhibited by 4-methylumbellifluorene (4-MU), which depletes the activated uridine diphosphate-glucuronic acid precursor pool and thus leads to decreased HA production [10]. Recently, 4-MU has been studied in different animal models and was shown to inhibit liver metastases of melanoma cells [11], to enhance chemotherapeutic action in pancreatic and breast cancer cells [12,13] and to attenuate tumour progression along with induction of apoptosis in prostate cancer cells [14].

HA activates membrane receptors such as the receptor of HA-mediated motility (RHAMM) and CD44 to induce signalling and specific cellular responses. Both CD44 and RHAMM have been implicated in tumour cell biology and tumour progression [15].

An HA-rich matrix is important for a variety of aspects of tumour pathobiology including anchorage-independent growth, migration, angiogenesis, suppression of apoptosis [15,16] and metastasis [8,17]. Recently strong evidence for the importance of HA in the microenvironment of tumours and in the tumour

stroma has been presented [18,19]. A variety of different types of cancer are characterised by either high amounts of tumour cell-associated HA (e.g., colon and gastric cancer) or high amounts of stromal HA (e.g., breast, ovarian, and prostate cancer) or both. In some of these malignancies (e.g., colon cancer), tumour-associated HA is an independent prognostic factor for poor outcome [20]. In other tumours (e.g., ovarian and prostate cancer) it is the stromal HA that is correlated with poor outcome, most likely because of the accelerated growth of the tumours and their metastases [4,21]. With respect to oesophageal cancer it is has been demonstrated that HA accumulates in the parenchyma and stroma [22].

The HA matrix of oesophageal carcinoma may contain novel targets for therapeutic approaches such as the HAS-isoforms, hyaluronidases and HA-receptors. Furthermore, the role of individual HAS enzymes and the factors that regulate HAS expression in oesophageal cancer have not been defined. In addition, the relative importance of stromal versus tumour cell HAS expression has not been addressed experimentally in any cancer yet, which is due to the fact that HAS2 deficient mice are lethal and HAS1 and HAS3 deficient mice are not available to the scientific community [23].

Previously it was demonstrated in ESCC cell lines that HA-synthesis mediated by HAS3, and to a lesser extent by HAS2, is required for the malignant cell phenotype characterised by filopodial plasma membrane extensions and high proliferative activity [24]. Knockdown of HAS3 and inhibition of HA-synthesis by the small molecule inhibitor, 4-MU, caused a rapid loss of focal contacts which was followed by resolution of filopodia and inhibition of proliferation and migration. Therefore, the aim of the present study was to elucidate whether HAS isoforms are specifically upregulated in human ESCC tumour specimens and if so whether inhibition of HA synthesis would be effective to inhibit tumour growth *in vivo*. Furthermore changes in tumour morphology and distribution of HA and HA receptors, following either systemic HA inhibition by 4-MU or inhibition of tumour HA production by lentiviral knockdown of HAS3, were examined. This approach may help to define and specify the molecular targets and to explore the therapeutic promises of pharmacologic HAS inhibition in ESCC.

## Methods

### Reagents and substances

Unless otherwise stated, all reagents were obtained from Sigma-Aldrich, Munich, Germany. Erlotinib was bought from LC Laboratories, Woburn, MA, USA. Cetuximab is a product of Merck Serono, Darmstadt, Germany.

### Cell culture

OSC1 cells were a gift from M. Sarbia [25] and were used for xenograft and cell culture experiments throughout the present study. The human foreskin fibroblast cell line Hs68 used in the co-culture experiments was purchased from ATCC (Wesel, Germany). OSC1 and Hs68 cells were maintained as monolayer cultures in RPMI-1640 (Sigma-Aldrich) supplemented with 10% fetal bovine serum, L-glutamine, penicillin, and streptomycin at 37°C, 5% CO<sub>2</sub> and 95% humidified air.

### Human ESCC specimens

Tissue samples from oesophageal squamous cell carcinomas (ESCC, n = 20) and normal oesophageal mucosa (n = 13) were collected from patients undergoing radical en bloc oesophagectomy at Düsseldorf University Hospital. The tissues were snap-frozen in liquid nitrogen immediately after resection and stored in liquid nitrogen until use. Written informed consent was obtained from all patients. The collection of the fresh tumour samples was approved by the ethics committee of the Heinrich Heine University Düsseldorf. Tumour stage and grading were classified by routine histopathologic assessment according to the UICC (Union Internationale Contre le Cancer) Classification for Malignant Tumours; the pathologists performing the assessment were unaware of the experimental data.

### Xenograft Model

NMRI nu/nu mice were used for subcutaneous tumour formation experiments after xenografting of OSC1 cells with or without previous lentiviral transduction *in vitro*. The tumours were initiated by the subcutaneous injection of 10<sup>6</sup> OSC1 cells into both flanks, and the mice were monitored after xenografting for 47 days in the 4-MU group and 65 days in the shHAS3 group, respectively. The mice were treated with 4-MU, which was pelleted into the chow, at a daily dose of 250 mg per mouse. Treatment started two days before xenografting. Biopsies for immunostaining and molecular studies were taken after sacrifice of the animals at the end of the experiment. The animal experiments were approved by the local animal facility and the *Landesamt für Natur, Umwelt und Verbraucherschutz, NRW*.

### Flat-Panel Detector Volume Computed Tomography Imaging (fpVCT)

After an iodine-containing contrast agent (Isovist 300<sup>®</sup>) was injected intravenously, mice were subjected to fpVCT, a nonclinical volume CT prototype (GE Global Research, Niskayuna, NY), as described previously [26].

### Immunostaining

Cryosections (8 µm) were derived from tumour tissue and fixed in acetone-methanol (2:3) for the following

immunostaining: human cytokeratin 18 (Progen Biotechnik, Heidelberg, Germany; 1:200), alpha-smooth muscle actin (Abcam; 1:50), secondary antibodies, goat anti-guinea-pig-FITC, goat anti-rat-RhodX (Dianova, Hamburg, Germany; 1:200), and sheep anti-rabbit-Cy3 (Sigma-Aldrich; 1:200); biotinylated HABP was detected with Cy3-labeled streptavidin (Dako; 1:200). Alternatively, fixation with 96% ethanol was used for staining with rabbit anti-human Ki67 (Abcam; 1:50) and rabbit anti- CD44 (Sigma-Aldrich; 1:1000), which were detected with sheep anti-rabbit-IgG F(ab)2-Cy3 (Sigma-Aldrich; 1:50/1:500). HA was detected by biotinylated HABP (Seikagaku, Tokyo, Japan; 6 µg/ml) and FITC- or Cy3-labeled streptavidin (Dako Deutschland, Hamburg, Germany; 1:200). Nuclei were counterstained by Hoechst 33342 (Invitrogen, Karlsruhe, Germany; 1:20000). Cell culture experiments were carried out on glass cover slides, fixed with 3.7% formalin solution and stained as above. Ki67 and HA staining were quantified by using ImageJ 1.37c software with the nucleus counter plug-in. For quantification five randomly selected images from each tumour section were analyzed and the average was used as n equals one.

### Real-time RT-PCR

The PCR reactions were performed according to standard procedures with the SYBR Green PCR Master Mix (Applied Biosystems). Relative expression levels were compared by using real-time PCR with the 2<sup>-ΔΔC(T)</sup> method. The primer sequences of the genes of interest are given in Table 1 [27,28].

### Lentiviral knockdown of HAS3

The ESCC cell line, OSC1, was used for xenografting and was maintained as described [25] in monolayer cultures. HAS3 knockdown was achieved by using the MISSION<sup>TM</sup> Lentiviral shRNA knockdown system (Sigma-Aldrich). The used hairpin sequence was 5'-CCGGGCTCTAACCTCTGTGGTTCTCGAGAACCACAGAGAGT TGTAGAGCTTT TTG-3'. A scrambled shRNA was used as a control. The transfer into the packaging line HEK 293T (ATCC, LGC Standards, Wesel, Germany) was

**Table 1** Primer sequences used for quantification of gene expression

Gene	Primer sequence
human EGFR	5'-GGA GAA CTG CCA GAA ACT GAC C-3' 5'-GCC TGC AGC ACA CTG GTT G-3'
human GAPDH	5'-GTGAAGGTGGAGTCACG-3' 5'-TGAGGTCAATGAAGGGTC-3'
human HAS2	5'-GTGGATTATGTACAGGTTGTGA-3' 5'-TCCAACCATGGGATCTTCTT-3'
human HAS3	5'-GAGATGTCAGATCTCAACAA-3' 5'-CCCACTAATACTGCACAC-3'

performed with the lipofection reagent Fugene 6 (Roche, Grenzach-Wyhlen, Germany). After 16 h, the medium was changed to Iscove's Modified Dulbecco's Medium (IMDM) for better stability of the produced lentiviral particles. The next day, the lentiviruses were harvested and concentrated by centrifugation with poly-L-lysine under the conditions reported previously [29]. After verification of HAS3 mRNA knockdown by RT-PCR target cells were transfected at a multiplicity of infection (MOI) of 10 and kept for 5 days in normal growth medium before injection.

### Statistical Analysis

Statistical analysis of mRNA levels in biopsy samples was performed by using the nonparametric Mann-Whitney test and the Spearman correlation analysis. All other datasets were analyzed either by ANOVA and the Bonferroni post hoc test or by Student's *t* test as appropriate. Data are presented as means  $\pm$  SEM. Statistical significance was assigned at the level of  $p < 0.05$ .

## Results

### HAS3 is upregulated in human oesophageal SCC biopsies and correlates with EGF receptor expression

We analysed the expression of HAS1-3 in human ESCC tumours by RT-PCR and compared to healthy oesophageal mucosa. HAS3 was the main isoform of the studied ESCC tumour samples. This result is in accordance with the HAS expression pattern found in the ESCC cell line OSC1 as determined earlier [28]. Therefore, OSC1 cells were used in this study for *in vitro* experiments and for the xenograft model. In addition, only HAS3 expression was significantly higher in ESCC than in normal mucosal tissue whereas there was no significant increase regarding HAS1 and HAS2 (data not shown). This result was true over all studied samples (2.34 $\pm$ 0.5 fold induction vs. control, mean $\pm$ SEM,  $p < 0.05$ ) as well as for the T = 1 (3.15 $\pm$ 1.2 fold induction vs. control, mean $\pm$ SEM,  $p < 0.05$ ) and the T = 2-4 (1.81 $\pm$ 0.3 fold induction vs. control, mean $\pm$ SEM,  $p < 0.05$ ) subgroups according to TNM classification (defining tumour size (T), lymph node involvement (N) and existence of metastases (M)) (Figure 1A). Furthermore, the mRNA levels of HAS3 were positively correlated with the mRNA levels of EGF receptor (HER1, ErbB1) in tumour cells, but no correlation between these mRNA levels was observed in normal mucosa (Figure 1B, C). Interestingly, T1 grade tumour samples showed a steeper correlation than did T2-4. This might indicate a stronger dependence of early tumour grades on EGF pathway signalling to maintain HAS3 activity. In line with these findings, EGF receptor activation led to induction of HAS3 in ESCC cells, which could be rescued by use of the EGF receptor tyrosine kinase inhibitor erlotinib and the monoclonal anti-EGFR antibody cetuximab (Figure 1D).

### 4-MU inhibits tumour growth *in vivo* and causes tumour-stroma remodelling

A xenograft tumour model was established by subcutaneously injecting the human ESCC line OSC1 into the flanks of NMRI nu/nu mice. The mice were given oral doses of the small molecule HAS inhibitor 4-MU starting 2 days before injection for the whole experimental period. During the first 47 days after xenografting calliper measurements showed that treatment with 4-MU strongly inhibited the time course of tumour progression (Figure 2A). At the end of the experimental period additional analysis using flat-panel volume computed tomography (fpVCT) revealed also significantly lower tumour volumes (control 100  $\pm$  20,0% vs. 4-MU 27,4  $\pm$  11,8%, Figure 2B).

Treatment with 4-MU not only was associated with decreased tumour size but also caused remarkable alterations in tumour morphology. Histopathological examination of tumour specimens from control mice showed that OSC1-derived xenograft tumours were poorly differentiated, with numerous loosely cohesive tumour cells (Figure 2C, left). In contrast, tumours from mice treated with 4-MU were characterised by the formation of distinct tumour cell clusters and large continuous areas of intratumoural stroma, as indicated by alpha-smooth muscle actin staining (Figure 2D, right). The outer circumference of the clusters exhibited a cell-rich border region (Figure 2C, right, arrows). Staining with the HABP probe showed that HA was found in the tumours but at levels lower in mice treated with 4-MU than in control mice (Figure 2E).

### Knockdown of HAS3 expression in OSC1 cells is sufficient to inhibit tumour progression and to mimic the morphological stroma redistribution as caused by systemic HAS inhibition

HAS3 is the major isoform in human ESCC as determined by real time RT-PCR and was correlated to EGFR expression, perhaps pointing to the functional importance of HAS3 in ESCC. Because the systemic application of 4-MU inhibits HA synthesis in both tumour cells and stromal fibroblasts independently of the involved HAS isoforms, the relative contribution and functional significance of HA derived specifically from tumour cell associated HAS3 was addressed. Transduction with shHAS3 lentivirus caused marked knockdown of HAS3 mRNA and protein expression (Figure 3).

The subcutaneous injection of the shHAS3 transduced OSC1 cells into nu/nu mice resulted in a marked inhibition of tumour growth (control 100  $\pm$  57.7% vs. shHAS3 10.1  $\pm$  5.3%, Figure 4A, B) and in a tumour morphology strikingly similar to that seen after systemic inhibition of HA synthesis. Specifically, tumours derived from shHAS3-transduced OSC1 cells exhibited a phenotype

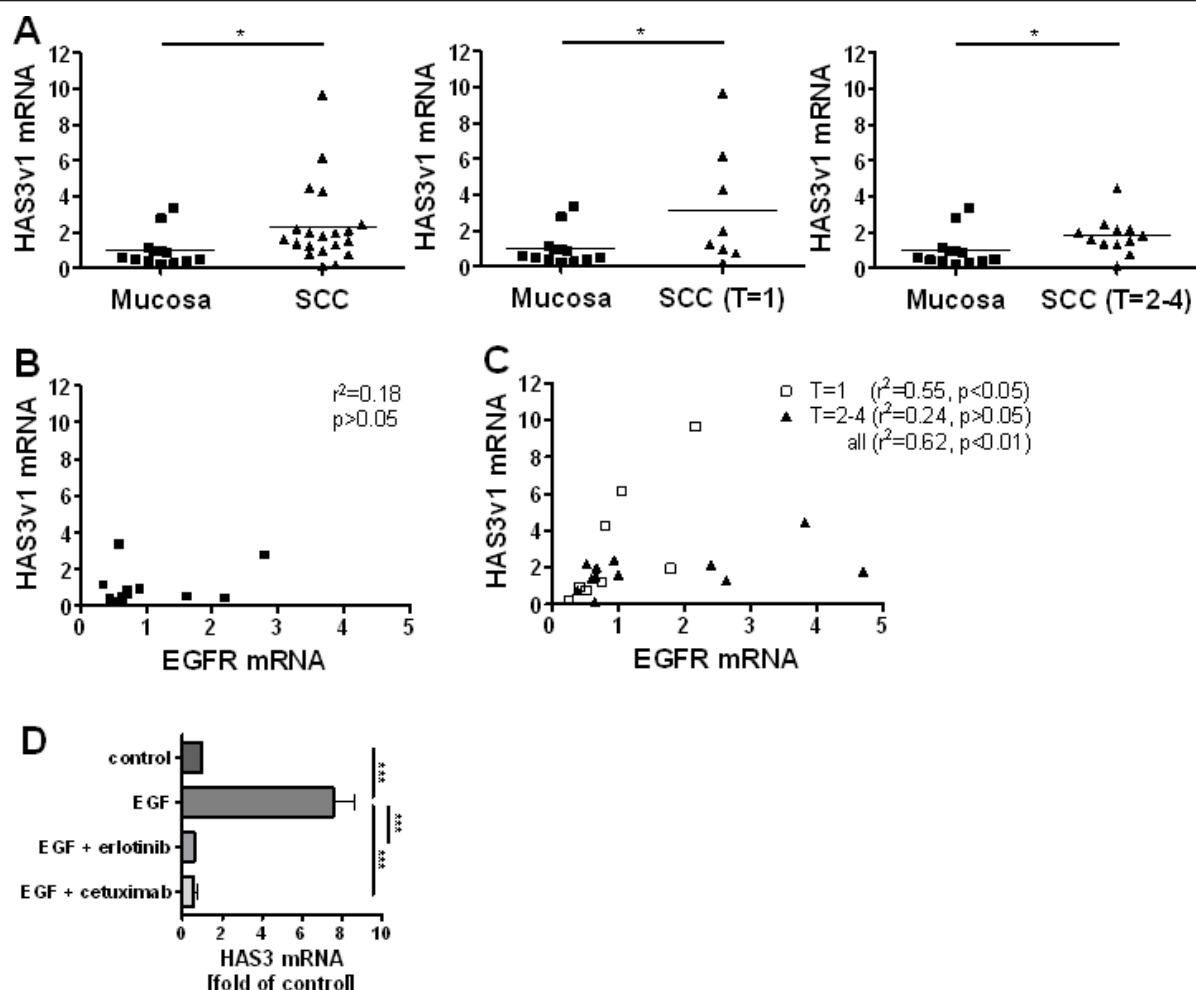


**Figure 1** HAS3 was upregulated and correlated with EGFR in human ESCC. (A) Real-time PCR of HAS3 mRNA from biopsy specimens from normal mucosa ( $n = 13$ ) and human ESCC differentiated into TNM staging (defining tumour size (T), lymph node involvement (N) and existence of metastases (M)) ( $n = 20$ ), mean  $\pm$  SEM, \*,  $p < 0.05$ . (B, C) EGFR expression was determined in the same biopsy specimens as in (A) and correlated to HAS3 expression in normal mucosa (B) and in ESCC (C). HAS3 expression was significantly correlated to EGFR expression in ESCC. (D) EGF stimulated HAS3 mRNA expression in the human ESCC cell line OSC1. This effect was rescued by use of the EGFR tyrosine kinase inhibitor erlotinib and the molecular anti-EGFR antibody cetuximab. Data are mean  $\pm$  SEM;  $n = 3-5$ ; \*\*\*,  $p < 0.001$ .

characterised by large tumour cell clusters with condensed cell-rich borders (Figure 4C, arrows) whereas the morphology of control tumours was characterised by numerous small clusters of OSC1 cells (Figure 4C, left).

Furthermore, alpha-smooth muscle actin staining showed that stromal tissue was strongly pronounced in shHAS3 tumours and separated the large OSC1 cell clusters (Figure 4D). The lentiviral knockdown of HAS3 in the xenografted OSC1 cells resulted in reduced stromal HA staining and in addition in pronounced association of the residual HA with the circumference of tumour cell clusters (Figure 4E). To identify the tumour cells anti-human cytokeratin 18 (CK18) immunostaining was performed in combination with HA staining (Figure 5). Strong stromal HA signals were detected in the

vicinity of CK18 positive tumour cell islands in shHAS3 xenografts (Figure 5B, arrows). However, within the tumour cell clusters HA was less pronounced.

In combination, these findings indicate that 4-MU and shHAS3 reduce the growth of OSC1-derived tumours in nude mice, cause a transition to a more differentiated tumour phenotype and cause formation of large tumour cell clusters that were separated by pronounced stromal tissue with reduced HA content.

#### Possible role of tumour cell CD44 for maintenance of pericellular HA matrix in OSC1

Next, immunostaining was used to determine the expression of the HA receptors CD44 and RHAMM in response to treatment with 4-MU and shHAS3. The

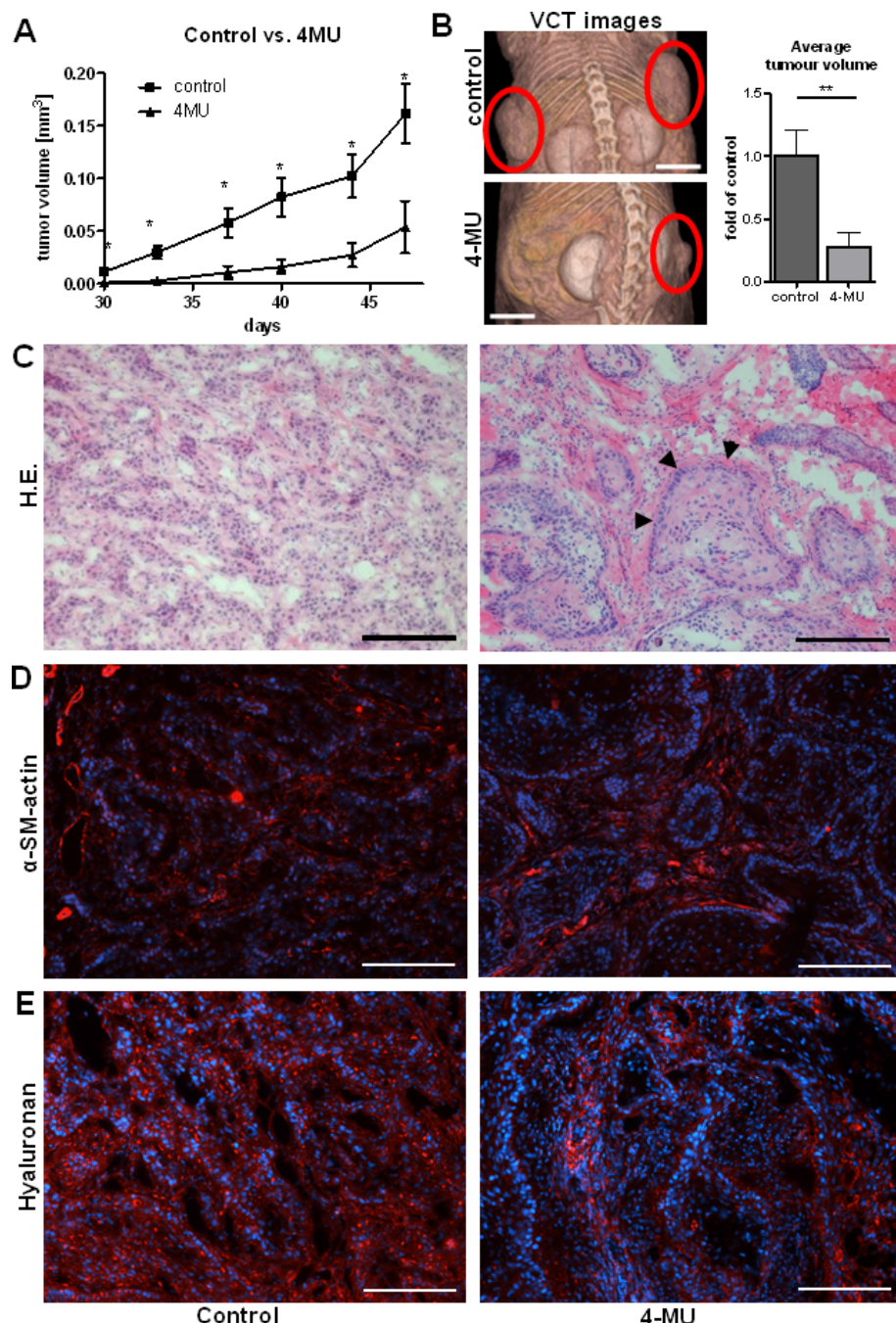


**Figure 2** 4-MU treatment inhibited tumour growth of OSC1 cells in nude mice. Nude mice received subcutaneous injection of  $10^6$  OSC1 cells, and tumour growth was monitored for 47 consecutive days. (A) Tumour volume as determined by calliper measurements; mean  $\pm$  SEM,  $n = 21$  (control), 17 (4MU); \* $p < 0.05$ . (B) Representative fpVCT images of control mice and 4-MU treated mice. Scale bars, 1 cm. Average tumour volumes after sacrifice of mice at the end of the experiment as measured by fpVCT showed a significant reduction in tumour volume in the 4-MU group. (C) Cryosections stained with H&E demonstrated a differentiated tumour phenotype in mice treated with 4-MU. This phenotype was characterised by larger tumour cell clusters with a cell-rich border region (arrows) and pronounced tumour stroma. Scale bars, 200  $\mu\text{m}$ . (D) Stromal fibroblasts were stained with alpha-smooth muscle actin staining (red). Scale bars, 200  $\mu\text{m}$ . (E) Hyaluronan staining (red) was associated with both tumour cells and stromal tissue and was markedly reduced by treatment with 4-MU. Scale bars, 200  $\mu\text{m}$ . Shown are representative images of  $n = 6$  (control) and  $n = 7$  (shHAS3) experiments.

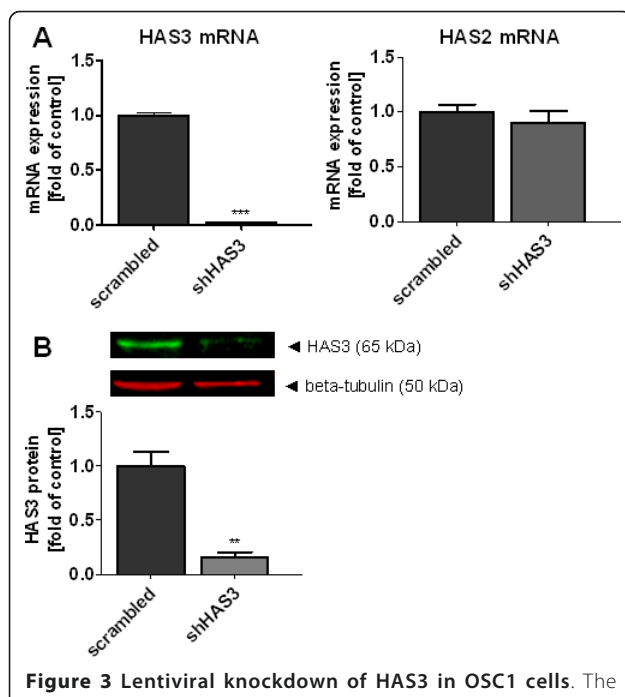


**Figure 3** Lentiviral knockdown of HAS3 in OSC1 cells. The transduction with lentiviral shHAS3 results in (A) a strong decrease of HAS3 mRNA without affecting HAS2 mRNA levels. (B) A significant reduction of HAS3 protein levels was found. Shown are the results of three independent RT-PCR experiments and a representative immunoblot of HAS3 with quantitative analysis of  $n = 3$  experiments, mean  $\pm$  SEM, \*\*  $p < 0.01$ , \*\*\*  $p < 0.001$ .

expression of human CD44 was pronounced in all tumour cells in controls and appeared to be redistributed and upregulated after 4-MU treatment in the tumour cells that faced the stromal tissue (Figure 6A, right). Similar changes in CD44 expression occurred in the shHAS3 group compared to mice that received OSC1 cells transduced with a control vector (Figure 6C, right). RHAMM was strongly expressed in tumour cells and to a weaker extent in stromal cells and did not respond to 4-MU or shHAS3 (Figure 6B, D). Next we considered that upregulated CD44 may bind stromal HA to the tumour cell surface. To further examine this possibility we compared CD44 and HA staining in monoculture of OSC1 with OSC1 and fibroblast co-culture. In monocultures the lentiviral knockdown of HAS3 resulted in an increased CD44 staining similar to the *in vivo* results whereas the pericellular HA signal was hardly detectable (Figure 7A, B). In contrast, in co-cultures of fibroblasts and OSC1 cells, strong pericellular HA signals were obtained in controls (Figure 7C) and were not diminished by knock down of HAS3 in OSC1 (Figure 7D, arrows). These observations suggest that HAS3 depleted OSC1 cells might utilise HA produced by stromal cells by means of increased CD44 expression to maintain the pericellular HA matrix.

### Inhibition of proliferation

To address the underlying mechanisms for inhibition of tumour progression, proliferation was determined by immunostaining in the xenograft tumours. Immunostaining of the proliferation marker Ki67 revealed numerous small clusters of proliferating tumour cells in the controls. The proliferative activity was lower in specimens treated with 4-MU than in controls and the proliferating cells were confined to the outer circumference of the large tumour cell clusters that tested positive for HA, CD44 and RHAMM (Figure 8A; proliferating cells in controls,  $25\% \pm 3\%$ ; proliferating cells in sections of mice treated with 4-MU,  $15\% \pm 3\%$ ;  $p < 0.05$ ;  $n = 4-5$ ).

Subsequently the above described staining patterns were compared to mice xenografted with shHAS3 transduced OSC1 cells. The percentage of proliferating tumour cells was lower in shHAS3-transduced tumours compared to control tumours (Figure 8B: control,  $35\% \pm 6\%$ ; shHAS3,  $20\% \pm 2\%$ ;  $p < 0.05$ ,  $n = 7$ ). As observed after 4-MU treatment, the remaining proliferative activity was confined to the CD44-positive circumference of tumour cell islands. These results strongly support the conclusion that inhibition of HAS3-mediated HA synthesis by OSC1, rather than HA synthesis by stromal cells, is sufficient to inhibit ESCC proliferation and progression and to cause stromal remodelling into a more differentiated tumour phenotype. In combination, tumour cell specific knock down of HAS3 pheno-copied the effect of systemic inhibition of HA synthesis.

### Discussion

HA synthesis is not sufficient for malignant transformation [30], but HA-binding proteins and HA receptors provide a matrix environment that supports the malignant phenotype of cancer cells, stromal cell recruitment, and, thus, the progression of cancer [31]. Recently, the importance of stromal HA-binding proteins was demonstrated for the proteoglycan versican, which triggers the invasion and retention of inflammatory cells in Lewis lung carcinoma and supports metastasis [17]. In human ESCC, HA accumulates in the parenchyma and stroma, and HA is produced by both tumour cells and stroma [22,28]. The amount of HA, which is supposed to be initially high in ESCC, decreases with progression to undifferentiated aggressive carcinomas; this finding suggests increased turnover [32].

Amount of HA and distribution are important prognostic factors in a variety of tumour types. However, important differences exist between tumours that originate from different types of tissue. Tumours arising from simple epithelia such as lung [33], gastric [34], salivary gland [35] and from the thyroid epithelium [36] show a strong correlation between tumour stage and increased HA content. In contrast, those derived from

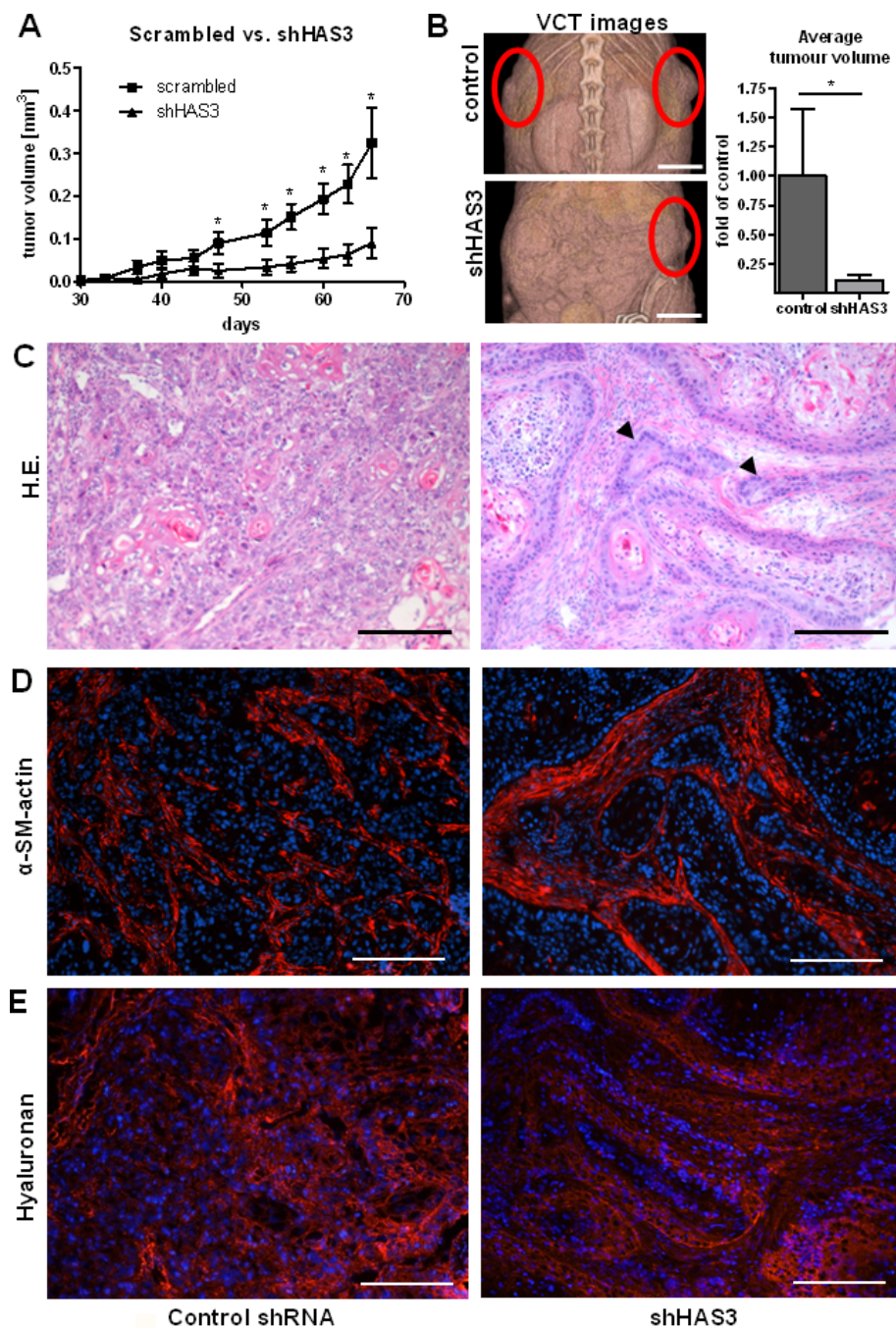


**Figure 4 Lentiviral knockdown of HAS3 in OSC1 cells inhibited tumour growth after xenografting of transduced cells into nude mice.**  
**(A)** Nude mice received subcutaneous injections of  $10^6$  OSC1 cells that had been transduced *in vitro* with a lentivirus containing either scrambled shRNA (control) or shHAS3. Tumour growth as assessed by calliper measurements; mean  $\pm$  SEM,  $n = 6$  (control), 7 (shHAS3); \*,  $p < 0.05$ . **(B)** Representative fpVCT images of mice after 65 days. Average tumour volumes after sacrifice of mice at the end of the experiment as measured by fpVCT showed also a significant reduction in tumour volume in the shHAS3 group. **(C)** H&E revealed changes in tumour morphology strikingly similar to those after 4-MU (compare Figure 2). **(D)** Tumour stroma was visualised by alpha-smooth muscle actin staining (red). **(E)** Xenografting shHAS3 tumour cells caused redistributed hyaluronan staining specifically localised to the outer layer of tumour cell clusters. Scale bars, 200  $\mu$ m. Shown are representative images of  $n = 6$  (control) and  $n = 7$  (shHAS3) experiments.

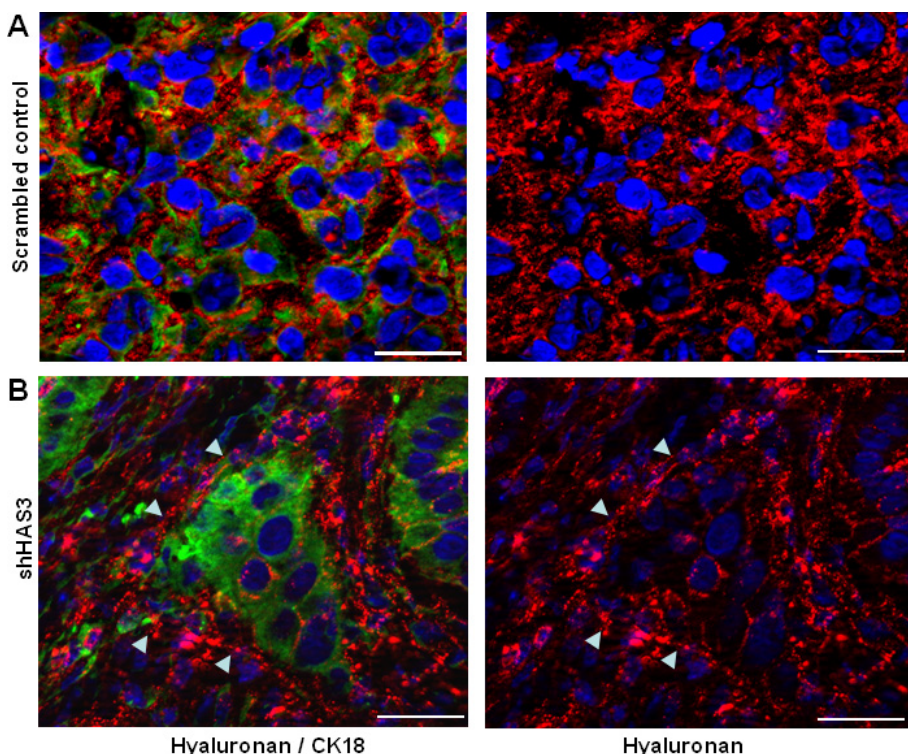


**Figure 5 Detection of the distribution of HA in shHAS3 knockdown xenografts by double staining for tumour cells (CK18) and HA.**

Section from the same series as in Figure 3 were double stained for HA (red) and CK18 (green) to determine the exact location of HA in the xenograft tumour sections. (A) Scrambled control sections revealed a strong HA signal in tumour and stroma. (B) HA staining in shHAS3 samples showed a strong signal in the stroma and tumour/stroma interface (arrows). However, HA was much less pronounced within the tumour cell clusters. Scale bars, 30  $\mu$ m. Shown are representative images of n = 6 (control) and n = 7 (shHAS3) experiments.

stratified epithelia i.e. oral, laryngeal, oesophageal and skin epithelium are characterized by an increase in HA abundance in early tumour stages which decreases in high grade poorly differentiated tumour stages [22,32]. In line with this, a tendency to increased HAS3 levels in the T = 1 stage compared to T = 2-4 stages was also seen in the present work (Figure 1A) although this was not significant.

The experiments reported here were performed to further increase our understanding about the role of HA synthesis in the progression of human ESCC, to evaluate the therapeutic potential of pharmacologic inhibition of HA synthesis for this tumour type and to attempt to differentiate the roles of tumour cell derived HA versus stromal cell-derived HA. Therefore, we analysed the response of ESCC xenografts to systemic versus tumour cell-targeted interference with HA synthesis. The inhibition of ESCC xenograft tumours by 4-MU is in line with reports showing that 4-MU has anti-tumour activity: it inhibits liver metastasis of melanoma cells; sensitises pancreatic cancer cells to gemcitabine and breast cancer cells to trastuzumab treatment in mice; and

decreases prostate cancer cell growth in a xenograft model [11-14]. However, this is the first demonstration that inhibition of a specific HAS isoform, HAS3, in tumour cells is as efficient as systemic HAS-inhibition by 4-MU.

Specifically, a more differentiated tumour phenotype, pronounced stromal strands, fewer singular tumour cells and reduced proliferation were observed. This *in vivo* phenotype shows strong similarities to the phenotype observed *in vitro* after treatment with 4-MU or shHAS3: specifically *in vitro* formation of tumour cell clusters with smooth cell borders occurred in response to inhibition of HA synthesis [24]. After knock down of HAS3 xenografted OSC1 cells still exhibited strong pericellular HA staining concomitant with pronounced CD44 staining suggesting that the elevated CD44 expression may cause binding of stroma derived HA to the tumour cell surface. The recruitment of stromal HA in response to knock down of HAS3 by tumour cells might be part of a compensatory mechanism. This thesis is corroborated by reports that melanoma cells stimulate stromal HA production by soluble factors to facilitate tumour

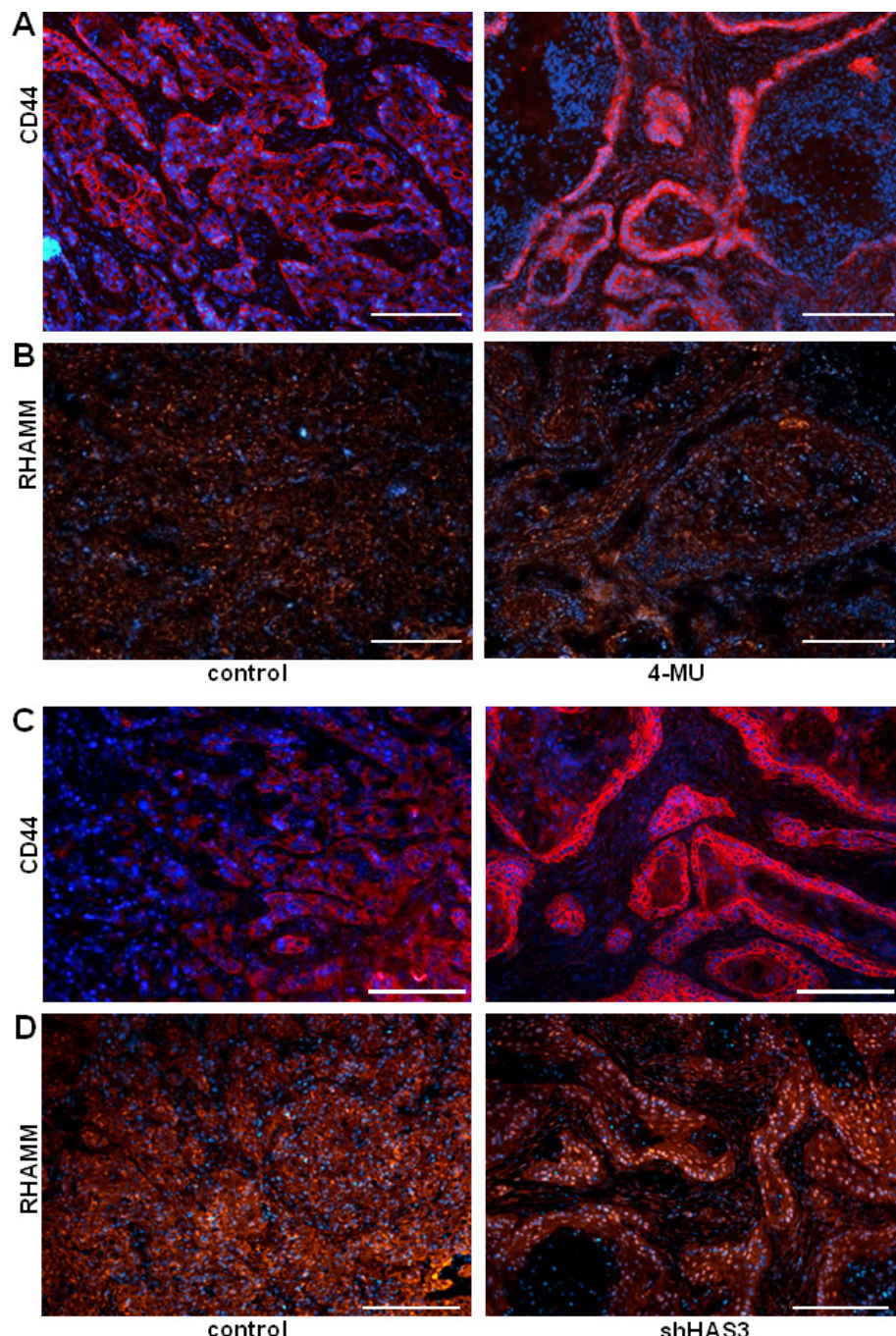


**Figure 6 Expression of CD44 and RHAMM in response to 4-MU versus shHAS3.** (A) 4-MU, immunostaining of human CD44 (red) revealed that CD44 was redistributed to the interface between tumour cells and stroma in response to 4-MU. (B) 4-MU, RHAMM was detected in both OSC1 cells and stromal cells. (C) shHAS3, shHAS3 transduction of tumour cells caused a similar redistribution of human CD44 (red) to the tumour-stroma interface. (D) shHAS3, RHAMM (red) was detected in both shHAS3 transduced OSC1 and stromal cells. Scale bars, 200  $\mu$ m. Shown are representative images of  $n = 6$  (control) and  $n = 7$  (shHAS3) experiments.

growth and invasion [37] and lung carcinoma cells using stimulatory membrane-bound glycoproteins to support locomotion and adhesion [38]. Functionally, the HA/CD44 interactions might contribute to tumour cell proliferation, because after inhibition of HA synthesis by 4-

MU or application of shRNA targeting HAS3 the remaining proliferative activity of tumour cells was confined to the CD44 positive tumour cell - stroma interface. The interaction between tumour cells and stromal fibroblasts mentioned above [38] might play an

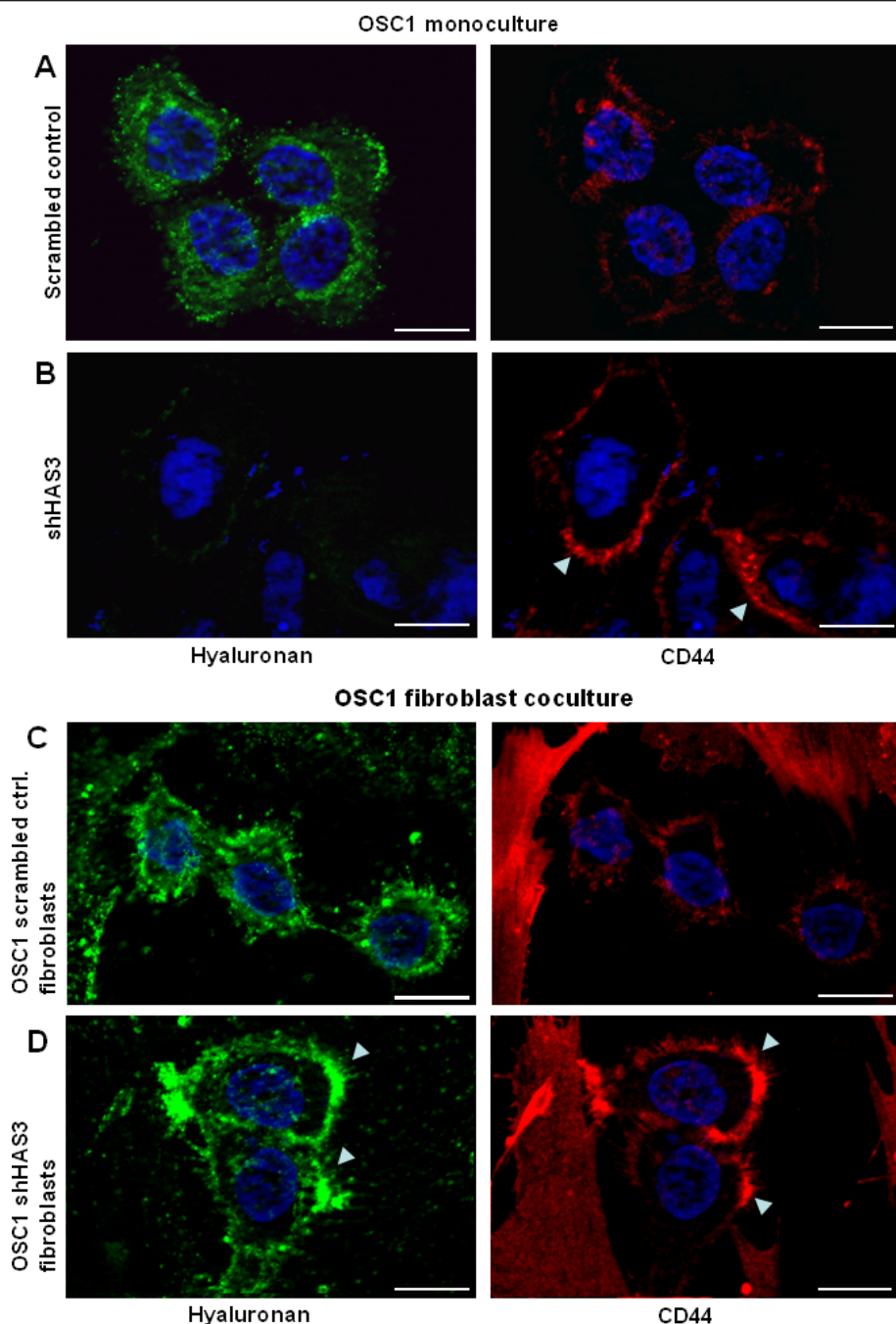


**Figure 7 Co-culture of OSC1 cells and fibroblasts suggested binding of stromal HA to the tumour cell surface via CD44.** OSC1 cells were cultured alone and with fibroblasts to gain mechanistic insight into the origin of OSC1-bound HA in shHAS3 transduced OSC1 cells. (A) In monoculture OSC1 cells showed a strong staining for HA (green) and a weak signal for CD44 (red). (B) Transduction with shHAS3 strongly decreased HA deposition (green) and increased CD44 expression (red, arrows). (C) In co-cultures OSC1 cells exhibited similar pericellular HA as compared to controls in A. (D) In contrast shHAS3 transduced OSC1 cell still exhibited a strong pericellular HA signal (green, arrows) in the presence of fibroblasts that co-localized with increased CD44 (red, arrows). Scale bars, 10  $\mu$ m. Shown are representative images of  $n = 3$ .

important role in this counterregulatory mechanism under HA deprived conditions as it was shown for breast carcinomas that the tumour-adjacent stroma showed elevated levels of HA and hyaluronectin to

facilitate invasion [39]. However, despite the utilisation of stromal HA the current findings clearly showed that tumour cell mediated HA synthesis is critical in this model of ESCC.

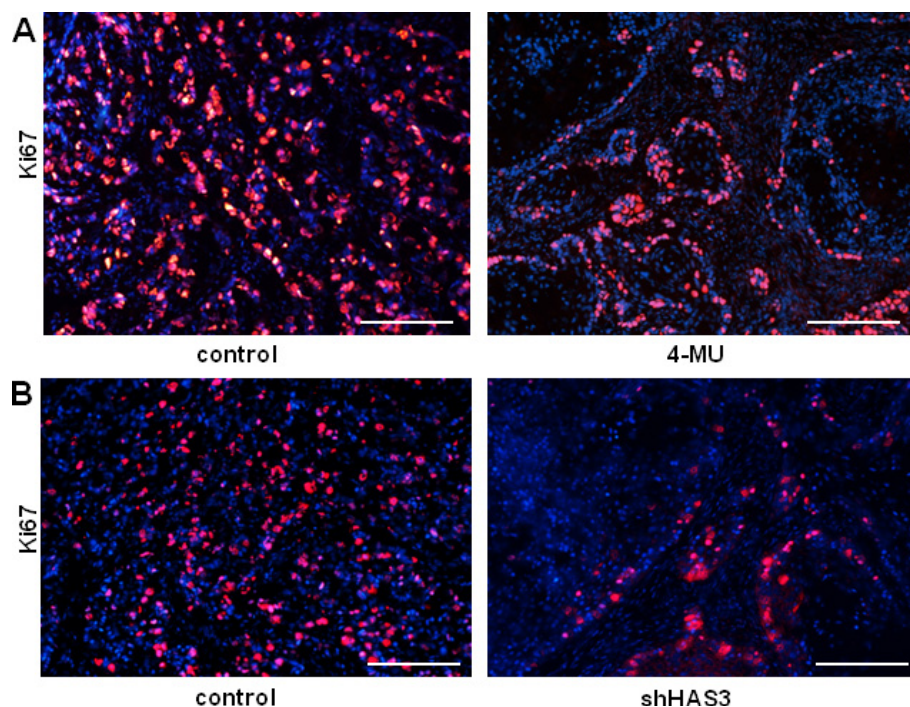


**Figure 8 Effects of 4-MU and tumour cell targeted shHAS3 on proliferation in OSC1 xenografts.** (A) 4-MU, staining of human Ki67 (red) was markedly reduced by 4-MU treatment and confined to the interface between tumour cells and stroma. (B) shHAS3, staining of human Ki67 (red) was markedly reduced in tumour cells transduced with shHAS3. Scale bars 200 μm. Shown are representative images of  $n = 6$  (control) and  $n = 7$  (shHAS3) experiments.

In contrast RHAMM remained more evenly distributed after both interventions. The previous characterisation of the molecular mechanisms underlying the inhibition of malignant ESCC phenotype by interference with HA synthesis *in vitro* suggested that both RHAMM and CD44 signalling are critically involved in the proliferative and migratory phenotype of ESCC [24] through activation of focal adhesion signalling and MAPK signalling. The abundant expression of RHAMM and the redistribution of CD44 upon treatment in xenograft tumours are therefore in line with the proposed role of RHAMM and CD44 in transducing the effects of HA in this model. In addition, in prostate carcinoma HAS3 and HAS2 have been shown to produce HA that is broken down by Hyal1 and that subsequently drives tumour progression and even metastasis [5,40,41]. Therefore, degradation of the high molecular weight HA into smaller fragments may contribute to tumour progression in ESCC and should be investigated in future studies.

Remarkably, the EGF receptor (EGFR, ErbB1) is over-expressed in 40% to 90% of ESCC tumours and overexpression of EGFR is associated with a poor prognosis [42,43]. As we show here, EGFR expression is positively correlated with HAS3 expression in human ESCC. Of note, a steeper correlation between HAS3 and EGFR

levels was found in the subgroup of  $T = 1$  tumours, which possibly suggests a stronger dependence of this early tumour stage on EGF stimulated HAS3 expression. In line with this finding, EGF receptor activation led to induction of HAS3 in ESCC. Induction of HAS3 expression by EGF and ErbB2 receptors has also been shown for keratinocytes, prostate and lung carcinoma cells [44-47]. Therefore, EGF may be an important regulator of HAS3 expression in ESCC, which would be especially relevant in cancers known to be responsive to EGF inhibition, such as head and neck squamous cell carcinoma and metastatic colorectal cancer.

On the other hand, HA has been shown to contribute to the EGFR pathway via HA-CD44 interaction. HA-CD44 complexes colocalize and potentially transactivate the EGF receptor leading to phosphorylation of ERK1 and ERK2 in glioblastoma cell lines [48] and to increase tumour growth, migration and resistance to a variety of chemotherapeutic drugs such as methotrexate, doxorubicin, adriamycin and cisplatin in head and neck cancer [49]. In line with this, reduction of HA synthesis by 4-MU enhances the anticancer activity of gemcitabine in pancreatic cancer cells [12]. Consistently, adding exogenous HA leads to increased resistance to the EGFR inhibitor gefitinib in non small lung cancer cells [47]. However, vice versa, EGFR was also

shown to modify the HA induced expression of a number of genes associated with cellular invasion and proliferation i.e. plasminogen activator inhibitor-1 (PAI-1) or tissue inhibitor of metalloproteinases (TIMP-1) in glioblastoma cell lines [48]. Moreover, in corneal epithelial cells, it was shown that HA and EGFR effects on migration were additive and that inhibition of either HA or EGFR signalling could not completely abolish the combined effects. This observation might indicate additional independent actions of EGFR and HA-CD44 [50]. Taken together, these reports show a close interrelationship between EGFR and HA-CD44 pathways and possibly a positive regulatory feedback in which EGF induces HA production which in turn amplifies the EGFR dependent signalling via CD44. Therefore, therapeutic modulation of the HA system may contribute new anticancer strategies in tumours dependent on EGFR signalling by disruption of this feedback cycle.

## Conclusions

In summary the present data extend the results from cell culture experiments [24] to *in vivo* growth of human oesophageal xenograft tumours. Specifically, it is proposed that ESCC tumour cells overexpress HAS3 in an EGFR dependent manner and that this overexpression supports a dedifferentiated proliferative tumour cell phenotype. Therefore, pharmacologic inhibition of HA synthesis may provide a novel therapeutic target for ESCC.

## Acknowledgements

This work was supported by the Deutsche Forschungsgemeinschaft, DFG Fi 682/4-2. ST was supported by a fellowship from the Gründerstiftung zur Förderung von Forschung und wissenschaftlichem Nachwuchs an der Heinrich Heine Universität Düsseldorf. WTK and NHS received a grant from the Vodafone Stiftung Germany, and NHS was supported by the DFG (STO 464/2-1). We acknowledge funding from The National Institutes of Health (HL073896, HL079090, and HL075930) to RCS. RCS is also funded in part by The William Buchanan Chair in Pediatrics of the University of Texas Southwestern Medical Center, Dallas, Texas, USA.

## Author details

<sup>1</sup>Institut für Pharmakologie und Klinische Pharmakologie, Universitätsklinikum Düsseldorf, Heinrich-Heine Universität Düsseldorf, 40225 Düsseldorf, Germany. <sup>2</sup>Abteilung Hämatologie/Oncologie, Zentrum Innere Medizin, Universitätsklinikum Göttingen, 37075 Göttingen, Germany. <sup>3</sup>Klinik für Visceral- und Gefäßchirurgie der Universität zu Köln, 50937 Köln, Germany.

<sup>4</sup>Klinik für Allgemein-, Viszeral- und Kinderchirurgie, Universitätsklinikum Düsseldorf, 40225 Düsseldorf, Germany. <sup>5</sup>Divisions of Pulmonary & Vascular Biology and Neonatal-Perinatal Medicine, Department of Pediatrics, The University of Texas Southwestern Medical Center, 75390 Dallas, Texas, USA.

<sup>6</sup>Hautklinik, Universitätsklinikum Düsseldorf, 40225 Düsseldorf, Germany.

## Authors' contributions

ST planned and carried out the cell culture and lentiviral experiments, supervised the animal studies and wrote the manuscript. TF carried out and supervised the animal experiments. EP performed the histological staining and analysed them. GD designed primers and performed real time PCR experiments. KJ and CD carried out the animal vCT experiments. FA analysed the vCT experiments and did counselling. KP, WTK, NHS acquired the human oesophageal cancer samples, performed staging and did

counselling. RCS provided the RHAMM antibody and participated in the planning of the experiments. BH participated in the design of the study and did counselling regarding growth factors. JWF designed and coordinated the study and drafted the manuscript. All authors read and approved the final manuscript.

## Competing interests

The authors declare that they have no competing interests.

Received: 12 December 2010 Accepted: 23 March 2011

Published: 23 March 2011

## References

1. Parkin DM, Bray F, Ferlay J, Pisani P: Global cancer statistics, 2002. *Cancer J Clin* 2005, 55:74-7108.
2. Enzinger PC, Mayer RJ: Esophageal cancer. *N Engl J Med* 2003, 349:2241-2252.
3. Cooper JS, Guo MD, Herskovic A, Macdonald JS, Martenson JA, Al-Sarraf M, Byhardt R, Russell AH, Bejtler JJ, Spencer S, et al: Chemoradiotherapy of locally advanced esophageal cancer: long-term follow-up of a prospective randomized trial (RTOG 85-01). *Radiation Therapy Oncology Group*. *JAMA* 1999, 281:1623-1627.
4. Itano N, Sawai T, Yoshida M, Lenas P, Yamada Y, Imagawa M, Shinomura T, Hamaguchi M, Yoshida Y, Ohnuki Y, et al: Three isoforms of mammalian hyaluronan synthases have distinct enzymatic properties. *J Biol Chem* 1999, 274:25085-25092.
5. Bharadwaj AG, Rector K, Simpson MA: Inducible hyaluronan production reveals differential effects on prostate tumor cell growth and tumor angiogenesis. *J Biol Chem* 2007, 282:20561-20572.
6. Li Y, Li L, Brown TJ, Heldin P: Silencing of hyaluronan synthase 2 suppresses the malignant phenotype of invasive breast cancer cells. *Int J Cancer* 2007, 120:2557-2567.
7. Udabage L, Brownlee GR, Nilsson SK, Brown TJ: The over-expression of HAS2, Hyal-2 and CD44 is implicated in the invasiveness of breast cancer. *Exp Cell Res* 2005, 310:205-217.
8. Tofuku K, Yokouchi M, Murayama T, Minami S, Komiya S: HAS3-related hyaluronan enhances biological activities necessary for metastasis of osteosarcoma cells. *Int J Oncol* 2006, 29:175-183.
9. Kim HR, Wheeler MA, Wilson CM, Iida J, Eng D, Simpson MA, McCarthy JB, Bullard KM: Hyaluronan facilitates invasion of colon carcinoma cells in vitro via interaction with CD44. *Cancer Res* 2004, 64:4569-4576.
10. Kakizaki I, Kojima K, Takagaki K, Endo M, Kannagi R, Ito M, Maruo Y, Sato H, Yasuda T, Mita S, et al: A novel mechanism for the inhibition of hyaluronan biosynthesis by 4-methylumbelliferone. *J Biol Chem* 2004, 279:33281-33289.
11. Yoshihara S, Kon A, Kudo D, Nakazawa H, Kakizaki I, Sasaki M, Endo M, Takagaki K: A hyaluronan synthase suppressor, 4-methylumbelliferone, inhibits liver metastasis of melanoma cells. *FEBS Lett* 2005, 579:2722-2726.
12. Nakazawa H, Yoshihara S, Kudo D, Morohashi H, Kakizaki I, Kon A, Takagaki K, Sasaki M: 4-methylumbelliferone, a hyaluronan synthase suppressor, enhances the anticancer activity of gemcitabine in human pancreatic cancer cells. *Cancer Chemother Pharmacol* 2006, 57:165-170.
13. Palyi-Krekk Z, Barok M, Isola J, Tammi M, Szollosi J, Nagy P: Hyaluronan-induced masking of ErbB2 and CD44-enhanced trastuzumab internalisation in trastuzumab resistant breast cancer. *Eur J Cancer* 2007, 43:2423-2433.
14. Lokeshwar VB, Lopez LE, Munoz D, Chi A, Shirodkar SP, Lokeshwar SD, Escudero DO, Dhir N, Altman N: Antitumor activity of hyaluronic acid synthesis inhibitor 4-methylumbelliferone in prostate cancer cells. *Cancer Res* 2010, 70:2613-2623.
15. Toole BP: Hyaluronan: from extracellular glue to pericellular cue. *Nat Rev Cancer* 2004, 4:528-539.
16. Liu N, Gao F, Han Z, Xu X, Underhill CB, Zhang L: Hyaluronan synthase 3 overexpression promotes the growth of TSU prostate cancer cells. *Cancer Res* 2001, 61:5207-5214.
17. Kim S, Takahashi H, Lin W-W, Descargues P, Grivennikov S, Kim Y, Luo J-L, Karin M: Carcinoma-produced factors activate myeloid cells through TLR2 to stimulate metastasis. *Nature* 2009, 457:102-106.

18. Itano N, Zhuo L, Kimata K: Impact of the hyaluronan-rich tumor microenvironment on cancer initiation and progression. *Cancer Sci* 2008, 99:1720-1725.
19. Koyama H, Kobayashi N, Harada M, Takeoka M, Kawai Y, Sano K, Fujimori M, Amano J, Ohhashi T, Kannagi R, et al: Significance of tumor-associated stroma in promotion of intratumoral lymphangiogenesis: pivotal role of a hyaluronan-rich tumor microenvironment. *Am J Pathol* 2008, 172:179-193.
20. Ropponen K, Tammi M, Parkkinen J, Eskelinen M, Tammi R, Lipponen P, Agren U, Alhava E, Kosma VM: Tumor cell-associated hyaluronan as an unfavorable prognostic factor in colorectal cancer. *Cancer Res* 1998, 58:342-347.
21. Lippinen P, Aaltomaa S, Tammi R, Tammi M, Agren U, Kosma VM: High stromal hyaluronan level is associated with poor differentiation and metastasis in prostate cancer. *Eur J Cancer* 2001, 37:849-856.
22. Wang C, Tammi M, Guo H, Tammi R: Hyaluronan distribution in the normal epithelium of esophagus, stomach, and colon and their cancers. *Am J Pathol* 1996, 148:1861-1869.
23. Camenisch TD, Spicer AP, Brehm-Gibson T, Biesterfeldt J, Augustine ML, Calabro A, Kubalak S, Klewer SE, McDonald JA: Disruption of hyaluronan synthase-2 abrogates normal cardiac morphogenesis and hyaluronan-mediated transformation of epithelium to mesenchyme. *J Clin Invest* 2000, 106:349-360.
24. Twarock S, Tammi MI, Savani RC, Fischer JW: Hyaluronan stabilizes focal adhesions, filopodia, and the proliferative phenotype in esophageal squamous carcinoma cells. *J Biol Chem* 2010, 285:23276-23284.
25. Sarbia M, Bosing N, Hildebrandt B, Koldovsky P, Gerharz CD, Gabbert HE: Characterization of two newly established cell lines derived from squamous cell carcinomas of the oesophagus. *Anticancer Res* 1997, 17:2185-2192.
26. Missbach-Guentner J, Dullin C, Kimmina S, Zientkowska M, Domeyer-Missbach M, Malz C, Grabbe E, Stuhmer W, Alves F: Morphologic changes of mammary carcinomas in mice over time as monitored by flat-panel detector volume computed tomography. *Neoplasia* 2008, 10:663-673.
27. Pavan L, Tarrade A, Hermouet A, Delouis C, Titeux M, Vidaud M, Therond P, Evain-Brion D, Fournier T: Human invasive trophoblasts transformed with simian virus 40 provide a new tool to study the role of PPARgamma in cell invasion process. *Carcinogenesis* 2003, 24:1325-1336.
28. Twarock S, Rock K, Sarbia M, Weber AA, Janicke RU, Fischer JW: Synthesis of hyaluronan in oesophageal cancer cells is uncoupled from the prostaglandin-cAMP pathway. *Br J Pharmacol* 2009, 157:234-243.
29. Zhang B, Xia HQ, Cleghorn G, Gobe G, West M, Wei MQ: A highly efficient and consistent method for harvesting large volumes of high-titre lentiviral vectors. *Gene Ther* 2001, 8:1745-1751.
30. Itano N, Atsumi F, Sawai T, Yamada Y, Miyaishi O, Senga T, Hamaguchi M, Kimata K: Abnormal accumulation of hyaluronan matrix diminishes contact inhibition of cell growth and promotes cell migration. *Proc Natl Acad Sci USA* 2002, 99:3609-3614.
31. Tammi RH, Kultti A, Kosma V-M, Pirinen R, Auvinen P, Tammi MI: Hyaluronan in human tumors: pathobiological and prognostic messages from cell-associated and stromal hyaluronan. *Semin Cancer Biol* 2008, 18:288-295.
32. Kosunen A, Ropponen K, Kellokoski J, Pukkila M, Virtaniemi J, Valtonen H, Kumpulainen E, Johansson R, Tammi R, Tammi M, et al: Reduced expression of hyaluronan is a strong indicator of poor survival in oral squamous cell carcinoma. *Oral Oncol* 2004, 40:257-263.
33. Pirinen R, Tammi R, Tammi M, Hirvikoski P, Parkkinen JJ, Johansson R, Bohm J, Hollmen S, Kosma VM: Prognostic value of hyaluronan expression in non-small-cell lung cancer: Increased stromal expression indicates unfavorable outcome in patients with adenocarcinoma. *Int J Cancer* 2001, 95:12-17.
34. Setala LP, Tammi MI, Tammi RH, Eskelinen MJ, Lipponen PK, Agren UM, Parkkinen J, Alhava EM, Kosma VM: Hyaluronan expression in gastric cancer cells is associated with local and nodal spread and reduced survival rate. *Br J Cancer* 1999, 79:1133-1138.
35. Xing R, Regezi JA, Stern M, Shuster S, Stern R: Hyaluronan and CD44 expression in minor salivary gland tumors. *Oral Dis* 1998, 4:241-247.
36. Bohm J, Niskanen L, Tammi R, Tammi M, Eskelinen M, Pirinen R, Hollmen S, Alhava E, Kosma VM: Hyaluronan expression in differentiated thyroid carcinoma. *J Pathol* 2002, 196:180-185.
37. Edward M, Gillan C, Micha D, Tammi RH: Tumour regulation of fibroblast hyaluronan expression: a mechanism to facilitate tumour growth and invasion. *Carcinogenesis* 2005, 26:1215-1223.
38. Knudson W, Biswas C, Li XQ, Nemec RE, Toole BP: The role and regulation of tumour-associated hyaluronan. *Ciba Found Symp* 1989, 143:150-159, discussion 159-169, 281-155.
39. Bertrand P, Girard N, Delpech B, Duval C, d'Anjou J, Daucé JP: Hyaluronan (hyaluronic acid) and hyaluronectin in the extracellular matrix of human breast carcinomas: comparison between invasive and non-invasive areas. *Int J Cancer* 1992, 52:1-6.
40. Bharadwaj AG, Kovar JL, Loughman E, Elowsky C, Oakley GG, Simpson MA: Spontaneous metastasis of prostate cancer is promoted by excess hyaluronan synthesis and processing. *Am J Pathol* 2009, 174:1027-1036.
41. Simpson MA: Concurrent expression of hyaluronan biosynthetic and processing enzymes promotes growth and vascularization of prostate tumors in mice. *Am J Pathol* 2006, 169:247-257.
42. Ozawa S, Ueda M, Ando N, Abe O, Shimizu N: High incidence of EGF receptor hyperproduction in esophageal squamous-cell carcinomas. *Int J Cancer* 1987, 39:333-337.
43. Shimada Y, Imamura M, Watanabe G, Uchida S, Harada H, Makino T, Kano M: Prognostic factors of oesophageal squamous cell carcinoma from the perspective of molecular biology. *Br J Cancer* 1999, 80:1281-1288.
44. Bourguignon LY, Gilad E, Peyrollier K: Heregulin-mediated Erbb2-ERK signaling activates hyaluronan synthases leading to CD44-dependent ovarian tumor cell growth and migration. *J Biol Chem* 2007, 282:19426-19441.
45. Pasonen-Seppanen S, Karvinen S, Torronen K, Hyttinen JM, Jokela T, Lammi MJ, Tammi MI, Tammi R: EGF upregulates, whereas TGF-beta downregulates, the hyaluronan synthases Has2 and Has3 in organotypic keratinocyte cultures: correlations with epidermal proliferation and differentiation. *J Invest Dermatol* 2003, 120:1038-1044.
46. Pasonen-Seppanen SM, Maytin EV, Torronen KJ, Hyttinen JM, Hascall VC, MacCallum DK, Kultti AH, Jokela TA, Tammi MI, Tammi RH: All-trans retinoic acid-induced hyaluronan production and hyperplasia are partly mediated by EGFR signaling in epidermal keratinocytes. *J Invest Dermatol* 2008, 128:797-807.
47. Chow G, Tauler J, Mulshine JL: Cytokines and growth factors stimulate hyaluronan production: role of hyaluronan in epithelial to mesenchymal-like transition in non-small cell lung cancer. *J Biomed Biotechnol* 2010, 2010:485468.
48. Tsatsas D, Kanagasundaram V, Kaye A, Novak U: EGF receptor modifies cellular responses to hyaluronan in glioblastoma cell lines. *J Clin Neurosci* 2002, 9:282-288.
49. Wang SJ, Bourguignon LY: Hyaluronan and the interaction between CD44 and epidermal growth factor receptor in oncogenic signaling and chemotherapy resistance in head and neck cancer. *Arch Otolaryngol Head Neck Surg* 2006, 132:771-778.
50. Nishida T, Nakamura M, Mishima H, Otori T: Hyaluronan stimulates corneal epithelial migration. *Exp Eye Res* 1991, 53:753-758.

doi:10.1186/1476-4598-10-30

**Cite this article as:** Twarock et al: Inhibition of Oesophageal Squamous Cell Carcinoma Progression by *in vivo* Targeting of Hyaluronan Synthesis. *Molecular Cancer* 2011 10:30.

**Submit your next manuscript to BioMed Central and take full advantage of:**

- Convenient online submission
- Thorough peer review
- No space constraints or color figure charges
- Immediate publication on acceptance
- Inclusion in PubMed, CAS, Scopus and Google Scholar
- Research which is freely available for redistribution

Submit your manuscript at  
[www.biomedcentral.com/submit](http://www.biomedcentral.com/submit)



# Hyperglycaemia and aberrated insulin signalling stimulate tumour progression via induction of the extracellular matrix component hyaluronan

Sören Twarock , Christina Reichert, Ulrike Peters, Daniel J. Gorski, Katharina Röck and Jens W. Fischer

Institut für Pharmakologie und Klinische Pharmakologie, Universitätsklinikum der Heinrich-Heine-Universität, Düsseldorf, Germany

Epidemiological studies have detected a higher incidence of various tumour entities in diabetic patients. However, the underlying mechanisms remain insufficiently understood. Glucose-derived pericellular and extracellular hyaluronan (HA) promotes tumour progression and development. In our study, we tested the hypothesis that a diabetic metabolic state, characterised by hyperglycaemia and concomitant aberrant insulin signalling, stimulates tumour progression via the induction of HA synthesis. In a streptozotocin-induced diabetic nude mouse tumour xenograft model, hyperglycaemia and lack of insulin caused an increased formation of tumour-associated HA-matrix, which in turn accelerated tumour progression and neoangiogenesis. This process was effectively attenuated by treatment with 4-methylumbellifrone, a pharmacological inhibitor of HA-synthesis. To define the mechanisms behind these *in vivo* observations, we investigated the impact of hyperglycaemia and insulin on the glucose metabolism in oesophageal squamous cell cancer cells (ESCC). Hyperglycaemia induced HA synthesis while insulin diminished HA production by directing glucose metabolites to glycolysis. *Vice versa*, inhibition of glycolysis, either by knockdown of the glycolytic key enzyme phosphofructokinase or by an experimental abrogation of insulin signalling (knockdown of the insulin receptor and long-term treatment with insulin) augmented HA synthesis. Consequently, these processes induced invasion, anchorage-independent growth and adhesion of ESCC to endothelial cells *in vitro*. Thus, the cellular shift in glucose usage from catabolism of glucose to anabolism of HA driven by hyperglycaemia and insulin resistance may represent an important link between diabetes and cancer progression. Hence, therapeutical inhibition of HA synthesis may represent a promising approach for tumour treatment in diabetic patients.

## Introduction

Diabetes is a widespread disease and is accountable for a plethora of sequelae and pathologies. In recent epidemiological studies, both Type 1 and Type 2 diabetes have been linked to an

**Key words:** diabetes, oesophageal cancer, extracellular matrix, hyaluronan, 4-methylumbellifrone, pharmacological therapy

**Abbreviations:** ESCC: oesophageal squamous cell cancer cells; FACE: fluorophore-assisted carbohydrate electrophoresis; G6P: glucose-6-phosphate; HA: hyaluronan; HCAECs: human coronary artery endothelial cells; HAS: HA synthase; IGF: insulin-like growth factor; INSR: insulin receptor; INSR- $\beta$ : insulin receptor subunit beta; IRS-1: insulin receptor substrate 1; MAPK: mitogen-activated protein kinase; 4-MU: 4-methylumbellifrone; PFKM: phosphofructokinase M.; UDP: uridine diphosphate; TUNEL: TdT-mediated dUTP-biotin nick end labeling

Additional Supporting Information may be found in the online version of this article.

**DOI:** 10.1002/ijc.30776

**History:** Received 6 Oct 2016; Accepted 26 Apr 2017; Online 10 May 2017

**Correspondence to:** Sören Twarock, Institut für Pharmakologie und Klinische Pharmakologie, Universitätsklinikum der Heinrich-Heine-Universität, Düsseldorf, Germany, E-mail: soeren.twarock@uni-duesseldorf.de; Tel. +49-211-81-12500, Fax +49-211-81-14781

increased prevalence of several types of tumour entities<sup>1</sup> including oesophageal cancer.<sup>2</sup> Furthermore, some malignancies, such as hepatocellular carcinoma, respond poorly to chemotherapeutic intervention in diabetic patients.<sup>3</sup> The mechanisms underlying these findings are insufficiently understood but presumably involve high glucose uptake by tumour cells, anabolic actions of insulin and the production of inflammatory cytokines by adipose tissue.<sup>4</sup> Increased uptake and metabolism of glucose, termed the Warburg effect, is regarded as an import hallmark of cancer cells.<sup>5,6</sup> These processes provide an increase in energy substrates and further fuel biomass synthesis.<sup>7</sup> Besides an indirect increase in insulin and insulin-like growth factor (IGF), hyperglycaemia can directly induce pathways that promote proliferation, antiapoptosis and invasion.<sup>8</sup> Furthermore, hyperglycemia causes epigenetic changes, which result in a prolonged activation of tumour cell proliferation.<sup>9</sup> However, many aspects of the direct effects of hyperglycemia on cancer cell progression need further investigation.<sup>10</sup>

Oesophageal cancer occurs with approximately equal probability as either adenocarcinoma or squamous cell carcinoma (ESCC). It is the sixth leading cause of cancer-related deaths worldwide, with a rapid increase in the last decades. Despite technical advances in surgery, intensified use of neoadjuvant chemoradiotherapy, and the introduction of new cytotoxic drugs, the mortality rate associated with

**What's new?**

The mechanisms by which hyperglycemia and other diabetes-related factors promote tumourigenesis are not fully understood, and while glucose metabolites and glycolytic precursors are implicated, their involvement remains largely undefined. In this investigation of hyperglycemia and glucose metabolism in esophageal squamous cell cancer cells, abrogated insulin signalling was found to work in combination with hyperglycemia to redirect glucose usage from glycolytic catabolism to anabolism of HA, an extracellular matrix polysaccharide synthesized from precursors in the first stages of glycolysis. Augmented HA facilitated the development of a malignant phenotype and tumour progression. Its synthesis was blocked by the inhibitor 4-methylumbelliflferone.

oesophageal cancer is similar to its incidence rate. The 5-year survival rate ranges from 15 to 25%.<sup>11</sup>

HA has been identified as a determinant of cancer progression, neoangiogenesis, metastasis and resistance to chemotherapy.<sup>12,13</sup> Of note, HA is an important protumourigenic component of the microenvironment of oesophageal cancer.<sup>14</sup> HA is an unbranched high-molecular-weight polysaccharide, composed of D-glucuronic acid and D-N-acetylglucosamine disaccharide units, and is exclusively synthesised from precursors that are generated during the first steps of glycolysis. The production of HA is facilitated by three isoforms of the HA synthase family (HAS1–3), which are located at the plasma membrane and extrude HA into the extracellular space.<sup>15</sup> HA synthesis can be blocked by the HAS inhibitor 4-methylumbelliflferone (4-MU).<sup>16</sup>

Both hyperglycaemia and elevated HA synthesis have been shown to enhance tumour progression, metastasis and chemotherapy resistance.<sup>10,12,13</sup> Insulin plays a major role in diabetes as well as the cell's glucose metabolism, especially by governing glucose metabolites to distinct downstream pathways.<sup>17</sup> Hence, in the study reported here we addressed the question of whether diabetes-associated hyperglycaemia and aberrant insulin signalling may account for the overproduction of tumour-promoting HA in ESCC cells and whether this process is mediated by a crosstalk between glycolysis and HA synthesis. *In vivo*, in a diabetic nude mouse tumour xenograft model, we investigated the influence of this process on tumour progression and tested systemic HA synthesis inhibition as a potential treatment option. Thus, we evaluated the efficacy of 4-MU, an orally available HAS inhibitor with documented safety in humans, for the treatment of diabetes-induced cancer growth.

**Material and Methods****Reagents and substances**

Unless denoted otherwise, all reagents were obtained from Sigma-Aldrich (St. Louis, MO).

**Cell culture**

The primary ESCC lines OSC1 and OSC2 were isolated and kindly provided by M. Sarbia.<sup>18</sup> KYSE-30, KYSE-270, KYSE-410 and KYSE-520 cells were obtained from DSMZ (Braunschweig, Germany). The identity of the four KYSE cell lines was validated by short tandem repeat (STR) analysis. Briefly, multiplex PCR reactions were performed by amplifying

genomic DNA using Identifier-1 Kit (ABI, Waltham, MA) and ESI17 Kit (Promega, Fitchburg, WI). Analyses were performed in the Institut of Forensic Medicine, University Hospital Duesseldorf. The identity of OSC1 and OSC2 was validated by karyotype analysis in the Institute of Human Genetics, University Hospital Duesseldorf. The cells were maintained as previously described.<sup>19</sup> Insulin resistance was induced *in vitro* by incubation with 100 nM insulin and high-glucose media for 3 days, as previously described.<sup>20</sup> HAS activity was inhibited by treatment with 4-MU, sodium salt (0.3 mM, 24 hr).

**Quantitative real-time reverse-transcriptase polymerase chain reaction**

Total RNA from cultured cells was isolated, reverse transcribed and analysed by qRT-PCR as described previously.<sup>19</sup> The following primers were used (gene of interest, sense and antisense sequences): INSR, 5'-GCTGCCACCAGTACGTCAATT-3' (sense), 5'-GTCGATGGTCTTCGCCTT-3' (antisense); PFKM, 5'-TC ATGACCCATGAAGAGCAC-3' (sense), 5'-GCACCGGTGAAG ATACCAAC-3' (antisense); HAS1, 5'-TTCTTCAGTCTGGAC TATATTGGGA-3' (sense), 5'-CCTGATCACACAGTAGAAAT GG-3' (antisense); HAS2, 5'-GTGGGAAGAACATCAAACAT TTAAGA-3' (sense), 5'-AATGCATCTGTTAGCTCTTG-3' (antisense); HAS3, 5'-GGAGGAGGATCCCCAAGTAG-3' (sense), 5'-CTGCTCAGGAAGGAAATCCA-3' (antisense); GLUT1, 5'-CTGAAGTCGCACAGTGAATA-3' (sense), 5'-TGGGTGGAGT TAATGGAGTA-3' (antisense); GLUT4, 5'-CCTGGTCCTTG CTGTGTTCT-3' (sense), 5'-CCAGGCCACGTCTCATTGTAG-3' (antisense).

**Immunoblot analysis**

Immunoblots were performed as previously described.<sup>19</sup> Primary antibodies against the following target proteins were used: IRS-1 (D23G12), p-IRS1 (Ser307) from Cell Signaling Technology (Danvers, MA); p-Tyr (PY99, Santa Cruz, Dallas, TX); insulin receptor beta (ab69508; Abcam, Cambridge, UK) and beta tubulin I (T7816; Sigma-Aldrich). Detection was performed with IR fluorescent secondary antibodies (IrDye; LI-COR, Lincoln, NE) using an Odyssey Infrared Imaging System (LI-COR).

**Transfection and gene silencing**

Knockdown of the genes of interest was achieved by lipotransfection of siRNAs or scrambled control siRNA (Qiagen, Hilden,

Germany) with Lipofectamine RNAiMaxx (Thermo Fisher, Waltham, MA) according to the manufacturer's instructions. The following siRNAs were used (gene of interest, Qiagen order numbers): INSR SI00004508, SI00004515, PFKM SI00604835, SI00604828, HAS3 SI04201246, SI00433895, AllStars Negative Control siRNA SI03650318.

#### HA measurement

HA in supernatants was measured by a commercially available HABP immunoaffinity assay (Corgenix, Broomfield, CO). For detection of HA newly synthesised from glucose, a radioactive HA assay was used. This assay was performed analogously to HA purification as described in literature.<sup>21</sup>

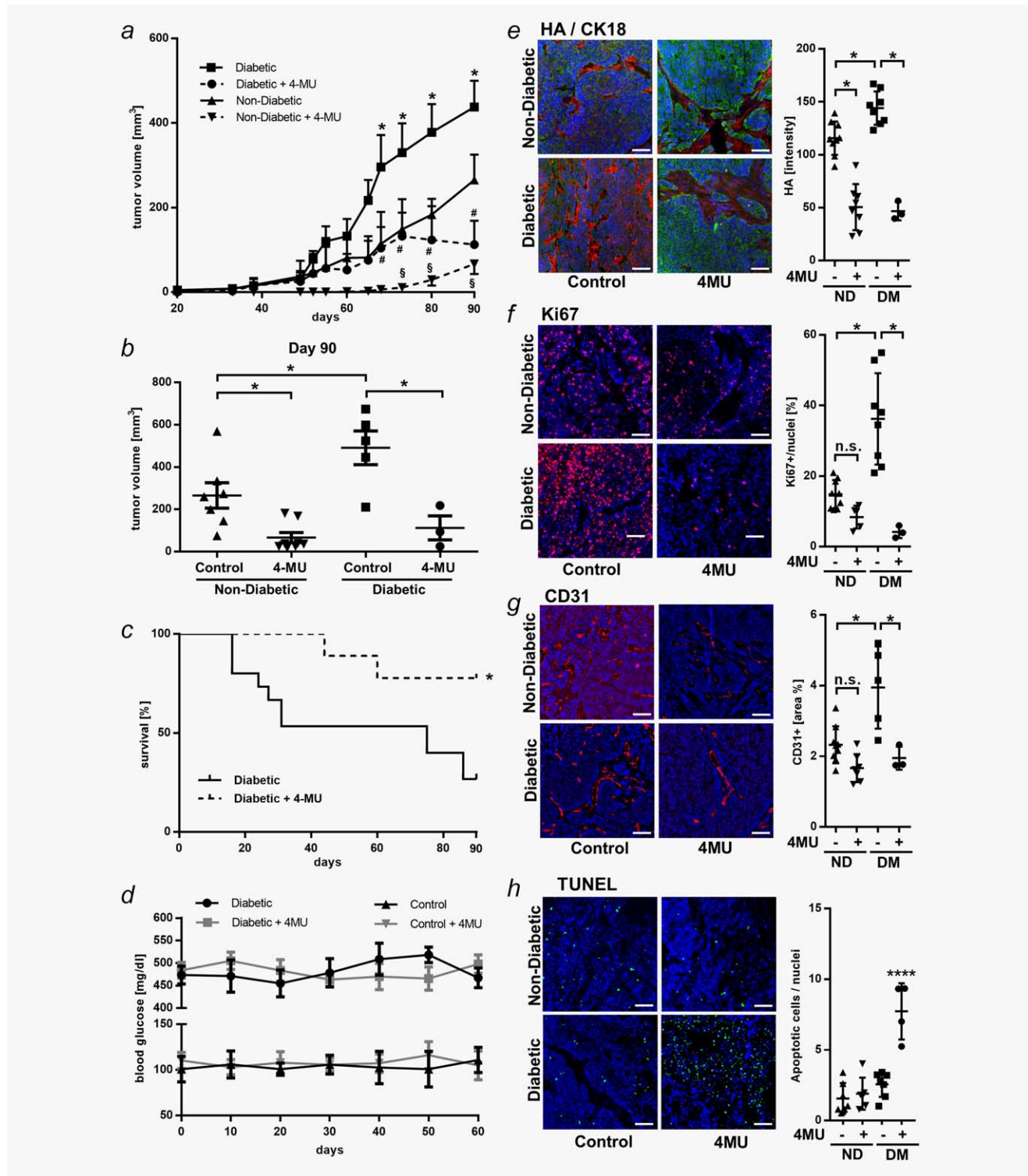


Figure 1.

Briefly, cells were incubated with [<sup>14</sup>C]-labelled glucose (20  $\mu$ Ci/ml; Hartmann Analytic, Braunschweig, Germany). Next, pronase (200  $\mu$ M/ml) was used to break up HA protein complexes, and half of the extract was digested with bovine hyaluronidase (10 U/ml, H3506, Sigma-Aldrich). To remove any unincorporated radiolabels, low-molecular-weight sugars and peptides, both samples were separately applied to a DEAE-Sephacel column (GE Healthcare, Little Chalfont, UK). Eluted HA was mixed with scintillation fluid (Rotiszint; Roth, Karlsruhe, Germany) and counted in a scintillation counter. The amount of HA was defined as the number of hyaluronidase-susceptible counts per minute (cpm) normalised to the protein content of the cell layer, as determined by Bradford assay.

#### Quantification of glucose metabolites

Intracellular glucose-6-phosphate and pyruvate as well as extracellular lactate concentrations were quantified with commercially available colorimetric assays (Lactate Assay Kit II, Glucose-6-Phosphate Assay Kit; Sigma-Aldrich and Pyruvate Assay Kit; abcam) according to manufacturer's instructions. Intracellular uridine diphosphate (UDP)-glucose/galactose, UDP-glucuronic acid and UDP-N-acetylglucosamine were quantified by fluorophore-assisted carbohydrate electrophoresis (FACE) as previously described.<sup>22</sup> Briefly, cultures were given low or high glucose containing media for 24 hr. Cell layers were collected on ice and sonicated, nucleotide sugars were then purified using solid phase extraction with ENVI-Carb SPE columns (Sigma-Aldrich). Monosaccharides were released from nucleotide residues by mild acid hydrolysis and conjugated to 2-aminoacridone (Invitrogen) before separation by gel electrophoresis. Samples were run alongside a control ladder of glucose, N-acetylglucosamine and glucuronic acid (Sigma-Aldrich). Band intensities were then integrated using image J and normalized to DNA content determined by a Quant-iT PicoGreen dsDNA Assay Kit (Invitrogen).

#### Proliferation assay

Proliferation was measured by a <sup>3</sup>[H]-thymidine assay as previously described.<sup>19</sup>

#### Adhesion assay

The impact of HA on the adhesion of cancer cells to endothelial cells was assessed as previously described<sup>23</sup> but with microscopic analysis instead of a radioactive assay. In detail, human coronary artery endothelial cells (HCAECs; Promocell, Heidelberg, Germany) were grown to confluence in monolayers in a 12-well plate. OSC1 cells were labelled with calcein (1  $\mu$ M) for 20 min and were then seeded at a density of  $5 \times 10^4$  cells per well on top of the confluent HCAEC monolayers, followed by a 45 min incubation at 4°C with gentle shaking. After washing with PBS, the bound cells were visualised and counted by fluorescence microscopy. To verify HA-dependency of the adhesion, each condition was also treated with hyaluronidase (10 U/ml), and the remaining cells were subtracted.

#### Matrigel invasion assay

The invasive capability of OSC1 cells over 24 hr was determined with a BD BioCoat Matrigel Invasion Chamber (Cat. 354480; BD Biosciences, Franklin Lakes, NJ) according to the manufacturer's instructions. Cells were counted with a bright-field microscopy after HE staining.

#### Soft agar assay

The capability for anchorage-independent growth in response to glucose and insulin was assessed as follows: To inhibit adhesion of the cells, the bottom of each well in a 24-well plate was coated with 0.5% Noble agar (BD Difco Agar; BD Biosciences) in RPMI-1640 full medium. OSC1 cells were suspended in a 0.3% agar-RPMI mixture and applied onto the solidified bottom layer. The medium was changed twice weekly, and the assay was analysed after three weeks by

**Figure 1. Hyperglycaemia and insulin depletion enhance hyaluronan-dependent tumour progression in a Type 1 diabetes nude mouse xenograft model.** (a) Xenograft OSC1 tumour growth over 90 days in diabetic and nondiabetic mice with (dashed lines) or without (solid lines) application of the hyaluronan synthase inhibitor 4-MU. Two-way ANOVA with Tukey's post-test: \*,  $p < 0.05$  diabetic vs. nondiabetic; #,  $p < 0.05$  diabetic vs. diabetic + 4-MU; \$,  $p < 0.05$  nondiabetic vs. nondiabetic + 4-MU (b) Mean tumour volumes at Day 90. One-way ANOVA with Tukey's post-test of seven nondiabetic, five diabetic, eight nondiabetic + 4-MU and three diabetic + 4-MU tumours. Shown are scatter-plots with mean  $\pm$  SEM. \*,  $p < 0.05$  vs. indicated condition. (c) Survival rate of tumour-bearing diabetic nude mice  $\pm$  4-MU within 90 days after xenografting. Fifteen diabetic vs. nine diabetic mice with 4-MU treatment were observed. At the end of the experiment, four diabetic mice and seven 4-MU treated diabetic mice remained alive. Log-rank (Mantel-Cox) test: \*,  $p < 0.05$ . (d) Blood glucose levels. Fifteen nondiabetic (ND), nine diabetic (DM), seven ND + 4-MU and seven DM + 4-MU were observed over 60 days. There was no statistical difference between control and 4-MU treated mice in diabetic and nondiabetic mice, respectively. (e) HA deposition (HABP staining, red) in tumour (cytokeratin 18, CK18, green) and stroma; nuclei (blue, Hoechst). Bar, 100  $\mu$ m. Shown are representative images. Quantification of nine nondiabetic (ND), eight diabetic (DM), eight ND + 4-MU and three DM + 4-MU tumours, presented as scatterplot with mean  $\pm$  SEM. Statistical significance by one-way ANOVA: \*,  $p < 0.05$  vs. indicated condition. (f) Proliferation rate in tumour tissue (Ki67 staining, red); nuclei (blue, Hoechst). Bar, 100  $\mu$ m. Shown are representative images. Quantification of nine nondiabetic (ND), eight diabetic (DM), five ND + 4-MU and three DM + 4-MU tumours, presented as scatterplot with mean  $\pm$  SEM. Statistical significance by one-way ANOVA: \*,  $p < 0.05$  vs. diabetic condition without 4-MU. (g) Endothelial cell staining (CD31 staining, red) in tumour tissue; nuclei (blue, Hoechst). Bar, 100  $\mu$ m. Shown are representative images. Quantification of nine nondiabetic (ND), five diabetic (DM), seven ND + 4-MU and three DM + 4-MU tumours, presented as scatterplot with mean  $\pm$  SEM. Statistical significance by one-way ANOVA: \*,  $p < 0.05$  vs. diabetic condition without 4-MU. (g) Apoptotic cells (TUNEL staining, green); nuclei (blue, Hoechst). Bar, 100  $\mu$ m. Shown are representative images. Quantification of seven nondiabetic (ND), six diabetic (DM), seven ND + 4-MU and four DM + 4-MU tumours, presented as scatterplot with mean  $\pm$  SEM. Statistical significance by one-way ANOVA: \*,  $p < 0.05$  vs. all other conditions. [Color figure can be viewed at [wileyonlinelibrary.com](http://wileyonlinelibrary.com)]

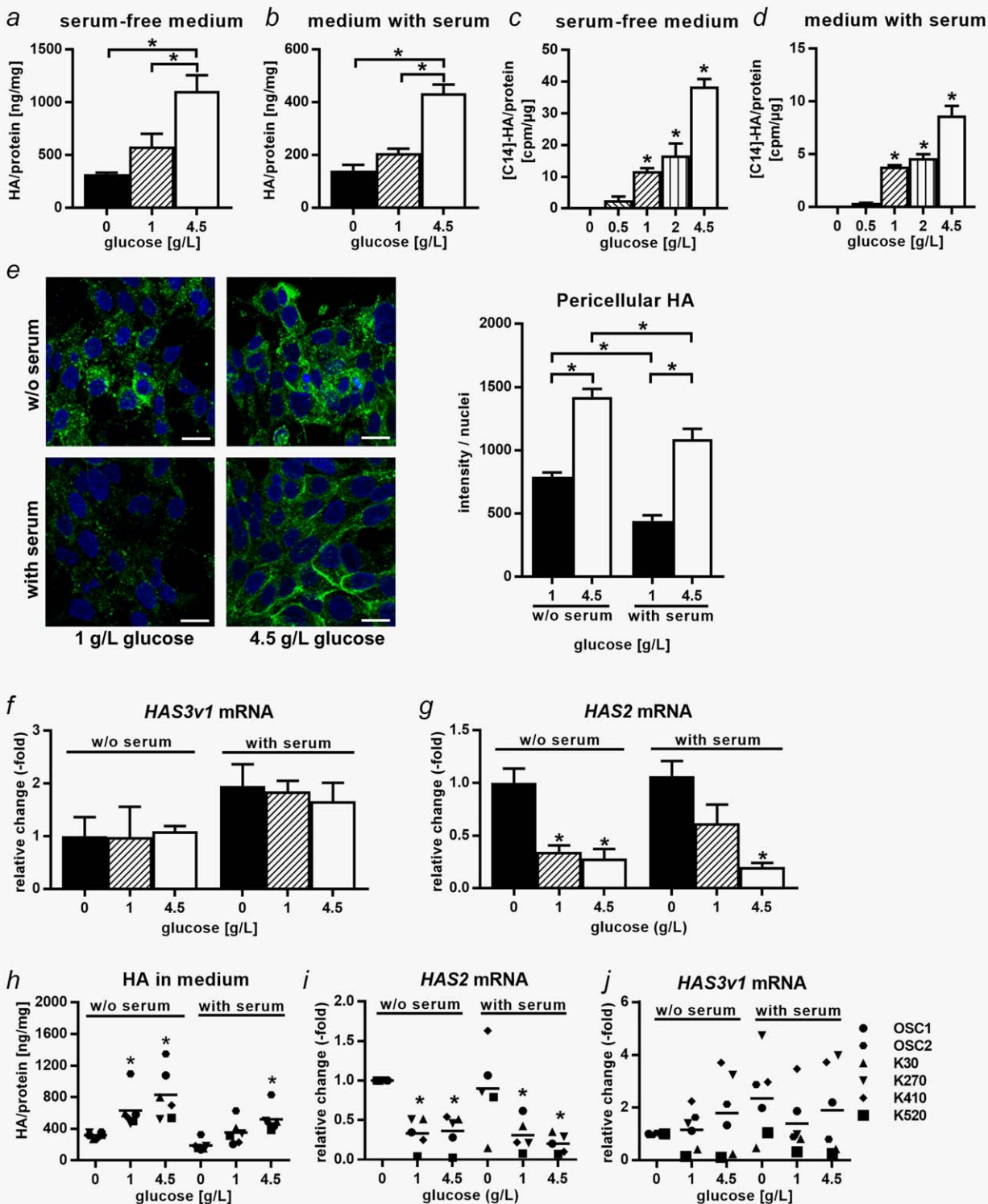


**Figure 2. Elevated glucose concentrations facilitate the production of hyaluronan in oesophageal squamous cell carcinoma cell lines.** (a, b) Hyaluronan (HA) concentrations in the medium of OSC1 cells normalised to cell layer protein in response to glucose and serum (10% FCS) after 24 hr measured by hyaluronic acid binding protein (HABP) assay. Data are mean  $\pm$  SEM from three independent experiments. \*,  $p < 0.05$  vs. 4.5 g/L glucose. (c, d) [ $^{14}$ C]-glucose integration in HA synthesis normalised to protein of OSC1 cell layer in response to glucose and serum after 24 hr. Data are mean  $\pm$  SEM from three independent experiments. \*,  $p < 0.05$  vs. 0 g/L glucose. (e) Pericellular HA coat of OSC1 cells in response to glucose and serum visualised by HA affinity cytochemistry after 24 hr (HABP, green); nuclei (blue, Hoechst). Scale bar, 10  $\mu$ m. Shown are representative results from three independent experiments, mean  $\pm$  SEM. \*.  $p < 0.05$ . (f, g) Transcriptional changes in hyaluronan synthase (HAS) 2 and 3v1 mRNA expression in OSC1 cells in response to glucose and serum after 24 hr. HAS1 mRNA was not detectable. Data are mean  $\pm$  SEM from three independent experiments. \*,  $p < 0.05$  vs. 0 g/L glucose. (h, i, j) HA production and HAS mRNA expression in six oesophageal squamous cell carcinoma (ESCC) cell lines: OSC1, OSC2, Kyse 30, Kyse 270, Kyse 410 and Kyse 520 (each cell line represents one n). HAS1 mRNA was not detectable in any cell line. Data are mean  $\pm$  SEM from six independent experiments. \*,  $p < 0.05$ , \*\*,  $p < 0.01$ , \*\*\*,  $p < 0.001$  vs. 0 g/L glucose. [Color figure can be viewed at [wileyonlinelibrary.com](http://wileyonlinelibrary.com)]

counting formed colonies larger than 50 µm with a bright-field microscope.

#### Nude mouse xenograft model and diabetes induction

T cell-immunodeficient male Crl:NU-Foxn1<sup>nu</sup> mice were obtained from Charles River Laboratories (Wilmington, MA).<sup>24</sup> At the age of 6 weeks, a single dose of streptozotocin (240 mg/kg body weight) was injected. When blood sugar levels (tail vein blood glucose test; GlucoSmart, MSP boddman, Bobingen, Germany) of all mice were verified to be within the target range of 400–600 mg/dl, half of the diabetic and nondiabetic mice was treated with 4-MU (AlfaAesar, ThermoFisher, Waltham, MA), which was pelleted into chocolate flavoured chow at a daily dose of 10 mg/g body weight; the other half of the mice received respective placebo chow. Two days later,  $1 \times 10^6$  OSC1 cells were injected into both flanks of each mouse. Palpable tumours were detected at approximately Day 20 after xenografting. The mice were observed for a total period of 90 days. The tumour volume was calculated by calliper measurements with the formula  $height \times length \times depth \times 0.52$  as described.<sup>25</sup> At the end of the observation period, the mice were sacrificed, and tumour xenografts were explanted for histological analysis. The animal experiments were approved by the local animal facility and the corresponding authority (LANUV NRW) and were carried out following the rules and guidelines of the German animal welfare law (*Tierschutzgesetz*).

#### Immunostainings

Cryosections (8 µm) were derived from tumour tissue and fixed with formalin. Targets stained comprise HA (HABP; Calbiochem, San Diego, CA), Ki67 (rabbit anti-Ki67; Novus, Littleton), CK18 (guinea pig anti-CK18; Progen, Heidelberg, Germany), CD31 (rat anti-CD31; Abcam) and CD44 (rabbit anti-CD44; Sigma-Aldrich). Apoptotic cells were detected with the Click-it Plus TdT-mediated dUTP-biotin nick end labeling (TUNEL) assay (C10617; Thermo Fisher) according to manufacturer's instructions. Nuclei were counterstained using Hoechst 33342 (Invitrogen, Carlsbad, CA).

#### Statistical analysis

All datasets were analysed either with ANOVA plus Tukey's or Sidak's *post hoc* test, with Log-rank (Mantel-Cox) test or with Student's *t*-test, as appropriate. All statistical analyses were carried out using GraphPad Prism 6 (Graphpad Software, La Jolla, CA). Data are presented as mean ± SEM. Statistical significance was set at the level of  $p < 0.05$ .

## Results

#### Diabetic conditions facilitate HA-mediated tumour progression *in vivo*

To investigate the impact of a diabetic metabolic state on tumour growth and morphology, we developed a Type 1 diabetes nude mouse tumour xenograft model characterised by hyperglycaemia and insulin deprivation: Induction of diabetes

in nude mice by a single injection of streptozotocin yielded blood sugar levels of approximately 400 mg/dl. Starting at around Day 55 after injection of the OSC1 squamous carcinoma tumour cells, the tumour growth curves of nondiabetic and diabetic mice diverged. On Day 90, the tumour volume in diabetic mice was significantly higher than that in nondiabetic mice, which indicates tumour promotion by Type I diabetes conditions. To assess the contribution of HA to this observation and to evaluate pharmacological HA synthesis inhibition as a therapeutic measure, nondiabetic and diabetic mice were fed the HAS inhibitor 4-MU. Of note, 4-MU substantially decreased the rate of tumour growth in diabetic and control mice, however with a more pronounced absolute effect in diabetic mice (Figs. 2a and 2b). Strikingly, 4-MU also increased the mean survival time of the diabetic mice (Fig. 2c). These effects were not accompanied by significant changes in blood glucose concentrations (Fig. 2d). Diabetic conditions resulted in an increase of the total HA deposition in xenograft tumour tissue, which was effectively reduced by treatment with 4-MU (Fig. 2e). Moreover, diabetic conditions strongly increased important histological parameters of tumour progression, i.e., the rate of Ki67-positive proliferating cells (Fig. 2f) and the amount of CD31-positive vessel formation (Fig. 2g). Intriguingly, only under diabetic conditions did 4-MU treatment significantly reduce proliferation (Fig. 2f) and vessel formation (Fig. 2g), and also cause a strong induction of apoptosis (Fig. 2h). The expression of the main HA receptor in ESCC, CD44, was not altered in response to hyperglycemia or 4-MU treatment (supporting information Fig. S1). These results indicate that elevated HA synthesis is of particular importance for tumour growth under diabetic conditions and that 4-MU may be an effective therapeutic drug under these conditions.

#### Elevated glucose supply augments HA production independently of HAS transcription

*In vivo*, elevated tumour growth under diabetic conditions was accompanied by increased histological deposition of HA while the inhibition of HA synthesis by 4-MU inhibited tumour growth. To elucidate the mechanism by which diabetic metabolic conditions induce HA synthesis, we performed the following *in vitro* experiments.

As the glycosaminoglycan HA is exclusively synthesised from glucose precursors, we first investigated the influence of glucose supply on HA synthesis. Elevated glucose concentrations caused a dose-dependent increase in HA production by OSC1 cells in medium without (Fig. 3a) and with (Fig. 3b) addition of serum. Strikingly, the presence of serum resulted in lower HA synthesis than did the same glucose concentration in serum-free medium. To verify that the observed increase of HA in the medium was caused by *de novo* synthesis originating from increased glucose uptake, we additionally measured the incorporation of radioactive labelled [<sup>14</sup>C]-glucose into newly synthesised HA. In agreement with the aforementioned results, radioactive HA also strongly increased with higher glucose

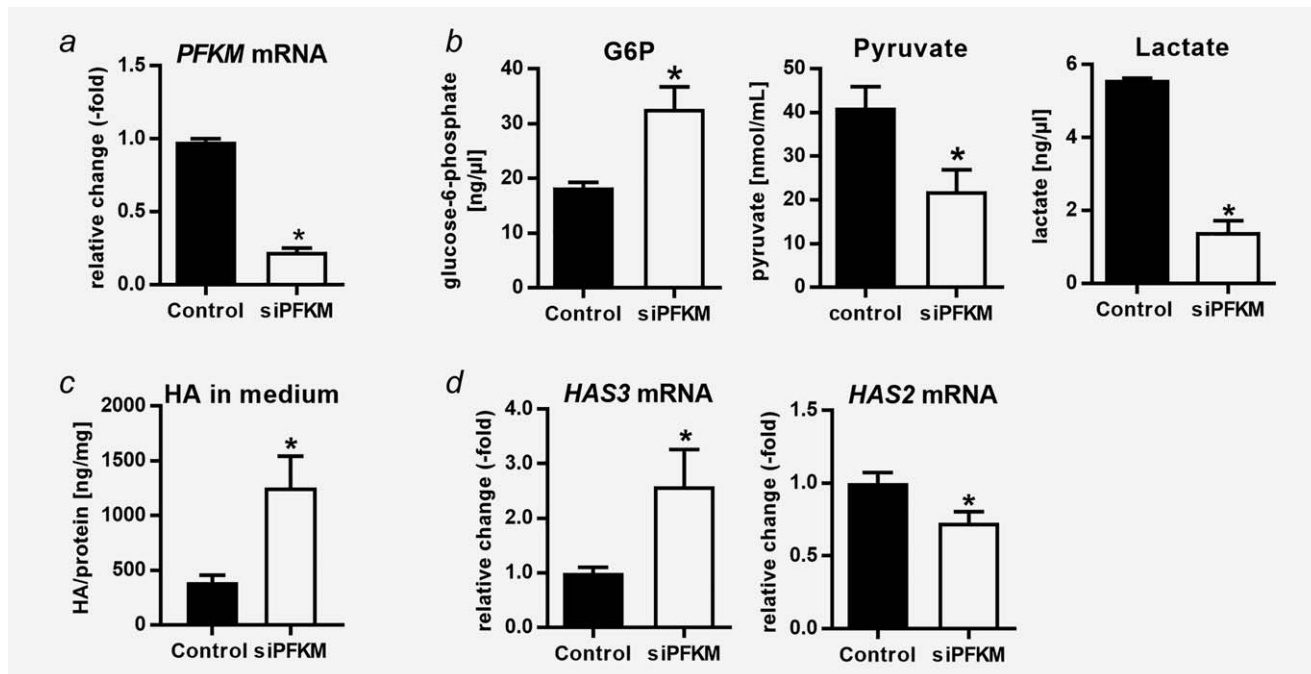


**Figure 3. Abrogation of glycolysis directs glucose usage to HA synthesis.** (a–d) Changes in the concentration of the glucose metabolites glucose-6-phosphate (G6P,  $n = 3$ ), pyruvate ( $n = 6$ ) and lactate ( $n = 3$ ), in the amount of hyaluronan (HA,  $n = 8$ ) and in the hyaluronan synthase (HAS) mRNA expression (HAS3v1,  $n = 8$ ; HAS2,  $n = 6$ ) in response to abrogation of glycolysis by knockdown of phosphofructokinase M (PFKM) in OSC1 cells with presence of serum after 24 hr ( $n = 5$ ). Data are mean  $\pm$  SEM from three to eight independent experiments. \*,  $p < 0.05$  vs. control.

concentrations in medium without (Fig. 3c) and with (Fig. 3d) serum. Consistently, the pericellular HA coat also increased strongly in response to glucose and also to serum deprivation (Fig. 3e). These results indicate that increased substrate supply is a driving factor for elevated HA synthesis. Interestingly, transcriptional changes in HAS genes were not causally involved in this process, since there was no upregulation of HAS3 (Fig. 3f) and HAS2 mRNA was even reduced with higher glucose concentrations (Fig. 3g); HAS1 was not detected. The results observed in OSC1 cells were confirmed in a total of six different ESCC cell lines (OSC1, OSC2, KYSE-30, KYSE-270, KYSE-410 and KYSE-520) (Figs. 3h–3j). To investigate the direct effect of hyperglycemia on HA precursors, sugar nucleotides were quantified by FACE, this showed elevated UDP-glucose/galactose concentrations under stimulation with high glucose media (supporting information Fig. S2a). In this assay, UDP-glucuronic acid (supporting information Fig. S2b) and UDP-N-acetylglucosamine (supporting information Fig. S2c) showed only trends toward increased concentrations, which is likely the result of rapid metabolism by the HAS enzymes.

#### Direct inhibition of glycolysis stimulates hyaluronan synthesis

The observation that HA synthesis is dependent on the availability of glucose precursors raises the question, whether other pathways metabolising these precursors may interfere with HA synthesis. Among these pathways, downstream glycolysis and the pentose phosphate pathway are the most relevant. To

analyse the flux of glucose metabolites, we measured the intracellular concentration of glucose-6-phosphate (G6P), the pivotal upstream metabolite of both HA synthesis and glycolysis, as well as extracellular lactate concentrations as an indicator of glycolytic activity. Silencing of the glycolytic key enzyme phosphofructokinase M (PFKM, Fig. 4a) yielded a pronounced disruption of glycolysis, which presented as a strong increase in the intracellular G6P pool and a decrease in pyruvate and lactate concentrations (Fig. 4b). As a result, HA synthesis (Fig. 4c) as well as HAS3 mRNA were increased while HAS2 mRNA was reduced (Fig. 4d). The rise in HAS3 mRNA expression, which was not detected in the experiments involving glucose stimulation (see Figs. 3f and 3j), may be the result of a transcriptional feedback loop between substrate supply to the HAS enzymes and HAS mRNA expression. Experiments with different PFKM knockdown efficiencies show that HAS3 mRNA expression is positively correlated with PFKM knockdown efficiency (supporting information Fig. S3a) while HAS2 mRNA shows a trend to a negative correlation (supporting information Fig. S3b). Thus, these experiments show a strong cross-talk between those two pathways metabolising glucose, i.e., glycolysis and HA synthesis.

#### Insulin diminishes HA synthesis by stimulation of glycolysis

The combination of the observations that the presence of serum decreased HA synthesis (see Fig. 3) and that HA synthesis is counteracted by glycolytic activity (see Fig. 4) led us

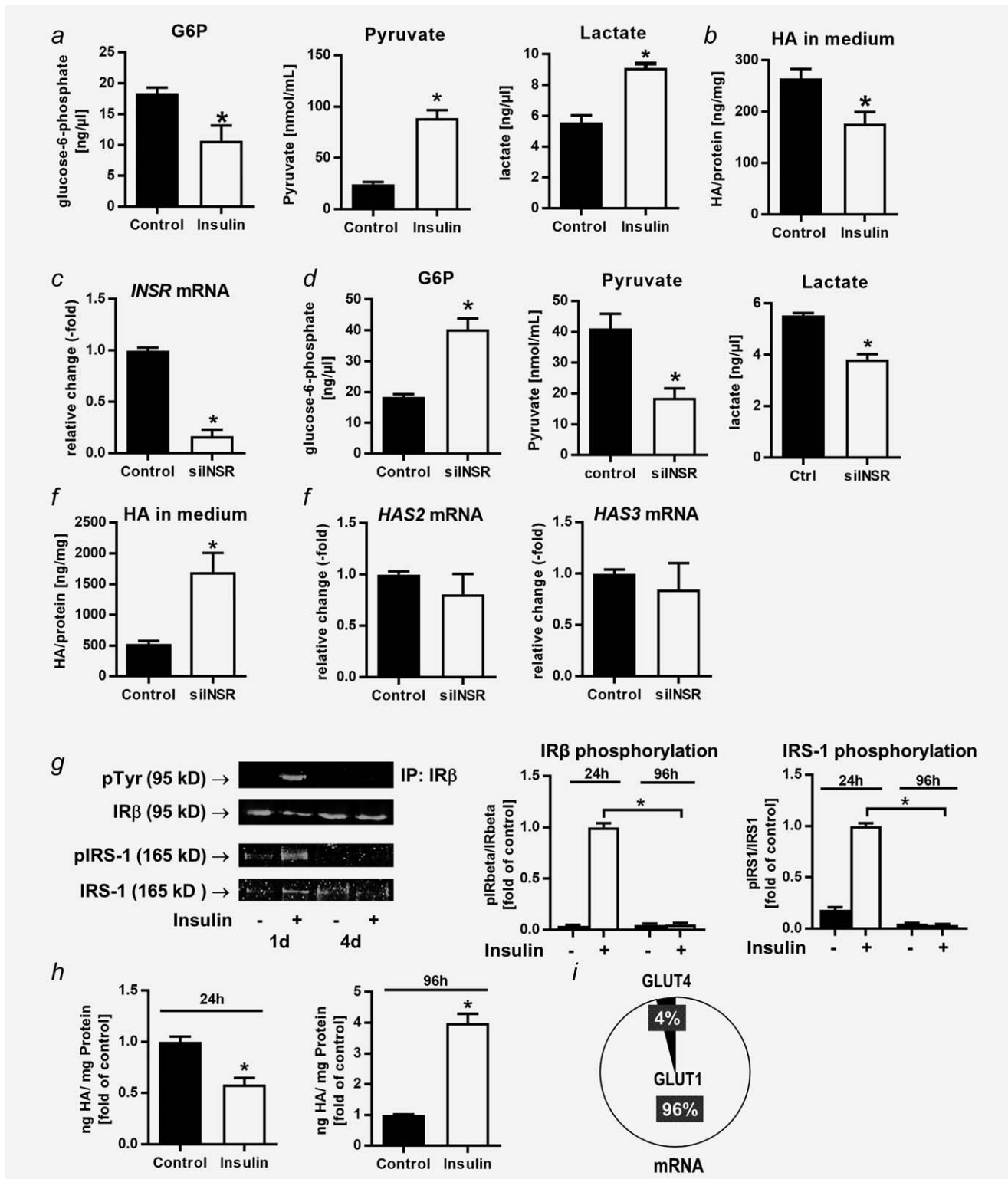


**Figure 4. Insulin actions are inversely correlated with hyaluronan synthesis.** (a–c) Changes in the concentration of the glucose metabolites glucose-6-phosphate (G6P,  $n = 3$ ), pyruvate ( $n = 5$ ) and lactate ( $n = 3$ ), hyaluronan (HA,  $n = 4$ ) and HAS mRNA expression ( $n = 3$ ) in response to stimulation with insulin (50 nM, 24 hr). Data are mean  $\pm$  SEM from three to four independent experiments. \*,  $p < 0.05$  vs. control. (d–f) Effects of insulin receptor (INSR) silencing (INSR mRNA,  $n = 4$ ) on G6P ( $n = 3$ ), pyruvate ( $n = 6$ ) and lactate ( $n = 3$ ) concentrations, hyaluronan synthesis ( $n = 4$ ) and HAS mRNA expression ( $n = 4$ ). Data are mean  $\pm$  SEM from three to four independent experiments. \*,  $p < 0.05$  vs. control. (g) Prolonged stimulation with insulin as a model for insulin resistance. Downregulation of insulin receptor activity by long-term (96 hr) insulin stimulation (100 nM), as measured by detection of phosphotyrosine (pTyr)-containing proteins after immunoprecipitation (IP) with antiinsulin receptor subunit beta (IR $\beta$ ) antibody normalised to total IR $\beta$  protein and detection of phospho-insulin receptor substrate 1 (IRS-1) normalised to total IRS-1. Data are mean  $\pm$  SEM from three independent experiments. \*,  $p < 0.05$  vs. short-term stimulation with insulin. (h) Effects of simulated insulin resistance on HA production. Short-term (24 hr) insulin stimulation vs. long-term (96 hr) insulin resistance. Data are mean  $\pm$  SEM from three independent experiments. \*,  $p < 0.05$  vs. unstimulated control. (i) Expression of glucose transporter 1/4 (GLUT1/4) mRNA in OSC1 cells. Exact percentages: GLUT1,  $95.91 \pm 0.5\%$ ; GLUT4,  $4.09 \pm 0.5\%$ . Data are mean  $\pm$  SEM from three independent experiments.

to the hypothesis that serum-derived factors may trigger pathways for glucose metabolism, thus reducing the availability of glucose precursors for HA synthesis. Since stimulation of glycolysis is a well-established metabolic function of insulin, we tested the effects of insulin on glycolysis and HA synthesis. As expected, stimulation with insulin (50 nM) triggered glycolysis, as determined by lowered intracellular G6P levels as well as increased intracellular pyruvate and extracellular lactate concentrations (Fig. 5a). In turn, the amount of HA in the supernatant of the cells was reduced (Fig. 5b).

Accordingly, silencing of the insulin receptor (*INSR*, Fig. 5c) increased the G6P precursor pool, reduced pyruvate and lactate concentrations (Fig. 5d), and strongly triggered HA synthesis (Fig. 5e) independently of changes in HAS transcription (Fig. 5f). Under diabetic conditions, both insulin depletion as found in Type 1 diabetes and insulin resistance, a characteristic feature of Type 2 diabetes, may result in diminished glycolysis and thus yield a larger supply of glucose precursors to HA synthesis. To mimic Type 2 diabetes conditions, we next established a model of experimentally induced insulin resistance in cancer cells, which used prolonged stimulation with insulin to downregulate the downstream signalling of *INSR*, as previously described.<sup>20</sup> To validate this approach, we measured the phosphorylation of insulin receptor subunit beta (*INSR-β*) and insulin receptor substrate 1 (IRS-1) with immunoblotting after 24 and 96 hr (Fig. 5g). In this experimental setup, short-term insulin stimulation (24 hr, 100 nM) consistently reduced HA synthesis, while simulated insulin resistance (insulin stimulation for 96 hr, 100 nM) led to a pronounced increase in HA production (Fig. 5h). This observation is in agreement with our observations using *INSR* silencing. To preclude any influence of insulin on glucose uptake in this experimental setup, we determined the expression of *GLUT1*, which facilitates basal glucose uptake independently of insulin, and *GLUT4*, which is largely regulated by insulin, by qPCR. Measurements of the mRNA expression of *GLUT1* and *GLUT4* showed that *GLUT1* is the predominantly expressed isoform in OSC1 cells; therefore, it can be assumed that glucose uptake in OSC1 is also largely independent of insulin effects (Fig. 5i).

#### **Augmented HA production in response to hyperglycaemia and insulin depletion promotes the malignant cancer cell phenotype**

Elevated HA production has been shown to exhibit tumour-promoting effects. Therefore, we performed experiments regarding the HA-mediated proliferation, invasion, and metastatic potential of OSC1 cells in response to high glucose supply, diminished insulin actions, and inhibition of glycolysis. In addition to a strong mitogenic effect of insulin, we detected a pronounced increase in proliferation with higher glucose supply (Fig. 6a). Next, we measured the invasive potential of OSC1 cells in response to hyperglycaemia and insulin. OSC1 cells exhibited stronger invasion when cultured

in high-glucose, instead of low-glucose, media. Likewise, the presence of insulin reduced invasion (Fig. 6b). Conversely, abrogating insulin signalling and glycolysis by silencing *INSR* or *PFKM* caused increased invasion (Fig. 6c). For detection of anoikis-resistant cells featuring anchorage-independent growth, we evaluated colony formation in a soft agar assay. The largest number of colonies was consistently observed in response to high glucose concentrations and insulin deprivation, the condition with the highest HA synthesis in previous experiments. Of note, insulin treatment in combination with high glucose concentrations yielded fewer but larger colonies than those found under other conditions (Fig. 6d). This observation may be explained by the anabolic effect of insulin in stimulating colony growth. Also, the inhibitory effect of higher HA content on cell-cell interaction and colony agglomeration in colonies lacking insulin may explain this effect. To address the adhesive capability of OSC1 cells in response to hyperglycaemia and insulin, we performed an endothelial cell adhesion assay. The largest number of adherent cells was again found under conditions that increased HA production: hyperglycaemia and insulin depletion (Fig. 6e) and direct (*siPFKM*) and indirect (*siINSR*) inhibition of glycolysis (Fig. 6f). These findings indicate enhanced cancer cell malignancy in response to conditions under which HA production is increased (cf. Figs. 3–5).

#### **Discussion**

Revealing the mechanisms behind the connection between the wide-spread diseases diabetes and cancer can lead to new strategies for prevention and targeted therapy.<sup>4</sup> Here we focus on the metabolic impact of hyperglycaemia and concomitant aberration of insulin signalling on the extracellular matrix component HA, which exhibits crucial functions in tumour progression.<sup>26</sup> In our study, we used ESCC cell lines as a model, which have been well characterised with respect to the impact of the extracellular matrix and especially HA on tumour progression.<sup>19,27,28</sup> Further research is needed to verify these findings in other tumour entities.

First evidence for the dependence of HA production on glucose supply was provided by studies using bacteria<sup>29</sup> that have shown increased concentrations of glucose to induce HA production. Moreover, diabetic rats<sup>30</sup> as well as patients with Type 1<sup>31</sup> and Type 2 diabetes<sup>32,33</sup> exhibit elevated HA levels in the circulating bloodstream and peripheral tissues. Hyperglycaemia-induced HA was identified to impair wound healing in diabetic patients.<sup>34</sup> In COS-1 and MCF-7 cells with overexpression of HAS isoforms, it was shown that HA synthesis depends on the availability of its direct precursors UDP-N-acetyl glucosamine and UDP-glucuronic acid.<sup>35,36</sup> Here we show that HA production in oesophageal cancer cells natively depends on the early glucose metabolite pool. This observation may indicate a proprietary overexpression of HAS genes in ESCC cells conceivably providing a survival factor for these cancer cell type.

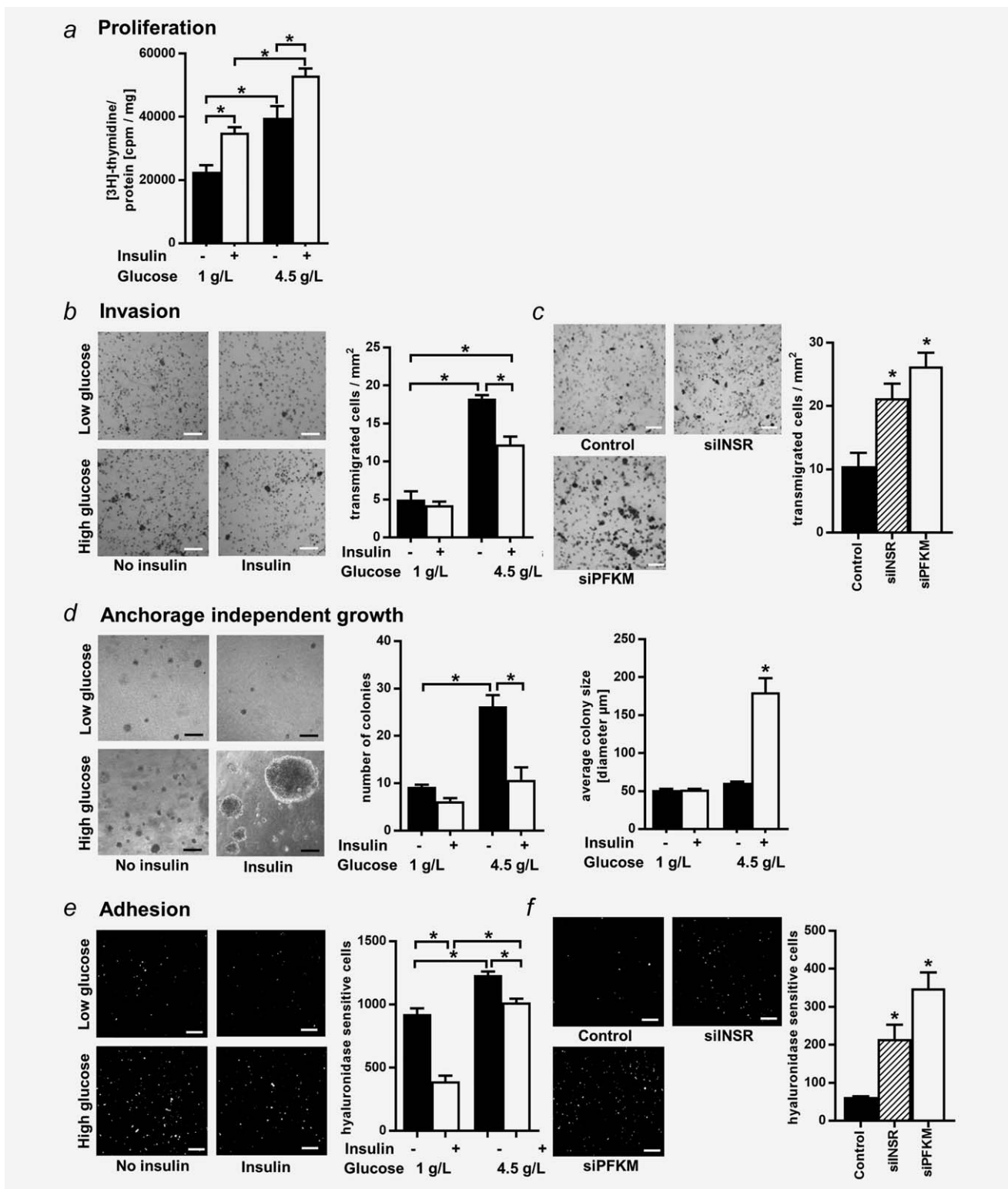


**Figure 5. Conditions favouring hyaluronan synthesis cause an increase in proliferation, invasion, anchorage-independent growth and adhesion to endothelial cells *in vitro*.** (a) Proliferation of OSC1 cells in response to glucose and insulin (10 µg/ml), as determined by [<sup>3</sup>H]-thymidine incorporation. Data are mean ± SEM from three independent experiments. \*, p < 0.05 between indicated conditions. (b) Influence of glucose and insulin (10 µg/ml) on the invasion of OSC1 cells through matrigel. Bar, 200 µm. Data are mean ± SEM from four independent experiments (dark dots: tumour cells, bright dots: pores in the inset membrane). \*, p < 0.05 vs. indicated condition. (c) Impact of inhibition of glycolysis by silencing of insulin receptor (INSR) and phosphofructokinase M (PFKM) on the invasion of OSC1 cells through matrigel (dark dots: tumour cells, bright dots: pores in the inset membrane). Data are mean ± SEM from four independent experiments. (d) Anchorage-independent growth of OSC1 cells as determined by colony formation in a soft agar assay. Bar, 200 µm. Data are mean ± SEM from four independent experiments. Number of colonies: \*, p < 0.05 vs. indicated condition. Average colony size: \*, p < 0.05 vs. all other conditions. (e) Influence of glucose and insulin (10 µg/ml) on hyaluronan-mediated adhesion of OSC1 cells to endothelial cells. Bar, 200 µm. Data are mean ± SEM from three independent experiments. \*, p < 0.05 vs. indicated condition. (f) Impact of inhibition of glycolysis by silencing of insulin receptor (INSR) and phosphofructokinase M (PFKM) on hyaluronan-mediated adhesion of OSC1 cells to endothelial cells. Bar, 200 µm. Data are mean ± SEM from three independent experiments. \*, p < 0.05 vs. control.

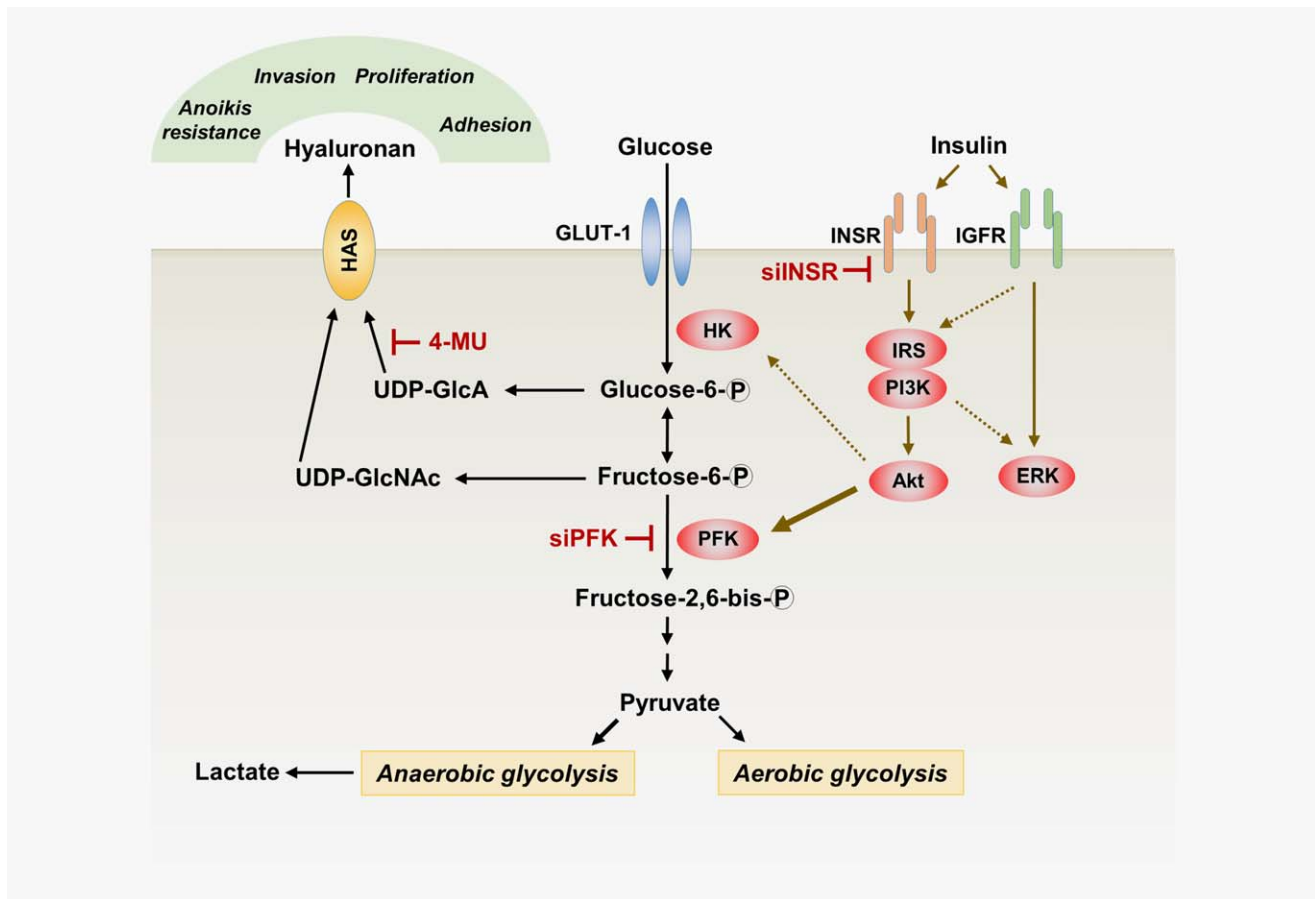


**Figure 6. Schematic of interactions between glycolysis and hyaluronan synthesis.** Glucose is taken up independently of insulin in most cancer cells by GLUT-1 and is subsequently converted to glucose-6-phosphate (G6P), which is the starting point for glycolysis and the synthesis of HA. Insulin orchestrates the metabolism of glucose toward glycolysis, thus depleting the precursor pool for HA synthesis. The inhibition of glycolysis by abrogated insulin actions or knock down of the glycolytic key enzyme phosphofructokinase (PFK) increases the usage of glucose for HA synthesis, which is inhibited by 4-methylumbellifera (4-MU). ERK, extracellular signal-regulated kinase; GlcA, glucuronic acid; GlcNAc, N-acetyl-glucosamine; HAS, hyaluronan synthase; HK, hexokinase; IGFR, insulin-like growth factor receptor; INSR, insulin receptor; IRS, insulin receptor substrate; PFK, phosphofructokinase; PI3K, phosphoinositide 3-kinase. [Color figure can be viewed at [wileyonlinelibrary.com](http://wileyonlinelibrary.com)]

It is important to mention that in most of our experiments the transcriptional regulations of the HAS enzymes do not correspond to the changes in HA synthesis. Most experiments in our study showed that higher HA precursor availability (i.e., hyperglycemia and abrogation of glycolysis by silencing of INSR) caused no significant changes in *HAS3* mRNA expression and a decrease in *HAS2* mRNA expression. These findings are in line with recent research on the regulation of HA synthesis showing that the transcriptional control of *HAS2*, its activation and the eventual production of HA is regulated by precursor availability, epigenetic changes in the promoter, O-GlcNAc modifications, ubiquitinations, phosphorylations and translocation to the cell surface.<sup>37–39</sup> Presumably, these processes are also involved in the regulation of the other HAS isoforms HAS1 and HAS3, this area is under investigation in the HA field. Taken together, current knowledge in this field shows that HAS expression and HA production do not always exhibit a direct relationship, even though HAS mRNA and HAS protein expression show a correlation. In the light of this,

our data indicate that indeed transcriptional changes were not accountable for increased HA synthesis but that an increase of substrates caused an increase of HA. However, it is remarkable that an abrogation of glycolysis by silencing of PFKM resulted in an increase of HAS3 expression. Therefore, we performed experiments with different PFKM knockdown efficiencies, which showed that *HAS3* mRNA expression is positively correlated with PFKM knockdown efficiency (yielding more substrates for HA synthesis) while there is a trend to a negative correlation with *HAS2* mRNA. In summary, we propose a substrate triggered feedback-loop leading to upregulation of HAS3 and downregulation of HAS2 in response to an afflux of glucose precursors.

Importantly, we show that the activity of glycolysis, the main pathway metabolising glucose, counteracts the use of glucose precursors for HA synthesis. Insulin plays a pivotal role in the regulation of glucose homeostasis and proliferation. Thus, aberrant insulin signalling is a crucial characteristic of diabetes. In the context of tumour progression, the two

most important effects of insulin are growth promotion and metabolic regulation of glycolysis.<sup>4</sup> The anabolic and mitogenic actions of insulin on tumour cells are well documented.<sup>40</sup> However, the metabolic actions of insulin on tumour progression are not well studied. Concerning glucose metabolism, it is important to differentiate between control of glucose uptake and glycolysis.

Insulin induces glucose uptake in many nonmalignant cells, such as adipocytes and skeletal muscle cells. In most cancer cells, however, glucose uptake is not facilitated by insulin-regulated GLUT-4 but rather by insulin-independent GLUT-1 and, to a lesser degree, by GLUT-3 and other GLUT isoforms.<sup>41</sup> This switch toward uncontrolled glucose uptake is part of the Warburg effect,<sup>7</sup> which describes a highly enhanced aerobic glycolysis in tumour cells, and also constitutes a hallmark of tumour development that is accompanied by increased aggressiveness of the tumour.<sup>42</sup> Of note, overexpression of GLUT-1 among patients with ESCC is associated with a poor prognosis and is directly correlated with higher TNM stages.<sup>43</sup>

Thus, even if insulin may not be necessary for glucose uptake in most cancer cells, it remains an important regulator of glycolysis and proliferation. More precisely, binding of insulin to the IRS, especially subtype B, mediates metabolic effects via the PI3K/Akt pathway, whereas growth processes are promoted by insulin and IGF through the IGF receptor/mitogen-activated protein kinase (MAPK) pathway.<sup>44,45</sup> These pathways can act independently of each other, e.g., in human muscle cells and adipocytes inhibition of the MAPK pathway does not interfere with the metabolic effects of insulin.<sup>46</sup> Importantly, there is growing evidence that metabolic and mitogenic pathways triggered by insulin are not only highly separated but that diabetic conditions do not cause a total loss of insulin functions but rather induce a partial or selective insulin resistance with differential regulation of the mitogenic and metabolic pathways.<sup>47–49</sup> For instance, human skeletal muscle cells of Type 2 diabetes patients exhibiting a reduction of IRS-1 phosphorylation show only a selective reduction in the activity of the metabolic PI3K-Akt-pathway while the mitogenic MAPK pathway remains intact.<sup>50</sup> These findings imply that the anabolic and therefore growth-promoting effects of insulin can persist, whereas other pathways, such as control of glycolysis, are abrogated. These observations raise the question why an abrogation of glycolysis, eventually resulting in decreased ATP production, might be conducive to tumour cell growth; obviously, this process would be disadvantageous for the energy homoeostasis of the cell. However, research on the Warburg effect in cancer cells has provided evidence that cancer cells are prone to use glucose metabolites preferably for biomass gain and other cellular tasks rather than for ATP generation.<sup>7</sup> Of note, some cancer cells express the dimeric pyruvate kinase M2 protein which diminishes the activity of the glycolytic pathway and thus increases the availability of glucose precursors for use in anabolic pathways.<sup>51</sup>

In conclusion, a lack of insulin in untreated Type 1 diabetes, as well as insulin resistance in Type 2 diabetes, may reduce glycolysis, thereby making an increased number of glucose precursors available for production of biomass such as HA synthesis. Simultaneously, proliferation can remain promoted by insulin via IRS-A and IGFR. Indeed, we observed that abrogation of insulin signalling increased the glucose precursor pool and thus stimulated HA synthesis. Concurrently, insulin remains exerted a strong mitogenic effect on the OSC1 cells used in our study. Thus, our results indicate that the tumour-promoting mitogenic actions of insulin, e.g., via the MAPK pathway, combine with increased HA synthesis to further support tumour growth and spread. In line with this, we found an increase in HA-dependent tumour characteristics, i.e., invasion, anchorage-independent growth and adhesion to endothelial cells in response to hyperglycaemia and insulin depletion, conditions favouring HA synthesis.

In this article, we used a nude mouse tumour xenograft model with streptozotocin-induced diabetes to investigate the effects of a diabetic metabolic state on HA-mediated tumour growth. In this model, diabetic conditions produced a pronounced but delayed increase in tumour growth. An explanation for this late onset of growth induction could be that tumour growth in its early stages may depend more on the mitogenic actions conferred by insulin, whereas glucose supply becomes more important in later stages of tumour progression. Two older studies (1972) on tumour growth in diabetic mice reported a decreased growth under diabetic conditions. However, these studies had some critical limitations, i.e., a short observation period, the use of toxic alloxan concentrations, or a pronounced weight loss leading to nutrient depletion also affecting the tumour mass.<sup>52,53</sup>

Our results show that only in diabetic mice inhibition of HA synthesis by 4-MU caused a higher absolute decrease in tumour volume and significantly reduced proliferation and vessel formation while strongly increasing the fraction of apoptotic cells. In nondiabetic mice, 4-MU delayed the onset of tumour growth resulting in a smaller mean tumour volume at Day 90. However, in this group treatment with 4-MU resulted only in a trend toward less Ki67 and CD31 positive cells and no effects on the TUNEL staining. This observation may be caused by a slower, delayed tumour growth kinetic and a depletion of the HA-rich tumour matrix.

Remarkably, 4-MU treatment also resulted in a pronounced prolongation in survival time of diabetic mice. This effect may be explained by a role of 4-MU in either reduction of tumour burden as a result of diminished HA production, or in a so far unknown amelioration of diabetes-related complications in these mice. However, blood glucose concentrations in diabetic mice were not significantly affected by 4-MU treatment. Further research is needed to specify this interesting effect of 4-MU on the mortality rate associated with diabetic conditions. Notwithstanding, these data indicate that 4-MU may be a promising therapeutic approach for the

treatment of cancer in diabetic patients and may additionally ameliorate diabetes-induced diseases. The fact that 4-MU (INN: hymecromone) is an orally bioavailable small molecular compound drug that has been approved as a spasmolytic in several countries for human use over many decades facilitates further clinical trials.

In summary, here we show that HA production in oesophageal cancer is modulated by glucose supply and by the glycolytic activity controlled by insulin (Fig. 6). We demonstrate the functional relevance of increased HA synthesis in response to hyperglycaemia and insulin depletion for the malignant cancer cell phenotype *in vitro* and for tumour progression and survival *in vivo*. Thus, our findings reveal the

central role of HA metabolism as a link between chronic hyperglycaemia, insulin signalling, and ESCC tumour progression and suggest a future clinical use of HA synthesis inhibitors such as 4-MU as an add-on therapeutic for cancer patients with diabetic comorbidity.

### Acknowledgements

S.T. designed the experiments, researched data, and wrote the article. U.P. researched data. C.R., D.J.G. and K.R. researched data and reviewed the article. J.W.F. designed the experiments, contributed guidance and reviewed the article. We appreciate the support by Birte Möhlendick, Tanja Arent, Wolfgang Huckenbeck and Barbara Hildebrandt in validating the cell lines used in our study.

### References

- Vigneri P, Frasca F, Sciacca L, et al. Diabetes and cancer. *Endocr Relat Cancer*, 2009;16:1103–23.
- Huang W, Ren H, Ben Q, et al. Risk of esophageal cancer in diabetes mellitus: a meta-analysis of observational studies. *Cancer Causes Control*, 2012;23:263–72.
- Feng YH, Lin CY, Huang WT, et al. Diabetes mellitus impairs the response to intra-arterial chemotherapy in hepatocellular carcinoma. *Med Oncol*, 2011;28:1080–8.
- Giovannucci E, Harlan DM, Archer MC, et al. Diabetes and cancer: a consensus report. *Diabetes Care*, 2010;33:1674–85.
- Hanahan D, Weinberg RA. Hallmarks of cancer: the next generation. *Cell*, 2011;144:646–74.
- Warburg O. On the origin of cancer cells. *Science*, 1956;123:309–14.
- Vander Heiden MG, Cantley LC, Thompson CB. Understanding the Warburg effect: the metabolic requirements of cell proliferation. *Science*, 2009; 324:1029–33.
- Masur K, Vetter C, Hinz A, et al. Diabetogenic glucose and insulin concentrations modulate transcriptome and protein levels involved in tumour cell migration, adhesion and proliferation. *Br J Cancer*, 2011;104:345–52.
- Cencioni C, Spallotta F, Greco S, et al. Epigenetic mechanisms of hyperglycemic memory. *Int J Biochem Cell Biol*, 2014;51:155–8.
- Ryu TY, Park J, Scherer PE. Hyperglycemia as a risk factor for cancer progression. *Diabetes Metab J*, 2014;38:330–6.
- Pennathur A, Gibson MK, Jobe BA, et al. Oesophageal carcinoma. *Lancet*, 2013;381:400–12.
- Toole BP. Hyaluronan: from extracellular glue to pericellular cue. *Nat Rev Cancer*, 2004;4:528–39.
- Sironen RK, Tammi M, Tammi R, et al. Hyaluronan in human malignancies. *Exp Cell Res*, 2011; 317:383–91.
- Lin EW, Karakasheva TA, Hicks PD, et al. The tumor microenvironment in esophageal cancer. *Oncogene*, 2016;35:5337–5349.
- Itano N, Sawai T, Yoshida M, et al. Three isoforms of mammalian hyaluronan synthases have distinct enzymatic properties. *J Biol Chem*, 1999; 274:25085–92.
- Kakizaki I, Kojima K, Takagaki K, et al. A novel mechanism for the inhibition of hyaluronan biosynthesis by 4-methylumbelliferon. *J Biol Chem*, 2004;279:33281–9.
- Goalstone ML, Draznin B. Insulin signaling. *West J Med*, 1997;167:166–73.
- Sarbia M, Bosing N, Hildebrandt B, et al. Characterization of two newly established cell lines derived from squamous cell carcinomas of the oesophagus. *Anticancer Res*, 1997;17:2185–92.
- Twarock S, Tammi MI, Savani RC, et al. Hyaluronan stabilizes focal adhesions, filopodia, and the proliferative phenotype in esophageal squamous carcinoma cells. *J Biol Chem*, 2010;285: 23276–84.
- Kumar N, Dey CS. Development of insulin resistance and reversal by thiazolidinediones in C2C12 skeletal muscle cells. *Biochem Pharmacol*, 2003;65:249–57.
- Jenkins RH, Thomas GJ, Williams JD, et al. Myofibroblastic differentiation leads to hyaluronan accumulation through reduced hyaluronan turnover. *J Biol Chem*, 2004;279:41453–60.
- Barnes J, Tian L, Loftis J, et al. Isolation and analysis of sugar nucleotides using solid phase extraction and fluorophore assisted carbohydrate electrophoresis. *MethodsX*, 2016;3:251–60.
- Zhang L, Underhill CB, Chen L. Hyaluronan on the surface of tumor cells is correlated with metastatic behavior. *Cancer Res*, 1995;55:428–33.
- Graham ML, Janecek JL, Kittredge JA, et al. The streptozotocin-induced diabetic nude mouse model: differences between animals from different sources. *Comp Med*, 2011;61:356–60.
- Euhus DM, Hudd C, LaRegina MC, et al. Tumor measurement in the nude mouse. *J Surg Oncol*, 1986;31:229–34.
- Itano N, Zhuo L, Kimata K. Impact of the hyaluronan-rich tumor microenvironment on cancer initiation and progression. *Cancer Sci*, 2008;99:1720–5.
- Twarock S, Freudenberger T, Poscher E, et al. Inhibition of oesophageal squamous cell carcinoma progression by *in vivo* targeting of hyaluronan synthesis. *Mol Cancer*, 2011;10:30.
- Twarock S, Rock K, Sarbia M, et al. Synthesis of hyaluronan in oesophageal cancer cells is uncoupled from the prostaglandin-cAMP pathway. *Br J Pharmacol*, 2009;157:234–43.
- Pires AM, Santana MH. Metabolic effects of the initial glucose concentration on microbial production of hyaluronic acid. *Appl Biochem Biotechnol*, 2010;162:1751–61.
- Chajara A, Raoudi M, Delpech B, et al. Circulating hyaluronan and hyaluronidase are increased in diabetic rats. *Diabetologia*, 2000;43:387–8.
- Nieuwendorp M, Holleman F, de Groot E, et al. Perturbation of hyaluronan metabolism predisposes patients with type 1 diabetes mellitus to atherosclerosis. *Diabetologia*, 2007;50: 1288–93.
- Dasu MR, Devaraj S, Park S, et al. Increased toll-like receptor (TLR) activation and TLR ligands in recently diagnosed type 2 diabetic subjects. *Diabetes Care*, 2010;33:861–8.
- Kang L, Lantier L, Kennedy A, et al. Hyaluronan accumulates with high-fat feeding and contributes to insulin resistance. *Diabetes*, 2013;62:1888–96.
- Shakya S, Wang Y, Mack JA, et al. Hyperglycemia-induced changes in hyaluronan contribute to impaired skin wound healing in diabetes: review and perspective. *Int J Cell Biol*, 2015;2015: 701–38.
- Rilla K, Oikari S, Jokela TA, et al. Hyaluronan synthase 1 (HAS1) requires higher cellular UDP-GlcNAc concentration than HAS2 and HAS3. *J Biol Chem* 2013;288:5973–83.
- Siijsonen H, Karna R, Hyttinen JM, et al. Hyaluronan synthase 1 (HAS1) produces a cytokine- and glucose-inducible, CD44-dependent cell surface coat. *Exp Cell Res*, 2014;320:153–63.
- Hascall VC, Wang A, Tammi M, et al. The dynamic metabolism of hyaluronan regulates the cytosolic concentration of UDP-GlcNAc. *Matrix Biol*, 2014;35:14–7.
- Tammi RH, Passi AG, Rilla K, et al. Transcriptional and post-translational regulation of hyaluronan synthesis. *FEBS J*, 2011;278:1419–28.
- Vigetti D, Viola M, Karousou E, et al. Metabolic control of hyaluronan synthases. *Matrix Biol*, 2014;35:8–13.
- Gallagher EJ, Fierz Y, Ferguson RD, et al. The pathway from diabetes and obesity to cancer, on the route to targeted therapy. *Endocrine Practice*, 2010;16:864–73.
- Medina RA, Owen GI. Glucose transporters: expression, regulation and cancer. *Biol Res*, 2002; 35:9–26.
- Hockel M, Vaupel P. Tumor hypoxia: definitions and current clinical, biologic, and molecular aspects. *J Natl Cancer Inst*, 2001;93:266–76.
- Kato H, Takita J, Miyazaki T, et al. Glut-1 glucose transporter expression in esophageal squamous cell carcinoma is associated with tumor aggressiveness. *Anticancer Res*, 2002;22: 2635–9.
- Samani AA, Yakar S, LeRoith D, et al. The role of the IGF system in cancer growth and metastasis: overview and recent insights. *Endocrine Rev*, 2007;28:20–47.

45. Nakae J, Kido Y, Accili D. Distinct and overlapping functions of insulin and IGF-I receptors. *Endocrine Rev*, 2001;22:818–35.
46. Lazar DF, Wiese RJ, Brady MJ, et al. Mitogen-activated protein kinase inhibition does not block the stimulation of glucose utilization by insulin. *J Biol Chem*, 1995;270:20801–7.
47. Groop PH, Forsblom C, Thomas MC. Mechanisms of disease: pathway-selective insulin resistance and microvascular complications of diabetes. *Nat Clin Practice Endocrinol Metab*, 2005;1:100–10.
48. Brown MS, Goldstein JL. Selective versus total insulin resistance: a pathogenic paradox. *Cell Metab*, 2008;7:95–6.
49. Parker VE, Savage DB, O’Rahilly S, et al. Mechanistic insights into insulin resistance in the genetic era. *Diabetic Med*, 2011;28:1476–86.
50. Cusi K, Maezono K, Osman A, et al. Insulin resistance differentially affects the PI 3-kinase- and MAP kinase-mediated signaling in human muscle. *J Clin Invest* 2000; 105:311–20.
51. Mazurek S, Boschek CB, Hugo F, et al. Pyruvate kinase type M2 and its role in tumor growth and spreading. *Semin Cancer Biol*, 2005; 15:300–8.
52. Heuson JC, Legros N. Influence of insulin deprivation on growth of the 7,12-dimethylbenz(a)anthracene-induced mammary carcinoma in rats subjected to alloxan diabetes and food restriction. *Cancer Res*, 1972;32:226–32.
53. Puckett CL, Shingleton WW. The effect of induced diabetes on experimental tumor growth in mice. *Cancer Res*, 1972;32:789–90.

# Inhibition of the hyaluronan matrix enhances metabolic anticancer therapy by dichloroacetate *in vitro* and *in vivo*

Sören Twarock  | Christina Reichert | Katharina Bach | Oliver Reiners | Inga Kretschmer | Daniel J. Gorski | Katharina Gorges | Maria Grandoch | Jens W. Fischer

Institut für Pharmakologie und Klinische Pharmakologie, Universitätsklinikum der Heinrich-Heine-Universität, Düsseldorf, Germany

## Correspondence

Sören Twarock, Institut für Pharmakologie und Klinische Pharmakologie, Universitätsklinikum der Heinrich-Heine-Universität, Düsseldorf, Germany.

Email: soeren.twarock@uni-duesseldorf.de

## Funding information

Forschungskommission der Heinrich-Heine-Universität Düsseldorf, Grant/Award Number: 51/2015

**Background and Purpose:** Aerobic glycolysis is a unique feature of tumour cells that entails several advantages for cancer progression such as resistance to apoptosis. The low MW compound, dichloroacetate, is a pyruvate dehydrogenase kinase inhibitor, which restores oxidative phosphorylation and induces apoptosis in a variety of cancer entities. However, its therapeutic effectiveness is limited by resistance mechanisms. This study aimed to examine the role of the anti-apoptotic hyaluronan (HA) matrix in this context and to identify a potential add-on treatment option to overcome this limitation.

**Experimental Approach:** The metabolic connection between dichloroacetate treatment and HA matrix augmentation was analysed *in vitro* by quantitative PCR and affinity cytochemistry. Metabolic pathways were analysed using Seahorse, HPLC, fluorophore-assisted carbohydrate electrophoresis, colourimetry, immunoblots, and immunochemistry. The effects of combining dichloroacetate with the HA synthesis inhibitor 4-methylumbelliferyl was evaluated in 2D and 3D cell cultures and in a nude mouse tumour xenograft regression model by immunoblot, immunochemistry, and FACS analysis.

**Key Results:** Mitochondrial reactivation induced by dichloroacetate metabolically activated HA synthesis by augmenting precursors as well as O-GlcNAcylation. This process was blocked by 4-methylumbelliferyl, resulting in enhanced anti-tumour efficacy in 2D and 3D cell culture and in a nude mouse tumour xenograft regression model.

**Conclusions and Implications:** The HA rich tumour micro-environment represents a metabolic factor contributing to chemotherapy resistance. HA synthesis inhibition exhibited pronounced synergistic actions with dichloroacetate treatment on oesophageal tumour cell proliferation and survival *in vitro* and *in vivo* suggesting the combination of these two strategies is an effective anticancer therapy.

**Abbreviations:** 4-MU, 4-methylumbelliferyl; CK18, cytokeratin 18; ECM, extracellular matrix; ESCC, oesophageal squamous cell carcinoma; FACE, fluorophore-assisted carbohydrate electrophoresis; G6P, glucose 6-phosphate; GlcNAc, N-acetyl-glucosamine; HA, hyaluronan; HABP, HA binding protein; HAS, hyaluronan synthase; HYAL, hyaluronidase; OXPHOS, oxidative phosphorylation; PDC, pyruvate dehydrogenase complex; PDK, pyruvate dehydrogenase kinase; RHAMM, receptor for hyaluronan-mediated motility

Sören Twarock and Christina Reichert should be considered joint first authors.

This is an open access article under the terms of the Creative Commons Attribution-NonCommercial-NoDerivs License, which permits use and distribution in any medium, provided the original work is properly cited, the use is non-commercial and no modifications or adaptations are made.  
© 2019 The Authors. British Journal of Pharmacology published by John Wiley & Sons Ltd on behalf of British Pharmacological Society.

## 1 | INTRODUCTION

Cancer cell metabolism has regained substantial attention as a potential drug target that distinguishes cancer cells from their non-malignant counterparts. Several new strategies have emerged and have provided promising new anticancer drugs (Martinez-Outschoorn, Peiris-Pages, Pestell, Sotgia, & Lisanti, 2017; Vernieri et al., 2016). One of the most evident characteristics of cancer cells is the metabolic switch from oxidative phosphorylation (OXPHOS) to aerobic glycolysis, which was first described by the Nobel laureate Otto Warburg, hence termed the Warburg effect (Warburg, 1956). It originates in reduced activity of the **pyruvate dehydrogenase complex** (PDC), which facilitates the conversion of pyruvate to acetyl-CoA and thus sustains mitochondrial OXPHOS. In a range of cancer cells, the activity of PDC is impeded by an increased **pyruvate dehydrogenase kinase** (PDK) activity, resulting in reduced mitochondrial activity. To compensate for the loss in ATP synthesis by mitochondrial OXPHOS, the glycolytic flux is increased, finally resulting in a much increased generation of lactate. Even though energy homeostasis is impaired by this process, the advantages for the growing cancer cell seem to outweigh this limitation. Inhibition of mitochondria-originated apoptosis, accumulation of biomass from early glucose metabolites, and creation of an acidified extracellular micro-environment are presumably supportive for tumour growth and spread (Vander Heiden, Cantley, & Thompson, 2009).

Intensive research on the Warburg effect led to the discovery of the low MW compound dichloroacetate, which was first used to reduce plasma glucose and triglycerides in patients with diabetes and hyperlipoproteinæmia (Stacpoole, Moore, & Kornhauser, 1978). In more recent years, it has been tested as an orphan drug to treat genetic mitochondrial diseases (Stacpoole, Kurtz, Han, & Langaeæ, 2008) such as lactate acidosis in children (Stacpoole et al., 2006) and the MELAS syndrome (Kaufmann et al., 2006). It was not before 2007 that dichloroacetate was also shown to reverse anaerobic glycolysis in tumour cells by dephosphorylation of PDK. This effect restores PDC activity, which enables reactivation of mitochondria and eventually results in the induction of mitochondria-driven apoptosis in transformed cells (Bonnet et al., 2007; Michelakis, Webster, & Mackey, 2008). As cell culture (Table S3) and animal experiments (Table S4) showed a considerable activity of this compound against a variety of tumour entities, dichloroacetate has gained wide attention in the scientific community in recent years (Kankotia & Stacpoole, 2014). Even though clinical studies confirm an overall good safety profile of dichloroacetate in humans, peripheral neuropathy emerged as the prominent dose-limiting side effect that often required dose reduction resulting in a loss of efficacy (Kaufmann et al., 2006). For instance, in recent phase I studies in NSCLC and glioblastoma patients, an effective dosage of  $25\text{--}50 \text{ mg}\cdot\text{kg}^{-1}\cdot\text{day}^{-1}$  was defined, but severe reversible neuropathy was reported in 38–86% of patients (Dunbar et al., 2014; Garon et al., 2014; Michelakis et al., 2010). A reduction of the dichloroacetate dose to  $6.5\text{--}12.5 \text{ mg}\cdot\text{kg}^{-1}\cdot\text{day}^{-1}$  generally ameliorated the emergence of this side effect but led to a loss of tumour growth reduction (Chu et al., 2015; Garon et al., 2014; Michelakis et al., 2010). Given these clinical results, there is a keen interest in exploring

### What is already known

- Dichloroacetate is a promising metabolic chemotherapeutic agent, but its efficacy needs further improvement.
- The hyaluronan matrix provides antiapoptotic signals via hyaluronan receptors.

### What this study adds

- Dichloroacetate treatment triggers hyaluronan synthesis metabolically via Krebs cycle activation.
- 4-Methylumbelliferone inhibits hyaluronan synthesis and counteracts this process, thus synergistically enhancing the efficacy of dichloroacetate.

### What is the clinical significance

- Both dichloroacetate and 4-methylumbelliferone, have been used in humans and show a favourable safety profile.
- This drug combination may represent a promising therapeutic option for tumours exhibiting the Warburg effect.

the mechanisms behind the diminished response to dichloroacetate treatment and in finding synergistic combination partners for therapy with dichloroacetate (Chu et al., 2015; Kaufmann et al., 2006; Sun, Board, & Blackburn, 2011; Zhou et al., 2015).

In order to identify potential compounds that enhance the efficacy of dichloroacetate or other strategies aiming at the restoration of mitochondrial OXPHOS, we focused on the extracellular matrix (ECM) as it is a pivotal component of the tumour stroma by forming a supportive tumour micro-environment (Pickup, Mouw, & Weaver, 2014). Specifically, we investigated the role of the ECM component hyaluronan (HA) as its synthesis is closely coupled to glycolysis intermediates (Moretto et al., 2015; Tammi et al., 2011; Twarock et al., 2017) and its abundance in the vicinity of cancer cells is a hallmark of tumour development, which has been shown to support tumour growth and spread, metastasis, chemotherapy resistance, and anti-apoptosis (Chanmee, Ontong, & Itano, 2016; Tammi et al., 2018). These processes are mediated by HA receptors, for example, CD44 and the receptor for hyaluronan-mediated motility (RHAMM), which trigger potent anti-apoptotic signalling pathways (Misra, Hascall, Markwald, & Ghatak, 2015). HA is an unbranched polysaccharide that is composed of alternating disaccharide units of **glucuronic acid** and N-acetyl-glucosamine (GlcNAc) and is synthesized by three membrane-bound isoforms of the HA synthase family (HAS1–3; Itano et al., 1999). Its synthesis can be inhibited by the orally available compound 4-methylumbelliferone (4-MU), which depletes the activated uridine diphosphate (UDP)-glucuronic acid precursor pool and thus interferes with HA production (Kakizaki et al., 2004). The efficacy of 4-MU in reducing the growth of a variety of tumour cell lines is well

documented (Table S5). In animal experiments, 4-MU was shown to attenuate tumour progression of, for example, oesophageal squamous cell carcinoma (ESCC) cells (Twarock et al., 2011; Twarock et al., 2017), hepatoma cells (Piccioni et al., 2015), bladder cancer cells (Morera et al., 2017), and prostate cancer cells (Lokeshwar et al., 2010). Moreover, it reduced metastatic spread of melanoma cells (Yoshihara et al., 2005) and chemotherapy resistance of pancreatic cancer cells (Nakazawa et al., 2006) and breast cancer cells (Chen & Bourguignon, 2014; Palyi-Krek et al., 2007). For further references, see also Table S6. Current research is aiming at identifying diseases and conditions in which 4-MU may present a valuable treatment option (Twarock et al., 2017).

For discovering a potential resistance mechanism involving the tumour micro-environment, we first investigated the effects of a dichloroacetate-induced restoration of the mitochondrial activity on the anti-apoptotic HA system. Subsequently, we established a mechanism that describes how reactivation of OXPHOS triggers HA synthesis (HAS) in two different ways. As proof of concept, we show that the inhibition of this process is effective to synergistically enhance dichloroacetate actions in terms of enhanced apoptosis in 2D and 3D cell cultures *in vitro* and in a nude mouse tumour xenograft regression model *in vivo*.

Our results provide insight in the counter-regulatory processes that emerge from the restoration of mitochondrial OXPHOS and show that the combination of dichloroacetate and 4-MU may be a promising pharmacological strategy for treatment of cancer entities exhibiting the Warburg effect. Our data suggest the combination of these two orally available compounds with a good safety profile in humans should be further investigated in clinical trials.

## 2 | METHODS

### 2.1 | Cell culture

The human ESCC cell line KYSE-410 (DSMZ Cat# ACC-381, RRID: CVCL\_1352; Braunschweig, Germany) was used to perform all experiments and was authenticated by short tandem repeat analysis. Cells were passaged in RPMI-1640 GlutaMAX medium (LifeTechnologies, Carlsbad, USA) containing 10% FBS supplemented with penicillin and streptomycin at 37°C in 5% CO<sub>2</sub> and 95% humidity. The number of viable cells was determined using a Countess cell counter (ThermoFisher, Waltham, USA). Cells were incubated with dichloroacetate in a concentration of 10, 20, or 40 mM as well as either 0.3- or 0.5-mM 4-MU, alone or in combination. With regard to dichloroacetate, we confirmed the doses to be used, with respect to growth inhibition (Figure S1) and the induction of a metabolic shift in our model cell line by quantification of lactate (Figure 2a) and mitochondrial ATP production (Figure 2b). For the experiments on the metabolic mechanism underlying elevated HAS under dichloroacetate, we chose the higher 40-mM dose as it produced a more striking metabolic phenotype (elevation of **glucose 6-phosphate** (G6P), acetyl-CoA, UDP-GlcNAc, and pericellular HA staining) than did the 20-mM dose.

Of note, even this strong induction of acetyl-CoA and HA in the medium was rescued by application of the ATP citrate lyase inhibitor SB-204990. For the experiments on *in vitro* tumour growth inhibition, we decided to use the mid-range concentration of 20-mM dichloroacetate, as this dose showed synergism with 300-μM 4-MU (Table S2) and we sought to explore in this study whether addition of 4-MU can reduce the dichloroacetate dose needed to achieve tumour growth inhibition. 4-MU alone only inhibited cell growth in a concentration of 300 μM (Figure 4a). As higher doses can also impair the synthesis of other glycosaminoglycans (unpublished data), we chose this dose as the highest concentration in our study. Based on the synergism calculation on growth reduction (Table S2) and our previous publications (Twarock et al., 2011; Twarock et al., 2017), we chose the 300-μM dose for further experiments.

### 2.2 | Animals

All animal care and experimental procedures were approved by the competent animal welfare authority (LANUV NRW) and the institutional animal welfare officer of the University of Düsseldorf under the administrative number 84.02.04.2013.A472 and performed according to the German and European animal welfare law. Animal studies are reported in compliance with the ARRIVE guidelines (Kilkenny et al., 2010; McGrath & Lilley, 2015) and with the recommendations made by the *British Journal of Pharmacology*. Male Cr: NMRI-Foxn1<sup>nu</sup> mice were obtained from Charles River (IMSR Cat# CRL:639, RRID:IMSR\_CRL:639; Wilmington, USA) and used for the experiments at the age of 4–6 weeks and a weight of 31.5 g ± 2 g. This mouse strain is commonly used for tumour xenograft experiments. The animals were bred and housed at the central animal housing facility of the Heinrich-Heine-University of Düsseldorf under specific pathogen-free conditions with standard housing and bedding material with four animals per cage. The mice had free access to nude mouse chow with chocolate aroma (Sniff, Soest, Germany) and water. In the groups receiving 4-MU, the drug was pelleted into the chow (see below); in the groups receiving dichloroacetate, the drug was dissolved in the drinking water. The animals were randomized to either treatment group. At the end of the experiment or if abort criteria were met (unusual behaviour as signs of pain or discomfort, tumour size exceeding 15 mm in any direction), the mice were killed by CO<sub>2</sub>. Power analyses with  $\alpha = .05$  and  $1 - \beta = .90$  using an estimated effect size of 1 (based on previous studies) yielded a minimum necessary sample size of 8 animals per treatment group.

### 2.3 | Tumour xenograft regression model

Tumour xenografts were induced by subcutaneous injection of 10<sup>6</sup> KYSE-410 cells into both flanks of the mice. After the injection, the tumour growth was assessed every second day, and the mice were randomized to the treatment groups placebo (nude mice standard chow with chocolate flavour), dichloroacetate, 4-MU, and dichloroacetate + 4-MU when the tumour volume reached at least

30 mm<sup>3</sup>. The tumour volume was calculated by caliper measurements with the formula Height × Length × Depth × 0.5. Dichloroacetate was added to the drinking water at a concentration of 0.3 g·L<sup>-1</sup>. Measurement of the volume of water consumed showed that the amount of dichloroacetate administered to each mouse was approximately equal to 50 mg·kg<sup>-1</sup> body weight·day<sup>-1</sup>. Here, we used a dichloroacetate dose that is established in the literature showing considerable effects on tumour growth in nude mouse xenograft models (Table S4). As in the *in vitro* experiments, we have chosen a dose of the lower range of published doses (Ishiguro, Ishiguro, Ishiguro, & Iwai, 2012; Ohashi et al., 2013). This dose was also used in clinical studies (Michelakis et al., 2010). 4-MU (AlfaAesar, ThermoFisher) was pelleted into the chow at a concentration of 50 g·kg<sup>-1</sup> (ssniff, Soest, Germany), which corresponds to a dose of 10 g·kg<sup>-1</sup> body weight·day<sup>-1</sup>. The 4-MU dose used here was first established by our group in a cardiovascular mouse model, in which the resulting plasma levels of 4MU (600 nM in blood plasma of mice) and the inhibition of HA synthesis were verified (Nagy et al., 2010). In two subsequent studies, our group confirmed the efficacy of this dose to inhibit tumour growth (Twarock et al., 2011; Twarock et al., 2017).

After the start of the treatment, the tumour growth was assessed every fifth day up to 60 days. At the end of the experiment, the mice were killed, and the tumours were excised and embedded for immunostaining. The mice had open access to food and pathogen-free water and were kept at a 12-hr day/night rhythm. All animal experiments were approved by the local animal facility and the responsible animal protection authority.

## 2.4 | HA assay

Cells were plated in 12-well dishes on glass cover slides and grown to 50% confluence. Next, the cells were incubated with dichloroacetate for 72 hr and fixed. HA was visualized using 1:200 biotinylated HA-binding protein (385911; Calbiochem, San Diego, USA) and 1:1,000 Streptavidin-Cy3 (SA1010; Invitrogen, Carlsbad, USA) in PBS. Nuclei were stained with Hoechst 33342 (H3570; Invitrogen). The HA deposition was calculated as integrated density and normalized to nuclei count using Fiji (Fiji, RRID:SCR\_002285; Schindelin et al., 2012). HA content of the supernatant was measured after 72 hr by an ELISA-like immunoaffinity assay (Corgenix, Broomfield, USA). Concentrations were normalized to protein content measured by Bradford assay.

## 2.5 | Quantitative real-time PCR

Total RNA was isolated after 72 hr of dichloroacetate treatment, and cDNA was synthesized from 1-μg RNA as described previously (Twarock, Tammi, Savani, & Fischer, 2010). The PCR reactions were performed according to standard procedures with SYBR Green PCR Master Mix (Applied Biosystems, Waltham, MA, USA). Relative expression levels were compared by using real-time PCR with the 2<sup>-ΔΔCt</sup> method. Primer sequences are given in Table S1.

## 2.6 | Quantification of metabolites

Intracellular acetyl-CoA and G6P were quantified using a colorimetric assay (Sigma) and normalized to total protein content. The ATP citrate lyase inhibitor SB-204990 (TOCRIS, Bristol, UK) was used as a negative control for the acetyl-CoA quantification. Fluorophore-assisted carbohydrate electrophoresis (FACE) was used to quantify intracellular (UDP)-sugars and executed as described previously (Twarock et al., 2017). Signal intensities were quantified by the Software Vision Works (Analytik Jena, Jena, Germany) and normalized to DNA content determined by Quant-iT PicoGreen dsDNA Assay Kit (Invitrogen).

## 2.7 | Real-time metabolism analysis

Oxygen consumption rate and extracellular acidification rate were measured by using a Seahorse XFe96 (Agilent Technologies, Santa Clara, USA) according to the manufacturer's instructions. Briefly, 12 × 10<sup>3</sup> KYSE-410 cells were seeded in an XFe96 well plate in standard cell culture medium 1 day in advance. On the day of analysis, the medium was changed to non-buffered RPMI-1640 supplemented with 10-mM glucose and 2-mM glutamine and incubated at 37°C without CO<sub>2</sub> for 1 hr. dichloroacetate was injected, and the cells were incubated for 15 min. Mitochondrial respiration was measured by XF Mito Stress Test Kit, and glycolysis was analysed by Glycolysis Rate Assay Kit (Agilent Technologies).

## 2.8 | Cell viability and apoptosis analysis

Cell viability and apoptosis were analysed by three different methods: living cell count, Annexin V-FITC binding, and cleaved PARP immunoblots. For cell count analysis, 3 × 10<sup>4</sup> cells were seeded per 12-well and incubated with the indicated amount of dichloroacetate and/or 4-MU and counted every 24 hr for 3 days. Annexin V (A13199; Invitrogen) binding to apoptotic cells was analysed at Day 3 by flow cytometry as previously described (Grandoch et al., 2009). For immunoblotting, at Day 3, cell extracts were separated by 10% SDS-PAGE and transferred to a nitrocellulose membrane by the semi-dry method. It was then incubated with 1:1,000 rabbit anti-cleaved-PARP antibody (Cell Signaling Technology Cat# v9532, RRID:AB\_659884; Danvers, USA) in 2.5% BSA in TBS-T and visualized by 1:10,000 RDye 800CW Goat anti-Rabbit (926-32211; Li-COR Bioscience, Lincoln, USA). The signal intensity was quantified and normalized to mouse anti-β-tubulin (Sigma-Aldrich Cat# T7816, RRID:AB\_261770) concentration.

## 2.9 | Quantification of O-GlcNAcylation

The amount of O-GlcNAcylated proteins was analysed by immunoblot and immunostaining. To this purpose, cells were incubated with dichloroacetate for 3 days, harvested in 2× Laemmli buffer, and proteins were separated by an 8% SDS-PAGE. After semi-dry transfer, the membrane was incubated with 1:1,000 mouse anti-O-GlcNAc

antibody (Abcam Cat# ab2739, RRID:AB\_303264, Cambridge, UK) in PBS followed by 1:1,000 goat anti-mouse AlexaFluor488 (A-11029; ThermoFischer) staining. Quantified protein content was normalized to tubulin concentration. The same antibody was used for immunostaining: The cells were grown on glass slides and fixed with 4% formalin. Next, the cells were permeabilized and blocked by 10% FBS, 0.3-M glycerine, 1% BSA, and 0.1% Triton X-100 in PBS. The cells were then incubated with the O-GlcNAc antibody and Hoechst. O-GlcNAc staining was analysed by Fiji and normalized to nuclei count. The O-GlcNAc transferase inhibitor alloxan (10 mM, Sigma) was used as negative control (Konrad et al., 2002).

## 2.10 | Gene silencing

The  $1 \times 10^5$  cells were reversely transfected with siRNA or scrambled control siRNA (Qiagen, Hilden, Germany) using lipofectamine RNAiMaxx (ThermoFisher) according to manufacturer's instructions. The following siRNAs were used (gene of interest, Qiagen order numbers): HAS3 (SI00433902, SI00433895), CD44 (SI00299705, SI03037419), RHAMM (SI02653196, SI05137384), and AllStars-Negative-Control-siRNA (SI03650318). Quantitative real-time RT-PCR was performed to confirm successful knockdown.

## 2.11 | 3D spheroid model

A multicellular tumour spheroid model was used to mimic three-dimensional growth: 5,000 KYSE-410 cells were planted in a round bottom 96-well BRAND microplate (Brand, Wertheim, Germany) and centrifuged for 10 min at 600 $\times$  g. After 4-day incubation time, the spheroids were treated with 20-mM dichloroacetate and/or 300- $\mu$ M 4-MU for 10 days. At Days 0, 3, 7, and 10 of treatment, pictures were taken with a Zeiss AxioObserverZ.1, and the diameter was measured using AxioVision Software (AxioVision, RRID:SCR\_002677, Carl Zeiss, Oberkochen, Germany). The volume was calculated from the diameter with the formula  $V = 1/6 \times \pi \times d^3$ . The medium was changed at the same time points.

## 2.12 | Living cell toxicity assay of 3D cultures

At Day 10, spheroids were stained with either 3- $\mu$ M ethidium homodimer 1 (46043; Sigma), 2- $\mu$ M calcein AM (206700; Calbiochem), and 33- $\mu$ M Hoechst 33342 or with 1:100 CellEvent Caspase-3/7Green Detection Reagent (C10423; Life Technologies) in combination with Hoechst as described previously (Sirenko et al., 2015). All dyes were directly added to 100- $\mu$ l RPMI culture media without washing and incubated for 3 hr at 4°C.

## 2.13 | Immunostaining

Tumour cryosections (8  $\mu$ m) were fixed with 10% formalin. Targets stained comprise 1:200 HA (HA binding protein [HAbP]), 1:200 cytokeratin 18 (CK18; guinea pig anti-CK18; GP-CK18; Progen,

Heidelberg, Germany), 1:1,000 Ki67 (rabbit anti-Ki67; NB500-170; Novus, Littleton, USA), and 1:1,000 CD31 (Abcam Cat# ab7388, RRID:AB\_305905). Click-it Plus TUNEL assay (C10617; ThermoFisher) was used to determine apoptotic cells according to manufacturer's instructions. Nuclei were counterstained by Hoechst. Staining was quantified by Fiji software. Five random images were selected from each tumour section and were averaged as one  $n$ .

## 2.14 | Randomization and blinding

In the in vivo experiments, the animals were randomized to either treatment group. After the tumours of the mice were harvested, the created histological slides were numbered, and the analysis was performed under blinded conditions. In vitro experiments regarding microscopic imaging were also carried out in a blinded manner. Other in vitro experiments were not conducted under blind conditions, but raw data were acquired directly from the experimental procedures and analysed through standardized procedures that reduce any possible operator bias.

## 2.15 | Data and statistical analysis

The data and statistical analysis comply with the recommendations of the *British Journal of Pharmacology* on experimental design and analysis in pharmacology. Statistical analysis was performed using GraphPad Prism Software 7.04 (GraphPad Prism, RRID:SCR\_002798, La Jolla, USA). All results are expressed as mean  $\pm$  SD of  $n$  independent experiments. Statistical comparison of two groups was performed by Student's *t* test. Three and more conditions were analysed by one-way ANOVA followed by Tukey's or Holm–Sidak's multiple comparison correction, if *F* test achieved the necessary level of statistical significance and there was no variance inhomogeneity. Statistical significance was considered at *P* values  $<0.05$ .

## 2.16 | Materials

If not noted otherwise, all reagents and chemicals were obtained from Sigma (St. Louis, MO, USA). Dichloroacetate and 4-MU doses used for the in vitro and in vivo experiments in this study are based on studies using these compounds in monotherapy and in combination with other drugs. These studies are summarized in Tables S3–S6 (dichloroacetate in vitro studies, Table S3; dichloroacetate in vivo studies, Table S4; 4-MU in vitro studies, Table S5; and 4-MU in vivo studies, Table S6).

## 2.17 | Nomenclature of targets and ligands

Key protein targets and ligands in this article are hyperlinked to corresponding entries in <http://www.guidetopharmacology.org>, the common portal for data from the IUPHAR/BPS Guide to PHARMACOLOGY (Harding et al., 2018), and are permanently archived in the Concise Guide to PHARMACOLOGY 2017/18 (Alexander et al., 2017).

## 3 | RESULTS

### 3.1 | Treatment with dichloroacetate triggers HA matrix synthesis

In this study, we aimed at the identification of strategies that synergistically enhance the efficacy of metabolic cancer treatments. Specifically, we chose dichloroacetate as a prototypical drug as it represents the most advanced approach exploiting aerobic glycolytic metabolism in cancer cells. Oesophageal cancer was selected as a model tumour entity since it presents with a poor prognosis and few treatment options (Enzinger & Mayer, 2003); in addition, we and others identified HA in the tumour micro-environment of oesophageal squamous cancer cells as a pivotal factor of tumour progression (Lin, Karakasheva, Hicks, Bass, & Rustgi, 2016; Twarock et al., 2011).

As a premise for further investigations, we first evaluated the influence of dichloroacetate treatment on the HA matrix system. Thus, we quantified the extracellular and pericellular HA content and determined the transcriptional regulation of pivotal genes of the HA matrix system in the ESCC cell line KYSE-410 in response to dichloroacetate. In this study, we used dichloroacetate concentrations of 10, 20, and 40 mM for the cell culture experiments as this range showed a dose-dependent reduction on the cell growth of KYSE-410 cells in preliminary experiments (Figure S1) and is also found in the literature (Kankotia & Stacpoole, 2014). On the product level, we measured HA concentrations in the cell supernatant by an ELISA-like assay (Figure 1a) and pericellular HA deposition by affinity-histological stainings, both using HAbP (Figure 1b). We observed a dose-dependent increase in both assays indicating enhanced HA deposition in response to dichloroacetate treatment. Quantitative PCR analyses of the main genes of the HA matrix system consistently revealed an up-regulation of the HAS 2 and 3 (HAS2,3; Figure 1c), the hyaluronidases 1 and 2 (HYAL1,2; Figure 1d), and the HA receptors RHAMM and CD44 (Figure 1e). As an up-regulated HA matrix can exhibit a strong anti-apoptotic activity, this observation might provide a basis for cellular resistance against dichloroacetate and was thus further scrutinized in the following experiments.

#### 3.1.1 | Reconstitution of mitochondrial function by dichloroacetate activates HA synthesis via an increase in HA precursor pool and O-GlcNAcylation

In order to identify the underlying mechanism of elevated HA synthesis following dichloroacetate treatment, we first validated the effects of dichloroacetate on aerobic glycolysis (Figure 2a) and ATP production (Figure 2b). Complete curves of mitochondrial respiration and glycolytic activity are shown in Figure S2. We observed a dose-dependent decline in glycolysis accompanied by a rise in intracellular ATP levels indicating activation of mitochondria-bound OXPHOS. HPLC measurements confirmed these findings (Figure S3). Pyruvate concentrations did not significantly change under these conditions, which is compatible with a shift in pyruvate usage from lactate

generation to OXPHOS (Figure S3B). In response to dichloroacetate treatment, the early glucose metabolite G6P, a key HA precursor molecule, increased in a dose-dependent manner (Figure 2C). However, FACE analysis showed that the downstream metabolite UDP-glucose, which is subsequently converted to UDP-glucuronic acid and finally integrated into the growing HA chain, did not increase with dichloroacetate stimulation (Figures 2d and S4). This finding may indicate a rapid metabolism and usage of this precursor in HA synthesis. A schematic overview of the suggested pathway is shown in Figure 3. As the second constituent of HA, GlcNAc, is synthesized by utilization of acetyl-CoA, we next investigated the effects of restored OXPHOS on GlcNAc levels and subsequent implications for HAS. Quantification of cellular acetyl-CoA levels revealed a strong dose-dependent increase in response to dichloroacetate treatment (Figure 2e) that was inhibited by the ATP citrate lyase inhibitor SB204990, which indicates its mitochondrial origin (Figure 2f). This rise in acetyl-CoA precursors also yielded a corresponding increase in cellular UDP-GlcNAc levels (Figures 2g and S4). This process was mainly accountable for the elevated HAS under dichloroacetate treatment as the inhibition of acetyl-CoA shuttling by SB204990 reversed the induction of HAS by dichloroacetate by about 75% (Figure 2h). These results indicate that the restoration of mitochondrial OXPHOS by dichloroacetate treatment causes an increase in the precursor pools of HA constituents, which provide the basis for the observed elevation of HAS. Furthermore, enhanced O-GlcNAcylation directly triggers the activity of the HAS enzymes (Tammi et al., 2011; Vigetti, Viola, Karousou, De Luca, & Passi, 2014). In line with the observed increase of the UDP-GlcNAc pool, dichloroacetate treatment resulted in a strong induction of O-GlcNAcylation of cellular proteins as determined by immunoblot (Figures 2i and S5) and immunohistochemistry (Figure 2j). This finding delineates an additional mechanism accountable for elevated HAS resulting from restored OXPHOS activity triggered by dichloroacetate.

#### 3.1.2 | Inhibition of HA synthesis synergistically enhances apoptosis and tumour growth suppression by dichloroacetate in 2D cell culture

The OXPHOS restoring agent dichloroacetate and the HA synthesis inhibitor 4-MU both showed a suppressing effect on the growth of cultured ESCC within 3 days. However, only the combination treatment was able to decrease the cell count (Figure 4a). We used the Software CompuSyn to identify synergistic combinations of dichloroacetate and 4-MU concentrations. For the combination of a mid-range concentration of 20-mM dichloroacetate with 300- $\mu$ M 4-MU, which is shown in Figure 4a, the CI value was calculated as 0.65545 denoting synergism for this combination (Table S2). Flow cytometry measurements for Annexin V<sup>+</sup> cells (Figure 4b) and immunoblots for PARP cleavage (Figure 4c) revealed that this effect was caused by an induction of apoptosis. In a next step, we aimed to identify the role of key parts of the HA system for mediating the synergistic enhancement of dichloroacetate by 4-MU. Therefore, we also performed growth experiments with cells that were treated with

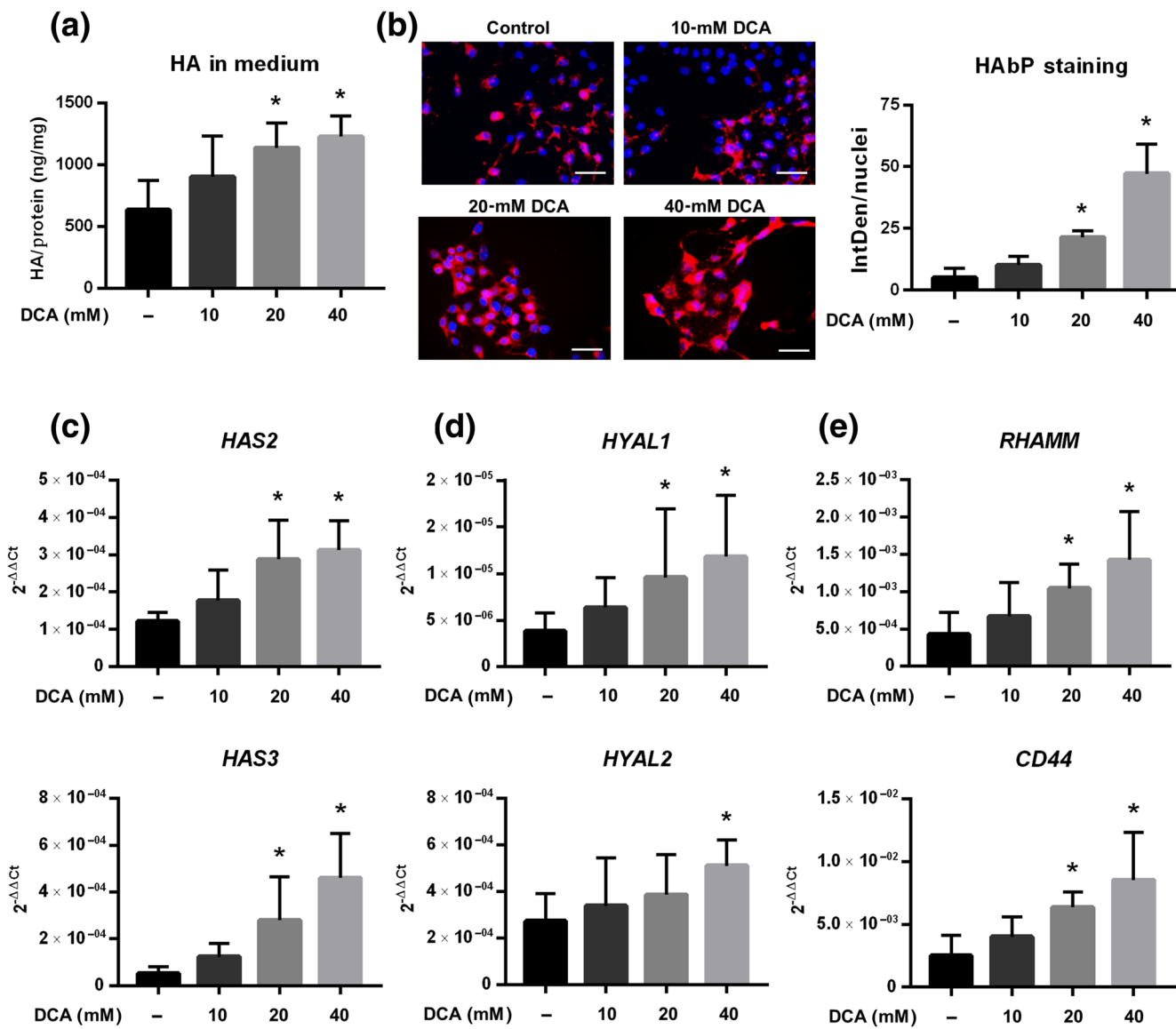


**FIGURE 1** Dichloroacetate up-regulates the hyaluronan matrix in oesophageal cancer cells on the product and transcriptional levels. KYSE-410 were incubated with 10-, 20-, 40-mM dichloroacetate (DCA) for 72 hr and analysed for their hyaluronan (HA) content and expression of genes relevant to HA synthesis, degradation, and signalling. (a) HA concentration in the medium was measured by an ELISA-like immunoaffinity assay and normalized to protein content ( $n = 6$ ). (b) Pericellular HA deposition (red) was stained by HA binding protein (HAbP), and its integrated density (IntDent) was normalized to nuclei (Hoechst, blue) count ( $n = 7$ , each  $n$  represents a pooled analysis of five replicates). Representative images are shown, scale bar: 100  $\mu$ m. Gene expression of (c) HA synthases (HAS2,3) and (d) hyaluronidases (HYAL1,2) and (e) HA receptors RHAMM and CD44 were determined and normalized to respective controls ( $n = 7$ ). Data shown are means  $\pm$  SD. \* $P < .05$ , significantly different from control (0-mM DCA); one-way ANOVA.

siRNAs against both HA receptors RHAMM and CD44 and HAS3, which is the main HAS isoform in the ESCC cells used in this project (Twarock et al., 2017). The knockdown of HAS3 resembled the effects of 4-MU in showing a substantial impairment of tumour cell growth that was, by trend, even more pronounced in combination with dichloroacetate. The knockdown of the HA receptors had a much weaker effect on cell growth, but this effect was strongly increased by addition of dichloroacetate (Figure 4d). These results indicate that interference with various components of the HA system, which is triggered by dichloroacetate treatment, result in a synergistic improvement of the anticancer actions of dichloroacetate.

### 3.2 | Combination treatment induces apoptosis and shrinkage of tumour spheroids

It has been reported that dichloroacetate shows different effectiveness in vivo and in cell culture experiments (Papandreou, Goliasova, & Denko, 2011). This observation may be connected to the fact that tumour metabolism is significantly modulated by oxygen availability, which alters with the growth of the tumour. In addition, also the ECM changes in response to the spatial interaction of the embedded cells. To consider these characteristics of a developing tumour, we established a 3D tumour spheroid model to investigate the interaction

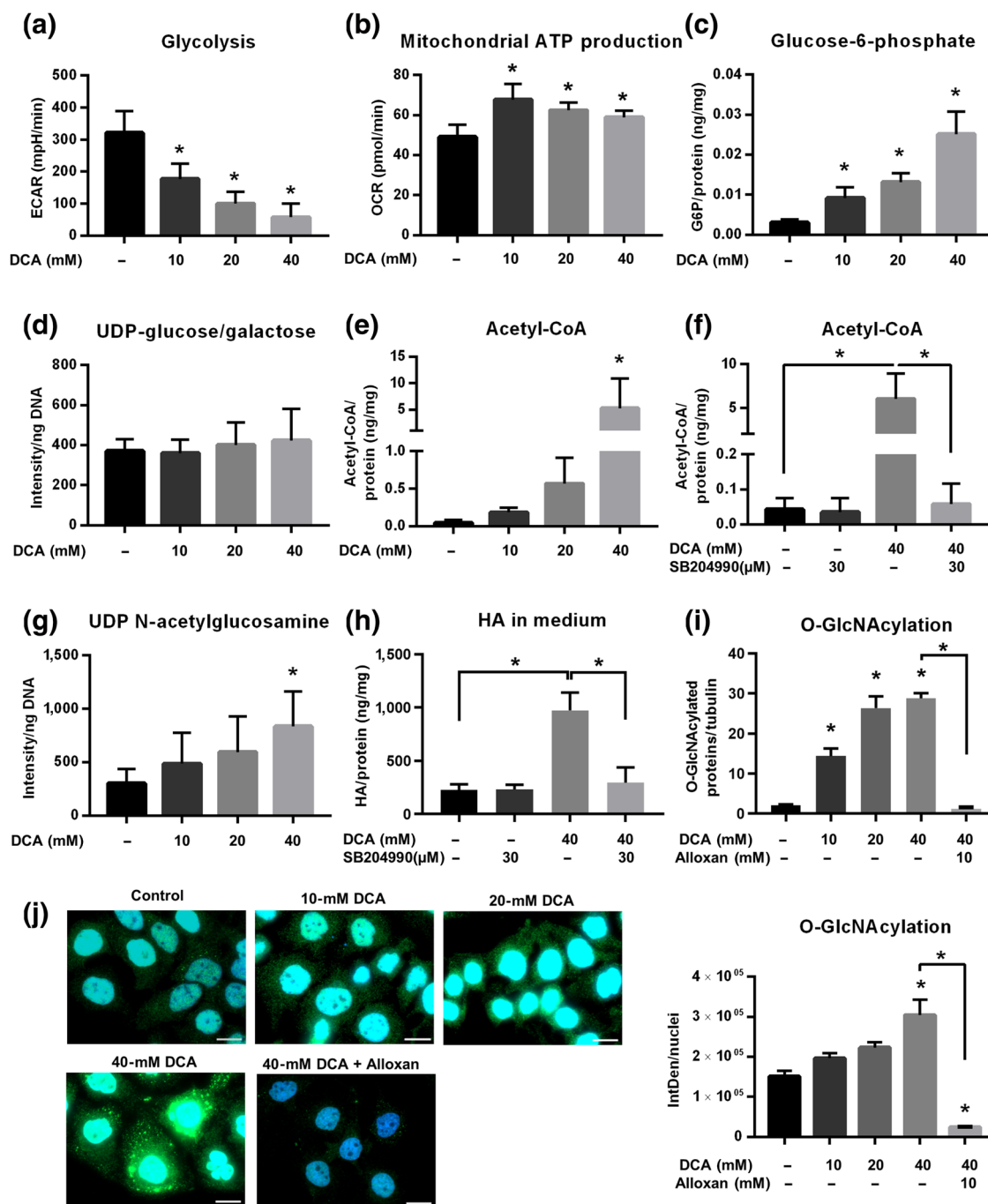


**FIGURE 2** Dichloroacetate (DCA) switches the tumour cells to OXPHOS resulting in increased hyaluronan precursors and protein O-GlcNAcylation. Real-time metabolism analysis by Seahorse XF96 with (a) Glycolysis Rate Assay Kit and (b) Mitochondrial Stress Test Kit was used to measure the acute response of KYSE-410 cells to dichloroacetate stimulation. Cells were seeded into Seahorse plates, and dichloroacetate was injected and incubated for 15 min before analysis was started. Extracellular acidification rate (ECAR) represents the amount of glycolysis, and oxygen consumption rate (OCR) defines the amount of mitochondrial respiration of  $12 \times 10^3$  cells per well (each  $n$  represents a pooled analysis of four replicates). (c) Glucose 6-phosphate concentration was measured after dichloroacetate incubation of 3 days by colorimetric analysis. (d) The hyaluronan (HA) precursor UDP-glucose/galactose was quantified by fluorophore-assisted carbohydrate electrophoresis (FACE) and normalized to total DNA content. UDP-sugars were isolated from KYSE-410 by ENVI-Carb columns. (e) Acetyl-CoA concentration was measured by colorimetry. (f) SB204990 inhibits the export of acetyl-CoA from the mitochondria to the cytosol and was used to abolish the effects of dichloroacetate on acetyl-CoA synthesis. (g) The HA precursor N-acetylglucosamine was isolated and determined by FACE analysis. (h) HA concentration in the medium after inhibition of acetyl-CoA shuttling with SB204990 was measured by an ELISA-like immunoaffinity assay. GlcNAcylation of proteins was quantified by (i) western blot analysis and (j) immunostaining (O-GlcNAcylation, green; nucleus, blue). The O-GlcNAc transferase (OGT) inhibitor alloxan was used as a negative control. (a-i)  $n = 6$ . (j) Representative images are shown, scale bar: 20 μm ( $n = 8$ , each  $n$  represents a pooled analysis of five replicates). Data shown are means  $\pm$  SD. \* $P < .05$ , significantly different from control (0-mM DCA) or as indicated; one-way ANOVA.

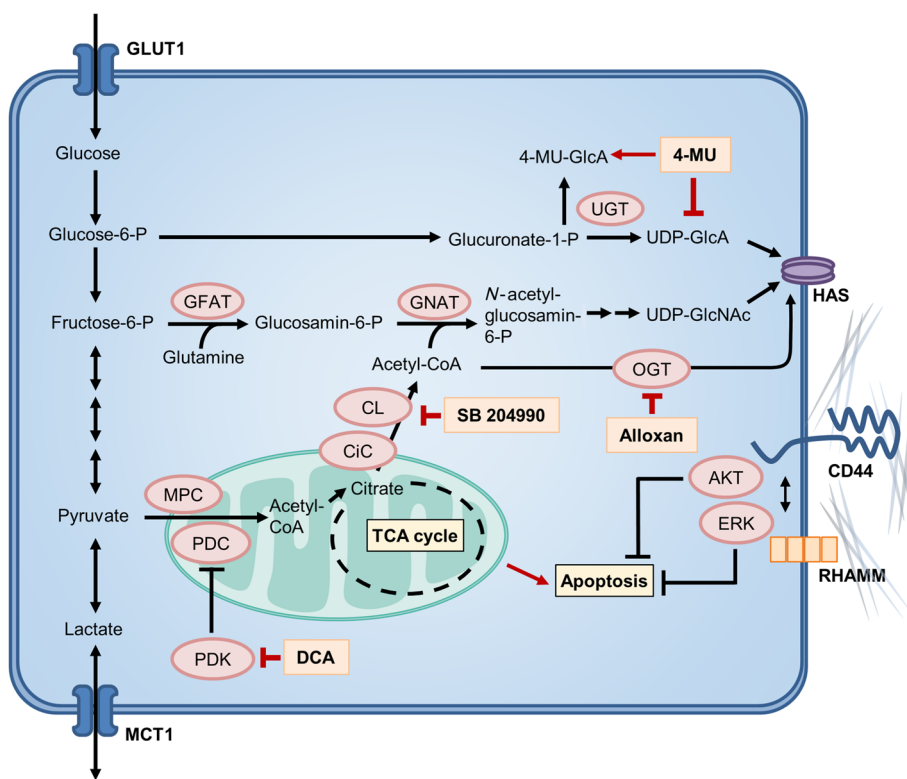


**FIGURE 3** Diagram of the pathways involved in the metabolic interaction of glycolysis, mitochondrial respiration, and hyaluronan synthesis. Glucose is taken up by the glucose transporters (e.g., GLUT1) and further metabolized in the glycolysis. For energy production, pyruvate is shuttled to the mitochondria via the mitochondrial pyruvate carrier (MPC) where it is converted to acetyl-CoA by the pyruvate dehydrogenase complex (PDC), whose activity is regulated by pyruvate dehydrogenase kinase (PDK). Acetyl-CoA is then further consumed in the tricarboxylic acid cycle (TCA) to fuel ATP synthesis. In most cancer cells, this pathway is aberrant due to an up-regulation of PDK leading to an inhibition of PDC activity. This switch is characteristic for hypoxic conditions but is regularly found also in the presence of oxygen in tumour cells (Warburg effect). Under these circumstances, pyruvate is reduced to lactate, which is exported by monocarboxylate transporters (e.g., MCT1). Restoration of mitochondrial oxidative phosphorylation (OXPHOS) by the PDK inhibitor dichloroacetate (DCA) yields an increased amount of acetyl-CoA in the mitochondria, which is also shuttled to the cytosol under involvement of the citrate carrier (CiC) and the ATP-citrate lyase (CL). A reactivation of mitochondrial metabolism in tumour cells has been connected to the induction of caspase-dependent apoptosis. Our study reveals that this process also yields an increase in the hyaluronan (HA) synthesis precursors glucose 6-phosphate and N-acetyl-glucosamine. The latter also triggers the O-GlcNAc transferase (OGT) mediating GlcNAcylation of proteins (e.g., hyaluronan synthase [HAS]). These processes result in a pronounced increase of the extracellular matrix compound HA that inhibits apoptosis via its receptors CD44 and RHAMM. HA synthesis can be blocked by 4-methylumbelliflone (4-MU), thus providing a countermeasure for this antiapoptotic counter-regulation. GFAT, glutamine:fructose-6-phosphate aminotransferase; GNAT, acetyl-CoA:D-glucosamine N-acetyltransferase; UGT, UDP-glucuronyltransferase

between metabolism and ECM in this setting and to determine the effect of dichloroacetate and 4-MU during this process. Quantitative PCR analyses showed that indeed two of the major enzymes supporting the Warburg Effect, that is, PDK 1 (PDK1) and LDH A (LDHA), showed a strong transcriptional induction compared to 2D culture indicating an increase in aerobic glycolysis under these conditions. Simultaneously, also, the mRNA expression of the main HA synthase (HAS3) in the examined cells was strongly increased. This may be attributable to the demanding scaffolding needs for three-dimensional growth (Figure 5a). Given the augmented activity of both systems in this set-up, we investigated whether the combination of dichloroacetate and 4-MU is also effectively inducing apoptosis under 3D conditions. In line with our earlier findings, the combination of dichloroacetate and 4-MU resulted not only in growth inhibition, as observed with the monotherapies, but caused a pronounced decrease

in spheroid volume below start size (Figure 5b). Live-Dead staining of native spheroids at Day 10 revealed that monotherapy with 4-MU (300 µM) diminished the size of the spheroid while only few dead cells were detectable. In contrast, monotherapy with dichloroacetate (20 mM) caused shedding of dead cells from the spheroid. However, only the combination of both compounds significantly reduced spheroid size and led to an extensive emergence of dead cells in and around the spheroid (Figure 5c, upper panel). This finding was corroborated by a caspase 3 staining that revealed an apoptotic core under 4-MU treatment, homogeneously distributed apoptotic cells with dichloroacetate treatment, and a widespread induction of apoptosis throughout the spheroids under the combination therapy (Figure 5c, lower panel). Silencing of RHAMM, CD44, and HAS3 basically resembled the results obtained in 2D cultures differing only in a weaker effect of the HAS3 knockdown, which may be caused by the

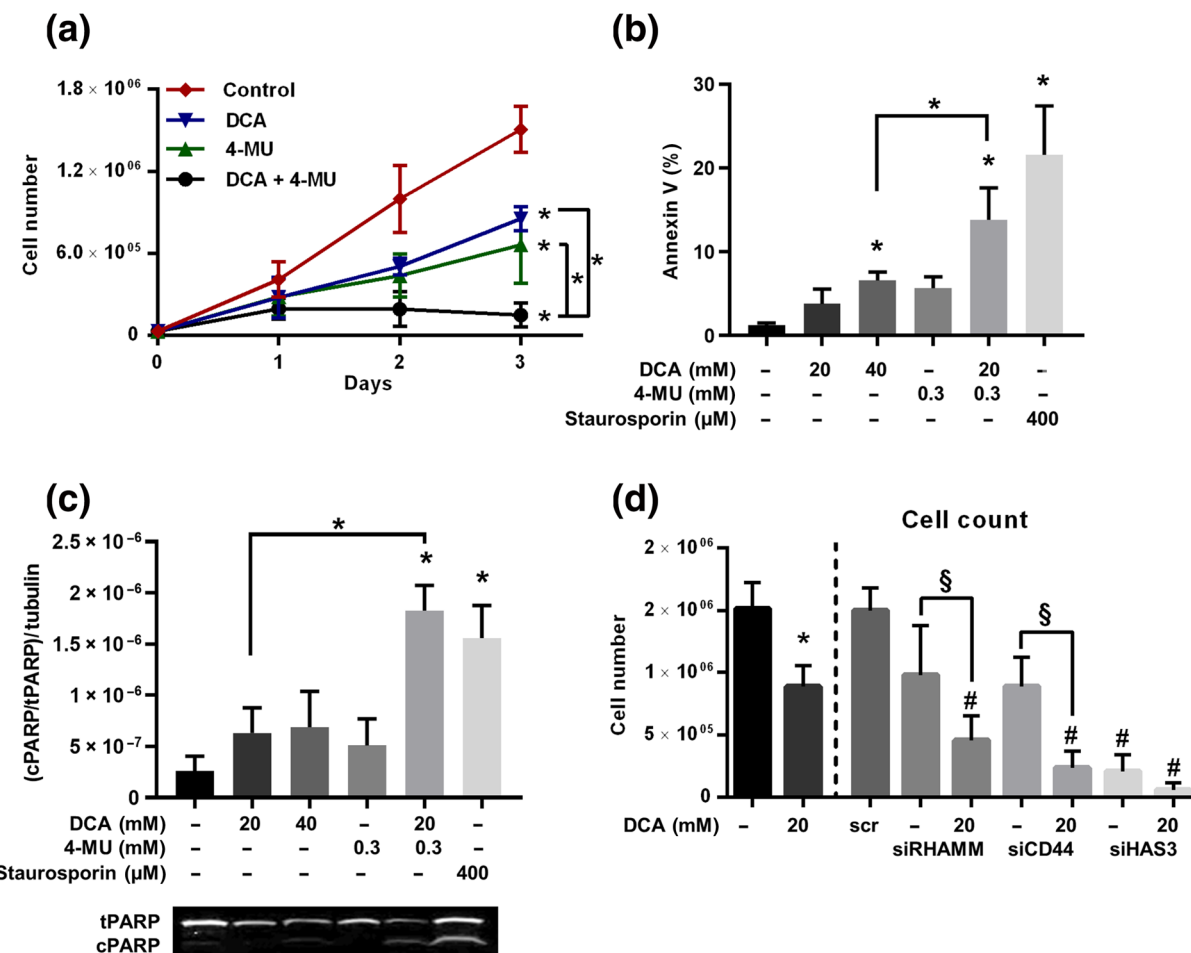


**FIGURE 4** Dichloroacetate (DCA) in combination with 4-methylumbelliferon (4-MU) leads to reduced cell growth and apoptosis induction in esophageal squamous cell carcinoma cells. (a) Cells were incubated with 20-mM dichloroacetate and/or 300- $\mu$ M 4-MU and counted daily for 3 days ( $n = 7$ ). After a 3-days of exposure to single or combination therapy, cells were collected for (b) FACS of annexin-positive cells ( $n = 6$ ) and (c) immunoblot of cleaved PARP (cPARP). cPARP was normalized to total PARP (tPARP). A typical immunoblot for seven individual experiments is shown. Staurosporine (400  $\mu$ M) was used as a positive control ( $n = 7$ ). (d) Cell numbers were determined 3 days after gene knockdown by siRNA for hyaluronan receptors RHAMM and CD44 and hyaluronan synthase (HAS) isotype HAS3 ( $n = 7$ ). Data shown are means  $\pm$  SD. \* $P < .05$ , significantly different from control or 0-mM DCA or as indicated; # $P < .05$ , significantly different from scrambled control; § $P < .05$ , significantly different from only siRNA treatment, one-way ANOVA.

strong overexpression of HAS3 in 3D culture (Figures 5, S6B, and S7A,B). The induction of cell death with dichloroacetate and 4-MU or siRHAMM, siCD44, and siHAS3 was validated by an APH assay (Figure S8A,B).

### 3.3 | Validation of the efficacy of the combination therapy in a nude mouse tumour xenograft regression model

To confirm our findings *in vivo*, we used a nude mouse tumour xenograft regression model. On Day 60, all treatments caused a significant reduction in tumour volume compared to the placebo control. However, only the combination treatment resulted in a sustained growth arrest of the tumour xenografts and in macroscopically detectable destruction of tumour tissue. In this group, the

tumour volume was also significantly reduced in comparison to the monotherapies with dichloroacetate and 4-MU (Figure 6a). In line with the *in vitro* experiments (Figure 1a,b), histological stainings for HA (HABP) and tumour cells (CK18) yielded an increase in HA deposition in the dichloroacetate treated group that was abolished in the 4-MU treated groups (Figure 6b). In order to detect the basis for the impeded xenograft growth in the treatment groups, we stained the tumour sections for the proliferation marker Ki67 (Figure 6c) and the endothelial cell marker CD31 (Figure 6d). Proliferating cells were diminished most in response to the combination treatment while the monotherapies also decreased the number of proliferating cells. Only dichloroacetate and dichloroacetate/4-MU resulted in a significant reduction of CD31 positive vessels. However, also, 4-MU treatment showed a similar tendency. Apoptotic cells were visualized by TUNEL staining (Figure 6e). Intriguingly, only the

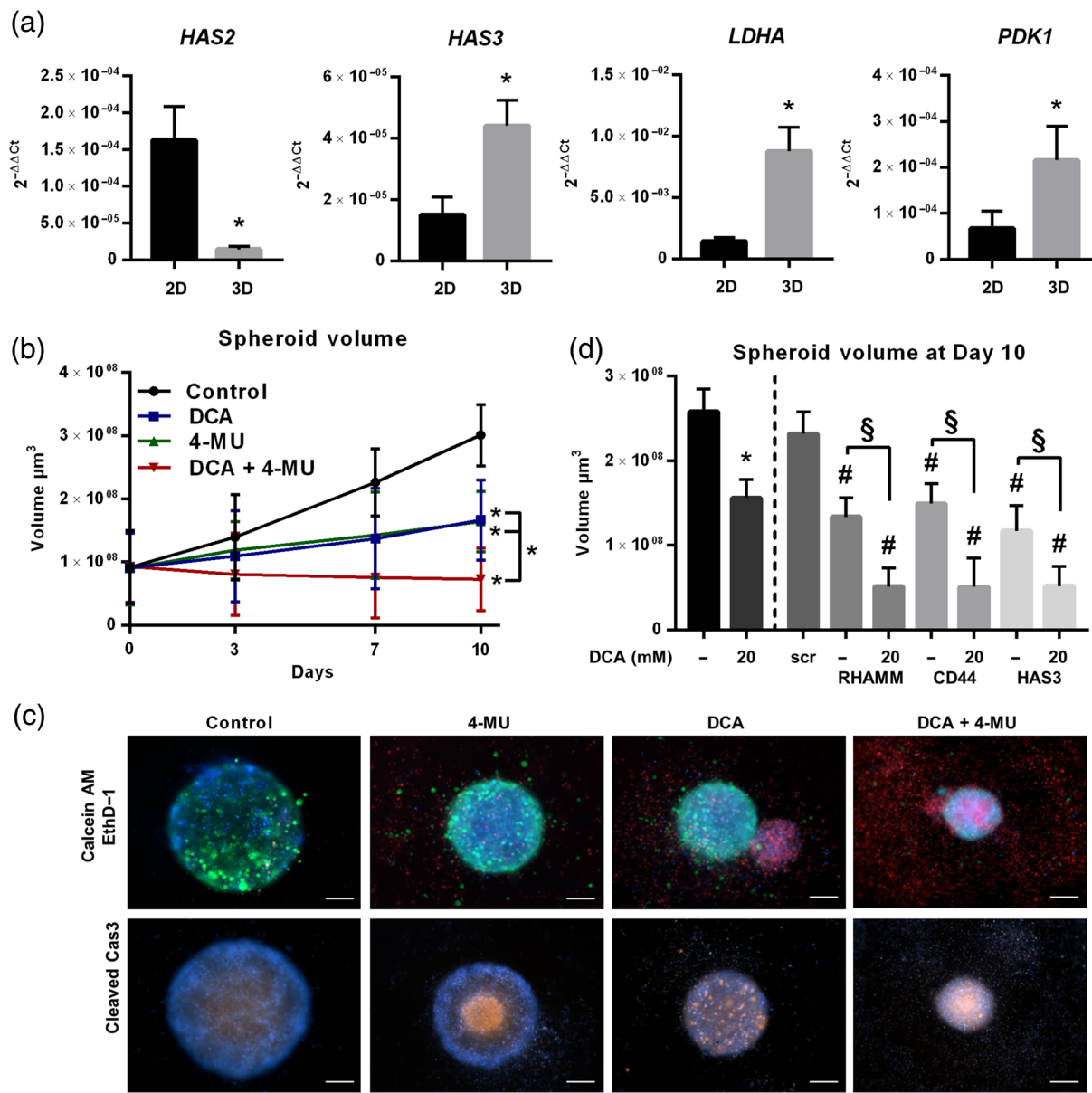


**FIGURE 5** Combination of dichloroacetate (DCA) and 4-methylumbelliferon (4-MU) causes reduction in tumour spheroid volumes and induction of apoptosis. (a) Comparison of the gene expression between 2D and 3D cultures of the most relevant components of the hyaluronan system and aerobic glycolysis ( $n = 6$ , each  $n$  represents a pooled analysis of eight replicates). (b) Spheroid volumes of 24 replicate spheroids per condition were measured. 3D cultures were grown for 4 days until incubation with drugs (20-mM dichloroacetate, 300- $\mu$ M 4-MU, or the combination of both) was started. The volume was measured over a 10-day period and observed by light microscopy. The volume of a sphere was calculated based on the diameter with the formula  $V = 1/6 \times \pi \times d^3$  ( $n = 6$ ). (c) At Day 10, spheroids were stained for living (calcein AM, green) and dead (ethidium homodimer 1 [EthD-1], red) cells or for cleaved caspase 3 (Cas3, orange). Nuclei were counterstained with Hoechst (blue). Representative images are shown, scale bar: 200  $\mu$ m. (d) siRNA knockdown of RHAMM, CD44, and HAS3 was performed prior to spheroid formation. Additional stimulation with 20-mM dichloroacetate was performed at Day 4. The experiments were followed for 10 d. Scrambled siRNA was used to exclude adverse effects of siRNA incorporation ( $n = 6$ ; one  $n$  included 24 spheroids per condition). Data shown are means  $\pm$  SD. \* $P < .05$ , significantly different from 2D values or as indicated; # $P < .05$  significantly different from scrambled control; § $P < .05$ , significantly different from only siRNA treatment; one-way ANOVA.

combination treatment caused a pronounced increase in apoptotic cells. The therapy was well tolerated in all treatment groups. Taken together, these experiments show that the combination of dichloroacetate and 4-MU may be a safe and effective treatment option for oesophageal cancer *in vivo*.

#### 4 | DISCUSSION

This study provided a deeper insight into the close connection between tumour metabolism and ECM regulation. It demonstrated that reconstitution of mitochondrial OXPHOS and subsequent

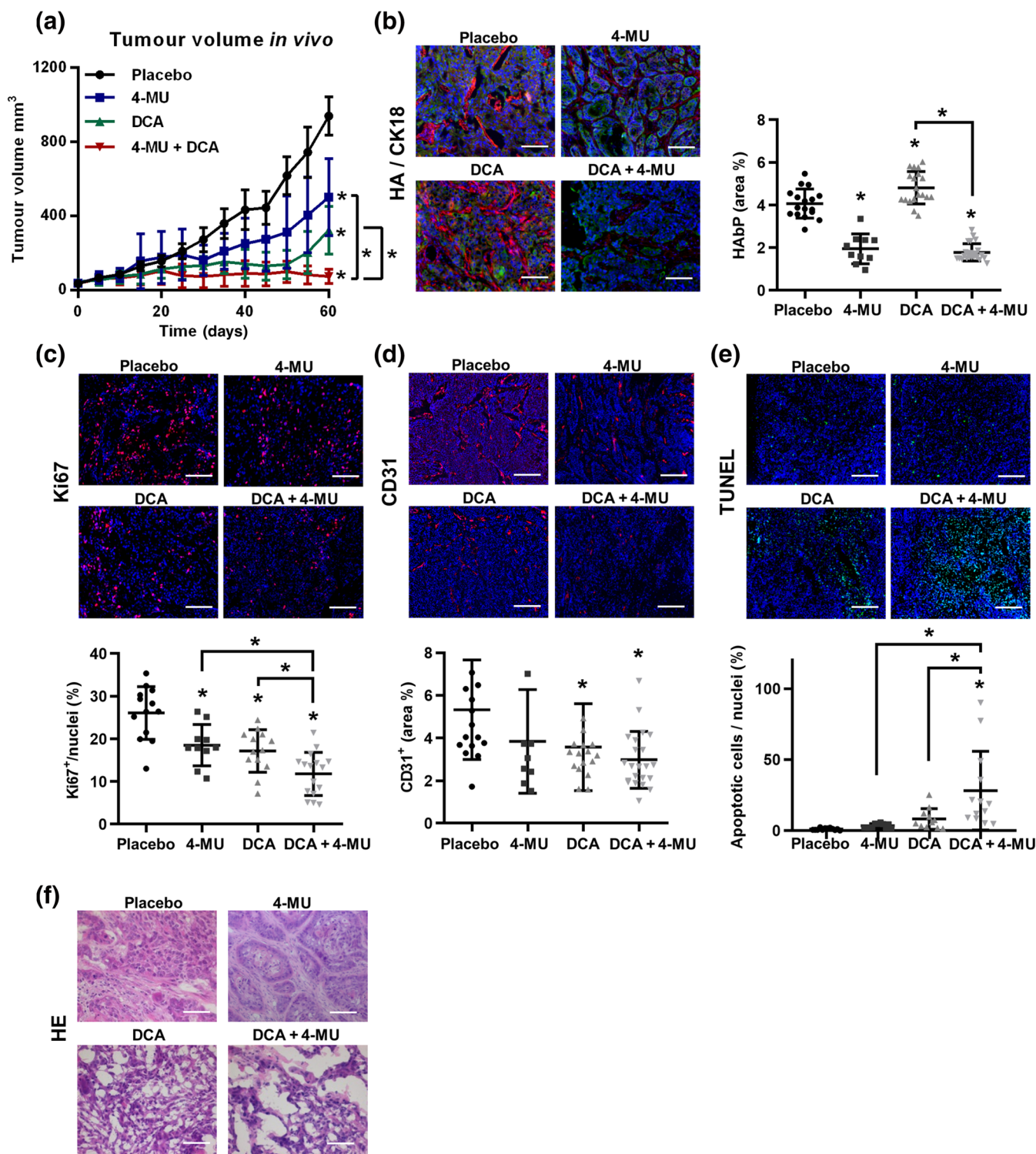


**FIGURE 6** The combination of dichloroacetate (DCA) and 4-methylumbelliferone (4-MU) reduces tumour growth and proliferation and induces hyaluronan (HA) synthesis and apoptosis *in vivo*. (a) Treatment with the testing substances started after a tumour volume of  $>30 \text{ mm}^3$  was detected. Tumour growth was measured by calipers and observed throughout 60 days. Placebo  $n = 15$ , 4-MU  $n = 9$ , dichloroacetate  $n = 10$ , dichloroacetate + 4-MU  $n = 13$ . Residual tumours were retrieved, and cryosections were drawn. The slides were stained for (b) HA deposition (HA binding protein [HAbP], red) in the tumour (CK18, green) and stroma, (c) proliferative activity of tumour cells (Ki67, red), and (d) vessels (CD31, red). (e) TUNEL staining (green) was used to measure the amount of apoptosis that is induced by single or combinational treatment. (f) HE staining of tumour tissues was used to evaluate the morphology of tumour and stroma. Representative images are shown, scale bars: (b–e)  $100 \mu\text{m}$ , (f)  $50 \mu\text{m}$ . Data shown are individual values, with means  $\pm$  SD. \* $P < .05$ , significantly different from placebo or as indicated; one-way ANOVA.

changes in the cellular glucose flux were metabolically coupled to the antiapoptotic HA system. This observation presents a new mechanism for resistance to metabolic anticancer therapies targeting the Warburg effect. This process may be further aggravated by the strong transcriptional activation of both aerobic glycolysis and HAS under three-dimensional growth, as observed in this study. To overcome this metabolic counter-regulation, we tested pharmacological inhibition of the HA matrix synthesis by the low MW compound 4-MU in combination with dichloroacetate treatment, which indeed caused increased apoptosis, eventually leading to synergistically enhanced anti-tumour effects *in vitro* and *in vivo*.

In detail, we describe two mechanisms that increase the HA synthesis when mitochondrial OXPHOS is restored by dichloroacetate. First, the G6P precursor pool is increased, thus providing more fuel for the synthesis of UDP-glucuronic acid, one of the two substrates for HA synthesis used by the HAS enzymes. This is in line with earlier reports in muscle cells showing that dichloroacetate inhibits glycolysis by an unknown mechanism resulting in an increase of G6P in this cell type (Clark et al., 1987). This observation may be explained by the inhibition of phosphofructokinase II via O-GlcNAcylation and is further discussed below. Second, activation of the PDC yielded a pronounced increase in mitochondrial acetyl-CoA that fuels OXPHOS but is also shuttled to the cytosol, where it serves as a cofactor for the synthesis of GlcNAc, which is the second substrate for HA synthesis.

In this context, it is noteworthy that HA is exclusively synthesized from these two early glucose metabolites. Accordingly, substrate availability directly correlates with the extent of HA synthesis (Tammi et al., 2011). For instance, UDP-sugar accumulation has been shown to enhance HA synthesis in breast cancer (Oikari et al., 2018). Interestingly, the synthesis of other glycosaminoglycans is modulated by UDP-GlcNAc availability, thus extending the effect of our findings beyond regulation of HA synthesis (Vigetti et al., 2012). One remarkable observation in our experiments is that we detected a rise in G6P and UDP-GlcNAc levels under dichloroacetate treatment but no increase in UDP-glucuronic acid. This may be caused by a rapid use of this immediate precursor for HA synthesis due to a high activity of the HAS enzymes triggered by the mechanisms discussed below.

In addition to providing fuel for HA synthesis, UDP-GlcNAc also holds the potential to induce HA synthesis by post-translational mechanisms (Moretto et al., 2015): UDP-GlcNAc concentrations control the activity of the O-GlcNAc transferase and thereby the O-GlcNAcylation of various proteins including the HAS enzymes. Indeed, a great extent of O-GlcNAcylation in breast cancer cells was found to correlate with the levels of HAS enzymes, accumulation of HA, and poor outcome (Tiainen et al., 2016). Specifically for HAS3, the predominant isoform in the ESCC cell line used in our study, it has been reported that cytosolic levels of UDP-GlcUA and UDP-GlcNAc regulate its activity by orchestrating the shuttling of this isoform from Golgi to the plasma membrane and facilitating its O-GlcNAcylation in melanoma cells (Deen et al., 2016). However, this study is the first to describe a connection between mitochondrial acetyl-CoA synthesis, UDP-GlcNAc levels, and HA matrix augmentation. To prove the link of

mitochondrial activity and increased cytosolic GlcNAc levels, we used the ATP citrate-lyase inhibitor SB-204990, which inhibits the cytosolic conversion of citrate to acetyl-CoA, thus prohibiting the shuttling of acetyl-CoA from mitochondria to the cytosol (Pearce et al., 1998). This experiment shows that mitochondria-dependent acetyl-CoA synthesis is an important step for the induction of HA synthesis via increased GlcNAc concentration under restored Krebs cycle activity.

Recently, these and other roles of O-GlcNAcylation as a nutrient-dependent regulator of cell functions have been summarised in a comprehensive review (Hart, 2019). The concentration of UDP-GlcNAc is a highly responsive sensor for the availability and flux of nutrients through major metabolic pathways and the activity of hexosamine biosynthesis. Thus, O-GlcNAcylation orchestrates a wide range of cellular processes in response to glycolytic activity including regulation of gene expression and methylation, cell cycle, cytokinesis, and the cytoskeleton. It is induced by cellular stress and mediates protection against cellular damage, by regulating DNA repair mechanisms, for instance. Moreover, O-GlcNAcylation is also an important factor connecting metabolism to epigenetic regulation (Hanover, Krause, & Love, 2012). Of note, O-GlcNAcylation and phosphorylation show a mutually exclusive interplay in protein activation and also exhibit a feedback crosstalk between the involved regulating enzymes. Prolonged elevation of O-GlcNAcylation promotes several age-associated chronic diseases, that is, diabetes, neurodegenerative diseases, and cancer. O-GlcNAcylation was also shown to inhibit phosphofructokinase II, thus increasing the flux of glucose metabolites into the pentose phosphate pathway (Yi et al., 2012). As the precursors of HA, G6P and fructose 6-phosphate, originate from earlier steps in glycolysis, this observation may explain the elevated G6P levels in response to dichloroacetate treatment. Aberrations in O-GlcNAc cycling enzymes are considered as a new characteristic of cancer and have been connected to the metabolic reprogramming in cancer cells and may represent a novel therapeutic target (Fardini, Dehennaut, Lefebvre, & Issad, 2013). As elevated O-GlcNAcylation has been reported in many cancer entities (Slawson & Hart, 2011), the increase of this process by dichloroacetate, which we report here, should be further explored in further studies to determine whether this may represent a negative dichloroacetate side effect, independent of HA elevation.

In addition to the effects of our findings on tumour cells, the induction of HA and GlcNAc levels by dichloroacetate may also contribute to its restorative effects on cellular stress, by regulation of cellular homeostasis. For instance, dichloroacetate has been proposed as a metabolic therapy for myocardial ischaemia and failure by facilitating aerobic oxidation of carbohydrates of fatty acids (Bersin & Stacpoole, 1997), a concept that has been assessed in several studies. These protective effects may be also dependent on increased O-GlcNAcylation, as discussed above, or on increased HA synthesis, as this process has been linked to inhibition of apoptosis. In support of this thesis, HA was recently found to promote healing after ischaemia-reperfusion injury (Petz et al., 2019). These considerations could also apply to other conditions such as septic shock (McCall et al., 2018), diabetes mellitus, and hyperlipoproteinemia (Stacpoole et al., 1978), as well as

pulmonary arterial hypertension and other diseases (James et al., 2017). Thus, the mechanisms elucidated in our study may also have long-term consequences on cellular processes beyond HA matrix regulation.

In addition to the observed metabolic stimulation of HA synthesis via an elevated supply of precursors and post-translational activation by GlcNAcylation, transcriptional changes were also involved in increasing HA synthesis following dichloroacetate treatment. We detected a strong dose-dependent up-regulation of the vital genes involved in HAS (HAS2-3), catabolism (HYAL1,2), and signalling (CD44, RHAMM). This effect may either be attributable to a positive transcriptional feedback loop that has been described (Tammi et al., 2011) or to a direct influence of the metabolic changes under dichloroacetate treatment on the respective gene promoters. Little is known about metabolic effects on HAS transcription but, in human smooth muscle cells, a drop in energy homeostasis causes a decline in HAS2 expression via **AMP kinase** (Vigetti et al., 2011).

This study also provides an explanation for the paradoxical observation that dichloroacetate was more active *in vivo* than *in vitro* in some experimental setups (Papandreou et al., 2011). The comparison of 2D and 3D cell cultures showed strong up-regulation of PDK1 and LDHA when grown as spheroids indicating that these systems are more active in this model, which better correlates to *in vivo* growth. This observation is in line with the fact that multicellular tumour spheroids are thought to be a better model for the hypoxia found in solid tumours, a condition that is linked to activation of aerobic glycolysis (Riffle & Hegde, 2017). In addition, we show for the first time that three-dimensional growth also causes strong transcriptional induction of HAS3. This may be the result of increased scaffolding needs but is likely also to present an important survival factor in advanced carcinogenesis. Indeed, only the targeting of both systems with the combination of dichloroacetate and 4-MU caused shrinkage of the tumour spheroids below their initial size. Our data suggest that the induction of the antiapoptotic HA matrix may be intrinsic to the mechanism of action of drugs that restore OXPHOS in cancer cells.

In our study, we first characterized a counter-regulatory mechanism involving a metabolic link between OXPHOS and elevated synthesis of the ECM compound HA. In a next step, we specifically targeted this rescue mechanism by abolishing the activity of the antiapoptotic HA system, which yielded a pronounced synergistic action of dichloroacetate and 4-MU. In contrast to most of the published studies on dichloroacetate combination therapies, we used a tumour xenograft regression model, which reflects the clinical situation more appropriately in that treatment starts after a defined tumour volume is detected. Of note, also under this condition, we found a sustained inhibition of tumour growth with a marked induction of apoptosis in the tumour tissue.

A limitation of this study is that our results have been produced using one tumour cell line. However, as summarized in Tables S3 and S4, the effects of dichloroacetate on mitochondria reactivation and subsequent tumour growth inhibition have been shown in a wide variety of tumour models *in vitro* and *in vivo*. As restored mitochondrial activity is most likely to result in elevated acetyl-CoA production in

general, we propose that the mechanism described here may also be valid for other cell types. Given that 4-MU was also reported to inhibit HAS, and consequently tumour growth, in a wide variety of tumour cells types (as summarised in Tables S5 and S6), it can be assumed that it would exhibit the same synergy with dichloroacetate as reported here in other cell types. Nevertheless, this assumption should be tested with other tumour entities and in other models.

This study shows that the metabolic changes induced by reactivation of mitochondrial OXPHOS result in a pronounced activation of HA matrix generation by an increase of the HA precursor pool and O-GlcNAcylation, which in turn supports the survival of the tumour cells. This process can be inhibited by the orally available HAS inhibitor 4-MU, which yielded strong synergistic actions with dichloroacetate *in vitro* and *in vivo*. As the resistance mechanism described in this study is likely to be inherent in therapies targeting the Warburg effect, 4-MU may also be a promising synergistic partner for these metabolic anticancer therapies as well. As 4-MU is approved for human use in many countries, the results of this study should be applicable to new clinical studies testing the therapeutic value of this combination for metabolic anticancer therapy. These findings provide the basis for further research on the effects of tumour metabolism on the tumour micro-environment and for testing this combination in clinical studies.

## ACKNOWLEDGEMENT

This work was supported by the Forschungskommission der Heinrich-Heine-Universität Düsseldorf (Grant 51/2015).

## AUTHOR CONTRIBUTIONS

S.T. designed the experiments, researched and interpreted data, and wrote the manuscript. C.R. researched and interpreted data and wrote parts of the manuscript. K.B., O.R., I.K., D.G., K.G., and M.G. researched data and reviewed the manuscript. J.W.F. designed the experiments, contributed guidance, and reviewed the manuscript.

## CONFLICT OF INTEREST

The authors declare no conflicts of interest.

## DECLARATION OF TRANSPARENCY AND SCIENTIFIC RIGOUR

This Declaration acknowledges that this paper adheres to the principles for transparent reporting and scientific rigour of preclinical research as stated in the **BJP** guidelines for **Design & Analysis**, **Immunoblotting and Immunoochemistry**, and **Animal Experimentation**, and as recommended by funding agencies, publishers and other organisations engaged with supporting research.

## DATA AVAILABILITY STATEMENT

All data generated or analysed during this study are included in this published article and its supplementary information files.

**ORCID**

Sören Twarock  <https://orcid.org/0000-0001-9252-1353>

**REFERENCES**

- Alexander, S. P. H., Fabbro, D., Kelly, E., Marion, N. V., Peters, J. A., Faccenda, E., ... Collaborators, C. G. T. P. (2017). THE CONCISE GUIDE TO PHARMACOLOGY 2017/18: Enzymes. *British Journal of Pharmacology*, 174, S272–S359. <https://doi.org/10.1111/bph.13877>
- Bersin, R. M., & Stacpoole, P. W. (1997). Dichloroacetate as metabolic therapy for myocardial ischemia and failure. *American Heart Journal*, 134, 841–855. [https://doi.org/10.1016/S0002-8703\(97\)80007-5](https://doi.org/10.1016/S0002-8703(97)80007-5)
- Bonnet, S., Archer, S. L., Allalunis-Turner, J., Haromy, A., Beaulieu, C., Thompson, R., ... Michelakis, E. D. (2007). A mitochondria-K<sup>+</sup> channel axis is suppressed in cancer and its normalization promotes apoptosis and inhibits cancer growth. *Cancer Cell*, 11, 37–51. <https://doi.org/10.1016/j.ccr.2006.10.020>
- Chanmee, T., Ontong, P., & Itano, N. (2016). Hyaluronan: A modulator of the tumor microenvironment. *Cancer Letters*, 375, 20–30. <https://doi.org/10.1016/j.canlet.2016.02.031>
- Chen, L., & Bourguignon, L. Y. (2014). Hyaluronan-CD44 interaction promotes c-Jun signaling and miRNA21 expression leading to Bcl-2 expression and chemoresistance in breast cancer cells. *Molecular Cancer*, 13, 52. <https://doi.org/10.1186/1476-4598-13-52>
- Chu, Q. S., Sangha, R., Spratlin, J., Vos, L. J., Mackey, J. R., McEwan, A. J., ... Michelakis, E. D. (2015). A phase I open-labeled, single-arm, dose-escalation, study of dichloroacetate (DCA) in patients with advanced solid tumors. *Investigational New Drugs*, 33, 603–610. <https://doi.org/10.1007/s10637-015-0221-y>
- Clark, A. S., Mitch, W. E., Goodman, M. N., Fagan, J. M., Goheer, M. A., & Curnow, R. T. (1987). Dichloroacetate inhibits glycolysis and augments insulin-stimulated glycogen synthesis in rat muscle. *The Journal of Clinical Investigation*, 79, 588–594. <https://doi.org/10.1172/JCI112851>
- Deen, A. J., Arasu, U. T., Pasonen-Seppanen, S., Hassinen, A., Takabe, P., Wojciechowski, S., ... Oikari, S. (2016). UDP-sugar substrates of HAS3 regulate its O-GlcNAcylation, intracellular traffic, extracellular shedding and correlate with melanoma progression. *Cellular and Molecular Life Sciences*, 73, 3183–3204. <https://doi.org/10.1007/s00018-016-2158-5>
- Dunbar, E. M., Coats, B. S., Shroads, A. L., Langae, T., Lew, A., Forder, J. R., ... Stacpoole, P. W. (2014). Phase 1 trial of dichloroacetate (DCA) in adults with recurrent malignant brain tumors. *Investigational New Drugs*, 32, 452–464. <https://doi.org/10.1007/s10637-013-0047-4>
- Enzinger, P. C., & Mayer, R. J. (2003). Esophageal cancer. *The New England Journal of Medicine*, 349, 2241–2252. <https://doi.org/10.1056/NEJMra035010>
- Fardini, Y., Dehennaut, V., Lefebvre, T., & Issad, T. (2013). O-GlcNAcylation: A new cancer hallmark? *Frontiers in Endocrinology*, 4, 99.
- Garon, E. B., Christofk, H. R., Hosmer, W., Britten, C. D., Bahng, A., Crabtree, M. J., ... Slamon, D. J. (2014). Dichloroacetate should be considered with platinum-based chemotherapy in hypoxic tumors rather than as a single agent in advanced non-small cell lung cancer. *Journal of Cancer Research and Clinical Oncology*, 140, 443–452. <https://doi.org/10.1007/s00432-014-1583-9>
- Grandoch, M., Bujok, V., Fleckenstein, D., Schmidt, M., Fischer, J. W., & Weber, A. A. (2009). Epac inhibits apoptosis of human leukocytes. *Journal of Leukocyte Biology*, 86, 847–849. <https://doi.org/10.1189/jlb.0109048>
- Hanover, J. A., Krause, M. W., & Love, D. C. (2012). Bittersweet memories: Linking metabolism to epigenetics through O-GlcNAcylation. *Nature Reviews Molecular Cell Biology*, 13, 312–321. <https://doi.org/10.1038/nrm3334>
- Harding, S. D., Sharman, J. L., Faccenda, E., Southan, C., Pawson, A. J., Ireland, S., ... NC-IUPHAR (2018). The IUPHAR/BPS guide to pharmacology in 2018: Updates and expansion to encompass the new guide to immunopharmacology. *Nucleic Acids Research*, 46, D1091–D1106. <https://doi.org/10.1093/nar/gkx1121>
- Hart, G. W. (2019). Nutrient regulation of signaling and transcription. *The Journal of Biological Chemistry*, 294, 2211–2231. <https://doi.org/10.1074/jbc.AW119.003226>
- Ishiguro, T., Ishiguro, M., Ishiguro, R., & Iwai, S. (2012). Cotreatment with dichloroacetate and omeprazole exhibits a synergistic antiproliferative effect on malignant tumors. *Oncology Letters*, 3, 726–728. <https://doi.org/10.3892/ol.2012.552>
- Itano, N., Sawai, T., Yoshida, M., Lenas, P., Yamada, Y., Imagawa, M., ... Kimata, K. (1999). Three isoforms of mammalian hyaluronan synthases have distinct enzymatic properties. *The Journal of Biological Chemistry*, 274, 25085–25092. <https://doi.org/10.1074/jbc.274.35.25085>
- James, M. O., Jahn, S. C., Zhong, G., Smeltz, M. G., Hu, Z., & Stacpoole, P. W. (2017). Therapeutic applications of dichloroacetate and the role of glutathione transferase zeta-1. *Pharmacology & Therapeutics*, 170, 166–180. <https://doi.org/10.1016/j.pharmthera.2016.10.018>
- Kakizaki, I., Kojima, K., Takagaki, K., Endo, M., Kannagi, R., Ito, M., ... Itano, N. (2004). A novel mechanism for the inhibition of hyaluronan biosynthesis by 4-methylumbelliferon. *The Journal of Biological Chemistry*, 279, 33281–33289. <https://doi.org/10.1074/jbc.M405918200>
- Kankotia, S., & Stacpoole, P. W. (2014). Dichloroacetate and cancer: New home for an orphan drug? *Biochimica et Biophysica Acta*, 1846, 617–629. <https://doi.org/10.1016/j.bbcan.2014.08.005>
- Kaufmann, P., Engelstad, K., Wei, Y., Jhung, S., Sano, M. C., Shungu, D. C., ... de Vivo, D. C. (2006). Dichloroacetate causes toxic neuropathy in MELAS: A randomized, controlled clinical trial. *Neurology*, 66, 324–330. <https://doi.org/10.1212/01.wnl.0000196641.05913.27>
- Kilkenny, C., Browne, W., Cuthill, I. C., Emerson, M., & Altman, D. G. (2010). Animal research: Reporting in vivo experiments: The ARRIVE guidelines. *British Journal of Pharmacology*, 160, 1577–1579.
- Konrad, R. J., Zhang, F., Hale, J. E., Knierman, M. D., Becker, G. W., & Kudlow, J. E. (2002). Alloxan is an inhibitor of the enzyme O-linked N-acetylglucosamine transferase. *Biochemical and Biophysical Research Communications*, 293, 207–212. [https://doi.org/10.1016/S0006-291X\(02\)00200-0](https://doi.org/10.1016/S0006-291X(02)00200-0)
- Lin, E. W., Karakasheva, T. A., Hicks, P. D., Bass, A. J., & Rustgi, A. K. (2016). The tumor microenvironment in esophageal cancer. *Oncogene*, 35, 5337–5349. <https://doi.org/10.1038/onc.2016.34>
- Lokeshwar, V. B., Lopez, L. E., Munoz, D., Chi, A., Shirodkar, S. P., Lokeshwar, S. D., ... Altman, N. (2010). Antitumor activity of hyaluronic acid synthesis inhibitor 4-methylumbelliferon in prostate cancer cells. *Cancer Research*, 70, 2613–2623. <https://doi.org/10.1158/0008-5472.CAN-09-3185>
- Martinez-Outschoorn, U. E., Peiris-Pages, M., Pestell, R. G., Sotgia, F., & Lisanti, M. P. (2017). Cancer metabolism: A therapeutic perspective. *Nature Reviews Clinical Oncology*, 14, 11–31. <https://doi.org/10.1038/nrclinonc.2016.60>
- McCall, C. E., Zabalawi, M., Liu, T., Martin, A., Long, D. L., Buechler, N. L., ... Vachharajani, V. (2018). Pyruvate dehydrogenase complex stimulation promotes immunometabolic homeostasis and sepsis survival. *JCI Insight*, 3. <https://doi.org/10.1172/jci.insight.99295>
- McGrath, J. C., & Lilley, E. (2015). Implementing guidelines on reporting research using animals (ARRIVE etc.): New requirements for publication in BJP. *British Journal of Pharmacology*, 172, 3189–3193. <https://doi.org/10.1111/bph.12955>

- Michelakis, E. D., Sutendra, G., Dromparis, P., Webster, L., Haromy, A., Niven, E., ... Petruk, K. C. (2010). Metabolic modulation of glioblastoma with dichloroacetate. *Science Translational Medicine*, 2, 31ra34.
- Michelakis, E. D., Webster, L., & Mackey, J. R. (2008). Dichloroacetate (DCA) as a potential metabolic-targeting therapy for cancer. *British Journal of Cancer*, 99, 989–994. <https://doi.org/10.1038/sj.bjc.6604554>
- Misra, S., Hascall, V. C., Markwald, R. R., & Ghatak, S. (2015). Interactions between hyaluronan and its receptors (CD44, RHAMM) regulate the activities of inflammation and cancer. *Frontiers in Immunology*, 6, 201.
- Morera, D. S., Hennig, M. S., Talukder, A., Lokeshwar, S. D., Wang, J., Garcia-Roig, M., ... Lokeshwar, V. B. (2017). Hyaluronic acid family in bladder cancer: Potential prognostic biomarkers and therapeutic targets. *British Journal of Cancer*, 117, 1507–1517. <https://doi.org/10.1038/bjc.2017.318>
- Moretto, P., Karousou, E., Viola, M., Caon, I., D'Angelo, M. L., De Luca, G., ... Vigetti, D. (2015). Regulation of hyaluronan synthesis in vascular diseases and diabetes. *Journal Diabetes Research*, 2015, 167283.
- Nagy, N., Freudenberg, T., Melchior-Becker, A., Rock, K., Ter Braak, M., Jastrow, H., ... Fischer, J. W. (2010). Inhibition of hyaluronan synthesis accelerates murine atherosclerosis: Novel insights into the role of hyaluronan synthesis. *Circulation*, 122, 2313–2322. <https://doi.org/10.1161/CIRCULATIONAHA.110.972653>
- Nakazawa, H., Yoshihara, S., Kudo, D., Morohashi, H., Kakizaki, I., Kon, A., ... Sasaki, M. (2006). 4-Methylumbelliferon, a hyaluronan synthase suppressor, enhances the anticancer activity of gemcitabine in human pancreatic cancer cells. *Cancer Chemotherapy and Pharmacology*, 57, 165–170. <https://doi.org/10.1007/s00280-005-0016-5>
- Ohashi, T., Akazawa, T., Aoki, M., Kuze, B., Mizuta, K., Ito, Y., & Inoue, N. (2013). Dichloroacetate improves immune dysfunction caused by tumor-secreted lactic acid and increases antitumor immunoreactivity. *International Journal of Cancer Journal International du Cancer*, 133, 1107–1118. <https://doi.org/10.1002/ijc.28114>
- Oikari, S., Kettunen, T., Tiainen, S., Hayrinne, J., Masarwah, A., Sudah, M., ... Auvinen, P. (2018). UDP-sugar accumulation drives hyaluronan synthesis in breast cancer. *Matrix Biology*, 67, 63–74. <https://doi.org/10.1016/j.matbio.2017.12.015>
- Palyi-Krek, Z., Barok, M., Isola, J., Tammi, M., Szollosi, J., & Nagy, P. (2007). Hyaluronan-induced masking of ErbB2 and CD44-enhanced trastuzumab internalisation in trastuzumab resistant breast cancer. *European Journal of Cancer*, 43, 2423–2433. <https://doi.org/10.1016/j.ejca.2007.08.018>
- Papandreou, I., Goliasova, T., & Denko, N. C. (2011). Anticancer drugs that target metabolism: Is dichloroacetate the new paradigm? *International Journal of Cancer Journal International du Cancer*, 128, 1001–1008. <https://doi.org/10.1002/ijc.25728>
- Pearce, N. J., Yates, J. W., Berkhouit, T. A., Jackson, B., Tew, D., Boyd, H., ... Groot, P. H. (1998). The role of ATP citrate-lyase in the metabolic regulation of plasma lipids. Hypolipidaemic effects of SB-204990, a lactone prodrug of the potent ATP citrate-lyase inhibitor SB-201076. *The Biochemical Journal*, 334(Pt 1), 113–119. <https://doi.org/10.1042/bj3340113>
- Petz, A., Grandoch, M., Gorski, D. J., Abrams, M., Piroth, M., Schneckmann, R., ... Fischer, J. W. (2019). Cardiac hyaluronan synthesis is critically involved in the cardiac macrophage response and promotes healing after ischemia reperfusion injury. *Circulation Research*, 124, 1433–1447. <https://doi.org/10.1161/CIRCRESAHA.118.313285>
- Piccioni, F., Fiore, E., Bayo, J., Atorrasagasti, C., Peixoto, E., Rizzo, M., ... Mazzolini, G. (2015). 4-Methylumbelliferon inhibits hepatocellular carcinoma growth by decreasing IL-6 production and angiogenesis. *Glycobiology*, 25, 825–835. <https://doi.org/10.1093/glycob/cwv023>
- Pickup, M. W., Mouw, J. K., & Weaver, V. M. (2014). The extracellular matrix modulates the hallmarks of cancer. *EMBO Reports*, 15, 1243–1253. <https://doi.org/10.15252/embr.201439246>
- Riffle, S., & Hegde, R. S. (2017). Modeling tumor cell adaptations to hypoxia in multicellular tumor spheroids. *Journal of Experimental & Clinical Cancer Research*, 36, 102. <https://doi.org/10.1186/s13046-017-0570-9>
- Schindelin, J., Arganda-Carreras, I., Frise, E., Kaynig, V., Longair, M., Pietzsch, T., ... Cardona, A. (2012). Fiji: An open-source platform for biological-image analysis. *Nature Methods*, 9, 676–682. <https://doi.org/10.1038/nmeth.2019>
- Sirenko, O., Mitlo, T., Hesley, J., Luke, S., Owens, W., & Cromwell, E. F. (2015). High-content assays for characterizing the viability and morphology of 3D cancer spheroid cultures. *Assay and Drug Development Technologies*, 13, 402–414. <https://doi.org/10.1089/adt.2015.655>
- Slawson, C., & Hart, G. W. (2011). O-GlcNAc signalling: Implications for cancer cell biology. *Nature Reviews Cancer*, 11, 678–684. <https://doi.org/10.1038/nrc3114>
- Stacpoole, P. W., Kerr, D. S., Barnes, C., Bunch, S. T., Carney, P. R., Fennell, E. M., ... Valenstein, E. (2006). Controlled clinical trial of dichloroacetate for treatment of congenital lactic acidosis in children. *Pediatrics*, 117, 1519–1531. <https://doi.org/10.1542/peds.2005-1226>
- Stacpoole, P. W., Kurtz, T. L., Han, Z., & Langae, T. (2008). Role of dichloroacetate in the treatment of genetic mitochondrial diseases. *Advanced Drug Delivery Reviews*, 60, 1478–1487. <https://doi.org/10.1016/j.addr.2008.02.014>
- Stacpoole, P. W., Moore, G. W., & Kornhauser, D. M. (1978). Metabolic effects of dichloroacetate in patients with diabetes mellitus and hyperlipoproteinemia. *The New England Journal of Medicine*, 298, 526–530. <https://doi.org/10.1056/NEJM197803092981002>
- Sun, R. C., Board, P. G., & Blackburn, A. C. (2011). Targeting metabolism with arsenic trioxide and dichloroacetate in breast cancer cells. *Molecular Cancer*, 10, 142. <https://doi.org/10.1186/1476-4598-10-142>
- Tammi, M. I., Oikari, S., Pasonen-Seppanen, S., Rilla, K., Auvinen, P., & Tammi, R. H. (2018). Activated hyaluronan metabolism in the tumor matrix—Causes and consequences. *Matrix Biology*, 78–79:147–164.
- Tammi, R. H., Passi, A. G., Rilla, K., Karousou, E., Vigetti, D., Makkonen, K., & Tammi, M. I. (2011). Transcriptional and post-translational regulation of hyaluronan synthesis. *The FEBS Journal*, 278, 1419–1428. <https://doi.org/10.1111/j.1742-4658.2011.08070.x>
- Tiainen, S., Oikari, S., Tammi, M., Rilla, K., Hamalainen, K., Tammi, R., ... Auvinen, P. (2016). High extent of O-GlcNAcylation in breast cancer cells correlates with the levels of HAS enzymes, accumulation of hyaluronan, and poor outcome. *Breast Cancer Research and Treatment*, 160, 237–247. <https://doi.org/10.1007/s10549-016-3996-4>
- Twarock, S., Freudenberg, T., Poscher, E., Dai, G., Jannasch, K., Dullin, C., ... Fischer, J. W. (2011). Inhibition of oesophageal squamous cell carcinoma progression by in vivo targeting of hyaluronan synthesis. *Molecular Cancer*, 10, 30. <https://doi.org/10.1186/1476-4598-10-30>
- Twarock, S., Reichert, C., Peters, U., Gorski, D. J., Rock, K., & Fischer, J. W. (2017). Hyperglycaemia and aberrated insulin signalling stimulate tumour progression via induction of the extracellular matrix component hyaluronan. *International Journal of Cancer Journal International du Cancer*, 141, 791–804. <https://doi.org/10.1002/ijc.30776>
- Twarock, S., Tammi, M. I., Savani, R. C., & Fischer, J. W. (2010). Hyaluronan stabilizes focal adhesions, filopodia, and the proliferative phenotype in esophageal squamous carcinoma cells. *The Journal of Biological Chemistry*, 285, 23276–23284. <https://doi.org/10.1074/jbc.M109.093146>
- Vander Heiden, M. G., Cantley, L. C., & Thompson, C. B. (2009). Understanding the Warburg effect: The metabolic requirements of cell

- proliferation. *Science*, 324, 1029–1033. <https://doi.org/10.1126/science.1160809>
- Vernieri, C., Casola, S., Foiani, M., Pietrantonio, F., de Braud, F., & Longo, V. (2016). Targeting cancer metabolism: Dietary and pharmacologic interventions. *Cancer Discovery*, 6, 1315–1333. <https://doi.org/10.1158/2159-8290.CD-16-0615>
- Vigetti, D., Clerici, M., Deleonibus, S., Karousou, E., Viola, M., Moretto, P., ... Passi, A. (2011). Hyaluronan synthesis is inhibited by adenosine monophosphate-activated protein kinase through the regulation of HAS2 activity in human aortic smooth muscle cells. *The Journal of Biological Chemistry*, 286, 7917–7924. <https://doi.org/10.1074/jbc.M110.193656>
- Vigetti, D., Deleonibus, S., Moretto, P., Karousou, E., Viola, M., Bartolini, B., ... Passi, A. (2012). Role of UDP-N-acetylglucosamine (GlcNAc) and O-GlcNAcylation of hyaluronan synthase 2 in the control of chondroitin sulfate and hyaluronan synthesis. *The Journal of Biological Chemistry*, 287, 35544–35555. <https://doi.org/10.1074/jbc.M112.402347>
- Vigetti, D., Viola, M., Karousou, E., De Luca, G., & Passi, A. (2014). Metabolic control of hyaluronan synthases. *Matrix Biology*, 35, 8–13. <https://doi.org/10.1016/j.matbio.2013.10.002>
- Warburg, O. (1956). On the origin of cancer cells. *Science*, 123, 309–314. <https://doi.org/10.1126/science.123.3191.309>
- Yi, W., Clark, P. M., Mason, D. E., Keenan, M. C., Hill, C., Goddard, W. A. 3rd, ... Hsieh-Wilson, L. C. (2012). Phosphofructokinase 1 glycosylation regulates cell growth and metabolism. *Science*, 337, 975–980. <https://doi.org/10.1126/science.1222278>
- Yoshihara, S., Kon, A., Kudo, D., Nakazawa, H., Kakizaki, I., Sasaki, M., ... Takagaki, K. (2005). A hyaluronan synthase suppressor, 4-methylumbelliferon, inhibits liver metastasis of melanoma cells. *FEBS Letters*, 579, 2722–2726. <https://doi.org/10.1016/j.febslet.2005.03.079>
- Zhou, X., Chen, R., Yu, Z., Li, R., Li, J., Zhao, X., ... Huang, G. (2015). Dichloroacetate restores drug sensitivity in paclitaxel-resistant cells by inducing citric acid accumulation. *Molecular Cancer*, 14, 63. <https://doi.org/10.1186/s12943-015-0331-3>

## SUPPORTING INFORMATION

Additional supporting information may be found online in the Supporting Information section at the end of the article.

**How to cite this article:** Twarock S, Reichert C, Bach K, et al. Inhibition of the hyaluronan matrix enhances metabolic anti-cancer therapy by dichloroacetate in vitro and in vivo. *Br J Pharmacol.* 2019;176:4474–4490. <https://doi.org/10.1111/bph.14808>